

**CATALYTIC OXIDATIVE CONVERSION OF METHANE TO
HIGHER HYDROCARBONS, SYNGAS OR CARBON DIOXIDE**

**A THESIS
SUBMITTED TO THE
UNIVERSITY OF PUNE
FOR THE DEGREE OF
DOCTOR OF PHILOSOPHY
IN CHEMISTRY**

By

BALU SHIVAJI UPHADE
M.Sc.

TH-1077

CHEMICAL ENGINEERING DIVISION
NATIONAL CHEMICAL LABORATORY
PUNE - 411 008, INDIA

FEBRUARY 1997

DEDICATED TO

MY FATHER : *Shri. Shivaji Bhimaji Uphade*

MY MOTHER : *Sau. Rakhmabai Shivaji Uphade*

AND UNCLES

CERTIFICATE AS PER FORM 'A'

Certified that the work incorporated in the thesis :

CATALYTIC OXIDATIVE CONVERSION OF METHANE TO HIGHER HYDROCARBONS, SYNGAS OR CARBON DIOXIDE

submitted by **Mr. Balu Shivaji Uphade** was carried out by the candidate under my guidance. Such material as has been obtained from other sources has been duly acknowledged in the thesis.



[Dr. Vasant R. Choudhary]

Research Guide

ACKNOWLEDGEMENTS

I express my deepest sense of gratitude to my thesis supervisor, Dr. Vasant R. Choudhary, Dy. Director, NCL, Pune, for his guidance. Working under his guidance has been a stimulating experience for me and I shall be having long lasting gratitude and respect for him.

My due kind gratitude to Dr. Paul Ratnasamy, Director, NCL and Dr. B.D. Kulkarni, Head, Chemical Engineering Division, NCL, for allowing me to carry out my research and extending me all the possible infrastructure facilities time-to-time.

I owe thanks to Profs. M.S. Wadia and R. S. Mali from Department of Chemistry, Pune University, Dr. A.C. Ranade (Vice-President R & D, Gufic Ltd., Valsad, Gujrat), Prof. U.G. Patil (Vice-Principal, Deolali Camp College, Nasik) and Drs. V.M. Nadkarni, S. Ponrathnam, C.R. Rajan and S.B. Pandit for cultivating research aptitude in me.

My collaborations with Drs. S.G. Pataskar, A.M. Rajput, A. Keshavaraja, A. Sudalai, Dr.(Mrs.) Belhekar, Mr. S.A.R. Mulla, Mr. A.S. Mamman, Mrs. G.A. Thite, Mr. Datta Ponde (Mama), Prabhakar Patil, Rajdeep, Miss. L.R. Kamath, Bulbule, Jakkam, Nandan, Miss. Roshan (all from NCL), Dr. K.S. Rane and his Ph.D. Student Mrs. Deepa from Goa University have provided with a first hand knowledge of academic excellence. They have been constant source of information and inspiration. I have enjoyed my numerous conversation with them. The help and cooperation provided from my seniors, Drs. V.H. Rane, S.T. Chaudhari and B. Prabhakar is duly acknowledged. I also wish to thank Dr. S.D. Sansare, Dr. V.R. Patwardhan, Dr. (Mrs) S. Mayadevi, Mr. A.K. Kinage, Mr. P. Devadas and Mr. C. Sivadinarayana for their helpful discussions and cooperation. The help received from the supporting staff of our group, Mr. V.L. Chandekar, Mr. V.L. Rajput and Mr. B.G. Pingale is also duly acknowledged.

The help I received from Mrs. A.P. Mitra and Mr. Deore for XRD and Mr. Sainkar for SEM (SIL), Mr. Bhujang for drawing/tracing of figures (PD), is invaluable to me. To them my thanks are due in no small amounts.

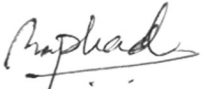
Many thanks are due to Dr. A.G. Shaikh, Mr. Dhaval Shirke, Mr. Shantanu Dhamne, Mrs. Neelam Bapat, and Miss. Kavita Wamwadi for their friendship and humor over the past years. My special thanks goes to Mr. Ravikant Thakkar, Mr. Prakash Ghule, Mr. Avinash Khalkar, Dr. Gautam Sakhala, my all the family members and other wellwishers for their patience to see me as a Doctor. I will be failing in my duties if I do not recall all my friends in NCL namely Vijay, Ulhas, Deepak, Sachin, Neepa, Zope, Patkar, Barhate, Mane, Bhawsar and all others in this laboratory who are not mentioned by person as well as my high school and college friends namely Bajirao, Sukhdeo, Balasaheb, Manik, Madhav, Narayan, Vasant, Shantaram, Paras, Appa, Anil, Babasaheb, Shaileja, Mini, Bagul, for their freindship.

The financial support provided by CSIR, Govt. of India, is gratefully acknowledged.

My special thanks and love go to my wife, SNEHAL, who provided much needed support and encouragement.

PUNE

February 1997


[B.S. Uphade]

LIST OF CONTENTS

Sl. No.	Description	Page No.
	OBJECTIVES/SCOPE, SUMMARY AND CONCLUSIONS	i-viii
	<i>PART-I : OXIDATIVE COUPLING OF METHANE TO HIGHER HYDROCARBONS</i>	
CHAPTER 1.1	OXIDATIVE COUPLING OF METHANE (OCM) TO C₂₊-HYDROCARBONS OVER SUPPORTED Li PROMOTED MgO AND La-PROMOTED CaO CATALYSTS	1-31
1.1.1	INTRODUCTION	1
1.1.2	EXPERIMENTAL	3
1.1.2.1	Catalyst Preparation	3
1.1.2.2	Catalyst Characterization	3
1.1.2.3	Catalytic Reaction	6
1.1.3	INFLUENCE OF SUPPORT ON SURFACE AND CATALYTIC PROPERTIES OF Li-MgO IN OCM	9
1.1.3.1	Comparison of Unsupported and Supported Li-MgO Catalysts for their performance in OCM	10
1.1.3.2	Catalyst-Support Interactions	11
1.1.4	INFLUENCE OF SUPPORT ON SURFACE AND CATALYTIC PROPERTIES OF La-CaO IN OCM	18
1.1.4.1	Comparison of Unsupported and Supported La-CaO Catalysts for their performance in OCM	18
1.1.4.2	Catalyst-Support Interactions	20
	REFERENCES	30
CHAPTER 1.2	OXIDATIVE COUPLING OF METHANE (OCM) OVER Sr-PROMOTED La₂O₃ CATALYSE SUPPORTED ON LOW SURFACE AREA POROUS CATALYST CARRIER	32-56
1.2.1	INTRODUCTION	32

RR
547.211:541.128(043)
UPH

Sl. No.	Description	Page No.
1.2.2	EXPERIMENTAL	33
1.2.2.1	Catalyst Preparation	33
1.2.2.2	Catalyst Characterization	33
1.2.2.3	Catalytic Reaction	34
1.2.3	RESULTS AND DISCUSSION	34
1.2.3.1	Catalyst Characterization	34
1.2.3.2	Oxidative Coupling of Methane	44
1.2.4	CONCLUSIONS	55
	REFERENCES	56

PART-II : CONVERSION OF METHANE TO SYNGAS

CHAPTER 21	OXIDATIVE CONVERSION OF METHANE TO SYNGAS OVER LaNiO₃ PEROVSKITE WITH OR WITHOUT SIMULTANEOUS STEAM AND CO₂ REFORMING REACTIONS: INFLUENCE OF PARTIAL SUBSTITUTION OF La AND Ni	57-76
2.1.1	INTRODUCTION	57
2.1.2	EXPERIMENTAL	58
2.1.2.1	Catalyst Preparation	58
2.1.2.2	Catalyst Characterization	59
2.1.2.3	Catalytic Reaction	59
2.1.3	RESULTS AND DISCUSSION	62
2.1.3.1	Catalyst Characterization	62
2.1.3.2	Oxidative Conversion of Methane to Syngas	65
2.1.3.3	Simultaneous Oxidative Conversion and Steam and CO ₂ Reforming of Methane to Syngas	71
2.1.4	CONCLUSIONS	74
	REFERENCES	75

S. No.	Description	Page No.
CHAPTER 2.2	PARTIAL OXIDATION OF METHANE TO SYNGAS WITH OR WITHOUT SIMULTANEOUS CO₂ AND STEAM REFORMING REACTIONS OVER Ni/AlPO₄	77-91
2.2.1	INTRODUCTION	77
2.2.2	EXPERIMENTAL	78
2.2.2.1	Catalyst Preparation	78
2.2.2.2	Catalytic Reaction	78
2.2.2.3	Catalyst Characterization	78
2.2.3	RESULTS AND DISCUSSION	79
2.2.3.1	Catalyst Characterization	79
2.2.3.2	Methane-to-Syngas Conversion over NiO/Silicalite-I	82
2.2.3.3	Methane-to-Syngas Conversion over NiO/ALPO-5	83
2.2.4	CONCLUSIONS	90
	REFERENCES	91
CHAPTER 2.3	OXIDATIVE CONVERSION OF METHANE TO SYNGAS WITH OR WITHOUT SIMULTANEOUS STEAM AND/OR CO₂ REFORMING OVER SUPPORTED NiO-MgO, NiO-CaO AND NiO-Yb₂O₃ CATALYSTS	92-98
2.3.1	INTRODUCTION	92
2.3.2	EXPERIMENTAL	93
2.3.2.1	Catalyst Preparation	93
2.3.2.2	Catalytic Reaction	93
2.3.3	RESULTS AND DISCUSSION	93
2.3.3.1	Oxidative Conversion of Methane to Syngas	95
2.3.3.2	Coupling of Catalytic Exothermic and Endothermic Reactions	96
2.3.4	CONCLUSIONS	97
	REFERENCES	98

Sl. No.	Description	Page No.
CHAPTER - 2.4	LARGE ENHANCEMENT IN METHANE-TO-SYNGAS CONVERSION ACTIVITY OF SUPPORTED Ni-CATALYSTS DUE TO PRECOATING OF CATALYST SUPPORTS WITH MgO, CaO OR RARE-EARTH OXIDE	99-104
2.4.1	INTRODUCTION	99
2.4.2	EXPERIMENTAL	99
2.4.2.1	Catalyst Preparation	99
2.4.2.2	Catalytic Reaction	100
2.4.3	RESULTS AND DISCUSSION	100
2.4.4	CONCLUSIONS	103
	REFERENCES	104
CHAPTER - 2.5	OXIDATIVE CONVERSION OF METHANE TO SYNGAS OVER NICKEL SUPPORTED ON COMMERCIAL LOW SURFACE AREA POROUS CATALYST CARRIERS PRECOATED WITH ALKALINE AND RARE EARTH OXIDES	105-128
2.5.1	INTRODUCTION	105
2.5.2	EXPERIMENTAL	106
2.5.2.1	Catalyst Preparation	106
2.5.2.2	Catalyst Characterization	107
2.5.2.3	Catalytic Reaction	107
2.5.3	RESULTS AND DISCUSSION	107
2.5.3.1	Influence of Support	109
2.5.3.2	Influence of Support Precoating Agent	114
2.5.3.3	Influence of MgO Loading on Support	117
2.5.3.4	Influence of NiO Loading on MgO Precoated Support	120
2.5.3.5	Influence of Calcination Temperature	121
2.5.4	CONCLUSIONS	126
	REFERENCES	128

Sl. No.	Description	Page No.
CHAPTER - 2.6	SIMULTANEOUS STEAM AND CO₂ REFORMING OF METHANE TO SYNGAS OVER NiO/MgO/SA-5205 IN PRESENCE AND ABSENCE OF OXYGEN	129-152
2.6.1	INTRODUCTION	129
2.6.2	EXPERIMENTAL	130
2.6.2.1	Catalyst Preparation	130
2.6.2.2	Catalyst Characterization	130
2.6.2.3	Catalytic Reaction	131
2.6.3	RESULTS	132
2.6.3.1	Catalyst Characterization	132
2.6.3.2	Steam and/or CO ₂ Reforming of Methane	132
2.6.3.3	Oxy-Steam Reforming of Methane	139
2.6.3.4	Oxy-CO ₂ Reforming of Methane	142
2.6.3.5	Oxy-Steam and CO ₂ Reforming of Methane	142
2.6.4	DISCUSSION	145
2.6.4.1	Steam and/or CO ₂ Reforming of Methane	147
2.6.4.2	Oxy-Steam and/or CO ₂ Reforming of Methane	147
2.6.5	CONCLUSIONS	150
	REFERENCES	151
PART-III	COMPLETE COMBUSTION OF METHANE FOR ITS EMISSION CONTROL	
CHAPTER 3.1	LOW-TEMPERATURE COMPLETE COMBUSTION OF METHANE OVER Mn-, Co- OR Fe-STABILIZED ZrO₂	153-163
3.1.1	INTRODUCTION	153
3.1.2	EXPERIMENTAL	153
3.1.2.1	Catalyst Preparation	153
3.1.2.2	Catalyst Characterization	154
3.1.2.3	Catalytic Reaction	154
3.1.3	RESULTS AND DISCUSSION	157
3.1.4	CONCLUSIONS	162
	REFERENCES	163

SL No.	Description	Page No.
CHAPTER 3.2	LOW TEMPERATURE TOTAL OXIDATION OF METHANE OVER Ag-DOPED LaMO₃ PEROVSKITE OXIDES	164-180
3.2.1	INTRODUCTION	164
3.2.2	EXPERIMENTAL	164
3.2.2.1	Catalyst Preparation	164
3.2.2.2	Catalyst Characterization	165
3.2.2.3	Catalytic Reaction	165
3.2.3	COMPLETE COMBUSTION OF METHANE OVER Ag-DOPED LaMO ₃ (M = CO, Mn, Ni)	171
3.2.4	COMPLETE COMBUSTION OF METHANE OVER Ag-DOPED LaFe _{1-y} Co _y O ₃	173
3.2.5	COMPLETE COMBUSTION OF METHANE OVER Ag-IMPREGNATED PEROVSKITES	177
	REFERENCES	180
APPENDICES		181-183
LIST OF PUNBICATIONS : PAPERS & PATENTS		184-187

**OBJECTIVE/SCOPE,
SUMMARY AND CONCLUSIONS**

OBJECTIVES/SCOPE, SUMMARY AND CONCLUSIONS

THESIS TITLE : CATALYTIC OXIDATIVE CONVERSION OF METHANE TO HIGHER HYDROCARBONS, SYNGAS OR CARBON DIOXIDE

Methane is a major constituent of natural gas and biogas. World reserves of natural gas are constantly being upgraded, and more and more natural gas is being discovered than oil. Methane is most inert among the hydrocarbons and therefore its direct conversion to ethylene and other value added and/or easily transportable products (viz., methanol, formaldehyde, liquid hydrocarbon fuels, lower olefins, etc.) is very difficult. Catalytic oxidative conversion of methane to ethylene (a key-stone to petrochemicals) and syngas (which is a mixture of CO and H₂, a versatile feedstock for NH₃, methanol and Fischer-Tropsch synthesis processes) and also low temperature catalytic complete combustion of methane to carbon dioxide (for methane emission control) are of great practical importance. In the past 13-15 years extensive studies has been carried out in the oxidative coupling of methane (OCM) to C₂-hydrocarbons over a number of catalysts, mostly unsupported ones. Since last 5-6 years research activities are also concentrated on catalytic oxidative conversion of methane to syngas and on catalytic complete combustion of methane (at low temperature) for its emission control.

The present work for the Ph.D. thesis was undertaken as a part of the comprehensive R & D programme in our laboratory for the development of catalysts and catalytic processes for the catalytic oxidative conversion of methane to ethylene and syngas and also for catalytic complete combustion of methane, with the following objectives.

1. To study the influence of physico-chemical catalyst-support interactions for Li-MgO and La-CaO OCM catalysts supported over commonly used low surface area porous catalyst carriers, on the surface and catalytic properties.
2. To develop a supported OCM catalyst (Sr-promoted La₂O₃) having high activity, selectivity and productivity in the OCM process and also having high thermal/hydrothermal stability and mechanical strength and to investigate thoroughly the influence of following catalyst and process parameters on the catalytic activity and selectivity in the OCM process at high space velocity.

- surface properties of silica-alumina support
 - Sr/La ratio
 - particle size
 - linear gas velocity
 - CH₄/O₂ ratio in the feed
 - catalyst dilution
3. To study oxidative conversion of methane to syngas with and without simultaneous steam and/or CO₂ reforming of methane using Ni/ALPO-5 and La_{1-x}Ca(or Sr)_xNi_{1-y}O₃ catalysts at different process conditions.
 4. To develop supported Ni catalyst for methane-to-syngas conversion processes using commercial low surface area porous catalyst carriers by thoroughly investigating the influence of various catalyst parameters (viz. support, precoating of support with alkaline and rare-earth oxides, loading of NiO and precoating metal oxide, calcination temperature, etc.) on the surface properties and activity/selectivity in the oxidative conversion of methane to syngas.
 5. To study the following methane-to-syngas conversion reactions over NiO/MgO/SA-5205 catalyst at different process conditions:
 - simultaneous steam and CO₂ reforming of methane
 - oxidative conversion of methane to syngas simultaneously with
 - steam reforming of methane
 - CO₂ reforming of methane
 - both steam and CO₂ reforming of methane
 6. To study low temperature complete combustion of methane over novel catalysts, such as Cr-, Mn-, Fe-, Co-, Ni-, or Cu-stabilised ZrO₂ and Ag-doped LaMO₃ perovskite oxide catalysts.

The thesis work has been divided into three parts, as follows.

PART-I: OXIDATIVE COUPLING OF METHANE (OCM) TO C₂+ HYDROCARBONS

CHAPTER - 1.1 : OCM OVER SUPPORTED Li-MgO AND La-CaO CATALYSTS: INFLUENCE OF CATALYST-SUPPORT INTERACTIONS

Oxidative coupling of methane to ethane/ethylene has been studied at atmospheric pressure over supported Li-promoted MgO and La-promoted CaO catalysts in the presence of free oxygen at different process conditions.

Deposition of Li-MgO catalyst on commonly used supports (containing SiO₂, Al₂O₃, SiC, ZrO₂, HfO₂, etc.) causes a drastic reduction in the catalytic activity/selectivity for the oxidative methane coupling reaction and also in both the total and strong surface basicity. The decrease in the catalytic activity/selectivity and basicity is attributed to strong chemical interactions between the catalyst and support, occurring during the high temperature (750°C) calcination/pretreatment of the catalyst. The chemical interactions result in catalytically inactive binary and ternary metal oxides containing Li and/or Mg, thus deactivating the Li-MgO catalyst by consuming its active components. As compared to Li-MgO, the deposition of La-CaO catalyst on the various supports caused a smaller decrease in its OCM activity.

CHAPTER - 1.2 : OXIDATIVE COUPLING OF METHANE OVER Sr-PROMOTED La₂O₃ CATALYST SUPPORTED ON LOW SURFACE AREA POROUS CATALYST CARRIER

Oxidative coupling of methane (OCM) to higher hydrocarbons over Sr-promoted La₂O₃ supported on commercial low surface area porous catalyst carriers (containing mainly alumina and silica) at 800° and 850°C and space velocity of 1,02,000 cm³.g⁻¹.h⁻¹ has been thoroughly investigated. Effects of support, catalyst particle size, linear gas velocity (at the same space velocity), Sr/La ratio, CH₄/O₂ ratio in the feed and catalyst dilution by inert solid particles on the conversion, yield or selectivity and product ratios (C₂H₄/C₂H₆ and CO/CO₂) in the OCM process have been studied. The catalysts have been characterised for their basicity, acidity and oxygen chemisorption by the TPD of CO₂, ammonia and oxygen, respectively from 50° to 950°C and also characterised for their surface area. The supported catalysts showed better performance than the unsupported one. The basicity is strongly influenced by the Sr/La ratio; the supported catalysts showed best performance for their Sr/La ratio of about 0.3. The methane/O₂ ratio also showed a strong influence on the OCM process. However, the influence

of linear gas velocity and particle size is found to be small; it is resulted mainly from the temperature gradient in the catalyst. The catalyst dilution has little or no effect on the conversion and selectivity. However, it has beneficial effects for achieving higher C_2H_4/C_2H_6 ratio and also for reducing the hazardous nature of the OCM process because of the coupling of the exothermic oxidative conversion reactions and the endothermic thermal cracking reactions and also due to the increased heat transfer area.

PART-II : CONVERSION OF METHANE TO SYNGAS

CHAPTER - 2.1 : OXIDATIVE CONVERSION OF METHANE-TO-SYNGAS OVER $LaNiO_3$ PEROVSKITE WITH OR WITHOUT SIMULTANEOUS STEAM AND CO_2 REFORMING REACTIONS: INFLUENCE OF PARTIAL SUBSTITUTION OF La AND Ni

Selective partial oxidation of methane to syngas over $LaNiO_3$, $La_{0.8}Ca(or Sr)_{0.2}NiO_3$ and $LaNi_{1-x}Co_xO_3$ (where $x = 0.2-1$) perovskites at extremely short contact time (≈ 0.8 ms) has been investigated. Also, simultaneous oxidative conversion and steam and CO_2 reforming of methane to syngas over $LaNiO_3$ at short contact time (≈ 9 ms) has been studied at different temperatures and CH_4/O_2 feed ratios. The catalysts, before and after reaction, were characterized by XRD and SEM. $LaNiO_3$ perovskite shows high activity and selectivity in the oxidative conversion of methane to syngas. However, the partial substitution of its La by Ca or Sr and also the partial or complete substitution of its Ni by Co causes a large decrease in its both activity and selectivity. $LaNiO_3$ is transformed to its catalytically active form, Ni^0/La_2O_3 , during the initial period of the process. This catalyst shows very good performance in the simultaneous oxidative conversion (which is exothermic) and steam and CO_2 reforming reactions (which are endothermic) of methane to syngas, at short contact time, operating in a most energy efficient manner and also requiring only a little or no external energy.

CHAPTER- 2.2 : PARTIAL OXIDATION OF METHANE TO SYNGAS WITH OR WITHOUT SIMULTANEOUS CO₂ AND STEAM REFORMING REACTIONS OVER Ni/ALPO₄ AND Ni/SILICALITE-I

Oxidative conversion of methane by O₂ to CO and H₂ (i.e. syngas) over NiO supported on microporous aluminophosphate (ALPO-5) and silicalite-I (i.e. high silica ZSM-5 zeolite) in the presence or absence of simultaneously occurring CO₂ and steam reforming reactions of methane has been investigated. During the catalytic reactions, the NiO/ALPO-5 is transformed into Ni^o/AlPO₄ (tridymite). The catalyst shows high activity and selectivity, particularly at high temperatures (at > 1073K) in the oxidative conversion of methane to syngas and also in the exothermic oxidative conversion which occurs simultaneously with the endothermic CO₂ and steam reforming of methane. In the latter case, the overall catalytic process can be made almost thermoneutral, requiring little or no external energy. The process also occurs in a most energy efficient and safe manner. The Ni/silicalite catalyst showed very poor performance in the oxidative conversion of methane to syngas.

CHAPTER - 2.3 : OXIDATIVE CONVERSION OF METHANE TO SYNGAS WITH OR WITHOUT SIMULTANEOUS STEAM AND/OR CO₂ REFORMING OVER SUPPORTED NiO-MgO, NiO-CaO AND NiO-Yb₂O₃ CATALYSTS

Influence of support on the performance of NiO-MgO, NiO-CaO, and NiO-Yb₂O₃ catalysts supported on a commercial catalyst carrier (SA-5205, containing alumina and silica) in the oxidative conversion of methane to syngas has been investigated. Coupling of the exothermic oxidative methane conversion with the endothermic steam and/or CO₂ reforming over NiO-MgO/SA-5205 catalyst has also been studied.

CHAPTER - 2.4 : LARGE ENHANCEMENT IN METHANE-TO-SYNGAS CONVERSION ACTIVITY OF SUPPORTED Ni-CATALYSTS DUE TO PRECOATING OF CATALYST SUPPORTS WITH MgO, CaO OR RARE-EARTH OXIDE

Supported NiO catalysts prepared using commercial sintered low surface area porous catalyst carriers (containing Al₂O₃, and/or SiO₂) precoated with MgO, CaO or rare-earth oxide show very much higher activity, selectivity and productivity in methane-to-syngas conversion reactions, than the catalyst prepared using without any precoating. Among the precoating metal oxides, the best performance is observed for MgO.

CHAPTER - 2.5 : OXIDATIVE CONVERSION OF METHANE TO SYNGAS OVER NICKEL SUPPORTED ON COMMERCIAL LOW SURFACE AREA POROUS CATALYST CARRIERS PRECOATED WITH ALKALINE AND RARE EARTH OXIDES

Partial oxidation of methane to CO and H₂ at very small contact times (about 1 ms) over different supported Ni-catalysts [prepared by depositing NiO-MgO on different commercial low surface area porous catalyst carriers (obtained from M/S Norton Co., USA) consisting of refractory compounds (viz. SiO₂, Al₂O₃, SiC, ZrO₂, HfO₂, etc.) at different concentrations and having different surface properties and also prepared by depositing NiO on the catalyst carriers precoated with different alkaline and rare earth oxides (viz. MgO, CaO, SrO, BaO, Sm₂O₃ and Yb₂O₃)] at 700° and 800°C, CH₄/O₂ ratio in feed of 1.8 and gas space velocity of $5.2 \times 10^5 \text{ cm}^3 \cdot \text{g}^{-1} \cdot \text{h}^{-1}$ has been investigated. The catalysts have been characterized by their TPR by H₂ from 100° to 900°C, degree of NiO reduction and H₂ chemisorption after the catalyst reduction at 900°C. The influence of support (its composition and surface properties), method of NiO and MgO deposition, support precoating agent, loadings of NiO and MgO (as support precoating agent) loadings and calcination temperature on the activity/selectivity, TPR and degree of NiO reduction and also on the H₂ chemisorption has been thoroughly studied. The catalyst characteristics are strongly influenced by the support (containing Al₂O₃ and/or SiO₂ at higher concentrations and having higher surface area), precoating agent, loading of MgO precoat on the support, particularly at lower loadings (below 2 wt.%), and also by the catalyst calcination temperature above 900°C. The catalyst prepared by depositing NiO on the commercial supports (except SA-5552 having much higher surface area) precoated with MgO (6 ± 1 wt.%) and calcined at 900°C shows excellent performance in the catalytic process (at 800°C) with very high methane conversion (> 91%), selectivity (> 95%) and CO productivity (> 13 mol.g⁻¹.h⁻¹). However, its activity and selectivity are reduced drastically when the MgO loading is decreased below 2 wt.%, the MgO precoat is replaced by that of SrO or BaO or when the catalyst is calcined above 1050°C.

CHAPTER - 2.6 : SIMULTANEOUS STEAM AND CO₂ REFORMING OF METHANE TO SYNGAS OVER NiO/MgO/SA-5205 IN PRESENCE AND ABSENCE OF OXYGEN

Steam reforming, CO₂ reforming and simultaneous steam and CO₂ reforming reactions of methane for its conversion into syngas (H₂ and CO) over NiO/MgO/SA-5205 catalyst (prepared by depositing NiO on MgO pre-coated SA-5205 support) in both the presence and absence of O₂ in the feed have been investigated at different process conditions. The catalyst has been characterised by its temperature programmed reduction and also, after its reduction, by temperature programmed desorption of hydrogen. It showed high activity and selectivity in the above methane-to-syngas conversion reactions at low contact times. The H₂/CO product ratio in the simultaneous methane conversion reactions showed a strong dependence on the feed composition; it is increased with increasing the concentration of steam relative to that of O₂ and/or CO₂ in the feed. In the oxy-steam and/or CO₂ reforming reactions, there is a direct coupling of the exothermic and endothermic reactions and hence these processes over the catalyst occur in the most energy efficient and safe manners, requiring little or no external energy. The net heat of reactions in these processes is strongly influenced by the reaction temperature and/or CH₄/O₂ ratio in the feed. In the simultaneous steam and CO₂ reforming of methane in both the presence and absence of O₂, it is possible to convert methane into syngas with high conversion (above 97%) and 100% selectivity for both CO and H₂.

PART-III: COMPLETE COMBUSTION OF METHANE FOR ITS EMISSION CONTROL

CHAPTER 3.1 : LOW-TEMPERATURE COMPLETE COMBUSTION OF METHANE OVER Mn-, Co-, AND Fe-STABILIZED ZrO₂

Complete combustion of methane to CO₂ and water over the transition metal (viz. Cr, Mn, Fe, Co, Ni or Cu) stabilised ZrO₂ (cubic) catalysts diluted with inert α -Al₂O₃ particles at different temperatures (250°-600°C) using 1 mol% CH₄ in air as a feed at a space velocity of 51,000 cm³.g⁻¹.h⁻¹ has been thoroughly investigated. Among the catalysts, Mn-stabilised ZrO₂ showed the best performance. Mn-, Fe- and Co-stabilised ZrO₂ (cubic) catalysts showed much higher methane combustion activity at low temperature than the perovskite oxide catalysts and have the activity comparable to that of the noble metal catalysts. Also, by incorporating the transition metal in the bulk

structure of ZrO_2 , not only the ZrO_2 is stabilized in its cubic (fluorite) form but also the reactivity of its lattice oxygen (at low temperature) for the complete combustion of methane is drastically increased.

CHAPTER 3.2 : LOW TEMPERATURE TOTAL OXIDATION OF METHANE OVER Ag-DOPED LaMO_3 PEROVSKITE OXIDES

Complete combustion of methane (at atmospheric pressure) over Ag (or Sr)-doped LaMO_3 (M = Mn, Fe, Co or Ni) catalysts diluted with inert $\alpha\text{-Al}_2\text{O}_3$ particles at different temperatures (300°-850°C) using 4 mol% CH_4 in air as a feed at a space velocity of 51,000 $\text{cm}^3\cdot\text{g}^{-1}\cdot\text{h}^{-1}$ has been thoroughly investigated. The catalysts were characterised for their surface area and crystalline phases and also for the reactivity of their lattice oxygen by their reaction with pure methane in the absence of free- O_2 . The pulse reactions of pure methane over the catalysts in the absence of free- O_2 indicated the involvement of lattice oxygen in the catalytic combustion of methane.

Partial substitution of La by Ag, instead of Sr, in LaMO_3 (M= Mn, Fe, Co or Ni) perovskite oxides causes a large increase in the catalytic activity of the perovskite in the complete combustion of dilute methane (for its emission control) at low temperature (< 700°C). Among the perovskite oxide catalysts Ag-doped LaCoO_3 and $\text{LaFe}_{0.5}\text{Co}_{0.5}\text{O}_3$ showed higher methane combustion activity and their lattice oxygen also showed higher reactivity.

PART - I

OXIDATIVE COUPLING OF METHANE (OCM) TO C₂₊-HYDROCARBONS

**CHAPTER - 1.1 : OXIDATIVE COUPLING OF METHANE (OCM) TO
C₂₊-HYDROCARBONS OVER SUPPORTED Li-
PROMOTED MgO AND La-PROMOTED CaO
CATALYSTS**

**CHAPTER - 1.2 : OXIDATIVE COUPLING OF METHANE OVER Sr-
PROMOTED La₂O₃ CATALYST SUPPORTED ON
LOW SURFACE AREA POROUS CATALYST
CARRIER**

CHAPTER - 1.1

OXIDATIVE COUPLING OF METHANE (OCM) TO C₂₊-HYDROCARBONS OVER SUPPORTED Li-PROMOTED MgO AND La-PROMOTED CaO CATALYSTS

1.1.1 INTRODUCTION

Direct conversion of methane, a major constituent of natural gas comprising over 90 mol% of the hydrocarbon fraction, to ethane and ethylene and C₂₊-hydrocarbons is a process of great practical importance. Methane is most inert among the hydrocarbons and hence its direct conversion to these highly valued and/or easily transportable products is a great challenge to the scientists working in this field. Since the first paper by Keller and Bhasin in 1982 [1], a very large number of unsupported basic solid catalysts have been reported for oxidative coupling of methane (OCM) to C₂-hydrocarbons. The studies on OCM have been compiled in several comprehensive reviews published time-to-time [2-14].

It is generally believed that oxidative coupling of methane on the catalyst involves the removal of hydrogen atom from methane molecule to form a methyl radical, the coupling of two methyl radicals to produce an ethane molecule and subsequent oxidative dehydrogenation of ethane to ethylene [6, 13].

India has large reserves of natural gas and the probability of finding new reserves for natural gas is estimated to be better than that for oil. But, due to lack of appropriate technology, NG produced in the country is mostly flared causing wastage of valuable energy source and global warming due to the CO₂ produced. It is, therefore, more appropriate to critically evaluate the technology options for converting natural gas to middle distillates via formation of ethylene. Hence, the present investigation was undertaken as a part of the comprehensive R & D programme in our laboratory for methane/NG conversion into lower olefins and syngas by energy efficient processes.

Li-promoted MgO [15, 16] shows high catalytic activity and selectivity in the OCM process. Since its introduction, this catalyst has been studied very extensively for its active centers, catalytic activity/selectivity and stability (or deactivation) and catalytic reaction mechanism for the

OCM process [6, 17-30]. Unsupported La-promoted CaO studied for the OCM process also shows high methane conversion activity and selectivity for C_{2+} -hydrocarbons and long term stability at high temperature (800°-850°C) [30-35]. However, a little or no information is available on the behavior of these catalysts when they are supported on commonly used catalyst carriers or supports. In industrial practice, active catalysts are generally supported on catalyst carriers which provide to the catalysts a porous matrix having a high mechanical strength (i.e. high crushing strength and resistance to attrition loss), a high thermal/hydrothermal stability and also a low pressure drop across the catalyst bed. It is, therefore, interesting to study the influence of different catalyst carriers (viz. low surface area porous supports containing refractory metal oxides, such as silica, alumina, zirconia and silicon carbide), used commonly for supporting oxidation catalysts, on the performance of supported Li-MgO and La-CaO catalysts. Since, the temperature involved in the catalyst calcination and/or catalytic OCM process is very high (about 700°-850°C), it is very interesting to know the interactions, particularly chemical ones, between the active components of the catalyst (both Li and MgO) and the support (viz. reactive metal oxides). It may be noted that although the strong metal-support interactions (commonly known as SMSI effect) have been extensively investigated [36,37], the information on metal oxide-support interactions is rare [38].

In the earlier studies reported by Choudhary et. al., the Li-MgO [22] (prepared using Li-acetate and Mg-acetate as catalyst precursors) and La-CaO [30] (prepared using La-nitrate and CaO as catalyst precursors) showed not only high activity and selectivity but also high productivity and catalyst stability in the OCM reaction. However, no information is available on the behavior of these catalysts when they are supported on commonly used catalyst carriers or supports. The present investigation was, therefore, undertaken to study the influence of commonly used catalyst supports on the performance of the above Li-MgO and La-CaO catalysts and also to know the interactions, particularly chemical ones, between the active components of both the catalyst and different supports.

1.1.2 EXPERIMENTAL

1.1.2.1 Catalyst Preparation

a) Unsupported and supported Li-MgO catalysts

Li-promoted MgO (unsupported) was prepared by impregnating powdered Mg-acetate with aqueous Li-acetate (Li/Mg mole ratio = 0.1), drying, calcining in air at 750°C for 6 h, powdering, pressing and crushing to 22-30 mesh size particles. Supported Li-MgO catalysts (Table 1.1.1) were prepared by impregnating different supports [viz. commercial low surface area ($< 1 \text{ m}^2 \cdot \text{g}^{-1}$) porous catalyst carriers : SA-5552, SC-5532, SS-5231 and SZ-5564 (obtained from M/S Norton Co., USA) (Appendix-1) and silica gel (Fuji-Davison, B-type) crushed to 22-30 mesh size particles and α -alumina in a form of fine powder] with an aqueous solution containing Li-acetate and Mg-acetate (Li/Mg mole ratio = 0.1), drying and calcining in air at 750°C for 6 h. The loading of Li-MgO in the supported catalysts was $9 \pm 0.5 \text{ wt.}\%$. Samples of Li_2O ($5.0 \pm 0.2 \text{ wt.}\%$) and MgO ($6.0 \pm 0.5 \text{ wt.}\%$) supported on the Norton catalyst carriers were also prepared by the above method.

b) Unsupported and supported La-CaO catalysts

Unsupported La-promoted CaO (La/Ca mole ratio = 0.1) was prepared using mixed La- and Ca-nitrates as precursors. The precursors were ground with distilled water sufficient to form a thick paste and dried at 110°C for 12 h. The dried catalyst mass was decomposed at 600°C for 6 h in static air, pressed binder-free, crushed to 22-30 mesh size particles and calcined at 900°C for 4 h in static air. Supported La-promoted CaO catalysts (Table 1.1.4) were prepared by impregnating different supports (viz. SA-5552, SC-5532, SS-5231 and SZ-5564 crushed to 22-30 mesh size particles) with an aqueous solution containing La- and Ca-nitrates (La/Ca = 0.1) with or without precoating the supports by MgO, CaO or La_2O_3 , drying and decomposing (or calcining) in air at 900°C for 4 h. The catalyst carriers were precoated with solid metal oxide by impregnating the catalyst carrier with corresponding metal nitrate, drying and decomposing as above.

1.1.2.2 Catalyst Characterization

a) Surface area

The surface area of the catalysts was measured by the single-point BET method by measuring the adsorption of nitrogen at liquid nitrogen temperature and at the N_2 concentration of 30 mol%

(balance helium), using a Monosorb Surface Area Analyser (Quantachrome Corp., USA) based on dynamic adsorption/desorption technique.

Before carrying out the surface area measurement experiments, the catalyst (1.0-3.0 g) was pretreated insitu in the sample cell at 300°C for 1 h in flow (30 cm³.min⁻¹) of a mixture of helium and nitrogen to remove the traces of moisture and also the analyser was calibrated by injecting a known amount of air.

The surface area was calculated from the observed desorption counts instead of the adsorption ones, as follows:

$$\text{Surface area (m}^2\text{.g}^{-1}\text{)} = \frac{\text{Desorption counts} \times 2.84}{\text{wt. of catalyst} \times \text{counts for a 1 cm}^3 \text{ of air}}$$

(2.84 m² area) = 1 cm³ of N₂ or air, counts are expressed in terms of surface area, m²

b) X-ray diffraction (XRD)

The XRD analysis of the catalysts used in the OCM process was done by the X-ray powder diffraction method using a Holland Philips, PW/1730 X-ray generator with the CuK_α radiation scintillation counter.

c) Measurement of basicity/base strength distribution

Chemisorption of CO₂ on Li-MgO

The catalysts used in the OCM process were characterized for their basicity (both total and strong basic sites) by the chemisorption of CO₂ at 100°C and 500°C, respectively, using g.c. pulse technique [39]. The experimental set-up used for the TPD studies is shown in Fig. 1.1.1

The catalyst (2.0 g) was packed in the quartz reactor and calcined in-situ in a flow of helium (30 cm³.min⁻¹) at 750°C for 1 h. The CO₂ pulse experiments on the same catalyst were carried out first at 500°C and then at 100°C. The chemisorption of CO₂ at 500°C was obtained directly as the amount of CO₂ adsorbed irreversibly on the catalyst. The chemisorption of CO₂ at 100°C was obtained as a sum of the chemisorption of CO₂ at 500°C and the amount CO₂ adsorbed irreversibly in the pulse experiments at 100°C due to decrease in the temperature from 500° to 100°C.

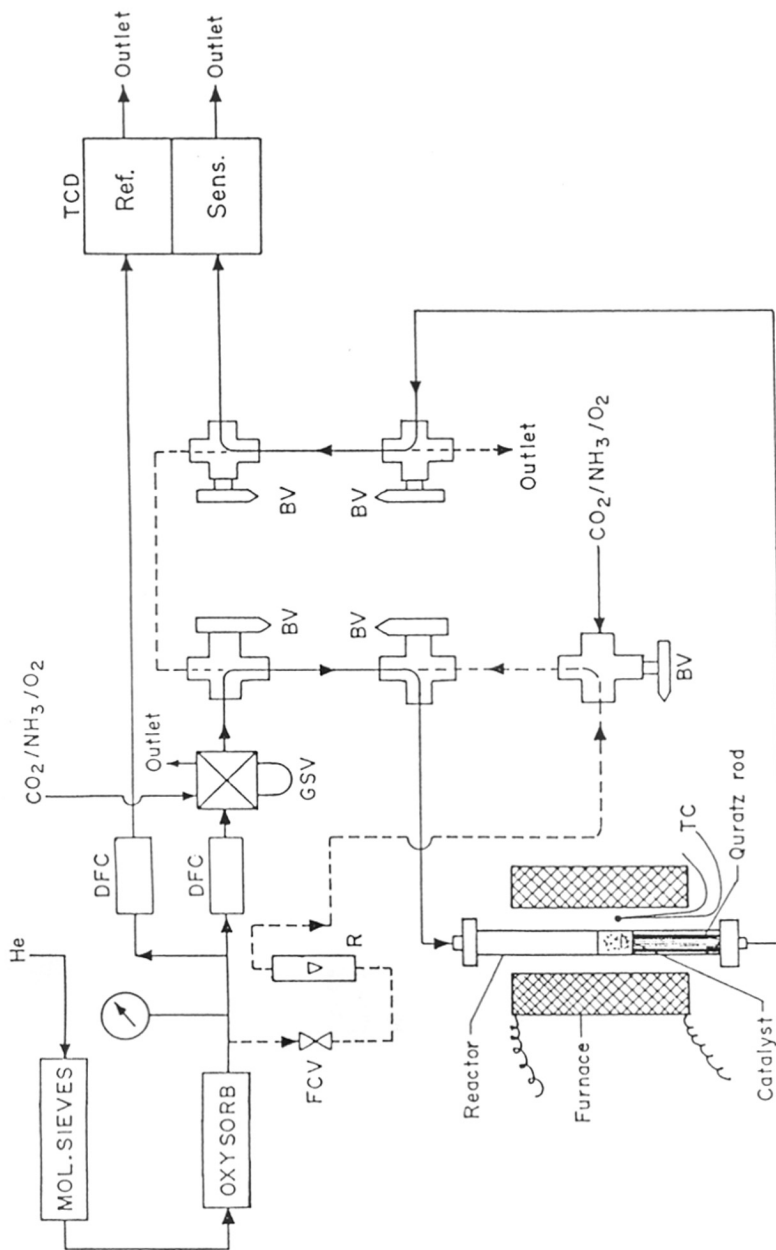


Fig. 1.1.1 : Experimental set-up for TPD studies [BV = Three way ball valve, DFC = Differential flow controller, FCV = Flow control valve, GSV = Gas sampling valve, R = Rotameter, TCD = Thermal conductivity detector, TC = Thermocouple]

TPD of CO₂ over La-CaO

The catalysts used in the OCM process were characterized for their basicity/base strength distribution by temperature programmed desorption (TPD) of carbon dioxide (chemisorbed at 100°C) from 50°C to 900°C. The experimental set-up used for the TPD studies is shown in Fig. 1.1.1

The catalyst (0.5-2.0 g) was packed in the quartz reactor and calcined in-situ in a flow of helium (30 cm³.min⁻¹) at 900°C for 1 h at a linear heating rate of 20°C.min⁻¹. The chemisorption of carbon dioxide at 100°C was carried out by saturating the catalyst with CO₂ and desorbing the physically adsorbed CO₂ at 100°C in a flow of helium for 30 min. The desorbed CO₂ in the TPD run was detected by a thermal conductivity detector (TCD).

In the present study, the chemisorption of CO₂ is considered as the amount of CO₂ retained by the presaturated catalyst after it was swept with pure helium for a period of 30 min.

1.1.2.3 Catalytic Reaction

The quartz reactor and experimental set-up used for the OCM reaction are shown in Figs. 1.1.2 and 1.1.3, respectively.

OCM over the catalysts was carried out at atmospheric pressure in a conventional flow quartz reactor (i.d.: 10 mm and o.d.: 12.0 mm) packed with 0.1 g or 1.0 g of catalyst. The reaction temperature was measured by a Chromel-Alumel thermocouple located in the catalyst bed. The catalyst was pretreated *in-situ* in the flow of N₂ (20 cm³.min⁻¹) at 750°C or 900°C (for unsupported and supported Li-MgO and La-CaO catalysts, respectively) for 1 h. The feed consists of pure methane and oxygen. The reactor effluent gases were analysed by an on-line gas chromatograph connected with thermal conductivity detector (TCD) and flame ionization detector, using Porapak-Q (3 mm x 3 m) and SpheroCarb (3 ft.) columns at the following GC operating conditions :

Detector temperature	:	150°C
Injector temperature	:	100°C
Oven temperature	:	37°C
Filament current	:	166 mA
Carrier gas	:	H ₂
Carrier gas flow	:	35 cm ³ .min ⁻¹

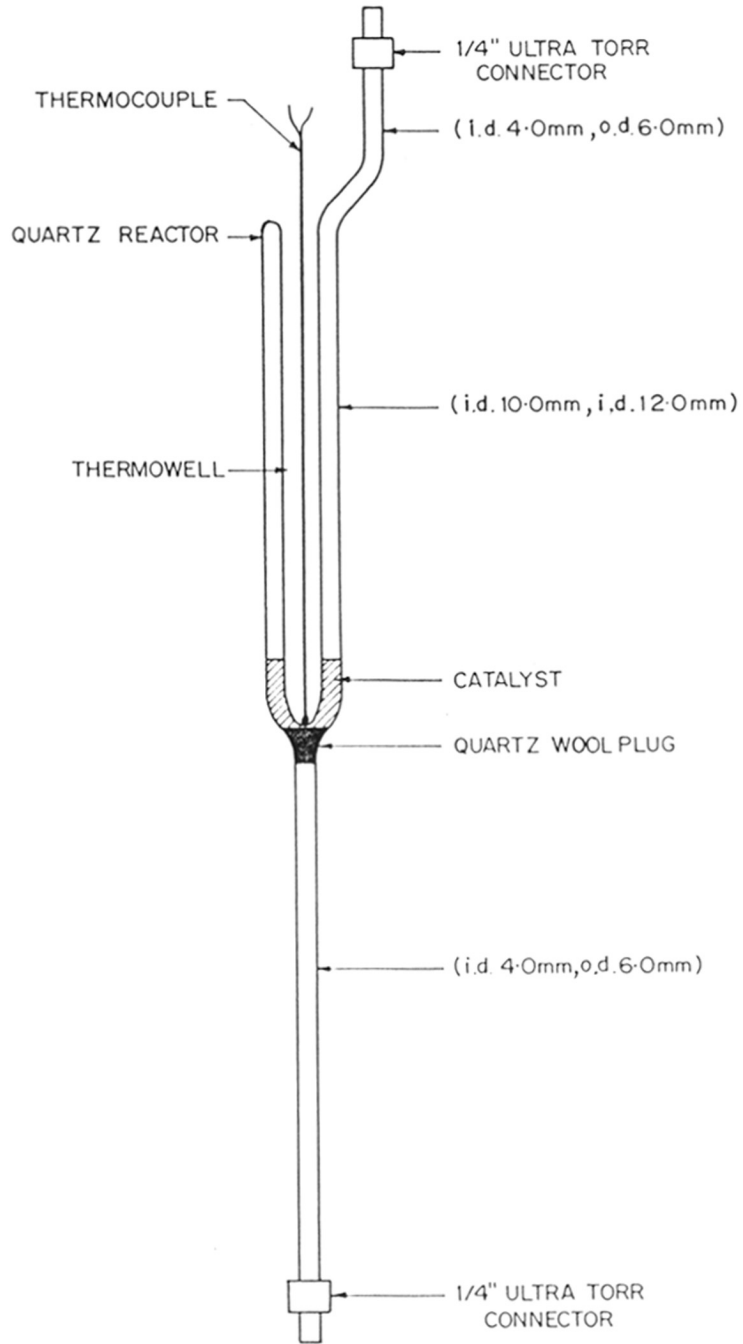


Fig. 1.1.2 : Quartz reactor for OCM reaction

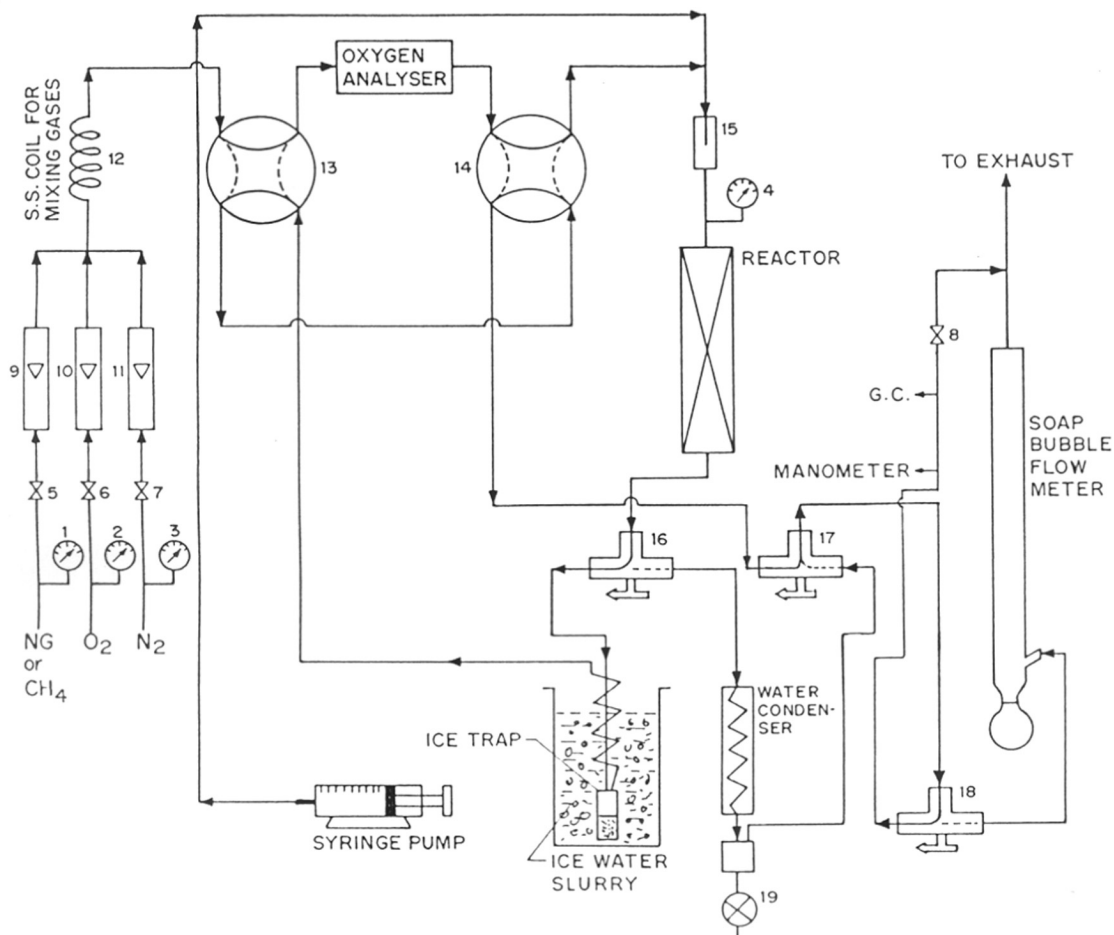


Fig. 1.1.3 : Experimental set-up for evaluation of catalyst performance in OCM process [1-4 : Pressure gauges, 5-8 : Needle valves, 9-11 : Rotameters, 12 : S.S. coil (dia. = 1/4", L = 10 ft), 13-14 : Stream selector valves, 15 : Preheater, 16-18 : Three way valves, 19 : Rota flow stop cocks]

Before carrying out the OCM reaction, the response factors and retention time of the product gases were obtained by injecting the high purity individual gas sample into the column. The detector response was linear.

The methane conversion, C₂-selectivity, C₂-yield, gas hourly space velocity (GHSV) and C₂-productivity (or STY) are defined/calculated as follows.

$$\begin{aligned} \text{Total CH}_4 \text{ conversion (\%)} &= \text{Conversion of CH}_4 \text{ to all the products} \\ &= \frac{\text{Total moles of CH}_4 \text{ converted}}{\text{Total moles of CH}_4 \text{ in feed}} \times 100 \\ \\ \text{C}_2\text{-Selectivity (\%)} &= \frac{\text{Conversion of CH}_4 \text{ to C}_2\text{-hydrocarbons (\%)}}{\text{Total conversion of CH}_4 \text{ (\%)}} \times 100 \\ \\ \text{C}_2\text{-Yield (\%)} &= \text{Conversion of CH}_4 \text{ to C}_2\text{-hydrocarbons} \\ &= \frac{\text{CH}_4 \text{ conversion (\%)} \times \text{C}_2\text{-selectivity (\%)}}{100} \\ \\ \text{C}_2\text{-Productivity (mol.g}^{-1}\text{.h}^{-1}\text{)} &= \frac{\text{GHSV} \times \text{mole fraction of CH}_4 \text{ in feed} \times \text{C}_2\text{-Yield (\%)}}{2 \times 22400 \times 100} \\ &= \frac{\text{GHSV} \times \text{mole fraction of CH}_4 \text{ in feed} \times \text{C}_2\text{-Yield (\%)}}{4.48 \times 10^6} \\ \\ \text{Gas Hourly Space Velocity (GHSV) (cm}^3\text{.g}^{-1}\text{.h}^{-1}\text{)} &= \frac{\text{Total flow rate of feed gases (measured at 0}^\circ\text{C and 1 atm) (cm}^3\text{.g}^{-1}\text{)}}{\text{Weight of catalyst (g)}} \end{aligned}$$

1.1.3 INFLUENCE OF SUPPORT ON SURFACE AND CATALYTIC PROPERTIES OF Li-MgO IN OCM

Results of the OCM over the unsupported and supported Li-MgO catalysts are presented in Table 1.1.1. XRD results showing the presence of different crystalline metal oxide phases, containing Li and/or magnesium, in the unsupported and supported catalysts and also in the samples of Li₂O supported on the different supports are given in Table 1.1.2.

1.1.3.1 Comparison of Unsupported and Supported Li-MgO Catalysts for their Performance in OCM

A comparison of the catalytic activity and selectivity of the unsupported Li-MgO with that of the supported Li-MgO catalysts (Table 1.1.1) indicates that, because of the deposition of Li-MgO on the catalyst carriers, the catalytic activity/selectivity and product ratios in the OCM are strongly influenced, as follows.

- The methane conversion activity is drastically reduced.
- The C₂ or C₂₊ selectivity is also drastically reduced.
- The C₂H₄/C₂H₆ ratio in products is decreased very markedly, indicating a large reduction in the ethane dehydrogenation activity.
- The CO/CO₂ ratio in products is increased very appreciably, indicating that the formation of CO over CO₂ is favored.

Table 1.1.1 : Results on OCM over Li-MgO supported on different supports [Reaction conditions feed = a mixture of 80 mol% CH₄ and 20 mol% O₂; temperature = 750°C].

Catalyst	Surface area (m ² .g ⁻¹)	GHSV (cm ³ .g ⁻¹ .h ⁻¹)	CH ₄ convn. (%)	Selectivity (%)			Product mole ratios	
				C ₂	C ₂₊	CO _x	C ₂ H ₄ /C ₂ H ₆	CO/CO ₂
Li-MgO (Unsupported)	5.0	11200	30.1	58.5	65.9	34.1	1.8	0.1
Li-MgO/SA-5552	1.6	11200 1120	No reaction 6.7	16.2	17.1	82.9	0.4	1.3
Li-MgO/SC=5532	0.6	11200 1120	1.9 8.9	21.4 23.2	22.8 25.5	77.2 74.5	0.5 0.6	2.5 1.2
Li-MgO/SS-5231	3.1	11200 1120	1.8 8.3	26.4 20.3	28.1 21.4	71.9 78.6	0.2 0.5	2.4 1.6
Li-MgO/SZ-5564	1.0	11200 1120	8.5 24.0	38.4 39.9	40.1 42.6	59.9 57.4	0.4 1.3	1.4 0.3
Li-MgO/∞-Al ₂ O ₃	-	1120	11.2	0.0	0.0	100.0	-	0.8
Li-MgO/SiO ₂	-	1120	2.5	13.0	15.8	84.2	0.4	3.5

Among the supported Li-MgO catalysts, Li-MgO/ α -Al₂O₃ shows the lowest (zero) selectivity for C₂ or C₂₊-hydrocarbons; whereas the lowest methane conversion activity is observed for the Li-MgO/SiO₂ catalyst. The best performance among the supported catalysts is, however, shown by the Li-MgO/SZ-5564 catalyst. Nevertheless, both the catalytic activity and selectivity of the Li-MgO is greatly reduced because of all the catalyst supports, indicating strong interactions between the support and the catalyst.

1.1.3.2 Catalyst-Support Interactions

In order to know the nature of the interactions between the catalyst and the different supports, the unsupported and supported Li-MgO catalysts were examined by XRD (Figs. 1.1.4-1.1.7) for formation of binary or ternary metal oxide phases, resulting from solid-solid reactions between the catalyst components (viz. : Li and Mg components) and the reactive components (e.g. Al₂O₃, SiO₂ etc.) of the supports, during the catalyst calcination at high temperature (750°C). The crystalline phases, identified by the XRD, in the Li-MgO (without any support) and supported Li-MgO catalysts are given in Table 1.1.2. The results confirm the formation of binary and ternary metal oxide phases (which are absent in the unsupported catalyst) in the supported catalysts. The chemical nature and extent of formation of a particular binary or ternary metal oxide phase containing lithium and/or magnesium depends on the presence of different reactive components, particularly SiO₂, Al₂O₃ and ZrO₂, and also on their concentrations in the different supports (Appendix-1). Because of the smaller concentration of lithium, particularly in the supported catalysts (Li/Mg = 0.1, before calcination), the binary or ternary metal oxide phases containing lithium are expected to be formed with a very low concentration, which may not be detected by XRD. In order to know the formation of Li-containing binary metal oxide which are not identified in the supported catalysts, Li₂O at higher concentration (5 wt.% Li₂O) is deposited on the supports and these supported Li₂O samples (prepared and calcined under identical conditions) were examined by XRD. The supported MgO samples were also examined by XRD. This study leads to the identification of a number of additional binary metal oxide phases containing lithium (Table 1.1.2). Although, the additional Li-containing phases observed in the supported Li₂O are not detected in the corresponding supported Li-MgO, there is a high possibility of the presence of these phases at a very low concentration in the supported catalysts.

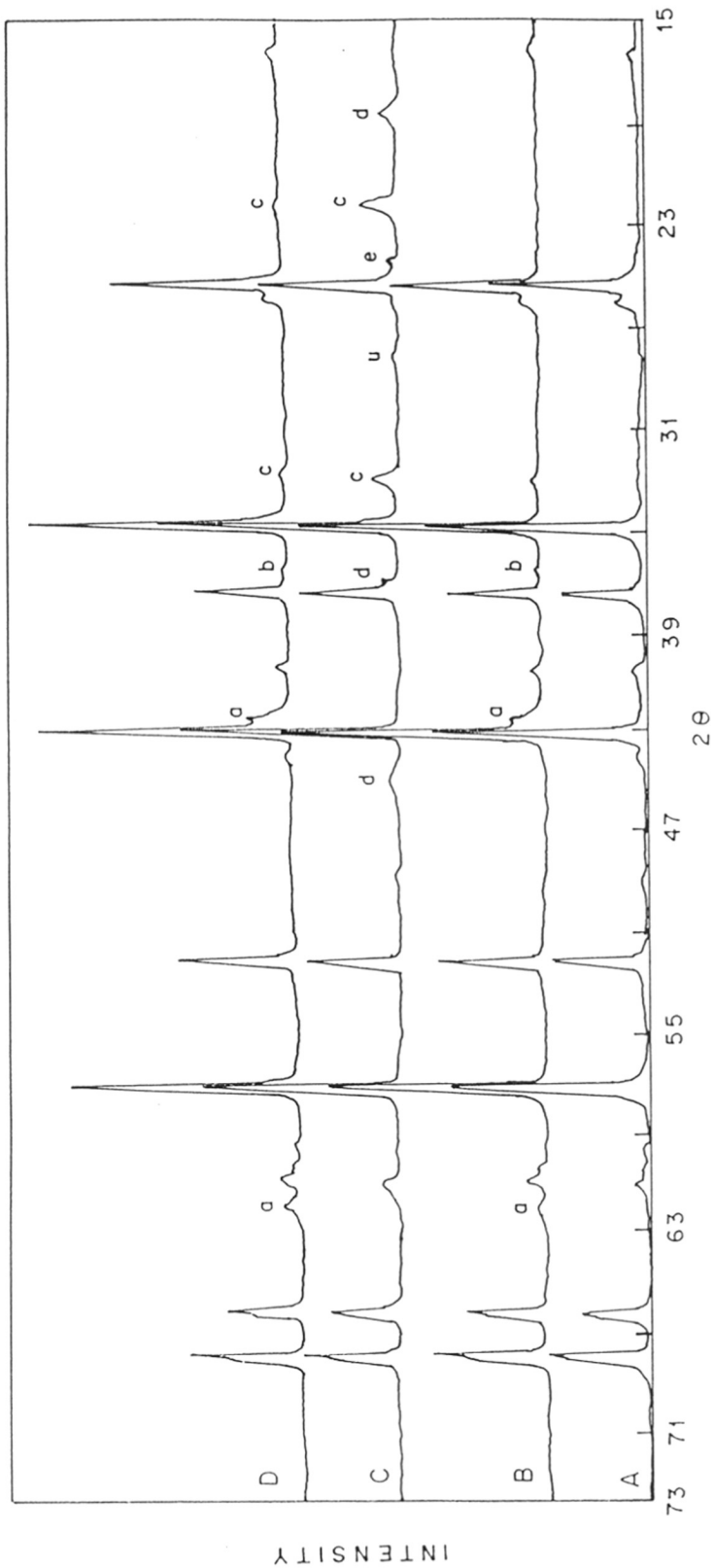


Fig. 1.1.4 : XRD spectra of SA-5552(A), MgO/SA-5552(B), Li₂O/SA-5552(C) and Li MgO/SA-5552(D) [a = MgO, b = Mg-Al-O, c = Li₄SiO₄, d = LiAlO₂, e = Li₂Si₂O₅, u = unidentified]

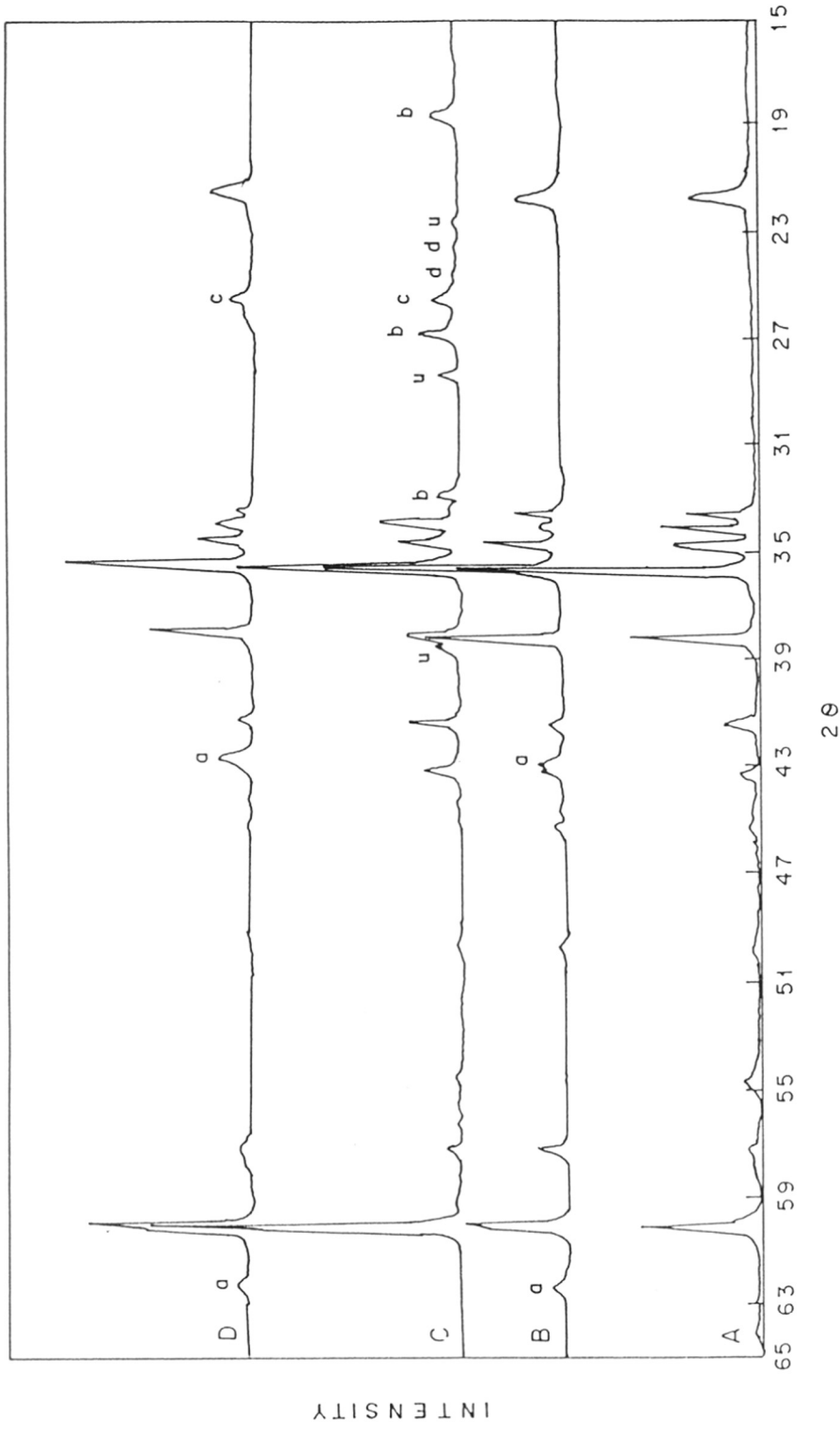


Fig. 1.1.5 : XRD spectra of SC-5532(A), MgO/SC-5532(B), Li₂O/SC-5532(C) and Li-MgO/SC-5532(D) [a = MgO, b = Li₂SiO₃, c = Li₆Si₂O₇, d = Li₂Si₂O₅, u = unidentified]

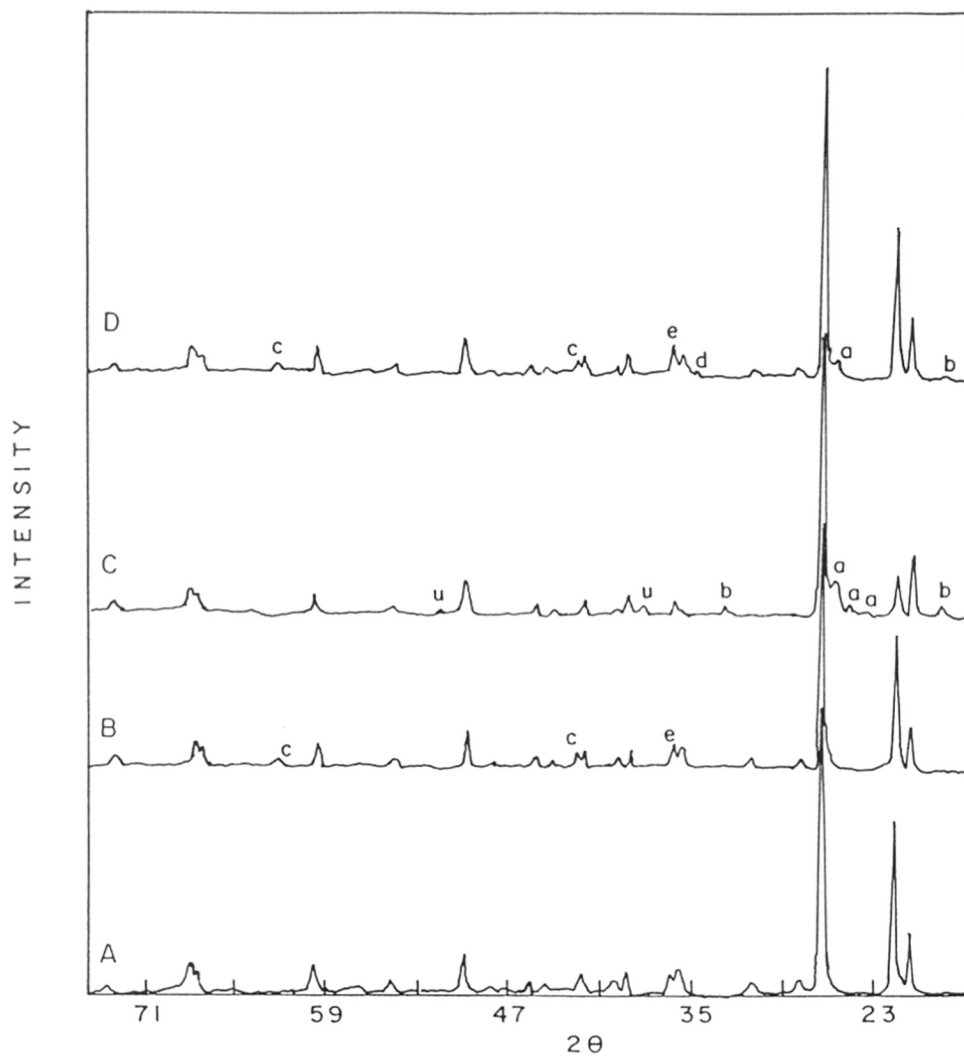


Fig. 1.1.6: XRD spectra of SS-5231(A), MgO/SS-5231(B), Li₂O/SS-5231(C) and Li-MgO/SS-5231(D) [a = Li₆Si₂O₇, b = Li₂SiO₃, c = MgO, d = Li₂MgSiO₄, e = Mg₂SiO₄]

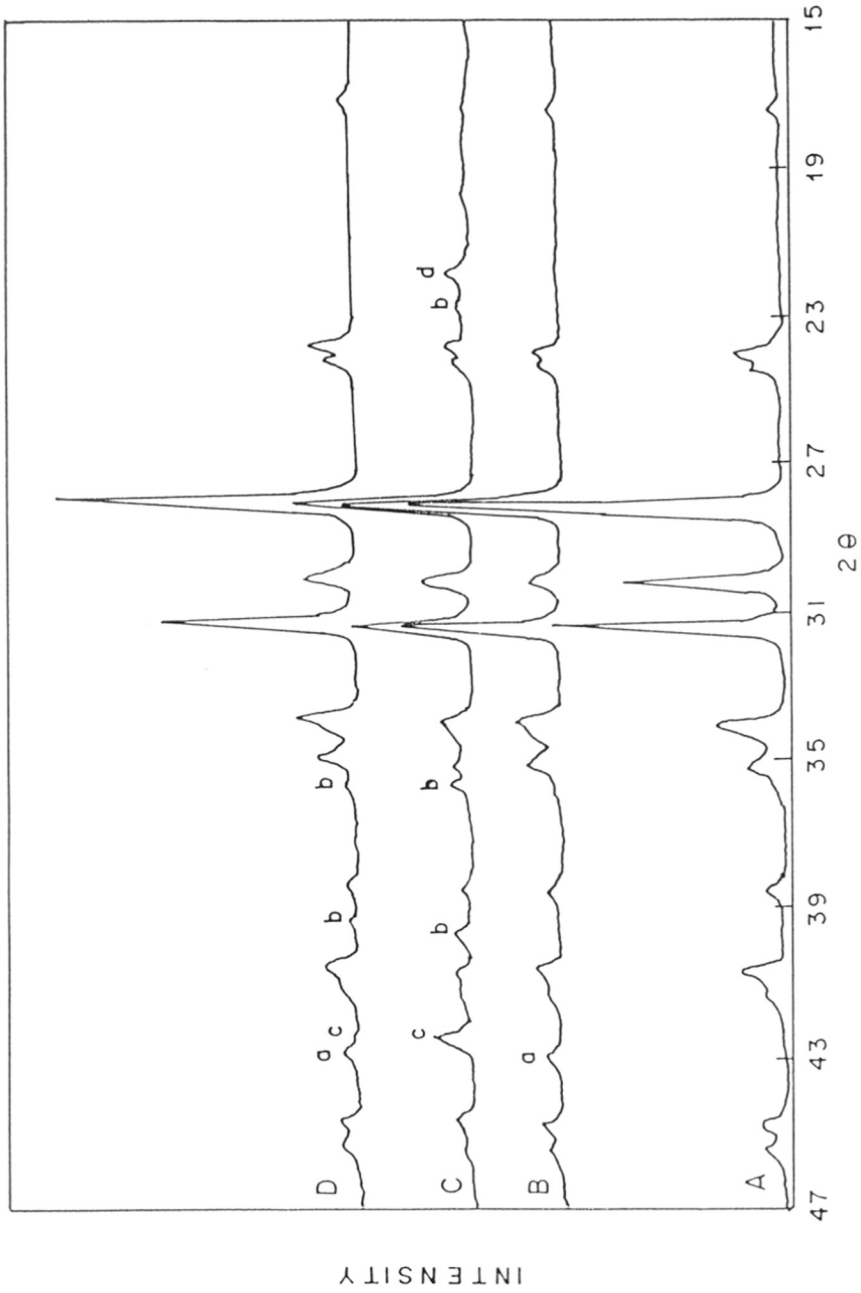


Fig. 1.1.7 : XRD spectra of SZ-5564(A), MgO/SZ-5564(B), Li₂O/SZ-5564(C) and Li-MgO/SZ-5564(D) [a = MgO, b = Li₂ZrO₃, c = Li₂ZrO₃, d = Li₂CO₃]

The formation of the various phases (both identified and unidentified ones) in the supported Li-MgO catalysts occurs due to different solid state reactions during the high temperature (750°C) catalyst calcination, as follows :

- Li_2CO_3 is formed due to reaction between Li_2O and CO_2 formed during the oxidative decomposition of Li- and Mg-acetates.
- $\alpha\text{-LiAlO}_2$ is formed by reaction of Li_2O with Al_2O_3
- Mg_2SiO_4 is formed by reaction of MgO with SiO_2
- Mg-Al-O is formed by reaction of MgO with Al_2O_3
- $\text{Li}_2\text{MgSiO}_4$ is formed by reaction of Li_2O and MgO with SiO_2
- Li_2SiO_3 , $\text{Li}_2\text{Si}_2\text{O}_5$, Li_4SiO_4 and $\text{Li}_6\text{Si}_2\text{O}_7$ are formed by reactions of Li_2O with SiO_2 .
- Li_2ZrO_3 and Li_4ZrO_4 are formed by reactions of Li_2O with ZrO_2 .

Table 1.1.2 : Crystalline phases identified in the supported and unsupported Li-MgO catalysts and the Li_2O supported on different catalyst carriers^a

Catalyst	Crystalline phases
Li-MgO (Unsupported)	MgO and Li_2CO_3
Li-MgO/SA-5552	MgO, Mg-Al-O and Li_4SiO_4
Li-MgO/SC-5532	MgO and $\text{Li}_6\text{Si}_2\text{O}_7$
Li-MgO/SS-5231	MgO, Mg_2SiO_4 , $\text{Li}_2\text{MgSiO}_4$, $\text{Li}_6\text{Si}_2\text{O}_7$ and Li_2SiO_3
Li-MgO/SZ-5564	MgO, Li_4ZrO_4 and Li_2ZrO_3
Li_2O /SA-5552	$\alpha\text{-LiAlO}_2$, Li_4SiO_4 , $\text{Li}_2\text{Si}_2\text{O}_5$ and unidentified
Li_2O /SC-5532	Li_2SiO_3 , $\text{Li}_6\text{Si}_2\text{O}_7$, $\text{Li}_2\text{Si}_2\text{O}_5$ and unidentified
Li_2O /SS-5231	$\text{Li}_6\text{Si}_2\text{O}_7$, Li_2SiO_3 , $\text{Li}_2\text{Si}_2\text{O}_5$ and unidentified
Li_2O /SZ-5564	Li_4ZrO_4 , Li_2ZrO_3 and Li_2CO_3

^aChemical composition of the supports is given in Appendix-1

In order to know the influence of the various commercial supports (viz. SA-5552, SS-5231, SC-5532 and SZ-5564) on the surface basicity, both the total and strong basic sites on the Li-MgO (unsupported) and supported Li-MgO catalysts have been measured in terms of the chemisorption of CO₂ at 100° and 500°C, respectively. The results showing a very strong influence of support on both the total and strong basic sites of the catalyst are presented in Table 1.1.3. The basicity is drastically reduced because of supporting the Li-MgO on the different catalyst carries. Since strong basicity is essential for high activity/selectivity in OCM process [21, 40, 41], the observed drastic reduction in the catalytic activity/selectivity is very much consistent with the drastic decrease in the strong basicity because of the strong chemical interactions between the catalyst and the different supports.

Table 1.1.3 : Results of chemisorption of CO₂ on Li-MgO catalyst with or without support. (loading of Li-MgO = 9 ± 0.5 wt.%)

Catalyst	CO ₂ Chemisorption (μmol.g ⁻¹)	
	100°C	500°C
Li-MgO (Unsupported)	73.0	69.50
Li-MgO/SA-5552	1.5	0.07
Li-MgO/SC-5532	2.1	0.02
Li-MgO/SS-5231	2.0	0.01
Li-MgO/SZ-5564	9.7	0.10

TH-1077

From this investigation, following important conclusions about strong influence of support on the basicity and catalytic activity/selectivity in OCM of Li-MgO catalyst have been drawn.

1. Both the activity and selectivity of Li-MgO catalysts are drastically reduced when the catalyst is supported on commonly used different catalyst carriers comprising of Al₂O₃, SiO₂, SiC or ZrO₂ as a major component.
2. The large reduction in the catalytic activity and selectivity is attributed to a drastic reduction in the surface basicity (both total and strong basic sites) caused by strong chemical interactions between the reactive components (viz. Al₂O₃, SiO₂ or ZrO₂) of the support and the active

RR
547.211:541.128 (043)
4PH

components (viz. Li and MgO) of the catalyst. The chemical interactions result in the formation of catalytically inactive binary or ternary metal oxide phases containing lithium and/or magnesium, thus consuming both the catalyst promoter (i.e. lithium) and the catalytically important other catalyst component (viz. MgO).

3. The catalyst carriers containing reactive components, particularly Al_2O_3 and SiO_2 , are not suitable for supporting Li-MgO catalyst. Also, the catalytically inactive solids containing these reactive components can not be used as an inert solid for diluting Li-MgO catalyst bed for the same reason.

1.1.4 INFLUENCE OF SUPPORT ON SURFACE AND CATALYTIC PROPERTIES OF La-CaO IN OCM

Results of the OCM over the unsupported and supported La-promoted CaO, with or without precoating the supports by MgO, CaO or La_2O_3 , are presented in Table 1.1.4. XRD results showing the presence of different crystalline metal oxide phases, containing La and/or Ca, in the supported CaO, La_2O_3 and La-CaO catalysts are given in Table 1.1.6.

1.1.4.1 Comparison of Unsupported and Supported La-CaO Catalysts for their performance in OCM

A comparison of the catalytic activity and selectivity of the unsupported La-CaO with that of the supported La-CaO catalysts (Table 1.1.4) reveals that, because of the direct deposition of La-CaO on the catalyst carriers, the catalytic activity/selectivity and product ratios (viz. $\text{C}_2\text{H}_4/\text{C}_2\text{H}_6$ and CO/CO_2) in the OCM are influenced appreciably, as follows.

- The methane conversion activity is reduced.
- The C_{2+} selectivity is also reduced.
- The $\text{C}_2\text{H}_4/\text{C}_2\text{H}_6$ ratio in products is decreased to a smaller extent indicating a reduction in the ethane dehydrogenation activity, and
- The CO/CO_2 ratio in the products is increased to an appreciable extent indicating more formation of CO over CO_2 .

However, the methane conversion activity and selectivity (or yield) for C_{2+} -hydrocarbons are increased due to the precoating of the catalyst carriers with MgO, CaO or La_2O_3 before depositing the La-CaO catalyst on them (Table 1.1.4) and the activity/selectivity of these catalysts is comparable to that of the unsupported catalyst. Among the supported catalysts, the best

performance is shown by the La-CaO/La₂O₃/SA-5552 and it is slightly superior than that of the unsupported La-promoted CaO catalyst, although, the loading of active catalyst mass in the supported La-CaO catalyst is much lower (15 wt%) than that (100 wt%) for the unsupported catalyst. The decrease in the catalytic activity/selectivity of La-CaO because of its direct deposition on the catalyst carriers is attributed mostly to the strong chemical interactions between the active components of the catalyst (viz. La and/or Ca) and the reactive components (viz. Al₂O₃, SiO₂, ZrO₂, etc.) of the supports, during catalyst calcination at high temperature (900°C).

Table 1.1.4 : Influence of support on the catalytic activity/selectivity in OCM of La-CaO precoated with or without by MgO, CaO or La₂O₃. [Reaction conditions: Feed, a mixture of pure methane and O₂ at a CH₄/O₂ feed ratio of 4.0; temperature, 800°C]

Catalyst	Surface area (m ² .g ⁻¹)	GHSV (cm ³ .g ⁻¹ .h ⁻¹)	CH ₄ convn. (%)	C ₂₊ sel. (%)	C ₂₊ yield (%)	Product mole ratios	
						C ₂ H ₄ /C ₂ H ₆	CO/CO ₂
La-CaO (Unsupported)	5.1	1,00,000	27.6	57.0	15.7	1.0	0.2
<u>Without precoating</u>							
La-CaO/SA-5552	1.3	51,000 25,700	17.0 18.9	48.1 43.2	8.2 8.2	0.7 2.0	0.6 0.5
La-CaO/SC-5532	0.8	51,000 25,700	12.7 16.4	47.6 40.1	6.0 6.6	0.6 0.7	0.5 0.5
La-CaO/SS-5231	1.3	1,00,000 10,000	3.2 19.8	46.1 48.2	1.5 9.5	0.2 0.9	1.4 0.9
La-CaO/SZ-5564	1.2	1,00,000 10,000	4.4 21.6	55.6 56.0	2.4 12.1	0.2 0.6	0.9 0.3
<u>With precoating</u>							
La-CaO/MgO/SA-5552	1.3	1,00,000	25.0	57.7	14.4	1.1	0.4
La-CaO/MgO/SC-5532	0.9	1,00,000	17.2	44.4	7.6	0.6	0.4
La-CaO/CaO/SA-5552	1.3	1,00,000	25.5	50.0	12.8	1.3	0.3
La-CaO/CaO/SC-5532	1.0	1,00,000	18.8	36.7	6.9	0.5	0.3
La-CaO/La ₂ O ₃ /SA-5552	0.5	1,00,000	31.2	57.0	17.8	1.0	0.5
La-CaO/La ₂ O ₃ /SC-5532	0.4	1,00,000	28.3	53.1	15.0	1.1	0.3

1.1.4.2 Catalyst Support Interactions

In order to know the possibility of strong chemical interactions between the active catalyst mass and the different supports, the supported and unsupported CaO, La₂O₃ and La-CaO catalysts were examined by XRD (Figs. 1.1.8-1.1.11) for the formation of binary or ternary metal oxide phases produced by solid-solid reactions between the active catalyst mass and the reactive components (e.g. Al₂O₃, SiO₂, etc.) of the supports, during the high temperature (900°C) catalyst calcination. The crystalline metal oxide phases containing the elements (viz. Ca and La) of active catalyst mass, detected in the unsupported and supported CaO, La₂O₃ and La-CaO catalysts are given in Table 1.1.5. These results reveal formation of following binary metal oxide phases.

- CaAl₂O₄ (in the CaO and La-CaO supported on SA-5552) due to reaction between CaO and Al₂O₃.
- CaSiO₃ (in the CaO supported on SC-5532 and SS-5231 and La-CaO supported on SC-5532 and SS-5231) due to reaction between CaO and SiO₂
- Ca₂SiO₄ (in the CaO supported on SA-5552, SC-5532 and SZ-5564 and La-CaO supported on SA-5552) due to reaction between CaO and SiO₂
- Ca₃SiO₅ (in the La-CaO supported on SC-5532 and SS-5231) due to reaction between CaO and SiO₂
- α-La₂Si₂O₇ (in the La₂O₃ supported on SC-5532 and SS-5231 and La-CaO supported on SA-5552 and SS-5231) due to reaction between La₂O₃ and SiO₂
- La₂Zr₂O₇ (in the La₂O₃ supported on SZ-5564) due to reaction between La₂O₃ and ZrO₂

The formation of above binary metal oxide phases clearly shows strong chemical interactions between CaO and the supports containing SiO₂ and Al₂O₃ at high concentration and also between La₂O₃ and supports containing SiO₂ at high concentration.

In order to know the effect of the catalyst-support interactions on the surface basicity and base strength distribution, the chemisorption of CO₂ at 100°C and TPD of CO₂ from 50° to 900°C for the unsupported La-CaO and supported La-CaO (with or without precoating the support by MgO or La₂O₃) catalysts have been measured (Figs. 1.1.12 and 1.1.13). The data on the surface basicity of the catalysts is included in Table 1.1.6.

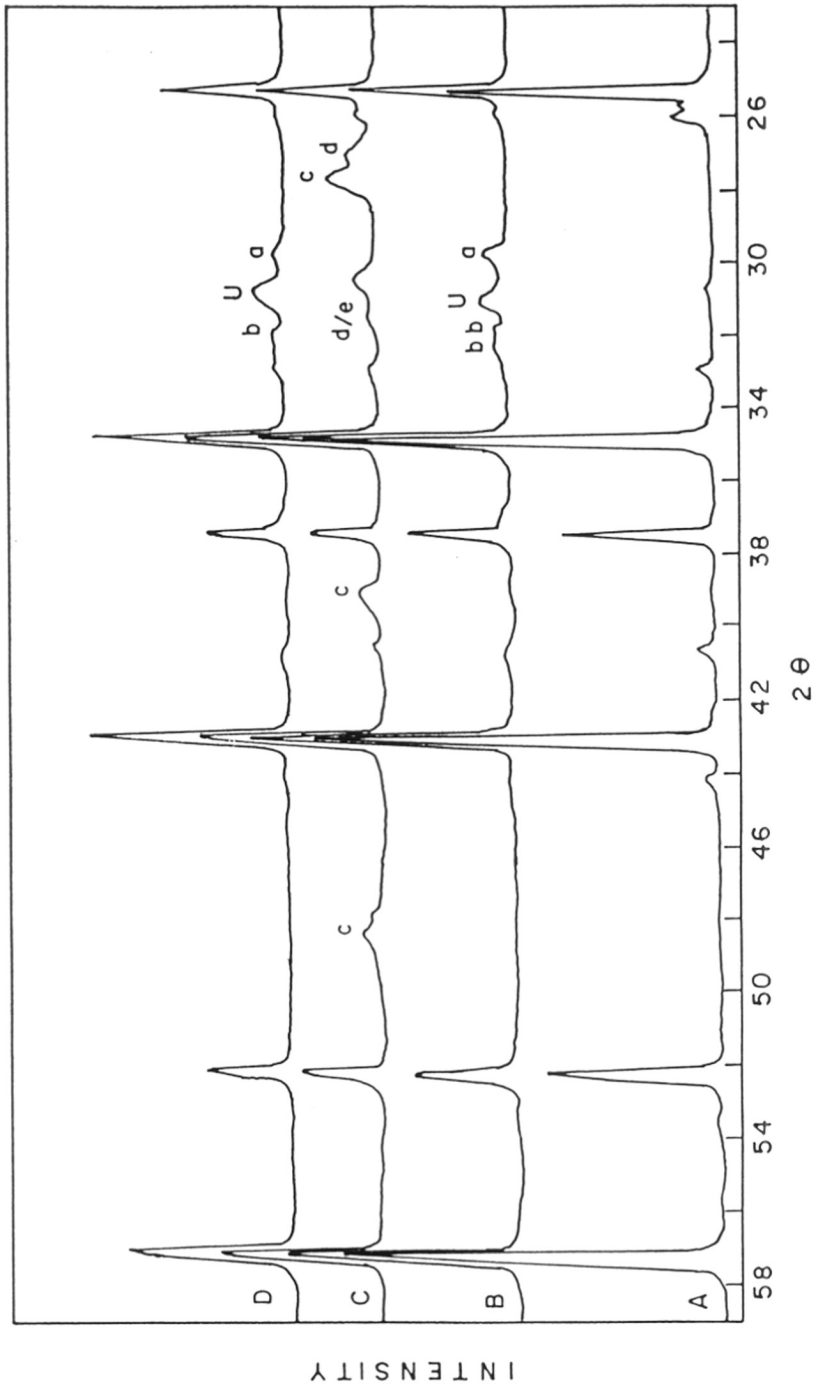


Fig. 1.1.8: XRD spectra of SA-5552(A), CaO/SA-5552(B), La₂O₃/SA-5552(C) and La-CaO/SA-5552(D) [a = CaAl₂O₄, b = Ca₂SiO₃, c = La(OH)₃, d = La₂O₃, e = α-La₂Si₂O₇ and U = unidentified]

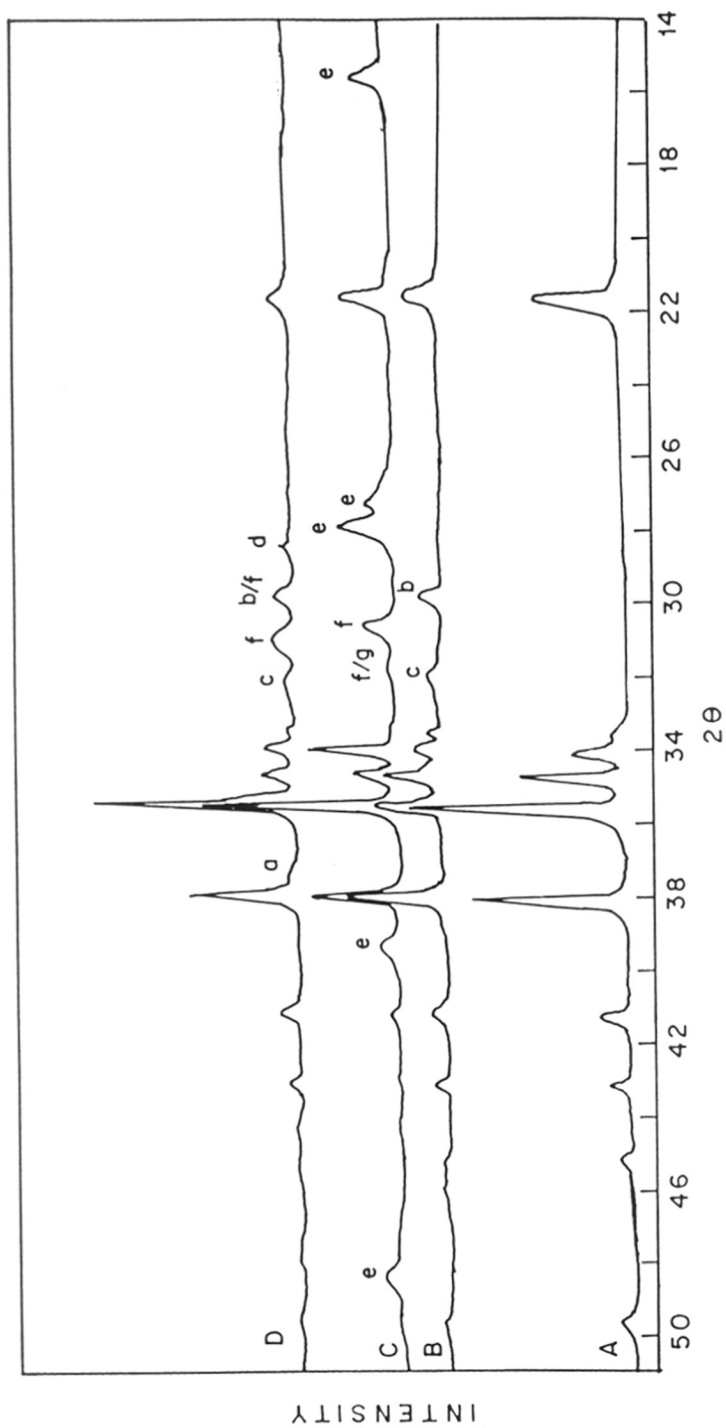


Fig. I.1.1.9: XRD spectra of SC-5532(A), CaO/SC-5532(B), $\text{La}_2\text{O}_3/\text{SC-5532(C)}$ and La-CaO/SC-5532(D) [a = CaO, b = CaSiO_3 , c = Ca_2SiO_3 , d = Ca_3SiO_5 , e = La(OH)_3 , f = La_2O_3 and g = $\alpha\text{-La}_2\text{Si}_2\text{O}_7$]

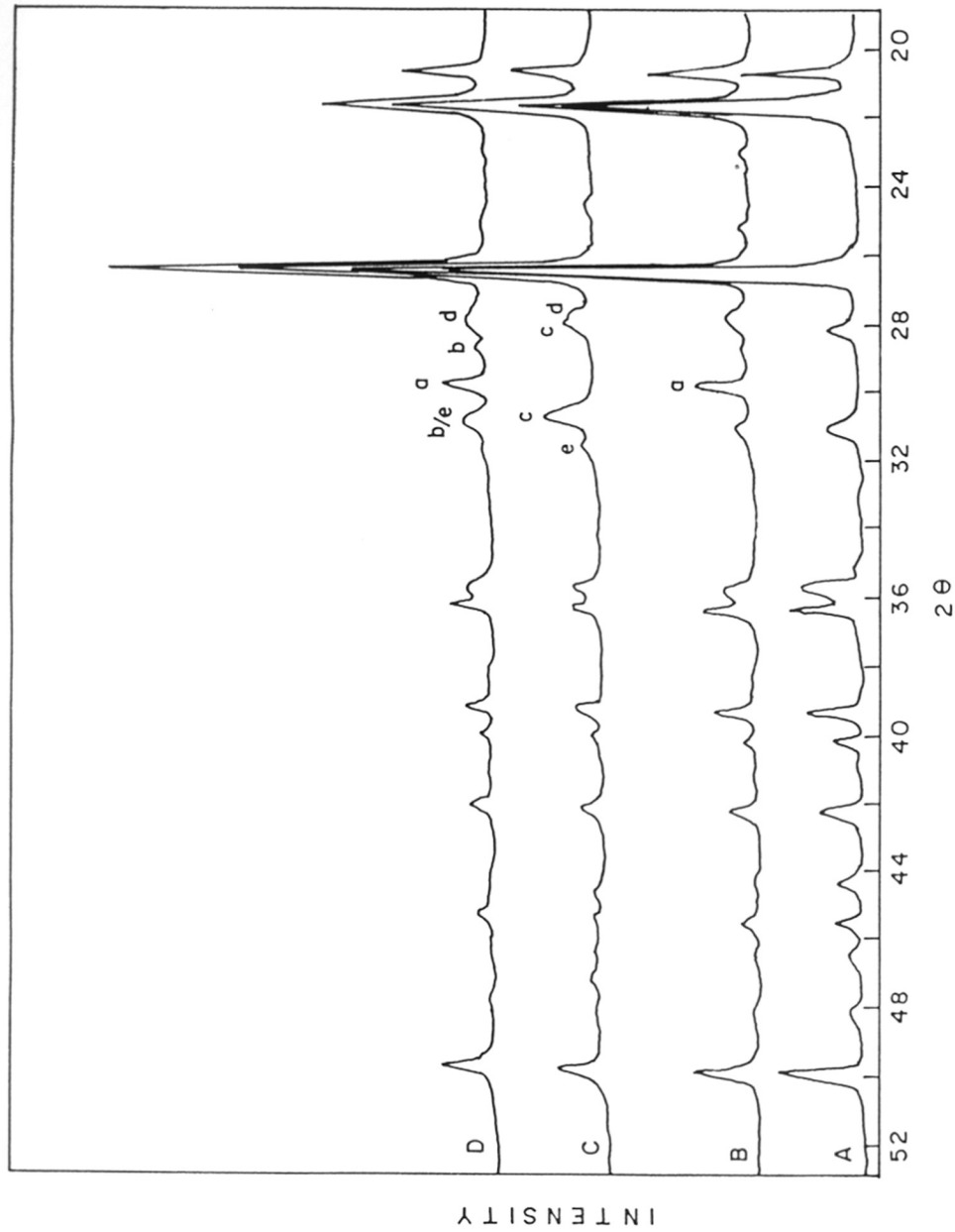


Fig. 1.1.10 : XRD spectra of SS-5231(A), CaO/SS-5231(B), La_2O_3 /SS-5231(C) and La-CaO/SS-5231(D) [a = CaSiO_3 , b = Ca_3SiO_5 , c = La_2O_3 , d = $\text{La}(\text{OH})_3$, and e = $\alpha\text{-La}_2\text{Si}_2\text{O}_7$]

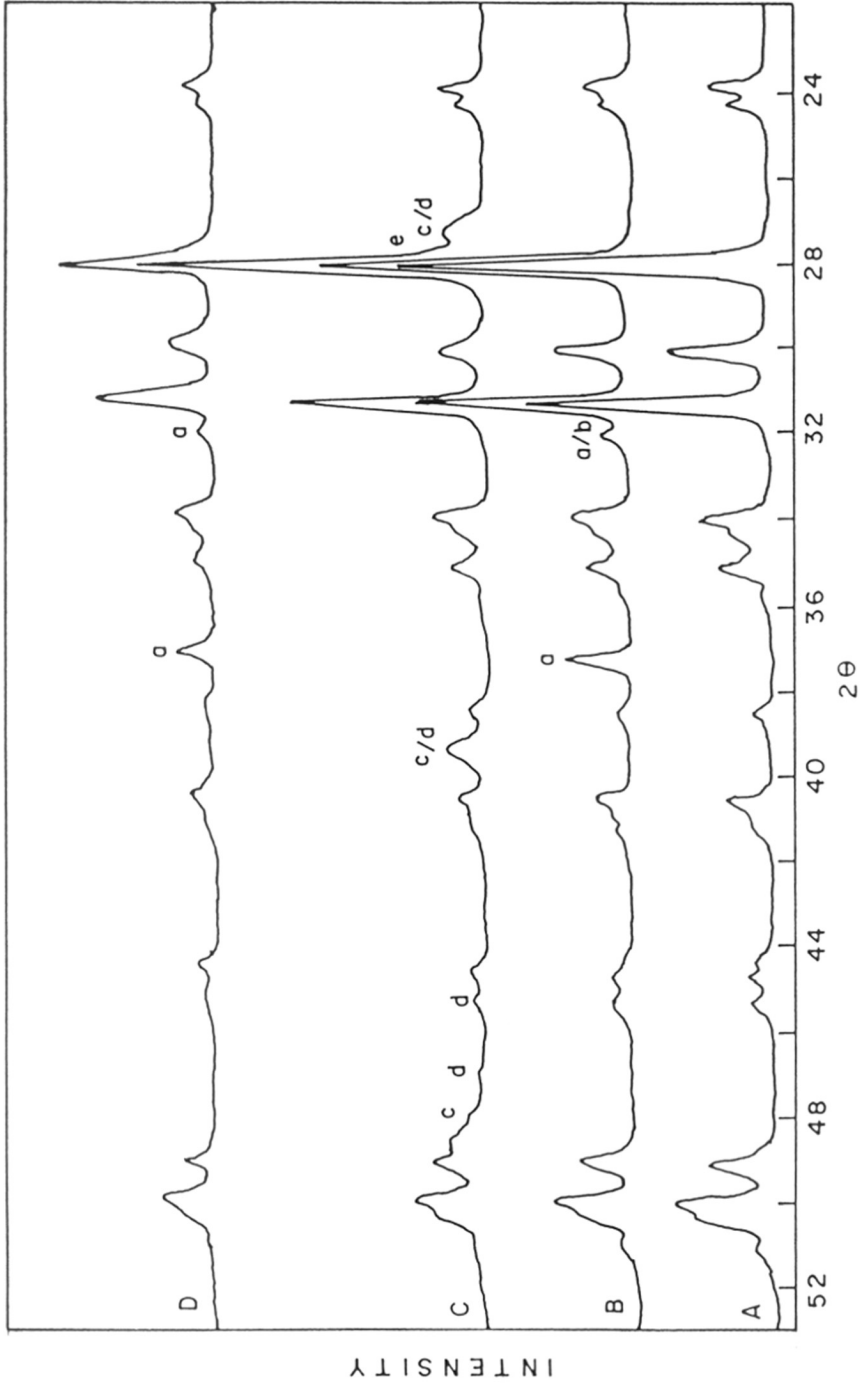


Fig. 1.1.11: XRD spectra of SZ-5564(A), CaO/SZ-5564(B), La₂O₃/SZ-5564(C) and La-CaO/SZ-5564(D) [a = CaO, b = Ca₂SiO₄, c = La(OH)₃, d = La₂O₃, AND e = La₂Zr₂O₇]

Table 1.1.5 : Crystalline phases containing Ca and/or La in supported CaO, La₂O₃ and La-CaO catalysts supported on different catalyst carriers^a

Catalyst	Crystalline phases		
	Major	Minor	Trace
CaO (Unsupported)	CaO	-	-
CaO/SA-5552	CaAl ₂ O ₄	Ca ₂ SiO ₄	-
CaO/SC-5532	CaSiO ₃ Ca ₂ SiO ₄	-	-
CaO/SS-5231	CaSiO ₃	-	-
CaO/SZ-5564	CaO	Ca ₂ SiO ₄	-
La ₂ O ₃ (Unsupported)	La(OH) ₃	La ₂ O ₃	-
La ₂ O ₃ /SA-5552	La(OH) ₃	La ₂ O ₃	-
La ₂ O ₃ /SC-5532	La(OH) ₃	La ₂ O ₃ α -La ₂ Si ₂ O ₇	-
La ₂ O ₃ /SS-5231	La ₂ O ₃	-	La(OH) ₃ α -La ₂ Si ₂ O ₇
La ₂ O ₃ /SZ-5564	La(OH) ₃	La ₂ O ₃	La ₂ Zr ₂ O ₇
La-CaO (Unsupported)	CaO	La ₂ O ₃ La(OH) ₃	-
La-CaO/SA-5552	CaAl ₂ O ₄	Ca ₂ SiO ₄	α -La ₂ Si ₂ O ₇
La-CaO/SC-5532	CaSiO ₃ La ₂ O ₃	CaO Ca ₃ SiO ₅	-
La-CaO/SS-5231	CaSiO ₃	Ca ₃ SiO ₅ La ₂ O ₃	α -La ₂ Si ₂ O ₇
La-CaO/SZ-5564	CaO	-	-

^aChemical composition of the supports is given in Appendix-1.

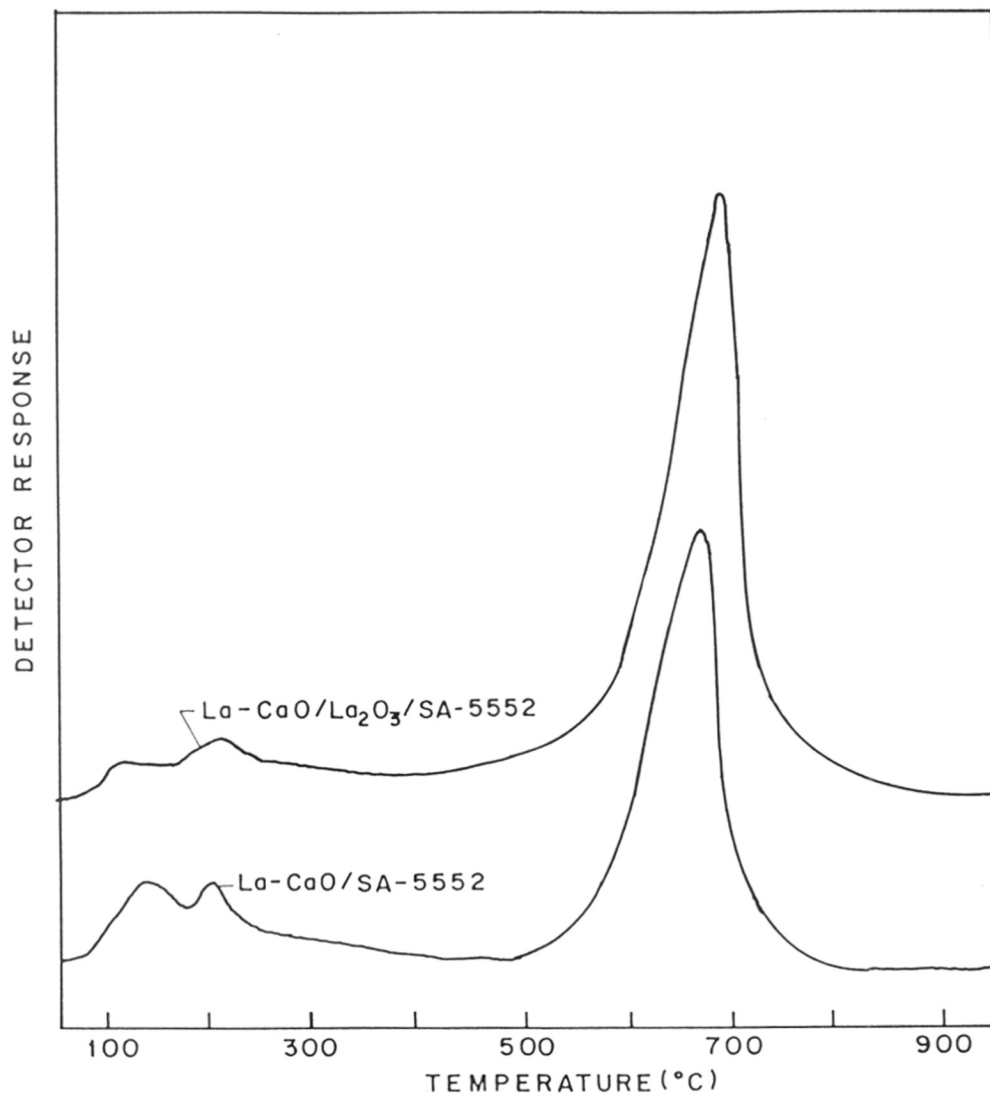


Fig. 1.1.12 : TPD of CO₂ on a) La-CaO/SA-5552 and b) La-CaO/La₂O₃/SA-5552 catalysts (La/Ca = 0.1, loading of La-CaO = 15 ± 1.5 wt %)

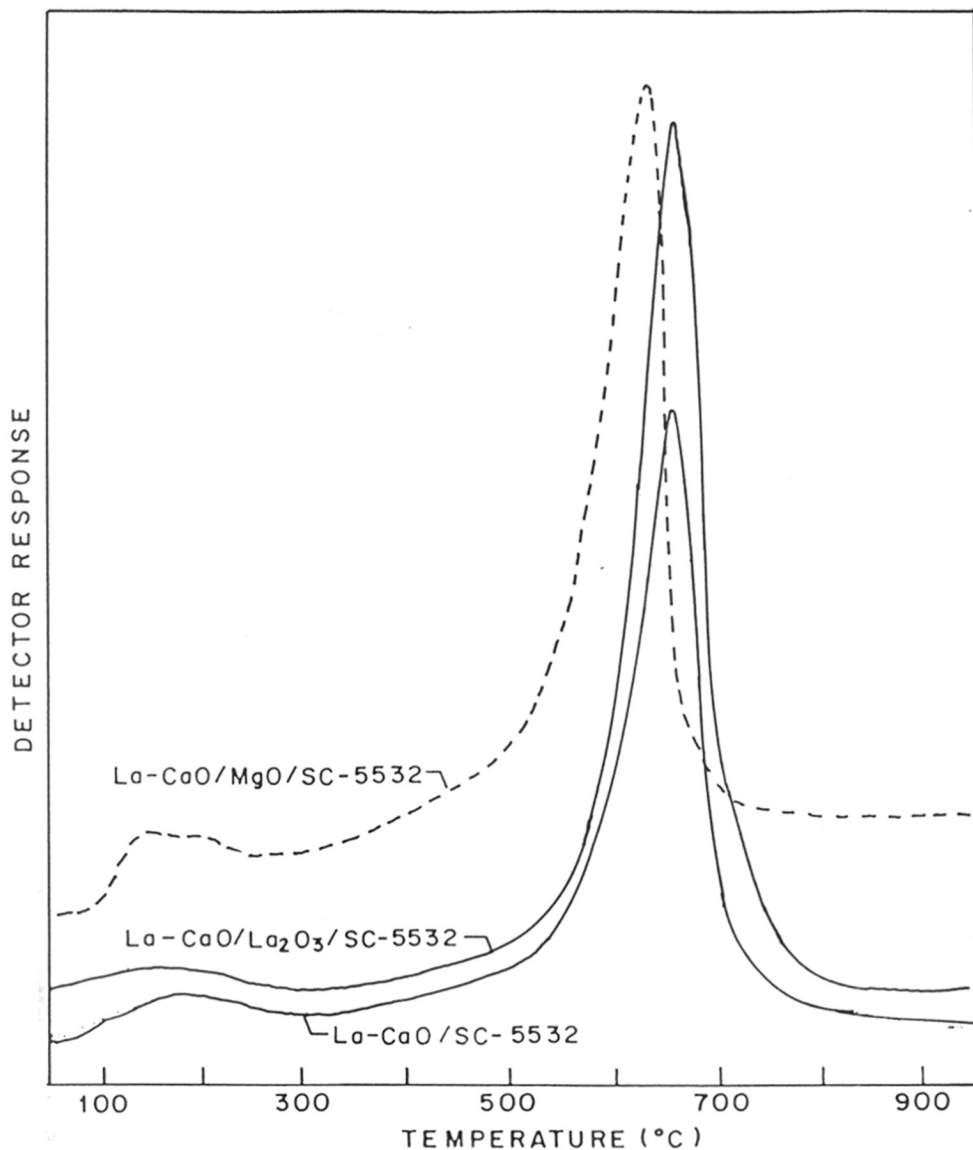


Fig. 1.1.13 : TPD of CO₂ on a) La-CaO/SC-5532, b) La-CaO/MgO/SA-5532 and c) La-CaO/La₂O₃/SC-5532 catalysts (La/Ca = 0.1, loading of La-CaO = 15 ± 1.5 wt %)

Table 1.1.6 : Distribution of weak and strong basic sites on unsupported and supported La-promoted CaO catalysts

Catalyst	Basic sites ($\mu\text{mol.g}^{-1}$)			CO ₂ TPD peak max. temp. (°C) ^d
	Total ^a	Weak ^b	Strong ^c	
La-CaO (Unsupported)	216.9	157.1	59.8	675
La-CaO/SA-5552	45.1	11.9	33.2	674
La-CaO/La ₂ O ₃ /SA-5552	147.3	4.5	142.8	698
La-CaO/SC-5532	72.2	10.0	62.2	663
La-CaO/MgO/SC-5532	100.8	15.0	85.8	642
La-CaO/La ₂ O ₃ /SC-5532	127.6	19.0	108.6	667

^aCO₂ desorbed from 50° to 900°C

^bCO₂ desorbed from 50° to 450°C

^cCO₂ desorbed from 450° to 900°C

^dcorresponding to the strong basic sites

The surface basicity (measured in terms of CO₂ chemisorbed at 100°C) is decreased due to the direct deposition of La-CaO on the both the SA-5552 and SC-5532 supports (Table 1.1.6). Since strong basicity is essential for the high activity/selectivity in OCM process [21, 40, 41], the observed reduction in the catalytic activity and selectivity is very much consistent with the decrease in the strong basicity because of the strong chemical interactions between the catalyst and the different supports. However, there is a large increase in the strong basicity of the La-CaO catalyst when it is supported on the La₂O₃ or MgO precoated catalyst carriers [i.e. on MgO (or La₂O₃)/SA-5552 and MgO (or La₂O₃)/SC-5532] (Table 1.1.6). The increase in the methane conversion activity and selectivity (or yield) for C₂₊-hydrocarbons (Table 1.1.4) due to the precoating of the catalyst carriers is very much consistent with the observed strong basicity (Table 1.1.6). The improvement in both the catalytic activity/selectivity and strong basicity is attributed to the formation of protective layer between the active catalyst mass and the reactive components of

the supports, eliminating or drastically reducing the chemical interactions between the two and for La_2O_3 precoated supports it may also be due to a formation of Ca-doped La_2O_3 .

Among the supported La-CaO catalysts with or without precoating of the supports, La-CaO/ La_2O_3 /SA-5552 showed the best performance in the OCM process (Table 1.1.4). It may be noted that this catalyst has not only the highest number of strong basic sites (Table 1.1.6) but also the strength of its strong basic sites is higher; the TPD peak maximum temperature corresponding to strong basic sites (698°C) for this catalyst is higher than that observed for the other catalysts.

From the above results and discussions following conclusions have been drawn.

1. Both the methane-to- C_{2+} -hydrocarbon activity (or C_2 -yield), C_2 -selectivity and ethane dehydrogenation activity of the La-promoted CaO catalysts are decreased appreciably by supporting these catalysts on different commonly used catalyst carriers containing Al_2O_3 , SiO_2 , SiC and ($\text{ZrO}_2 + \text{HfO}_2$). However, the methane conversion activity/selectivity (or yield for C_{2+} -hydrocarbons) of the catalyst are increased due to the precoating of the catalyst carrier with MgO, CaO or La_2O_3 , before depositing La-CaO on them.
2. The appreciable reduction in the catalytic activity of the supported La-CaO (without precoating) is attributed to a drastic reduction in the surface basicity (both total and strong) caused by strong chemical interactions between the reactive components (viz. Al_2O_3 , SiO_2 or ZrO_2) of the support and the active components, mainly CaO, of the catalyst. The chemical interactions result in the formation of catalytically inactive binary metal oxide phases (viz. CaAl_2O_4 , CaSiO_3 , Ca_2SiO_4 , Ca_3SiO_5 and $\alpha\text{-La}_2\text{Si}_2\text{O}_7$), thus consuming the active catalyst components and hence catalyst deactivation.
3. The improved catalytic activity/selectivity of the MgO, CaO and La_2O_3 precoated supported La-CaO catalysts is attributed to the formation of a protective layer of the precoated metal oxide between the reactive components of the support and the deposited La-CaO. The improved catalytic performance is consistent with the increase in the strong basicity of the catalyst.

REFERENCES

1. G.E. Keller and M.M. Bhasin, *J. Catal.*, 73 (1982) 9
2. P. Pitachi and K. Klier, *Catal. Rev. Sci. Eng.*, 28 (1986) 13
3. M.S. Scurrrell, *Appl. Catal.*, 32 (1987) 1
4. J.S. Lee and S.T. Oyama, *Catal. Rev. Sci. Eng.*, 30 (1988) 249
5. G.J. Hutchings, J.R. Woodhouse and M.S. Scurrrell, *Chem. Soc. Rev.*, 18 (1989) 251
6. J.H. Lunsford, *Catal. Today*, 6 (1990) 235
7. Y. Amenomiya, V.I. Briss, M. Goledzinowski, J.Galuszka and A.R. Sanger, *Catal. Rev. Sci. Eng.*, 32 (1990) 163
8. J.-L. Dubois and C.J. Cameron, *Appl. Catal.*, 67 (1990) 49
9. A.M. Maitra, *Appl. Catal. A: General*, 104 (1993) 11
10. O.V. Krylov, *Catal. Today*, 18 (1993) 209
11. III J.M. Fox, *Catal. Rev. Sci. Eng.*, 35 (1993) 169
12. J.H. Lunsford, *Stud. Surf. Sci. Catal.*, 75 (1993) 103
13. J.H. Lunsford, *Angew. Chem. Int. Ed. Engl.*, 34 (1995) 970
14. L. Mleczko and M. Baerns, *Fuel Processing Technology*, 42 (1995) 217
15. T. Ito and J.H. Lunsford, *Nature*, 314 (1985) 721.
16. T. Ito, J.X., Wang, C.H. Lin and J.H. Lunsford, *J. Am. Chem. Soc.*, 107 (1985) 5062
17. S.J. Korf, J.A. Roos, N.A. deBruijn, J.G. Van Ommen and J.R.H. Ross, *J. Chem. Soc. Chem. Commun.*, (1987) 1433.
18. G.A. Martin, P. Turlier, V. Ducarme, C. Mirodatos and M. Pinabiau, *Catal. Today*, 6 (1990) 373.
19. V.R. Choudhary, A.M. Rajput, D.B. Akolekar and V.A. Seleznev, *Appl. Catal.*, 62 (1990) 171.
20. S.J. Korf, J.A. Roos, N.A. deBruijn, J.G. Van Ommen and J.R.H. Ross, *Appl. Catal.*, 58 (1990) 131.
21. V.R. Choudhary, V.H. Rane and S.T. Chaudhari, *Catal. Lett.*, 6 (1990) 95.
22. V.R. Choudhary, S.T. Chaudhari and M.Y. Pandit, *J.Chem.Soc., Chem. Commun.*, (1991) 1158.
23. M.J. Holgado, V. Rives and S. San Roman, *React. Kinet. Catal. Lett.*, 48 (1992) 455
24. I.M. Slagtern, , Dahl, K.-J. Jens, E. Hansen and M. Seiersten, *Appl. Catal. A:General*, 91 (1992) 13.
25. M. Xu, C. Shi, X. Yang, M. P. Rosynek and J.H. Lunsford, *J. Phys.Chem.*, 96 (1992) 6395.

26. C. Shi, M. Xu, M. P. Rosynek and J.H. Lunsford, *J. Phys. Chem.*, 97 (1993) 216.
27. M.-C. Wu, C.M. Truong, K. Coulter and D.W. Goodman, *J.Catal.*, 140 (1993) 344
28. Y.E. Chang, G.A. Somorjai and H. Heinemann, *J.Catal.*, 141 (1993) 713.
29. J.H. Lunsford, P.G. Hinson, M. P. Rosynek, C. L. Shi, M. T. Xu and X. M. Yang, *J. Catal.*, 147 (1994) 301.
- 30 V.R. Choudhary, S.T. Chaudhari, A.M. Rajput and V.H. Rane, *Catal. Lett.*, 3 (1989) 85
31. S. Becker and M. Baerns, *J. Catal.*, 128 (1991) 512
32. X.-R. Xia, W. Cui, G.-X. Xiong and X.-X. Guo, *Catal. Today*, 13 (1992) 617
33. M.S. Holgado, V. Rives and S. San Roman, *React. Kinet. Catal. Lett.*, 48 (1992) 391
34. T.L. Yang, L.B. Feng and S.K Shen, *J. Catal.*, 144 (1994) 384
35. L. Mleczko, U. Pannek, M. Rothaemel and M. Baerns, *Can. J. Chem. Eng.*, 74 (1996) 279
36. S. J. Tauster, *Acc. Chem. Res.*, 20 (1987) 389.
37. G.L. Haller and D.F. Resasco, *Adv. Catal.*, 36 (1989) 173.
38. F.S. Stone, *J. Mol. Catal.*, 59 (1990) 147.
39. V. R. Choudhary and L. K. Doraiswamy, *Ind. Eng. Chem. Prod. Res. Dev.*, 10 (1971) 218.
40. V. R. Choudhary and V. H. Rane, *J. Catal.*, 130 (1991) 411.
41. V. D. Sokolovskii, *Catal. Rev. -Sci. Eng.*, 32 (1990), 1.

CHAPTER - 1.2

OXIDATIVE COUPLING OF METHANE OVER Sr-PROMOTED La_2O_3 CATALYST SUPPORTED ON LOW SURFACE AREA POROUS CATALYST CARRIERS

1.2.1 INTRODUCTION

In order to convert methane into higher hydrocarbons for its effective utilization, worldwide efforts have been made during the last 13-15 years for the oxidative coupling of methane (OCM) to ethane/ethylene over a number of basic solid catalysts [1-5]. The OCM process occurs at high temperatures ($750^\circ - 900^\circ\text{C}$). Hence, for avoiding catalyst deactivation due to the loss of volatile active components, efforts are concentrated on developing the OCM catalyst containing non-volatile promoters or active components, such as La-promoted MgO [6, 7], La-promoted CaO [8, 9], alkaline earth- promoted La_2O_3 and other rare earth oxides [10-16]. These catalysts show good activity/selectivity and high thermal stability and hence long life in the OCM process. However, for converting these laboratory catalysts into commercial ones, it is preferable to support them on a porous matrix (i.e. catalyst carriers or supports) for providing high mechanical strength and resistance to abrasion to avoid high pressure drop across the catalyst bed and also for increasing the dispersion of the catalyst.

Our earlier studies showed that when Li-promoted MgO [17] and La-promoted MgO [18] OCM catalysts (which showed high activity/ selectivity, high productivity and long life) [19, 6] were supported on commonly used catalyst carriers, their activity and selectivity are reduced drastically. The reduction in the catalytic activity and selectivity was attributed to the consumption of the active catalyst components (i.e. promoter) by their chemical interactions with the active components (viz. silica and alumina) of the catalyst carriers during the high temperature (900°C) calcination of the supported catalysts. However, in the case of La_2O_3 catalyst [18], its activity and selectivity is influenced only to a small extent by supporting it on different catalyst carriers. Lanthana, after promotion with strontium, shows lower activity but higher selectivity in the OCM process [15]. It is, therefore, interesting to study the influence of support on the catalytic

activity/selectivity of La_2O_3 promoted by strontium for developing a supported OCM catalyst having high activity/selectivity, high productivity and also high thermal stability or long life.

The present work was undertaken with the above objective. OCM process over Sr-promoted La_2O_3 catalyst supported on a low surface area porous silica-alumina catalyst carriers (SA-5205 and SA-5218, obtained from M/S Norton Co., USA) with different Sr/La ratios, support particle sizes and catalyst dilution's has been thoroughly investigated.

1.2.2 EXPERIMENTAL

1.2.2.1 Catalyst Preparation

Supported Sr-promoted La_2O_3 catalysts (Sr- La_2O_3 /SA-5205 and Sr- La_2O_3 /SA-5218 with Sr- La_2O_3 loading of 16 ± 1.5 wt.% and 13 ± 1.0 wt.%, respectively) were prepared by impregnating commercial low surface area porous inert catalyst carriers (viz. SA-5205 and SA-5218) by the active catalyst mass. The impregnation of mixed nitrates of Sr and La from their aqueous solution on the support particles was done by incipient wetness technique. The resulting supported catalyst mass was dried at 90°C for 16 h and then calcined in static air at 950°C for 4 h. The chemical composition and properties of the catalyst supports are given in Appendix-1.

1.2.2.2 Catalyst Characterization

The surface area of the catalysts was measured by the single-point BET method, using a Monosorb Surface-Area Analyser (Quantachrome Corp., USA), described earlier (Chapter - 1.1).

The supported catalysts were characterized by temperature-programmed desorption (TPD) of CO_2 , NH_3 and O_2 . The surface basicity/base strength distribution on the catalyst was measured by the TPD of CO_2 (chemisorbed at 100°C) on the catalyst (1.0 g) packed in a shallow bed quartz reactor with low dead volume, from 50°C to 950°C . The CO_2 desorbed in the TPD was measured quantitatively by the thermal conductivity detector. The acidity distribution on the catalyst was measured by the TPD of ammonia (chemisorbed at 100°C), from 50°C to 950°C . TPD of oxygen (chemisorbed at 100°C) was also measured from 50°C to 950°C . In all the TPD experiments, the linear heating rate was $20^\circ\text{C}.\text{min}^{-1}$ and carrier gas was helium ($40 \text{ cm}^3. \text{min}^{-1}$) passed over molecular sieves and oxysorb to remove traces of moisture and oxygen. Before the TPD, the catalyst was pretreated at 950°C in a flow of helium ($40 \text{ cm}^3. \text{min}^{-1}$) for a period of 1 h. In the

present case, the chemisorption of CO₂, NH₃ and oxygen is defined as the amount of a particular sorbate retained on the pre-saturated catalyst when it was swept with pure helium (40 cm³. min⁻¹) for a period of 30 min. The experimental set-up used and the procedure adapted for TPD of O₂ prechemisorbed at 100°C) is similar to that of used for the TPD of CO₂ and NH₃, described in Chapter - 1.1

In the present study, the chemisorption is considered as the amount of adsorbate retained by the presaturated catalyst after it was swept with pure helium for a period of 30 min.

1.2.2.3 Catalytic Reaction

The OCM reaction over the supported catalysts was carried out at atmospheric pressure in a continuous flow quartz reactor (i.d. 10 mm) (described in Chapter - 1.1) provided with a Chromel-Alumel thermocouple located axially in the catalyst bed. The catalyst was pretreated *in-situ* in a flow of N₂ (30 cm³. min⁻¹) at 950°C for 1 h. The feed was a mixture of pure methane and oxygen. The OCM reaction over the catalyst was carried out at a space velocity of 1,02,000 cm³.g⁻¹.h⁻¹ (measured at 0°C and 1 atm pressure). The reactor effluent gases, after the removal of water by condensation, were analysed by an on-line gas chromatograph using Porapak-Q and Sphero carb columns. The detailed procedure for the above is given in Chapter - 1.1.

1.2.3 RESULTS AND DISCUSSION

1.2.3.1 Catalyst Characterization

Data on the surface area and chemisorption (at 100°C) of CO₂, ammonia and oxygen for the Sr-promoted La₂O₃ catalysts with or without support are presented in Table 1.2.1.

a) Surface area

Surface area of the catalysts is, in general, decreased with increasing the Sr/La ratio. This indicates that the sintering or crystal growth of Sr-La₂O₃ is increased with increasing the concentration of Sr in the catalysts. A comparison of the supported and unsupported Sr-La₂O₃ catalysts (having the same Sr/La ratio) for their surface area of the active catalyst mass (i.e. Sr-La₂O₃) reveals that the surface area and hence the dispersion of the catalyst mass is increased markedly because of both the supports. The increase in the dispersion is, however, larger in case of the SA-5205 support. The surface basic sites measured in terms of the chemisorption of CO₂ (at

100°C) per unit mass of the active catalyst mass are also larger for the supported catalysts due to the higher dispersion of Sr-La₂O₃.

b) TPD of CO₂

The TPD of CO₂ (chemisorbed at 100°C) on the Sr-La₂O₃/SA-5205 catalysts from 50° - 950°C is shown in Fig. 1.2.1. A comparison of the TPD curves shows a strong influence of the Sr/La ratio on the CO₂ chemisorption sites (i.e. basic sites) of the supported catalyst. The dependence of the weak, intermediate strength and strong basic sites (measured in terms of the CO₂ desorbed in the TPD from 50° to 250°C, 250° to 650°C and 650° to 950°C, respectively) of the supported catalyst on its Sr/La ratio is shown in Fig. 1.2.2. The influence of Sr/La ratio on the weak basic sites is small but that on the intermediate strength and strong basic sites is very large. The intermediate strength basic sites are sharply decreased and the strong basic sites are sharply increased with increasing the Sr/La ratio; the influence is however smaller at the higher Sr/La ratios. The TPD peak (at 800°-950°C) corresponding to the strong basic sites is shifted towards the higher temperature side with increase in the Sr/La ratio. This indicates that the strength of the strong basic sites is higher for the catalyst with higher Sr/La ratio. Results of the TPD of CO₂ on the Sr-La₂O₃/SA-5218 catalysts are presented in Figs. 1.2.3 and 1.2.4. The observations made for the influence of Sr/La ratio on the TPD, dependence of weak, intermediate strength and strong basic sites and also on the strength of the strong acid sites of the catalyst are similar to that made for the Sr-La₂O₃/SA-5205 catalyst.

A comparison of the TPD of CO₂ on the Sr-La₂O₃ (Sr/La = 0.1) catalyst without and with support (Figs. 1.2.1 and 1.2.3) shows that the catalyst without support contains mainly the strong basic sites with much smaller amounts of both the intermediate strength and weak basic sites. The strength of its strong basic sites is also much larger than that of the strong basic sites of the supported catalyst as indicated by the shift of the TPD peak (corresponding to the strong basic sites) of the unsupported catalyst to the higher temperature side (Figs. 1.2.1 and 1.2.3). This clearly shows a strong influence of the supports on the basicity/base strength distribution of the catalyst.

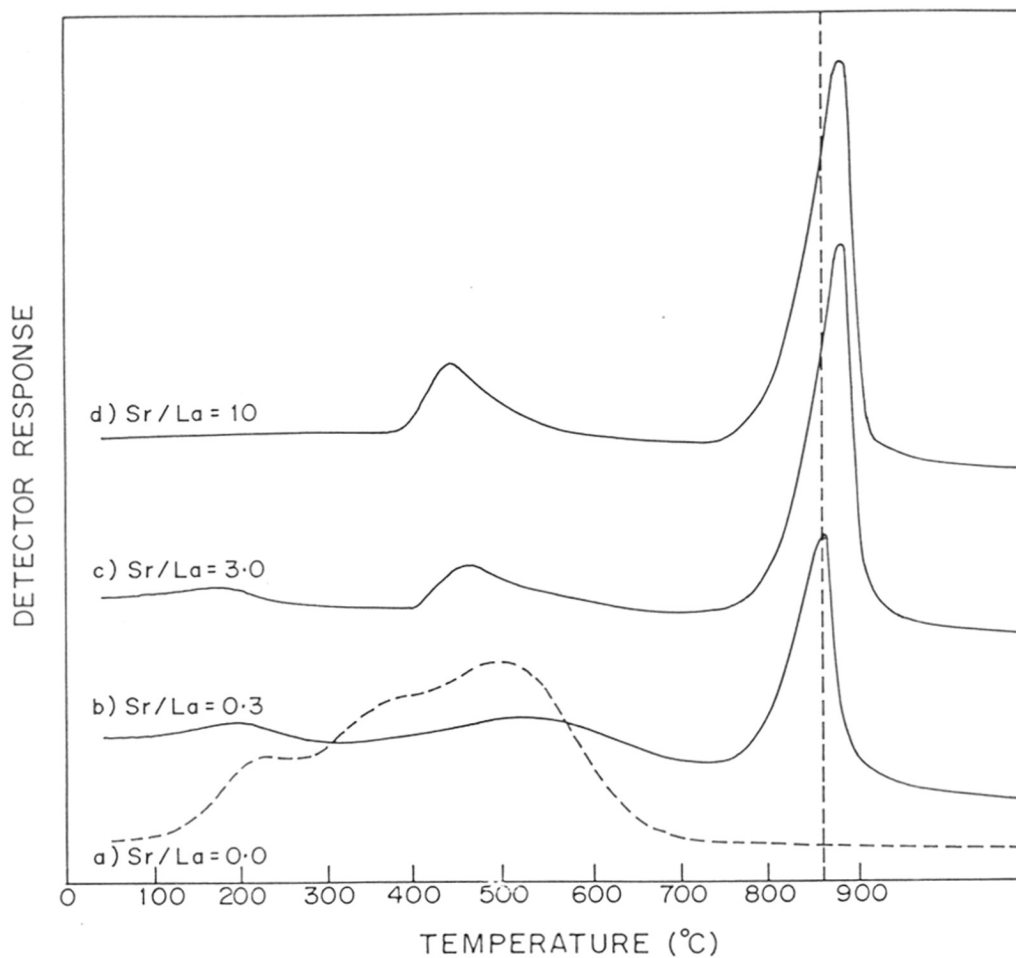


Fig. 1.2.1 : TPD of CO₂ on Sr-La₂O₃/SA-5205 catalysts with different Sr/La ratios (loading of Sr-La₂O₃ = 16.1 wt%)

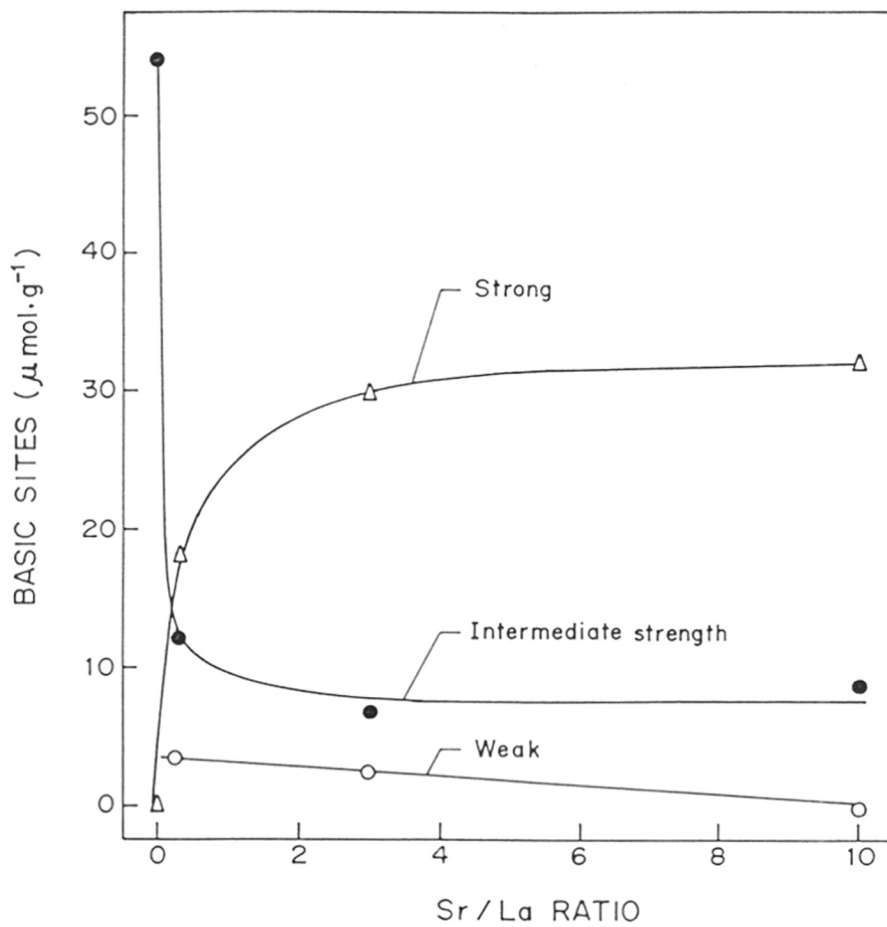


Fig. 1.2.2 : Effect of Sr/La ratio on the basic sites of Sr-La₂O₃/SA-5205 catalyst

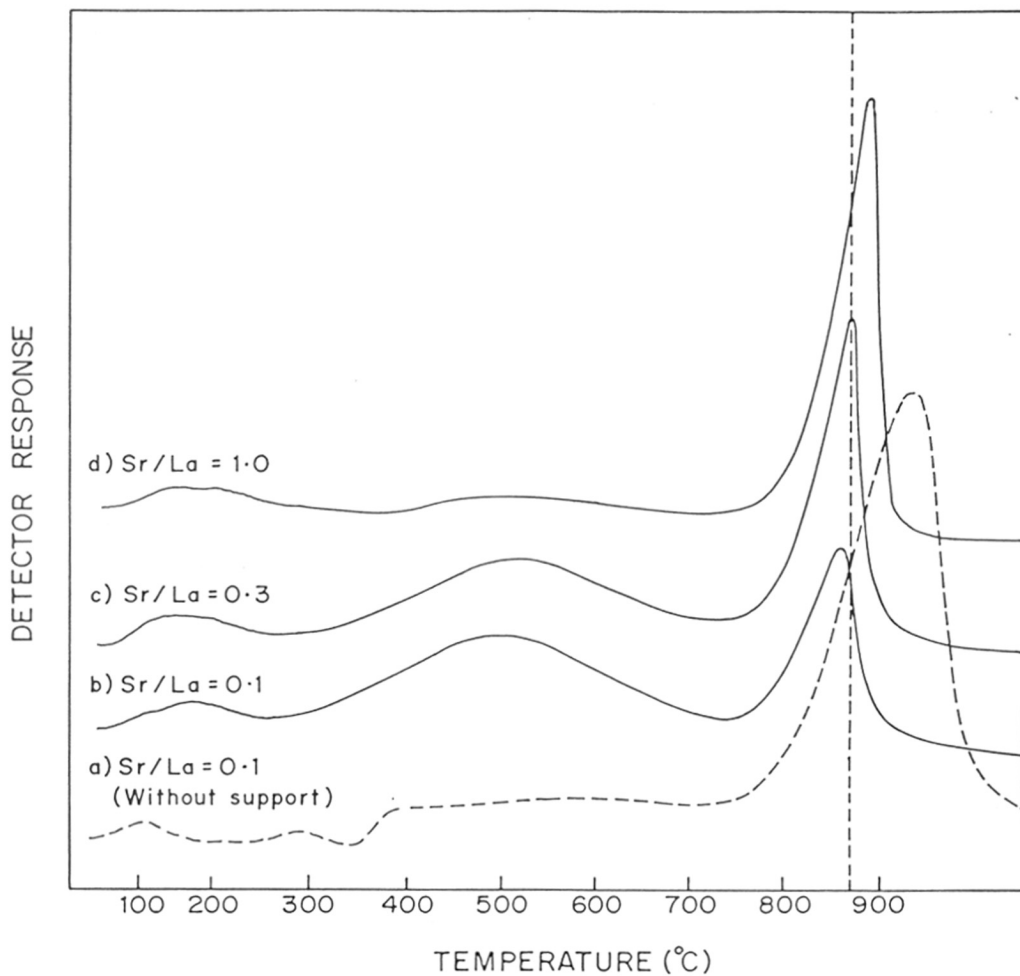


Fig. 1.2.3 : TPD of CO₂ on Sr-La₂O₃ (without support) and Sr-La₂O₃/SA-5218 with different Sr/La ratios (loading of Sr-La₂O₃ = 13.9 wt %)

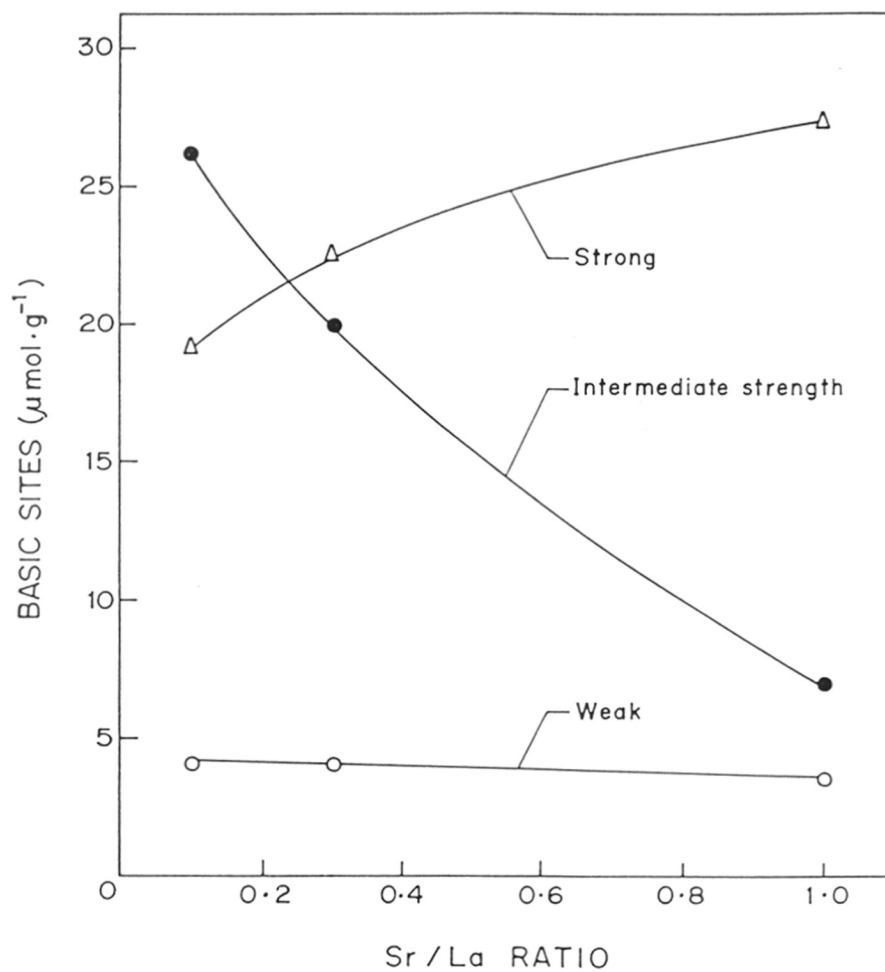


Fig. 1.2.4 : Effect of Sr/La ratio on the basic sites of Sr-La₂O₃/SA-5218 catalyst

c) TPD of NH_3

Results of the TPD of ammonia (chemisorbed at 100°C) on the Sr-La₂O₃/SA-5205 (Sr/La = 0.3 and 10) and Sr-La₂O₃/SA-5218 (Sr/La = 0.3) are presented in Fig. 1.2.5. The TPD for the supported catalysts consists of only a single peak. The peak maximum temperature (477°C) for the Sr-La₂O₃/SA-5205 with Sr/La of 0.3 is lower than that (500°C) for the other two catalysts. This shows that the strength of the acid sites of the former catalyst is lower than that of the other catalysts. A comparison of the Sr-La₂O₃/SA-5205 catalyst with Sr/La ratio of 0.3 and 10 (Table 1.2.1 and Fig. 1.2.5) indicates that both the number and strength of acid sites on the supported catalysts are lower for the catalysts having lower Sr/La ratio.

Table 1.2.1 : Surface area and chemisorption (at 100°C) of CO₂, ammonia and oxygen on Sr-La₂O₃/SA-5205, Sr-La₂O₃/SA-5218 and Sr-La₂O₃ (without support) catalysts with different Sr/La ratios

Sr/La ratio	Surface area (m ² .g ⁻¹)		CO ₂ chemisorbed (μmol.g ⁻¹)		NH ₃ chemisorbed (μmol.g ⁻¹)		O ₂ chemisorbed (μmol.g ⁻¹)	
	Supported catalyst	Active catalyst mass	Supported catalyst	Active catalyst mass	Supported catalyst	Active catalyst mass	Supported catalyst	Active catalyst mass
A) Sr-La₂O₃/SA-5205 (16 ± 1.5 wt% Sr- La₂O₃)								
0.0	1.6	9.8	56.7	347	-	-	-	-
0.1	1.2	7.5	-	-	-	-	-	-
0.3	1.0	6.3	34.1	215	8.8	55	7.6	48
1.0	0.9	5.4	-	-	-	-	-	-
3.0	0.5	3.0	39.4	236	-	-	-	-
10.0	0.2	1.2	41.1	246	11.1	67	28.6	172
B) Sr-La₂O₃/SA-5218 (13 ± 1.2 wt% Sr- La₂O₃)								
0.1	0.7	5.7	49.4	402	-	-	-	-
0.3	0.6	4.6	46.8	359	5.6	43	16.6	127
1.0	0.4	3.3	37.7	311	-	-	-	-
C) Sr-La₂O₃ (without support)								
0.1	-	2.9	-	160	-	46	-	-
1.0	-	0.9	-	55	-	-	-	-

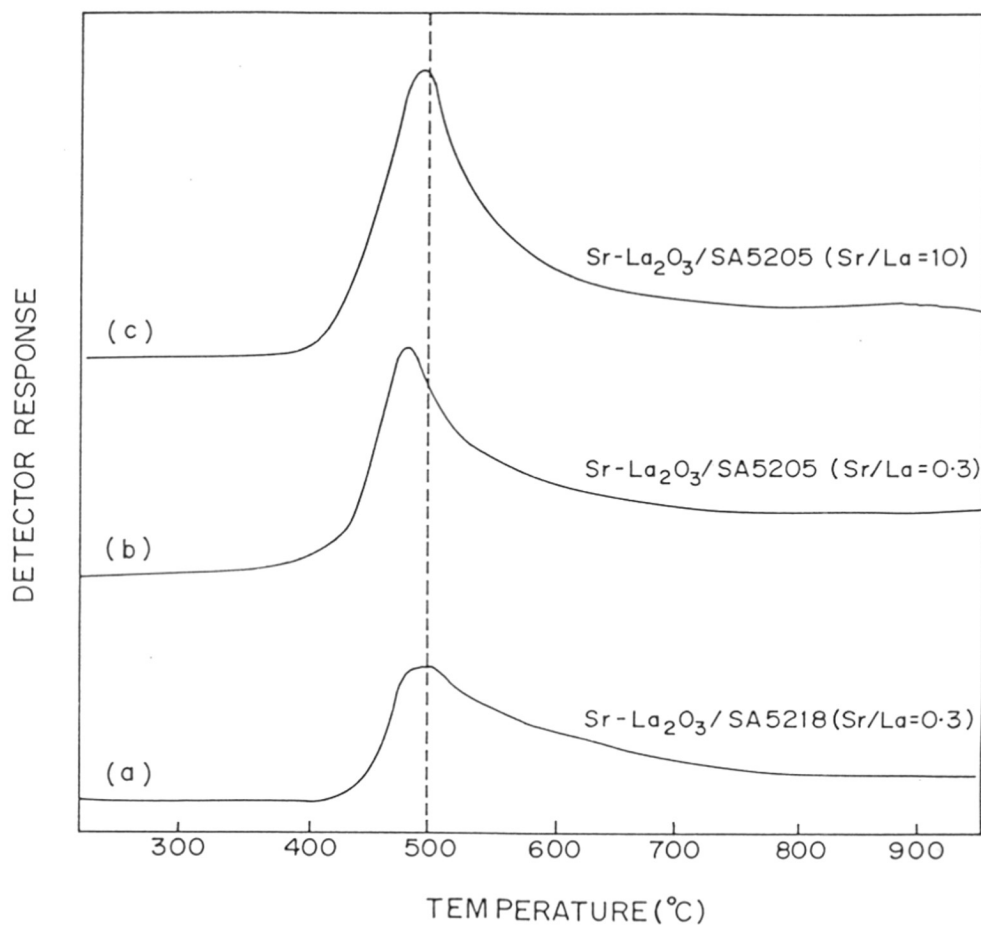


Fig. 1.2.5 : TPD of NH₃ on Sr-La₂O₃/SA-5205 (Sr/La = 0.3 and 10) and Sr-La₂O₃/SA-5218 (Sr/La = 0.3)

TPD of O₂

Figure 1.2.6 shows the results on the TPD of oxygen over the supported catalysts with different supports and Sr/La ratios. The O₂ TPD on the catalyst shows two distinct peaks. However, the peak maximum temperature and the shape of the TPD peaks differ from catalyst to catalyst. The amount of O₂ chemisorbed at 100°C is also different for the three catalysts (Table 1.2.1). In the Sr-La₂O₃/SA-5205 (Sr/La = 0.3) catalyst, the number of stronger O₂ chemisorption sites are more than that of the weaker O₂ chemisorption sites. Whereas, the other two catalysts have opposite distribution of the weak and strong O₂ chemisorption sites. This shows a strong influence of the support and Sr/La ratio on both the number and strength distribution of the O₂ chemisorption sites on the supported catalyst.

The observed influence of the Sr/La ratio and support on the basic sites/base strength distribution, acidity/acid strength distribution and O₂ chemisorption sites and their strength distribution is attributed to the formation of surface La³⁺ and O²⁻ species with different coordinations due to doping of La₂O₃ with Sr²⁺ at different concentrations and also because of the dispersion to different extents of the Sr-doped La₂O₃ on the supports. The crystal ionic diameter of Sr²⁺ cation (0.224 nm) is higher than that of La³⁺ (0.203 nm). Hence, the insertion of Sr in the structure of La₂O₃ is expected to cause a distortion of its crystal structure creating a defect structure with surface imperfections such as steps, kinks, corners, which provide sites for ions of low coordination, La³⁺_{LC} and O²⁻_{LC} (where LC = low coordination number, viz. 3 and 4). The acidity and basicity of the catalysts are attributed to the surface La³⁺ and O²⁻ ions. The base strength (or electron pair donor strength) of the surface sites is expected to vary depending upon the -ve charge on the anions (O²⁻) and/or their coordination on the surface. Similarly, the acid strength (or electron pair acceptor strength) of the surface sites is expected to be dependent upon the +ve charge on the metal cation (La³⁺ and also Sr²⁺) and/or their coordination on the catalyst surface. Thus the ions of low coordination, formed due to the doping of Sr in La₂O₃ and the dispersion and/or interaction of the Sr-doped La₂O₃ with support, are responsible for the presence of sites of different strength.

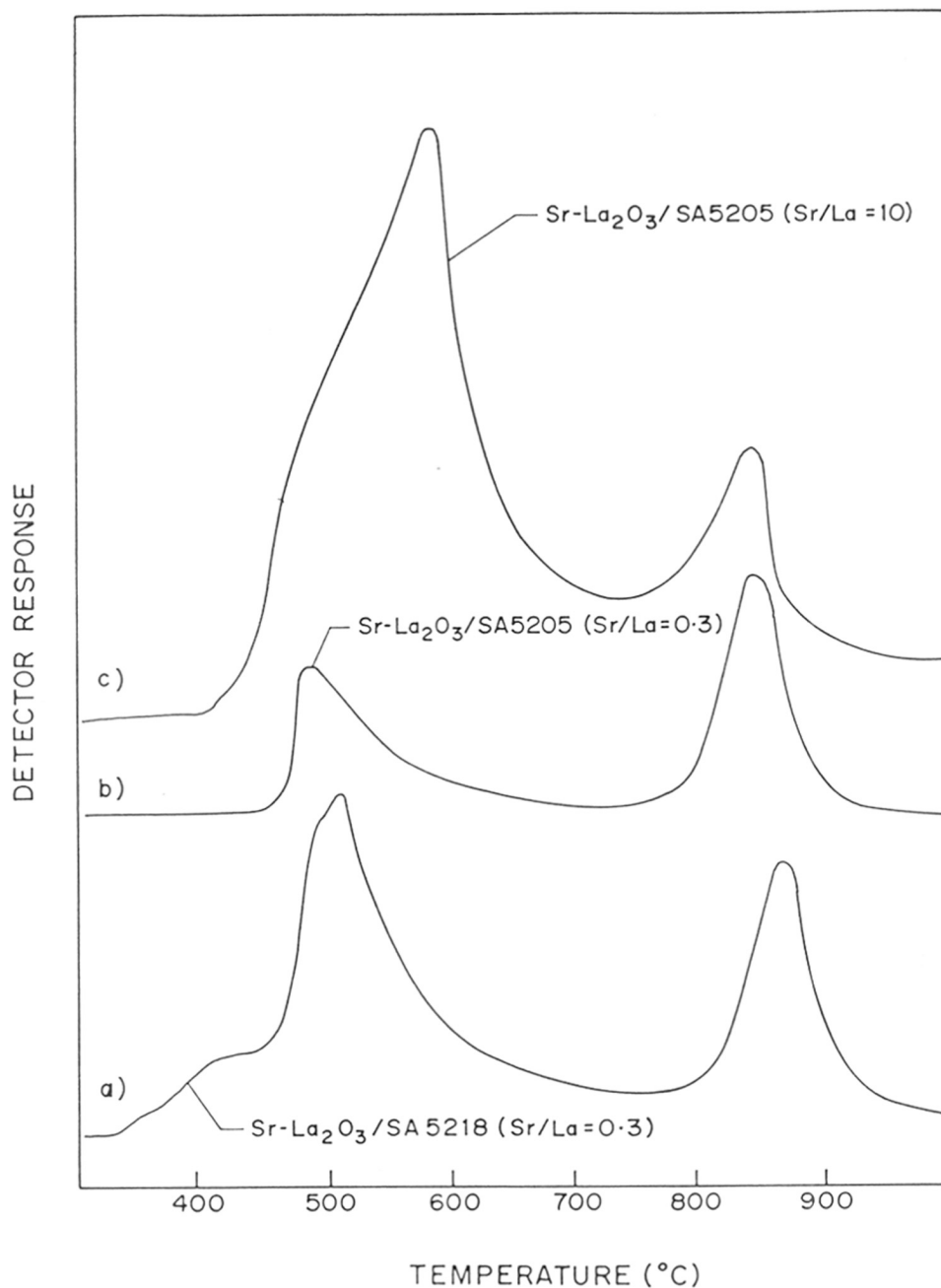


Fig. 1.2.6 : TPD of O₂ on Sr-La₂O₃/SA-5205 (Sr/La = 0.3 and 10) and Sr-La₂O₃/SA-5218 (Sr/La = 0.3)

1.2.3.2 Oxidative Coupling of Methane (OCM)

a) Influence of support

The performance in the OCM (at 800°C) of the supported Sr-promoted La₂O₃ catalysts is compared with that of the unsupported catalyst in Table 1.2.2. Both the conversion and C₂₊ selectivity or C₂₊ yield are increased to a small extent because of supporting the catalyst on both the catalyst carriers. Although the concentration of Sr-La₂O₃ in the supported catalysts is much lower than that in the unsupported catalyst, the activity and selectivity of the supported catalysts is even slightly higher, mostly due to the higher dispersion of the catalytically active components on both the supports. Among the supported catalysts, the one supported on SA-5205 shows better performance, probably because of the higher dispersion of Sr-La₂O₃.

Table 1.2.2 : Influence of support on the performance of Sr-promoted La₂O₃ (Sr/La = 0.1) catalyst in the OCM process at 800°C [GHSV = 1,00,200 cm³.g⁻¹.h⁻¹ and CH₄/O₂ mole ratio in feed = 4.0]

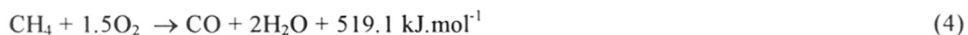
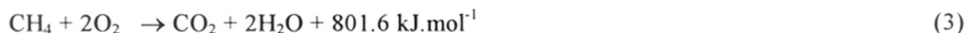
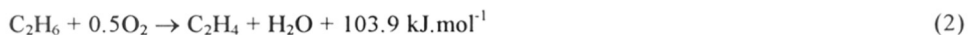
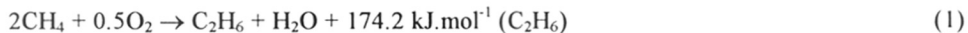
	Sr-La ₂ O ₃ (without support)	Sr-La ₂ O ₃ /SA-5205	Sr-La ₂ O ₃ /SA-5218
CH ₄ conversion (%)	26.7	29.1	28.4
C ₂₊ yield (%)	16.2	18.4	17.6
C ₂₊ selectivity (%)	60.7	63.3	61.9
C ₂ H ₄ /C ₂ H ₆ product ratio	1.1	0.9	1.0
CO/CO ₂ product ratio	0.2	0.4	0.4

The observed lower activity and selectivity of the unsupported Sr-La₂O₃ catalyst is also expected because of the fact that the strength of its strong basic sites is much larger (Fig. 1.2.3) and hence the strong basic sites of this catalyst are blocked by CO₂ formed during the OCM process. The effective strong basic sites available for the methane conversion reaction are therefore smaller.

b) Influence of linear gas velocity

In order to study the influence of film diffusional (or external) mass transfer or heat transfer resistance on the OCM, the conversion/selectivity data have been obtained by varying the linear gas velocity over the supported catalyst (Sr-La₂O₃/SA-5218 with Sr/La = 0.3 and particle size = 0.96 mm) at 850°C (CH₄/O₂ ratio in feed = 8 and 16, GHSV = 1,02,000 cm³.g⁻¹.h⁻¹). The results showing the influence of amount of catalyst in the reactor on the conversion and selectivity in the OCM at the same space velocity are presented in Fig. 1.2.7.

The methane conversion, C₂ or C₂₊ selectivity (except for the lowest amount of catalyst or linear gas velocity) and C₂₊ yield in the OCM process are increased to a small extent with increasing the amount of catalyst in the reactor (or the linear gas velocity). However, the ethylene/ethane product ratio is decreased appreciably. The small increase in the conversion and yield or selectivity is expected due to the increase in the external mass transfer rate with increasing the linear gas velocity. The observed decrease in the ethylene/ethane is, however, expected because of the increase in the heat transfer from the external surface of the catalyst particles to the bulk gas phase. The OCM process (at 800°C) involves following exothermic reactions.



Hence, under the heat transfer limitations, the temperature at the external surface of the catalyst particles is expected to be higher than that of the bulk gas phase. Conversion of ethane to ethylene by the thermal cracking reaction



is higher at higher temperatures and hence the ethylene/ethane is expected to be decreased with increasing the heat transfer rate. Alternatively, the decrease in the ethylene/ethane ratio shows that the temperature at the external surface of the catalyst particles at lower linear velocities is higher than that of the bulk gas flowing over the catalyst.

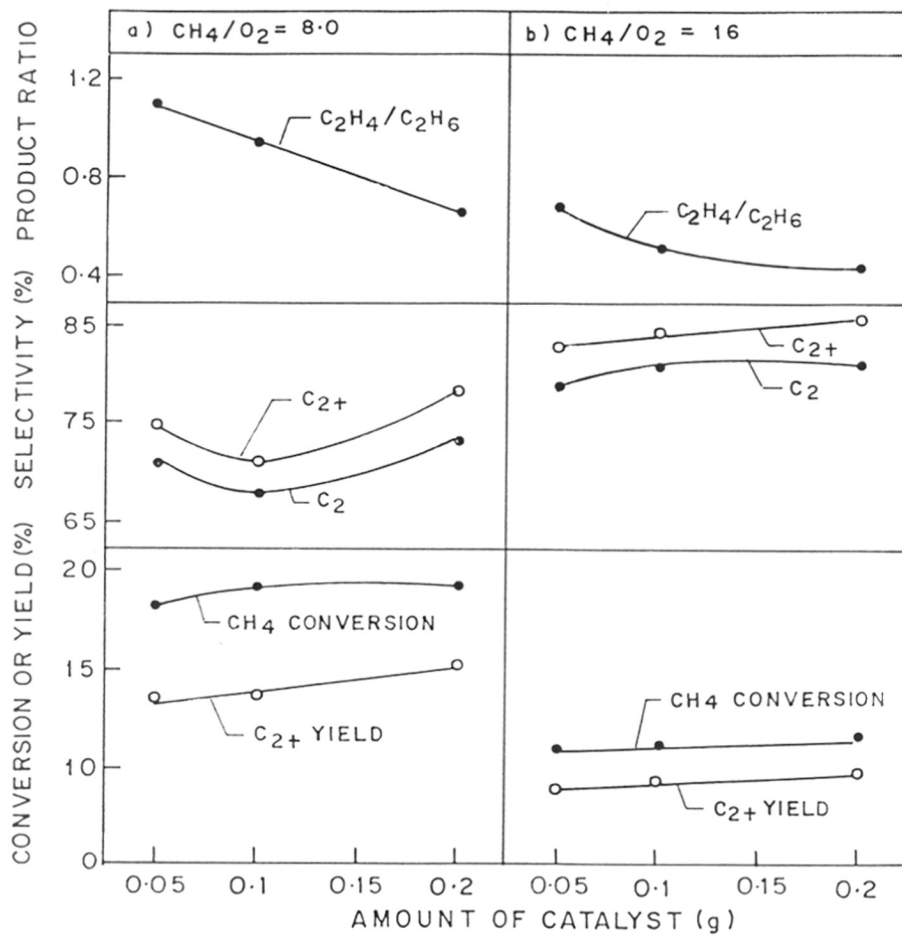


Fig. 1.2.7 : Effect of linear gas velocity on the OCM (at 850°C, GHSV = 102 000 cm³.g⁻¹.h⁻¹) over Sr-La₂O₃/SA-5218 catalyst (Sr/La = 0.3, particle size = 0.96mm)

c) Influence of catalyst particle size

For studying the influence of intraparticle (or pore diffusional) mass transfer or heat transfer in the OCM process, the reaction (at 850°C, $\text{CH}_4/\text{O}_2 = 8.0$ and $\text{GHSV} = 1,02,000 \text{ cm}^3 \cdot \text{g}^{-1} \cdot \text{h}^{-1}$) was carried out over the Sr-La₂O₃/SA-5218 catalyst (Sr/La = 0.3) by varying its particle size from 0.2 to 1.0 mm. The results (Fig. 1.2.8) show a small increase in the conversion of methane and ethylene/ethane ratio but a small decrease in the selectivity of C₂ and C₂₊ hydrocarbons with increasing the catalyst particle size. Because of this the C₂₊ yield is not changed significantly. The influence of the intraparticle mass and heat transfer on the conversion and selectivity is thus small. But the observed small decrease in the methane conversion and the appreciable increase in the ethylene/ethane ratio for the catalyst with larger particle size indicate that the temperature inside the catalyst particles is higher than that of the bulk gas phase, resulting in the catalyst effectiveness factor greater than 1, similar to that generally observed for most exothermic reactions [20].

d) Influence of Sr/La ratio

Results showing the influence of Sr/La ratio of the Sr-La₂O₃/SA-5205 catalyst on its methane conversion activity, C₂₊ yield, selectivity for C₂ and C₂₊ hydrocarbons and product ratios (viz. C₂H₄/C₂H₆ and CO/CO₂ mole ratios) in the OCM at two different process conditions are presented in Fig. 1.2.9. Also the results on the Sr-La₂O₃/SA-5218 catalysts with different Sr/La ratios at different process conditions are given in Fig. 1.2.10. The results on both the supported catalysts show a strong influence of the Sr/La ratio on the catalyst performance in the OCM process, as follows.

For both the supported catalysts, their methane conversion activity and C₂₊ yield or selectivity are increased by the promotion by Sr at lower concentration (when Sr/La < 1.0). The improvement in the catalyst performance due to the Sr promotion is attributed mainly to the large increase in the strong basic sites of the catalyst (Figs. 1.2.2-1.2.4). This is because of the requirement of strong basic sites for the OCM reaction [21-23].

In the case of both the supported catalysts, the methane conversion activity and selectivity and also the ethylene/ethane product ratio are first increased passed through a maximum and then decreased with increasing the Sr/La ratio. The Sr-La₂O₃/SA-5205 catalyst with Sr/La ratio of 10 shows very poor performance in the OCM process. This could be because of its much lower surface area and higher acidity (Table 1.2.1) and also may be due to smaller number of strong

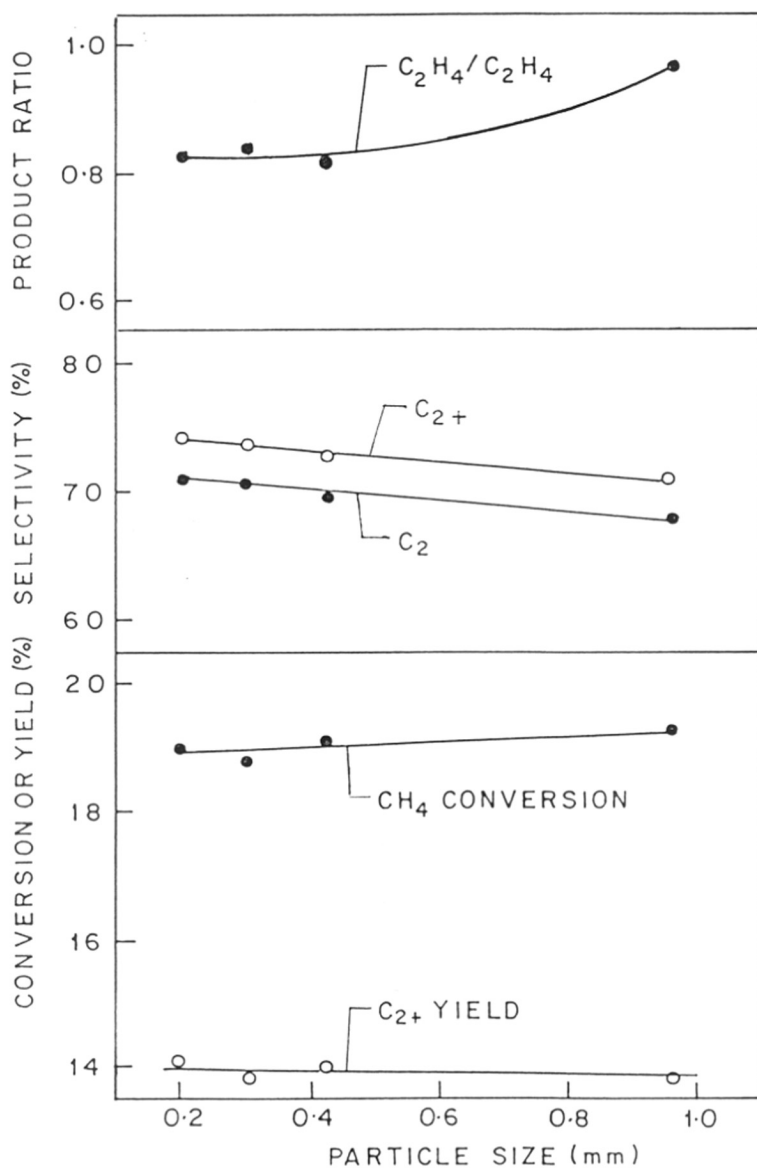


Fig. 1.2.8 : Effect of catalyst particle size on the OCM over Sr-La₂O₃/SA-5218 (Sr/La = 0.3) catalyst

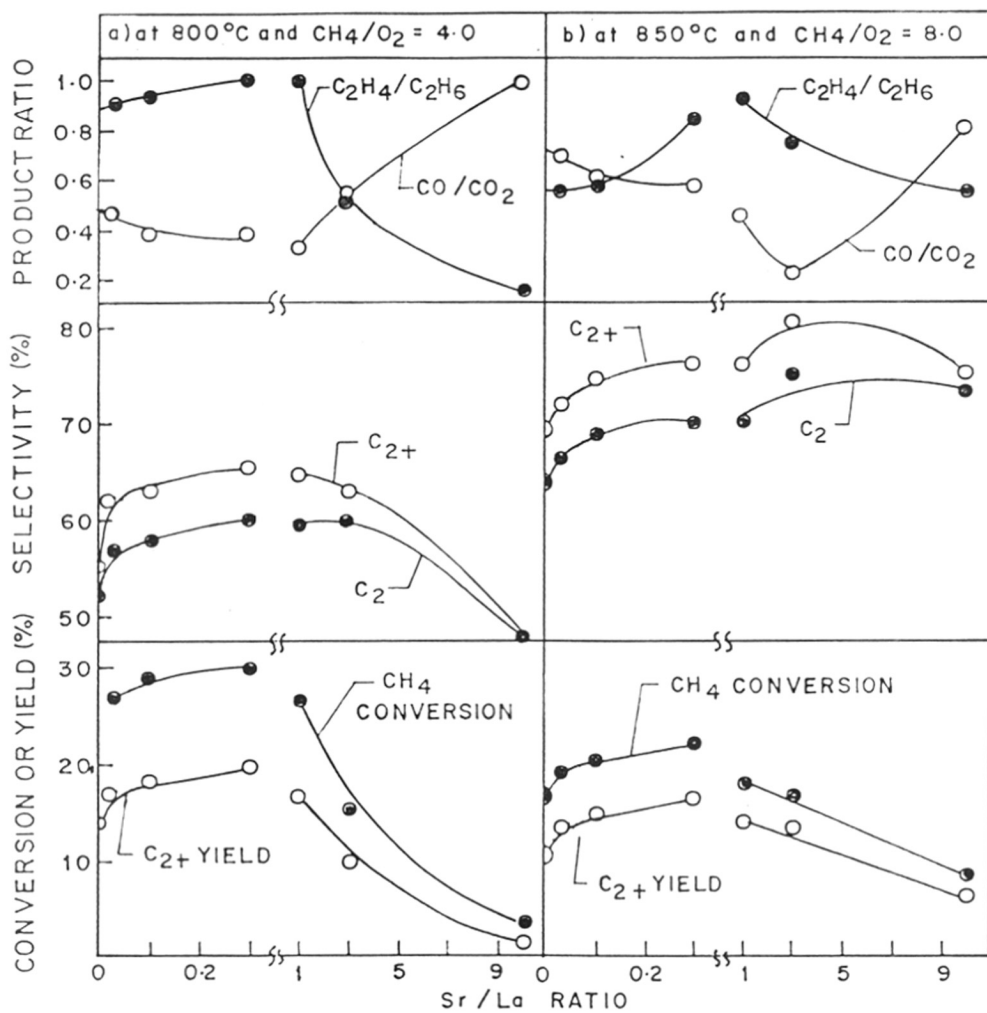


Fig. 1.2.9 : Effect of Sr/La ratio on the OCM over Sr-La₂O₃/SA-5205 catalyst

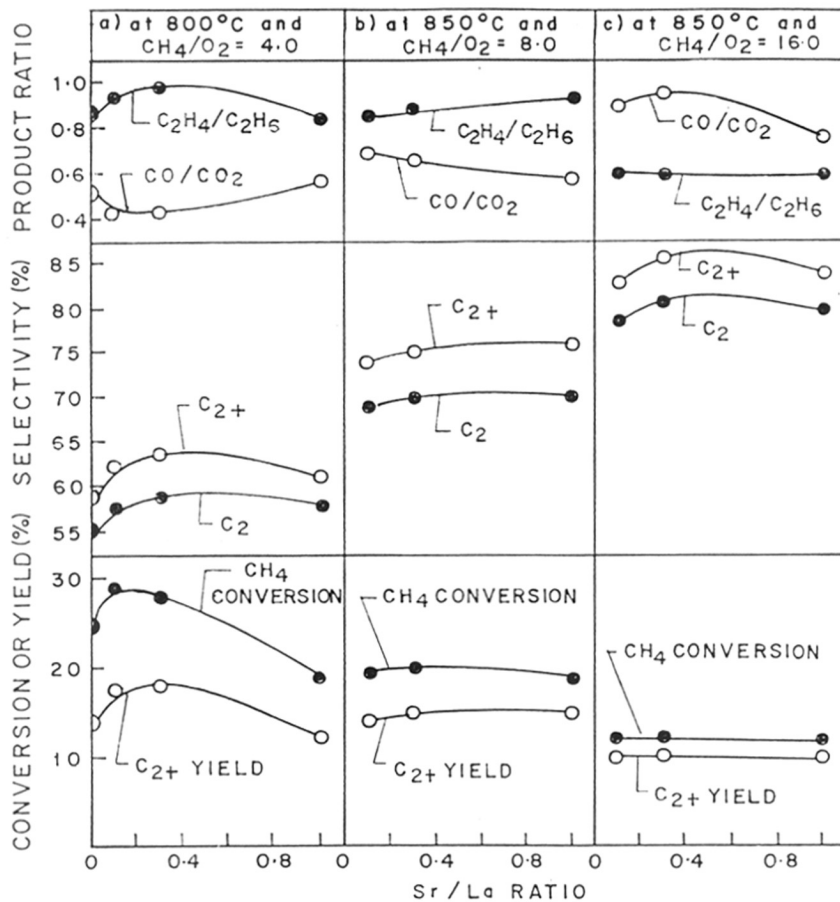


Fig. 1.2.10: Effect of Sr/La ratio on the OCM over Sr-La₂O₃/SA-5218 catalyst

chemisorption sites, corresponding to the O₂-TPD peak at about 850°C (Fig. 1.2.6). The formation of carbon monoxide related to that of CO₂ is also strongly affected by the Sr/La ratio. Based on the C₂ yield, both the supported catalysts show their best performance in the OCM process for the Sr/La ratio of about 0.3.

e) Influence of CH₄/O₂ ratio in the feed

Results showing a strong influence of CH₄/O₂ ratio in the feed on the performance of both the supported Sr-La₂O₃ catalysts (Sr/La = 0.3) in the OCM process are presented in Fig. 1.2.11. The influence of the CH₄/O₂ ratio on the performance for both the supported catalysts is similar.

When the CH₄/O₂ ratio is increased (or the O₂ concentration is decreased)

- the methane conversion and C₂ yield are decreased appreciably,
- the selectivity for C₂ or C₂₊ hydrocarbons is increased markedly,
- the C₂H₄/C₂H₆ ratio is decreased exponentially, and
- the CO/CO₂ ratio is increased markedly.

The increase in the selectivity is mostly due to the decrease in the methane conversion, as observed commonly in the OCM process. The decrease in the methane conversion and C₂H₄/C₂H₆ ratio and also the decrease in the formation of CO₂ relative to that of CO (i.e. the increase in the CO/CO₂ ratio) are expected due to the availability of less oxygen for the oxidative methane coupling reaction (Reaction-1), oxidative dehydrogenation of ethane (Reaction-2) and total combustion of methane (Reaction-3), respectively. The observed strong influence on the C₂H₄/C₂H₆ ratio may also be at least partly due to a decrease in the temperature gradient between the catalyst surface (at which the temperature is higher) and the bulk gas phase with decreasing the methane conversion and increasing the selectivity.

The results in Fig. 1.2.11 also confirms that the Sr-La₂O₃/SA-5205 catalyst shows slightly better performance than the catalyst supported on SA-5218. The Sr-La₂O₃/SA-5205 catalyst show a very high selectivity for C₂₊ hydrocarbons (85%) with a good conversion of methane (13%) at 850°C in the OCM process using CH₄/O₂ ratio of 16 in the feed.

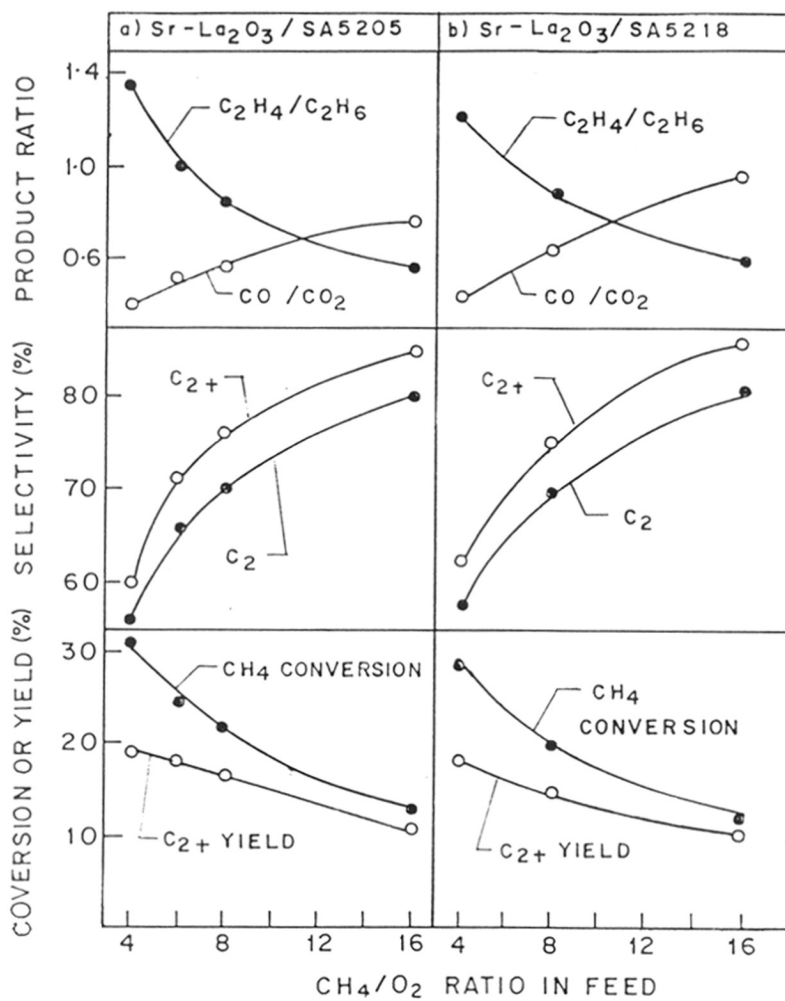


Fig. 1.2.11 : Effect of CH_4/O_2 ratio in feed on the OCM over $\text{Sr-La}_2\text{O}_3/\text{SA-5205}$ and $\text{Sr-La}_2\text{O}_3/\text{SA-5218}$ catalysts ($\text{Sr/La} = 0.3$) at 850°C

f) Influence of catalyst dilution

The OCM process involves highly exothermic combustion side reactions (Reactions 3 and 4) and hence a small decrease in the selectivity or a small increase in the formation of combustion products results in a large production of heat in a small catalyst zone, creating hot spots in the catalyst bed, particularly, for a larger scale operation. The creation of hot spots results in the irreversible catalyst deactivation due to the sintering or crystal growth and/or may cause reaction run-away if the reaction heat from the reactor is not removed instantly. Since the removal of large heat from a small catalyst zone is very difficult, the process may become highly hazardous. In order to overcome this problem, it is proposed to dilute the supported catalyst bed with the particles of inert solid having the same size as that of the supported catalyst. The results showing the influence of catalyst dilution on the performance of the OCM process over Sr-La₂O₃/SA-5218 catalyst diluted with the particles of the same support (SA-5218) at different process conditions are presented in Fig. 1.2.12.

The results show no influence of the catalyst dilution on the conversion but a small effect on the selectivity in the process. However, the influence on the product ratios (C₂H₄/C₂H₆ and CO/CO₂) is appreciable. Both the ethylene/ethane and CO/CO₂ ratios are increased markedly with increasing the catalyst dilution. The increase in the C₂H₄/C₂H₆ and CO/CO₂ ratios are expected due to the increase in the rates of thermal cracking of ethane and homogeneous oxidation of hydrocarbons, respectively, because of the increase in the contact time for both the non-catalytic (homogeneous) reactions with increasing the catalyst dilution.

The catalyst dilution in the OCM process thus plays two important roles. It increases the heat transfer area (which is wellknown) so that the heat removal from catalyst bed becomes easier. The second role, which is very important, is that it provides more contact time for the slow thermal cracking of ethane (Reaction-5), which is highly endothermic, in the vicinity of the supported catalyst [24]. Because of this the endothermic thermal cracking reaction occurs to an appreciable extent simultaneously in the vicinity of the exothermic oxidative conversion reactions over the catalyst. This results in a coupling of the exothermic and endothermic reactions, making the overall process non-hazardous or less hazardous. Our earlier studies [24] showed that by coupling of the exothermic oxidative dehydrogenation of ethane with its endothermic cracking using diluted catalyst, it is possible to make the overall process almost thermoneutral with a large energy saving.

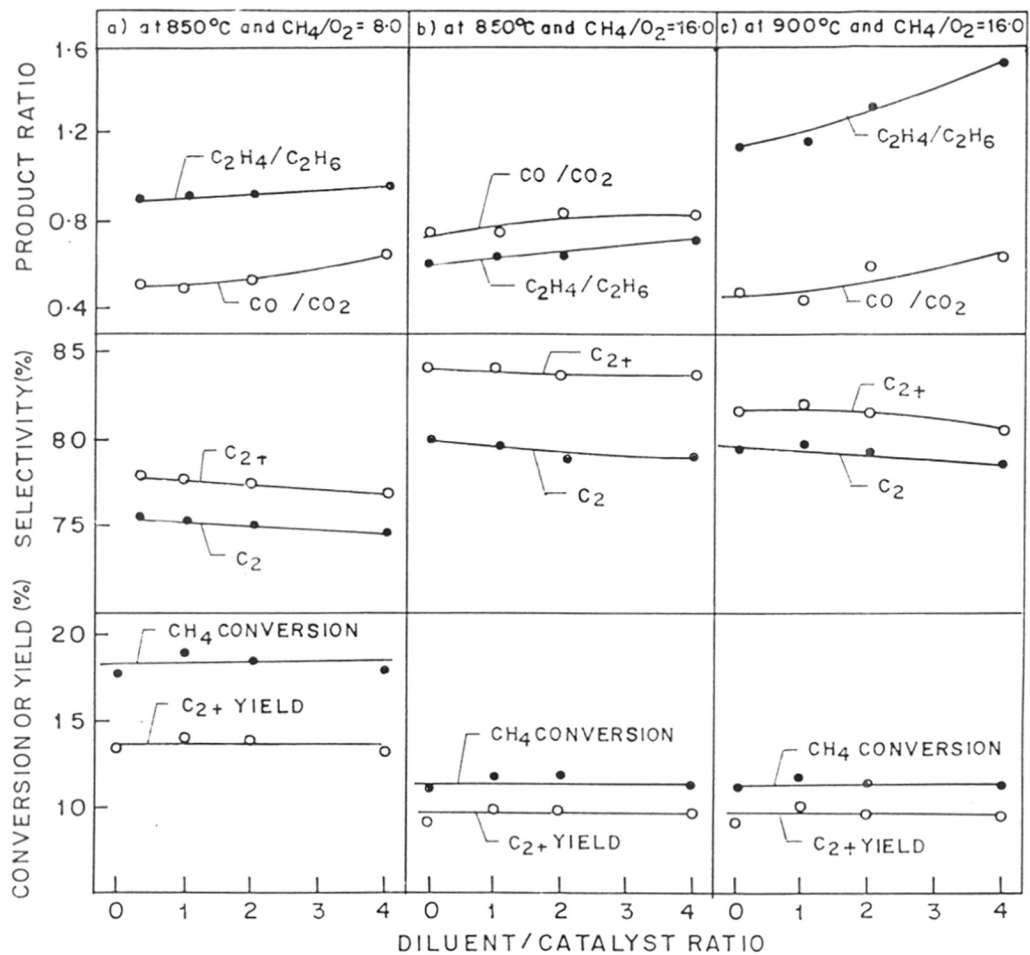


Fig. 1.2.12 : Effect of catalyst dilution by inert solid on the OCM over Sr-La₂O₃/SA-5218 (Sr/La = 0.3) catalyst

The results (Fig. 1.2.12) clearly show that the catalyst dilution has only a small effect on the selectivity; the methane conversion is not affected significantly. Hence the above advantages of the catalyst dilution (viz. the increase in the C_2H_4/C_2H_6 ratio, and the elimination or drastic reduction in the hazards because of the coupling of exothermic and endothermic reactions and the increase in the heat transfer area due to the catalyst dilution) can very well be utilised for the OCM process over the supported catalyst.

1.2.4 CONCLUSIONS

Sr-promoted La_2O_3 catalyst shows better performance when it is supported on a low surface area porous catalyst carriers containing silica and alumina. The improved performance is attributed to the increase in the dispersion and also to the reduction in the strength of the very strong basic sites of the Sr- La_2O_3 due to its deposition on the support. The performance in OCM of the supported Sr- La_2O_3 is strongly influenced by its Sr/La ratio; the best performance is shown by the catalyst with Sr/La ratio of about 0.3. The strong basic sites are increased and the intermediate strength ones are decreased with increasing the Sr/La ratio of the supported catalyst.

The linear gas velocity and particle size of the supported catalyst show a small effect on the conversion and selectivity but a large effect on the C_2H_4/C_2H_6 product ratio in the OCM process, most probably because of an appreciable temperature gradient in the catalyst. The CH_4/O_2 ratio in the feed shows a very strong influence on the conversion, selectivity and product ratios (C_2H_4/C_2H_6 and CO/CO_2). The dilution of the supported catalyst with the support particles, even at high diluent/supported catalyst ratio, show little or no influence on the conversion and selectivity but a strong influence on the product ratios. The catalyst dilution has beneficial effects for the OCM process; the ethylene/ethane ratio is increased markedly and also the hazardous nature of the exothermic process is expected to be reduced with increasing the catalyst dilution, particularly because of the coupling of the exothermic methane oxidative conversion reactions with the endothermic ethane thermal cracking.

REFERENCES

1. J.R. Anderson, *Appl. Catal.*, 47 (1989) 177.
2. J.S. Lee and S.T. Oyama, *Catal. Rev. Sci. Eng.*, 30 (1988) 249.
3. G.J. Hutchings, M.S. Scurrrell and J.R. Woodhouse, *Chem. Soc. Rev.*, 18 (1989) 251.
4. J.H. Lunsford, *Catal. Today*, 6 (1990) 235.
5. J.H. Lunsford, *Angew. Chem. Int. Ed. Engl.*, 34 (1995) 970.
6. V.R. Choudhary, S.T. Chaudhari, A.M. Rajput and V.H. Rane, *J. Chem. Soc. Chem. Commun.*, (1989) 555.
7. S.T. Chaudhari, *Ph.D. Thesis*, University of Bombay (1992).
8. V.R. Choudhary, S.T. Chaudhari, A.M. Rajput and V.H. Rane, *Catal.Lett.*, 3 (1989) 85.
9. S. Becker and M. Baerns, *J. Catal.*, 128 (1991) 512.
10. J.M. DeBoy and R.F. Hicks, *J. Chem. Soc. Chem. Commun.*, (1988) 982..
11. J.M. DeBoy and R.F. Hicks, *Ind. Eng. Chem. Res.*, 27 (1988) 1577.
12. N. Yamagata, Y. Abe, K. Igarashi, T. Ishikawa, M. Sahara and M. Okazaki, *Chem. Lett.* (1990) 1893
13. Z.L. Zhang, C.T. Au and K.R. Tsai, *Appl. Catal.*, 62 (1990) L29
14. H. Yamashita, Y. Machida and A. Tomita, *Appl. Catal.*, 79 (1991) 203
15. S.J. Conway, J.A. Greig and G.M. Thomas, *Appl. Catal. A: General*, 86 (1992) 199.
16. V.H. Rane, *Ph.D. Thesis*, University of Poona, (1992).
17. V.R. Choudhary, S.A.R. Mulla and B.S. Uphade; *Mater. Chem. Phys.* (communicated).
18. V.R. Choudhary, S.A.R. Mulla and B.S. Uphade, *Ind. Eng. Chem. Res.* (accepted).
19. V.R. Choudhary, S.T. Chaudhari, M.Y. Pandit, *J. Chem. Soc. Chem. Commun.*, (1991) 1158.
20. C.N. Satterfield, *Diffusion and Reaction in Porous Catalysts II. Complex Cases in Mass Transfer in Heterogeneous Catalysis*, M.I.T. Press Cambridge, (1970) 164-207.
21. V.R. Choudhary, V.H. Rane and S.T. Chaudhari, *Catal.Lett.*, (1990) 95.
22. V.R. Choudhary and V.H. Rane, *J. Catal.*, 130 (1991) 411.
23. V.D. Sokolovskii, *Cat. Rev. Sci. Eng.*, 32 (1990) 1.
24. V.R. Choudhary, B.S. Uphade and S.A.R. Mulla, *Angew. Chem. Int. Ed. Engl.*, 34 (1995) 665.

PART - II

CONVERSION OF METHANE TO SYNGAS

CHAPTER - 2.1 : OXIDATIVE CONVERSION OF METHANE TO SYNGAS OVER LaNiO_3 PEROVSKITE WITH OR WITHOUT SIMULTANEOUS STEAM AND CO_2 REFORMING REACTIONS: INFLUENCE OF PARTIAL SUBSTITUTION OF La AND Ni

CHAPTER - 2.2 : PARTIAL OXIDATION OF METHANE TO SYNGAS WITH OR WITHOUT SIMULTANEOUS CO_2 AND STEAM REFORMING REACTIONS OVER Ni/AlPO_4

CHAPTER - 2.3 : OXIDATIVE CONVERSION OF METHANE TO SYNGAS WITH OR WITHOUT SIMULTANEOUS STEAM AND/OR CO_2 REFORMING OVER SUPPORTED NiO-MgO , NiO-CaO AND $\text{NiO-Yb}_2\text{O}_3$ CATALYSTS

CHAPTER - 2.4 : LARGE ENHANCEMENT IN METHANE-TO-SYNGAS CONVERSION ACTIVITY OF SUPPORTED Ni-CATALYSTS DUE TO PRECOATING OF CATALYST SUPPORTS WITH MgO , CaO OR RARE-EARTH OXIDES

CHAPTER - 2.5 : OXIDATIVE CONVERSION OF METHANE TO SYNGAS OVER NICKEL SUPPORTED ON COMMERCIAL LOW SURFACE AREA POROUS CATALYST CARRIERS PRECOATED WITH ALKALINE AND RARE EARTH OXIDES

CHAPTER - 2.6 : SIMULTANEOUS STEAM AND CO_2 REFORMING OF METHANE TO SYNGAS OVER $\text{NiO}/\text{MgO}/\text{SA-5205}$ IN PRESENCE AND ABSENCE OF OXYGEN

CHAPTER - 2.1

OXIDATIVE CONVERSION OF METHANE-TO-SYNGAS OVER LaNiO_3 PEROVSKITE WITH OR WITHOUT SIMULTANEOUS STEAM AND CO_2 REFORMING REACTIONS: INFLUENCE OF PARTIAL SUBSTITUTION OF La AND Ni

2.1.1 INTRODUCTION

Syngas (i.e. a mixture of CO and H_2 , a versatile feed stock for ammonia, methanol and Fischer-Tropsch synthesis processes and also several carbonylation and hydrogenation processes) is produced from methane (or natural gas) mostly by its steam reforming [1,2].



This process suffers from severe limitations like very high energy requirements, high H_2/CO ratio (> 4 , which is not suitable for methanol and Fischer-Tropsch synthesis) and poor selectivity ($\approx 60\%$) for CO because of the water gas shift reaction,



Moreover, the syngas production cost by this process accounts for almost about 60% of the integrated cost of the plant. Syngas can also be produced by non-catalytic partial oxidation at about 1400°C using heavy hydrocarbons, pure oxygen and steam as a feed [1-3].



This process though yields syngas with desired H_2/CO ratio of about 2.0, it operates at very high temperature and extensive soot is formed in the reactor and, hence, is not commercially feasible route for the production of syngas.

Because of the severe energy crisis, worldwide efforts are being made to find a novel energy efficient (or less energy intensive) route for the production of syngas with H_2/CO ratio of about 2.0, which is desirable for methanol and Fischer-Tropsch synthesis processes. Recently, a number of studies on catalytic partial oxidation of methane to syngas (which is exothermic and hence not at all energy intensive) with high conversion, selectivity and desirable H_2/CO ratio, operating at extremely short (1-10 ms) [4-11], moderate [12-18] and high [19] residence times has been reported. The catalysts used in

this process are as follows: NiO-CaO [4], NiO-MgO [5], NiO-rare earth oxides [6], Ni/Al₂O₃ [7,19], supported noble metals [8-11,14,15], and pyrochlore and perovskite oxides containing noble metals, Ni or Co, such as Ln₂Ru₂(or Ir₂)O₇ (Ln = lanthanide) [12,13], LaMO₃ (M = Ni, Rh or Co) [16], (CaSr)(TiNi or Co)O_{3-x} [17] and Ba₃NiRuTaO₉ [18]. Coupling of exothermic and endothermic reactions in methane-to-syngas conversion by carrying out the partial oxidation of methane simultaneously with steam reforming [20] and CO₂ reforming [21, 22] or both [23] over NiO-CaO catalyst has also been reported for eliminating hazards associated with the oxidative conversion process without losing its advantages, thus increasing the process feasibility [20, 23]. Simultaneous CO₂ and steam reforming of methane over supported noble metals [24] and NiO-CaO [25] has also been investigated earlier.

Although the pyrochlore and perovskite oxide catalysts containing noble metals viz. La₂Ru₂(or Ir₂)O₇ [12,13] and LaRhO₃ [16] showed excellent performance in the oxidative conversion of methane to syngas, their use in the process is limited because of their extremely high cost. The catalytic properties of LaNiO₃ perovskite are expected to be altered by partial substitution for La by Sr or Ca and for Ni by Co [26, 27]. It is, therefore, interesting to know the influence of the partial substitutions in LaNiO₃ on the catalytic activity/selectivity in the oxidative conversion of methane to syngas. The present investigation was undertaken for this purpose and also for studying the coupling of exothermic and endothermic reactions involved in the simultaneous oxidative conversion and steam and CO₂ reforming of methane to syngas over the perovskite oxide catalyst.

2.1.2 EXPERIMENTAL

2.1.2.1 Catalyst Preparation

The LaNiO₃, LaNi_{1-x}Co_xO₃, LaCoO₃ and La_{0.8}Ca(or Sr)_{0.2}NiO₃ perovskite catalysts were prepared by co-precipitation method as follows. An aqueous solution containing equimolar quantities of nitrates of La (with or without Ca or Sr in requisite amounts) and Ni or Co or both (in requisite amounts) was added slowly to the aqueous solution of sodium carbonate under continuous stirring over a period of 1 h (the amount of sodium carbonate was 25% excess than that required for the complete precipitation). The precipitate formed was kept overnight for ageing and then filtered and washed thoroughly with distilled water. It was dried in an air oven at 100°C for 15 h and then decomposed at 500°C in static air for 5 h. The decomposed mass was washed thoroughly with boiling distilled water to

remove the remaining traces of Na^+ , NO_3^- and CO_3^{2-} ions and then filtered and dried at 100°C for 15h. It was pressed binder-free to 25 mm diameter pellets, using 5 ton pressure. The pellets are calcined in air at 900°C for 15 h and crushed to 22-30 mesh size particles (bulk density of particles = $1.8\text{-}2.0\text{ g.cm}^{-3}$).

2.1.2.2 Catalyst Characterization

The perovskite structure of all the catalysts was confirmed by XRD using a Holland Philips, PW/1730 X-ray generator with the CuK_α radiation scintillation counter. The crystal size and morphology of the perovskite catalysts were determined by using a JSM 5200, JEOL scanning electron microscope. The surface area of the catalysts was measured by the single-point BET method by measuring the adsorption of nitrogen at liquid nitrogen temperature from a N_2 -He mixture containing 30 mol% N_2 , using a Monosorb Surface Area Analyzer (Quantachrome Corp., USA).

2.1.2.3 Catalytic Reaction

The schematic diagram of experimental set-up and the quartz reactor used for the catalytic partial oxidation of methane to syngas are shown in Figs. 2.1.1 and 2.1.2, respectively. For the catalytic oxidative conversion of methane in the presence of steam and/or CO_2 , the reactor shown in Fig. 1.1.2 (Chapter-1.1) was used.

The catalytic partial oxidation of methane-to-syngas with or without the steam and CO_2 reforming reactions was carried out by passing continuously a gaseous feed containing pure methane ($> 99.95\%$) and oxygen ($> 99.9\%$) with or without steam and CO_2 ($> 99.99\%$) over the catalyst packed in a quartz reactor at different process conditions. The oxidative conversion reaction was carried out using 0.02 g catalyst packed in 4 mm i.d. quartz reactor (Fig. 2.1.1). Whereas, the simultaneous oxidative conversion and steam and/or CO_2 reforming reactions were carried out using 0.3 g catalyst packed in 9 mm i.d. quartz reactor (Fig. 1.1.2). In both the cases, the reactor was kept in a tubular furnace and its temperature was measured/controlled by a Chromel-Alumel thermocouple provided in the center of the catalyst bed. The reaction temperature could be controlled within 5°C . The gas hourly space velocity (GHSV) of feed was measured at 0°C and 1 atm pressure. The gaseous products (after condensing the water from the product stream at 0°C) were analyzed by an on-line gas chromatography using a Spherocarb column at the following GC operating conditions :

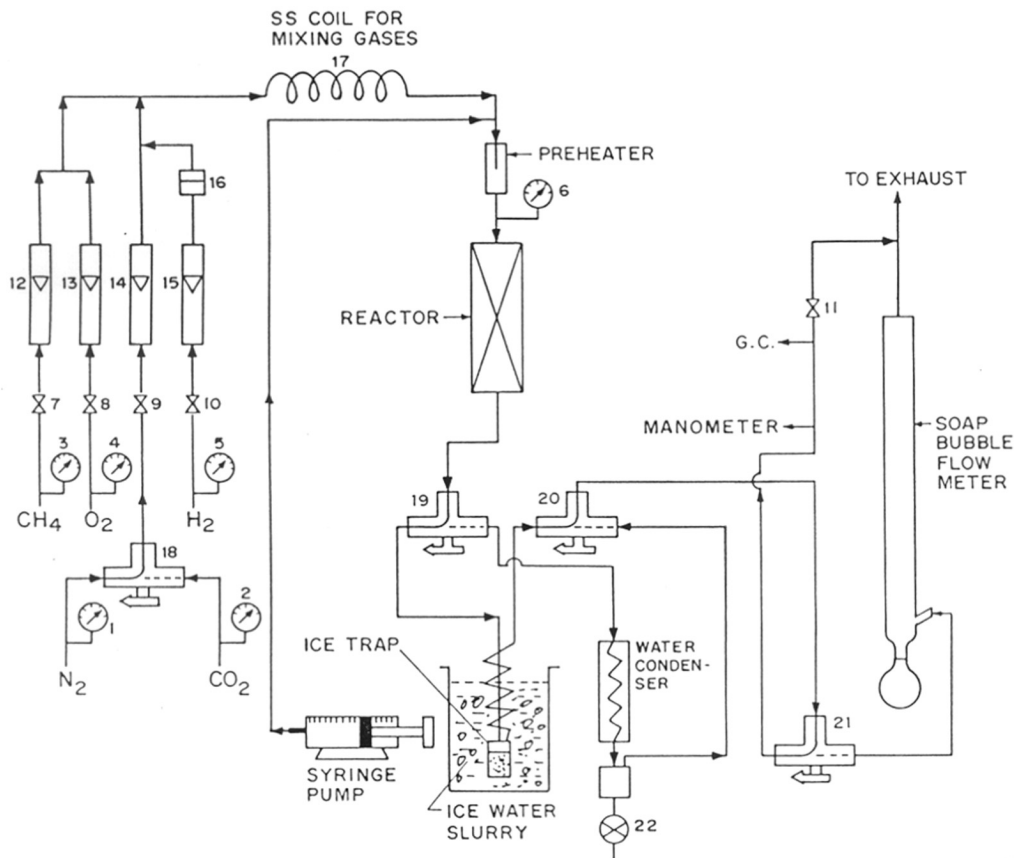


Fig. 2.1.1 : Experimental set-up for evaluation of catalyst performance in methane-to-syngas conversion [1-6 : Pressure gauges, 7-11 : Needle valves, 12-15 : Rotameters, 16 : Two way valve, 17 : S.S. coil (dia. = 1/4", L = 10 ft), 18-21 : Three way valves, 22 : Rota flow stop cocks]

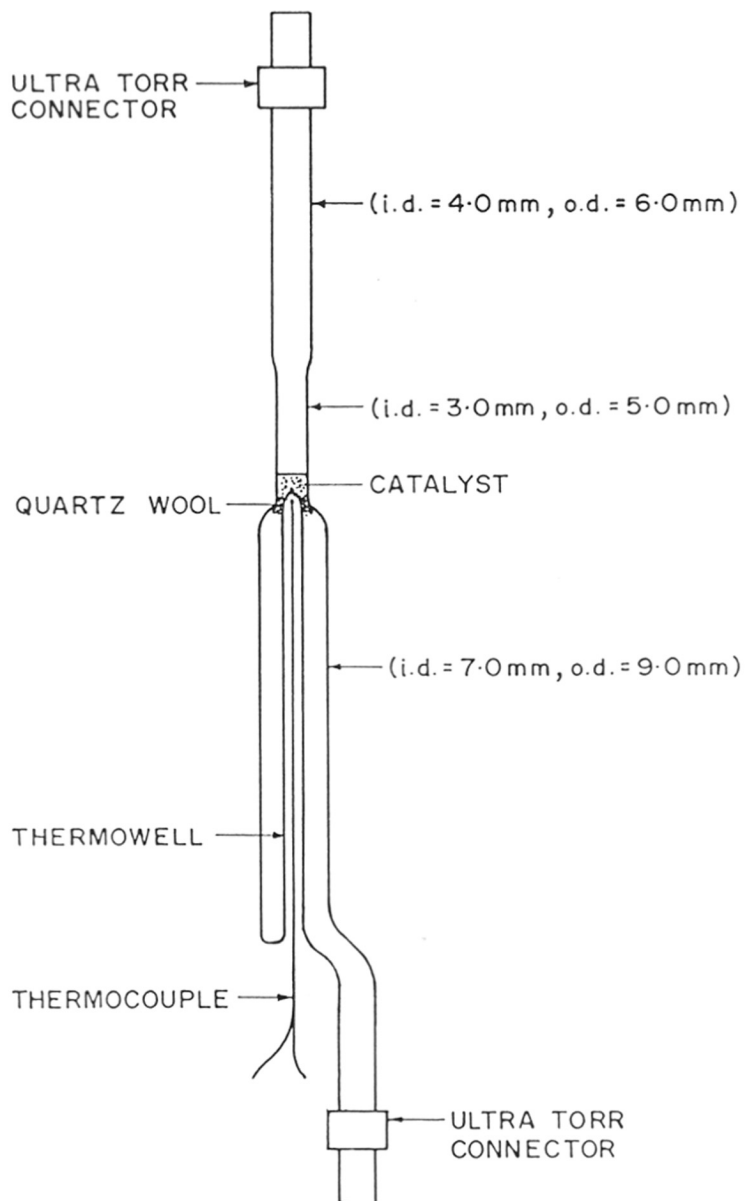


Fig. 2.1.2 : Quartz flow reactor for oxidative conversion of methane to syngas

Detector temperature	:	100°C
Injector temperature	:	100°C
Oven temperature	:	45°C
Current	:	132 mA
He-carrier gas flow rate	:	35 cm ³ .min ⁻¹

The methane conversion, CO-selectivity, H₂-selectivity, GHSV (gas hourly space velocity) and CO-productivity are defined/calculated as follows:

$$\text{Conversion (\%)} = \frac{\text{Reactant}|_{\text{Feed}} - \text{Reactant}|_{\text{product}}}{\text{Reactant}|_{\text{Feed}}} \times 100$$

$$\text{Selectivity (\%)} = \frac{\text{Conversion of reactant to a particular product}}{\text{Conversion of reactant}} \times 100$$

$$\text{GHSV (cm}^3\text{.g}^{-1}\text{.h}^{-1}\text{)} = \frac{\text{Total flow rate of feed gases (at }^\circ\text{C and 1 atm.) (cm}^3\text{.h}^{-1}\text{)}}{\text{wt. of catalyst (g)}}$$

$$\text{CO productivity (mol g}^{-1}\text{ h}^{-1}\text{)} = \frac{\text{GHSV} \times \text{FC of CH}_4 \times \text{MF of CH}_4 \times \text{FS of CO}}{22400}$$

where,	FC	=	Fractional conversion
	MF	=	Mole fraction
	FS	=	Fractional selectivity

2.1.3 RESULTS AND DISCUSSION

2.1.3.1 Catalyst Characterization

a) Surface area

Data showing the influence of partial or complete substitution of Ni by Co and also a partial substitution of La by Ca or Sr in LaNiO₃ perovskite on its surface area are presented in Table 2.1.1. The substitution at both the sides results in a decrease in the surface area of the perovskite. Its surface area is decreased continuously with increasing the extent of substitution of Ni by Co.

Table 2.1.1 : Surface area of perovskite oxide catalysts and their specific activity in oxidative conversion of methane to syngas at 800°C (feed = 64.3 mol% CH₄ and 35.7 mol% O₂, GHSV = 5.2 x 10⁵ cm³.g⁻¹.h⁻¹)

Perovskite composition	Surface area (m ² .g ⁻¹)	Specific activity (mmol.m ⁻² .s ⁻¹)		
		CH ₄ conversion	CO formation	H ₂ formation
LaNiO ₃	4.5	0.77	0.73	1.40
LaNi _{0.8} Co _{0.2} O ₃	4.1	0.64	0.54	0.92
LaNi _{0.6} Co _{0.4} O ₃	3.6	0.54	0.41	0.59
LaNi _{0.4} Co _{0.6} O ₃	3.4	0.54	0.32	0.43
LaNi _{0.2} Co _{0.8} O ₃	2.7	0.27	0.06	0.06
LaCoO ₃	2.4	0.12	0.09	0.00
La _{0.8} Ca _{0.2} NiO ₃	4.1	0.65	0.56	0.81
La _{0.8} Sr _{0.2} NiO ₃	3.5	0.48	0.29	0.38

b) X-ray diffraction (XRD)

XRD spectras of LaNi_{1-x}Co_xO₃ oxides (where x = 0-1), confirming their perovskite-type structure, are shown in Fig. 2.1.3. The spectra of LaNiO₃ before and after the simultaneous oxidative methane conversion and steam and CO₂ reforming reactions (at 850°C, CH₄/O₂ = 2.1, CH₄/CO₂ = CH₄/H₂O = 12, GHSV = 43,100 cm³.g⁻¹.h⁻¹) are also compared in Fig. 2.1.3. The comparison reveals that, after the reaction, the perovskite (LaNiO₃) undergoes a drastic structural change : LaNiO₃ → La₂O₃ + Ni⁰. The reduction of Ni³⁺ from the perovskite to metallic Ni is expected [26, 28] due to the syngas (H₂ + CO) produced in the reaction. The used catalyst shows a presence of La(OH)₃ phase along with Ni⁰. The formation of the La(OH)₃ phase is due to hydrolysis of La₂O₃ by steam during the reaction and also by the exposure of the used catalyst to atmospheric moisture. In earlier studies also, Ni/La₂O₃ [29] and Ni on lanthanum modified alumina [30] showed high activity/selectivity and stability

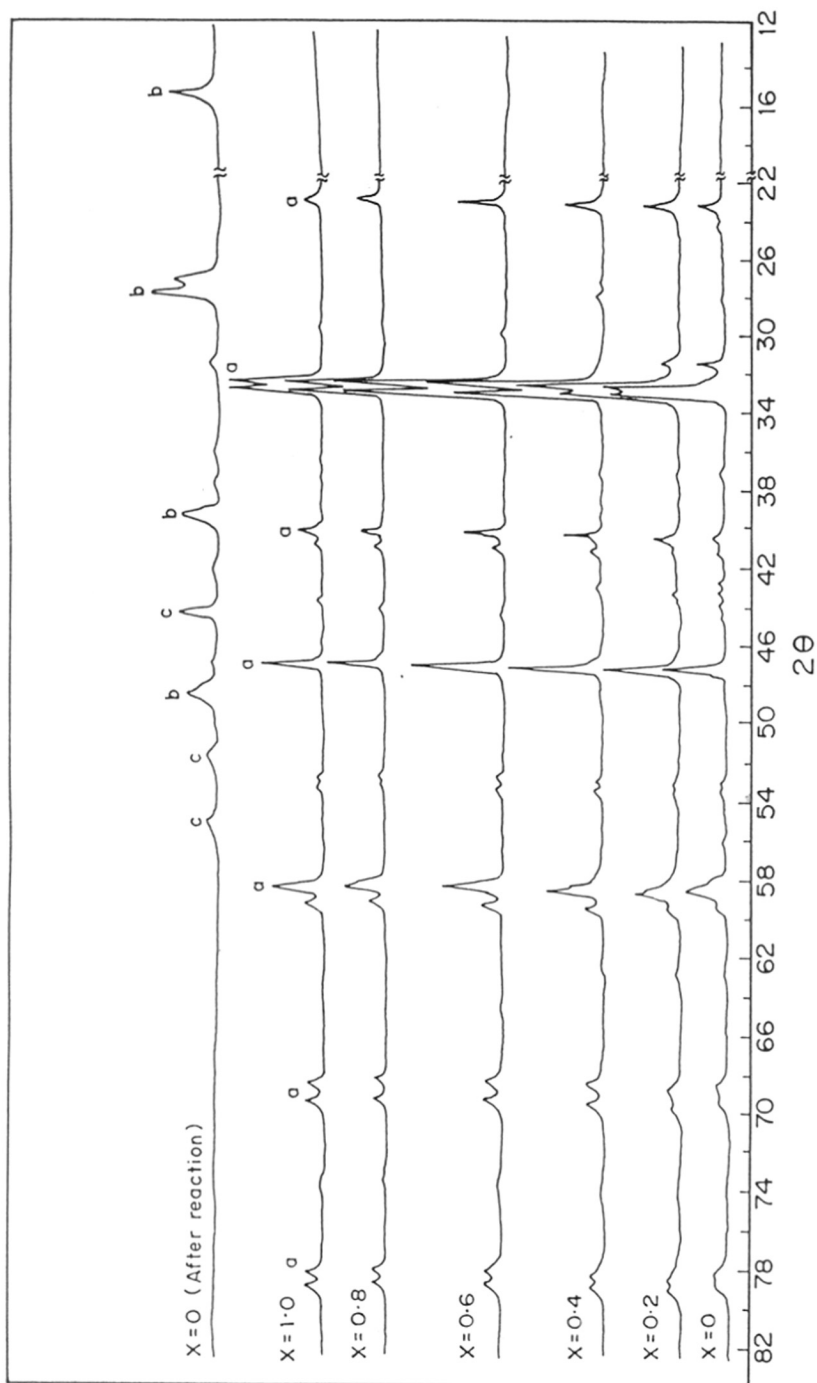


Fig. 2.1.3: XRD spectra of $\text{LaNi}_{1-x}\text{Co}_x\text{O}_3$ (where $x = 0, 0.2, 0.4, 0.6, 0.8, 1.0$) perovskite oxides before reaction and of LaNiO_3 after reaction (crystalline phases : a, perovskite; b, $\text{La}(\text{OH})_3$ and c, Ni^0).

in the CO₂ reforming of methane. The initial catalytic activity of supported Ni catalysts was found to be dependent upon metallic nickel phase [31].

c) Scanning electron microscope (SEM) studies

Scanning electron micrograms (SEM) of the LaNiO₃, LaNi_{0.4}Co_{0.6}O₃ and LaCoO₃ perovskites, before and after the oxidative conversion of methane to syngas (at 800°C) are presented in Fig. 2.1.4. A comparison of the catalysts before and after the reaction shows that the crystal size and morphology of the catalysts are changed after the reaction. This is expected because of the structural breakdown of the perovskites, resulting from their reduction by the H₂ and CO produced in the methane conversion reactions, followed by recrystallization of their reduction products (viz. La₂O₃ and partially and/or completely reduced Ni and Co-oxide species. After the use of the perovskites, the size of crystals for LaCoO₃ is larger than that for LaNiO₃. This coincides with the poor performance of LaCoO₃ (Fig. 2.1.5).

Earlier studies [32] showed that LaCoO₃ perovskite prepared from metal nitrate solutions contains amorphous Co₃O₄ impurity indicated by evaluation of oxygen (150 μmol.g⁻¹) between 527 - 837°C. However, in the present case, the amount of O₂ evolved from the LaCoO₃ is found to be much smaller (31.5 μmol.g⁻¹) indicating only a very small Co₃O₄ impurity. Nevertheless, the Co₃O₄ impurity alongwith the perovskite is expected to be reduced [26] in the initial period of the reaction, resulting in Co/La₂O₃ or Ni-Co/La₂O₃.

2.1.3.2 Oxidative Conversion of Methane to Syngas

The oxidative conversion of methane to syngas over the perovskite oxide catalysts was carried out at atmospheric pressure, using a mixture of pure methane and oxygen with CH₄/O₂ mole ratio of 1.8 as a feed at a GHSV of 5.2 × 10⁵ cm³.g⁻¹.h⁻¹. The catalysts are compared for their specific catalytic activity in Table 2.1.1.

Figure 2.1.5 shows the influence of the partial and complete substitution of Ni by Co in LaNiO₃ on its activity/selectivity in the oxidative conversion of methane to syngas at 800°C and extremely small contact time (≈ 0.8 ms). Both the conversion and the selectivity for CO and H₂ and consequently the CO space-time-yield are decreased with increasing the substitution of Ni by Co. The H₂/CO product ratio is also decreased with increasing the substitution, the decrease being very pronounced for the complete substitution of Ni by Co. These results reveal that, LaNiO₃ is highly

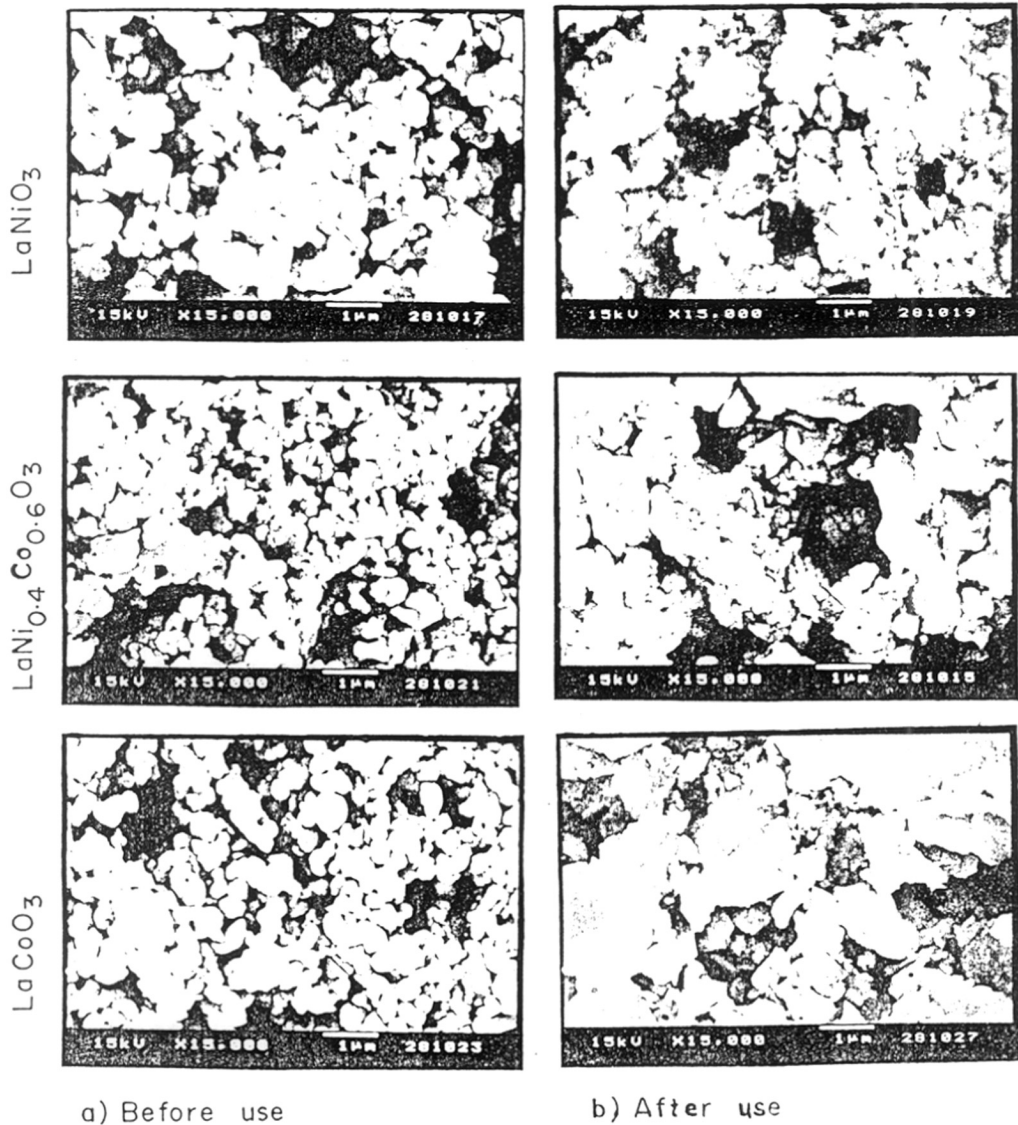


Fig. 2.1.4: SEM of LaNiO_3 , $\text{LaNi}_{0.4}\text{Co}_{0.6}\text{O}_3$ and LaCoO_3 perovskite oxides (before and after the oxidative conversion of methane to syngas at 800°C).

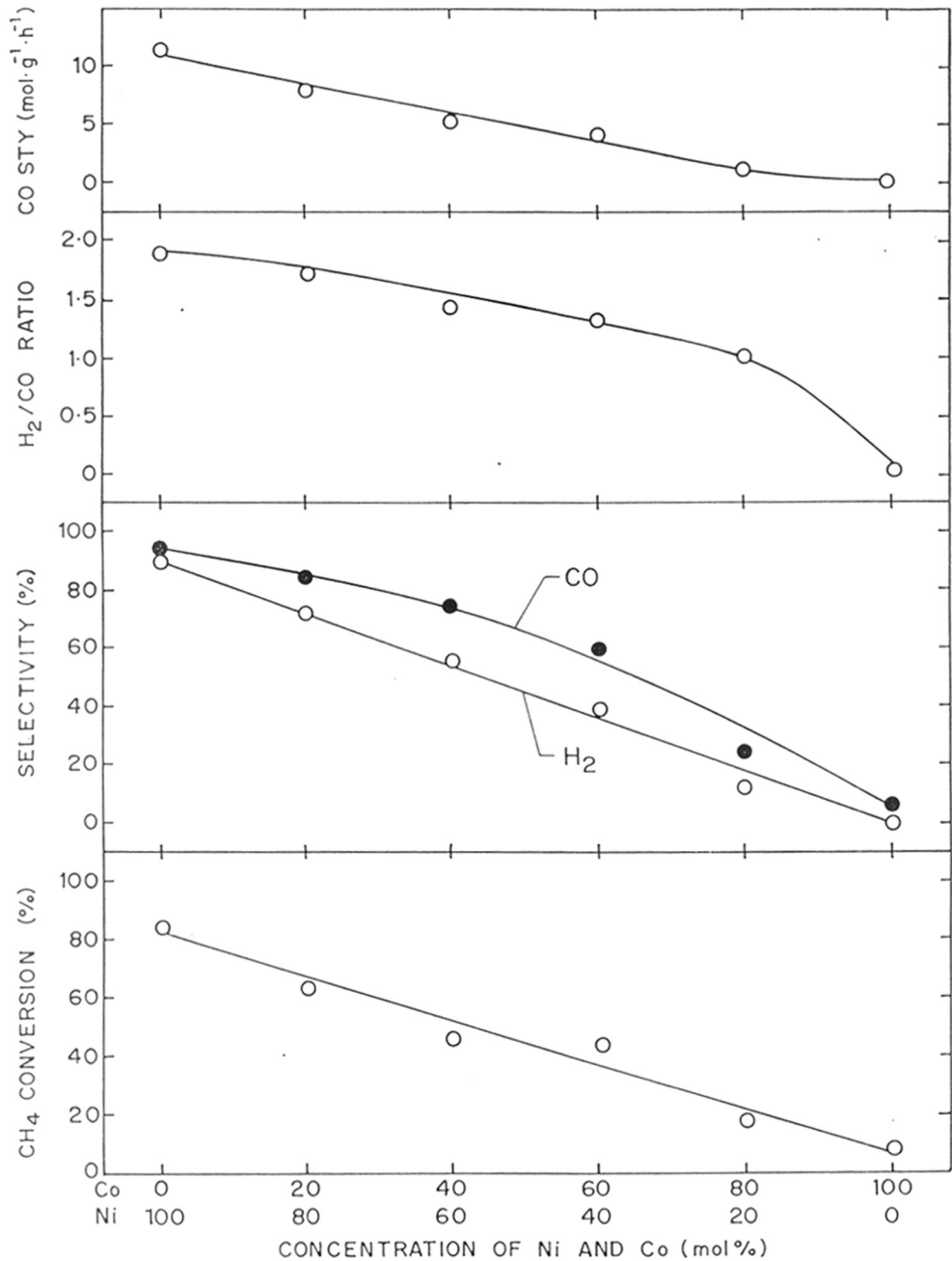


Fig. 2.1.5 : Influence of relative concentration of Ni and Co in $\text{LaNi}_{1-x}\text{Co}_x\text{O}_3$ perovskite on conversion, selectivity and space-time-yield in the oxidative conversion of methane to syngas at 800°C [$\text{CH}_4/\text{O}_2 = 1.8$ and $\text{GHSV} = 5.2 \times 10^5 \text{ cm}^3 \cdot \text{g}^{-1} \cdot \text{h}^{-1}$].

active and selective in the reaction but LaCoO_3 is much less active and not at all selective catalyst for the partial oxidation of methane to syngas. This is consistent with the fact that the latter is a good combustion catalyst [26, 27].

The selectivity (for H_2 and CO) of LaNiO_3 is almost same as that of the $\text{NiO-La}_2\text{O}_3$ [6], a non-perovskite catalyst, but the former is more active in the oxidative conversion of methane to syngas. This is probably because of a high dispersion and/or an uniform distribution of Ni^0 in the matrix of La_2O_3 due to the reduction of LaNiO_3 to $\text{Ni}^0/\text{La}_2\text{O}_3$ by the syngas produced during the initial period of the reaction. The reduction of LaNiO_3 by H_2 at different conditions has been reported earlier [26, 28, 33, 34]. Earlier studies on CaRuO_3 [35], LaCoO_3 [36] and LaNiO_3 [37] perovskites indicated that by reduction treatment, the metal (Ru, Co and Ni) is in highly disperse state on a matrix composed of the respective metal oxide. In the present case also, the average crystal size of Ni^0 (31.3 nm) for LaNiO_3 (after use/reaction), obtained from the XRD line broadening, is found to be much smaller than that (125 nm) for $\text{NiO-La}_2\text{O}_3$ [6].

The influence of temperature on the activity/selectivity of LaNiO_3 in the oxidative methane-to-syngas conversion is shown in Fig. 2.1.6. The results indicate that not only the conversion but also the selectivity for both H_2 and CO is increased with increasing the reaction temperature. The increase in the selectivity is consistent with the fact that the formation of H_2 and CO in the oxidative conversion of methane is thermodynamically favored at the higher temperatures. This is because of the fact that the water gas shift reaction ($\text{CO} + \text{H}_2\text{O} \rightleftharpoons \text{CO}_2 + \text{H}_2$), which governs H_2/CO ratio, is favored at lower temperatures (below 700°C).

The time-on-stream activity/selectivity of LaNiO_3 in the reaction at 800°C is shown in Fig. 2.1.7. There is no significant change in both the activity and selectivity of the catalyst for a time-on-stream of 10 h.

The time-on-stream activity and selectivity data for the $\text{La}_{0.8}\text{Ca}_{0.2}\text{NiO}_3$ and $\text{La}_{0.8}\text{Sr}_{0.2}\text{NiO}_3$ catalysts are included in Fig. 2.1.7. The results reveal that both the catalysts have poor activity and selectivity as compared to that of LaNiO_3 and also their activity and selectivity are decreased pronouncedly with increasing the time-on-stream, indicating their fast deactivation during the catalytic process. This leads to the conclusion that the partial substitution of La by Ca or Sr in LaNiO_3 results in a catalyst with inferior performance in the oxidative conversion of methane to syngas.

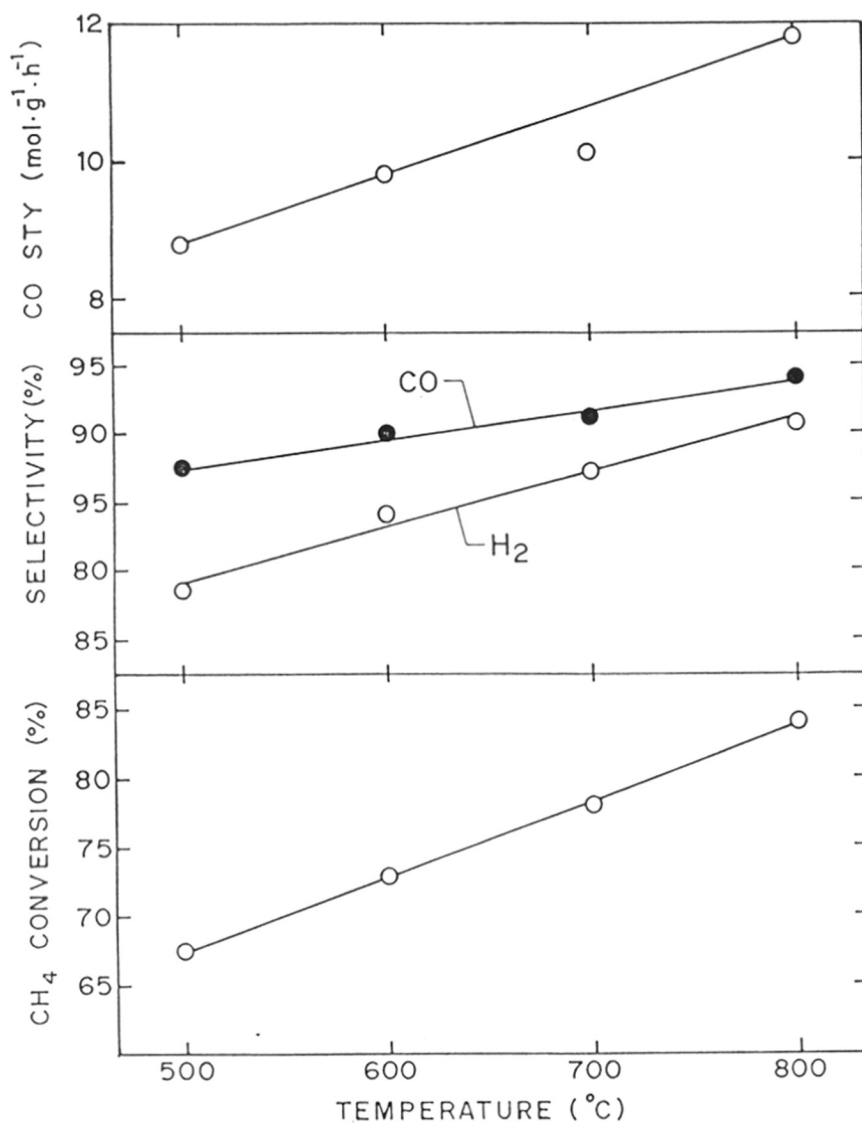


Fig. 2.1.6: Influence of temperature on conversion, selectivity and space-time-yield in the oxidative conversion of methane to syngas over LaNiO_3 perovskite catalyst [$\text{CH}_4/\text{O}_2 = 1.8$ and $\text{GHSV} = 5.2 \times 10^5 \text{ cm}^3 \cdot \text{g}^{-1} \cdot \text{h}^{-1}$].

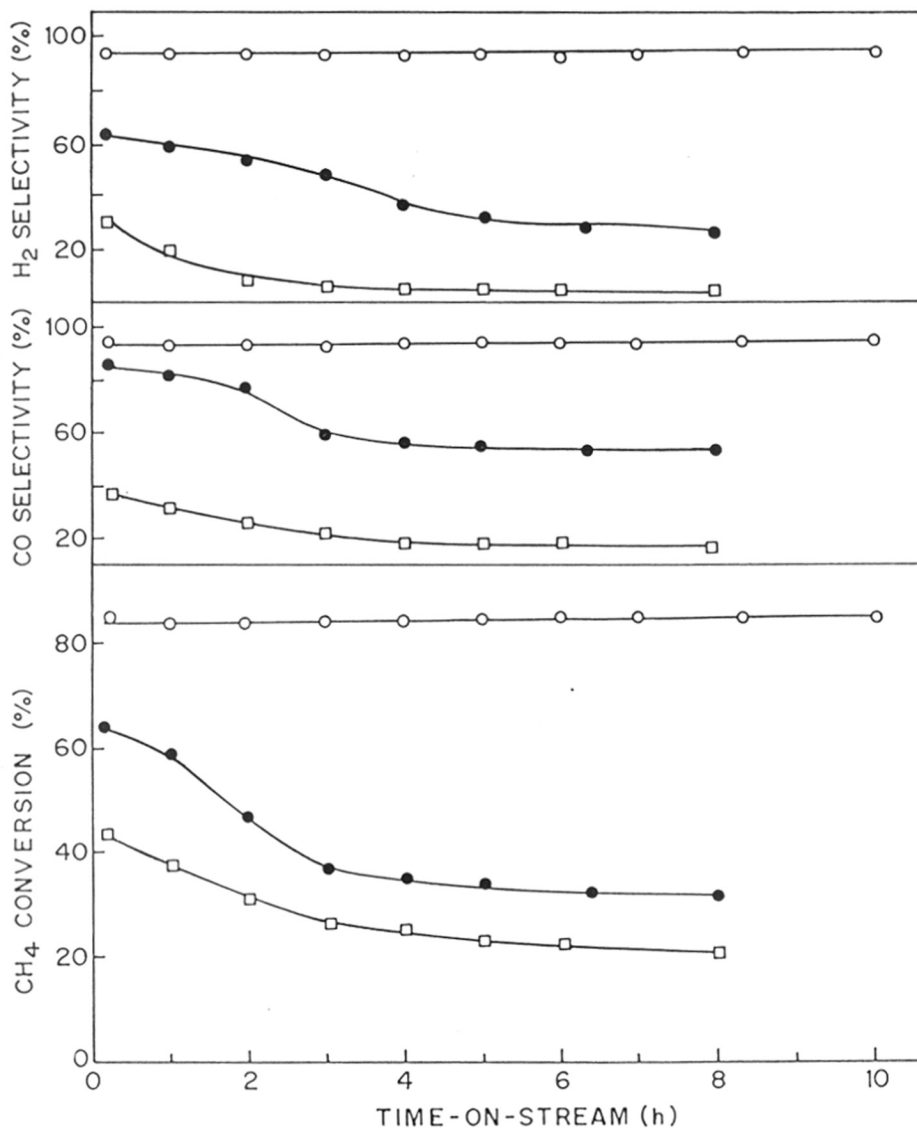


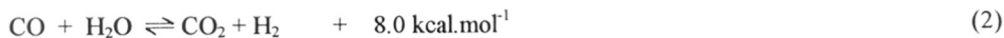
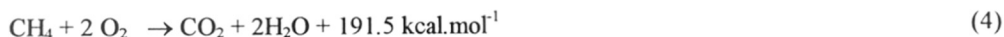
Fig. 2.1.7: Time-on-stream activity/selectivity of LaNiO₃ (○), La_{0.8}Ca_{0.2}NiO₃ (●) and La_{0.8}Sr_{0.2}NiO₃ (□) catalysts in oxidative conversion of methane to syngas at 800°C [CH₄/O₂ = 1.8 and GHSV = 5.2 × 10⁵ cm³·g⁻¹·h⁻¹].

2.1.3.3 Simultaneous Oxidative Conversion and Steam and CO₂ Reforming of Methane to Syngas

Results of the reactions of methane with O₂, CO₂ and steam, occurring simultaneously over LaNiO₃ perovskite, at different temperatures (at CH₄/O₂ = 2.1, CH₄/H₂O = CH₄/CO₂ = 12 and GHSV = 43,100 cm³.g⁻¹.h⁻¹) and CH₄/O₂ feed ratios [at 850°C, CH₄/(O₂ + 0.5CO₂ + 0.5H₂O) = 1.8, CO₂/H₂O = 1, GHSV = 47,200 cm³.g⁻¹.h⁻¹] are summarized in Figs. 2.1.8 and 2.1.9. The negative conversion of CO₂ and H₂O observed at temperatures < 800°C (Fig. 2.1.8), is just indicative of the formation of CO₂ and H₂O in the process, respectively. However, when the conversion of CO₂ and H₂O is ≥ 0, the selectivity (based on methane) for CO and H₂, respectively, is 100%. The net heat of reaction (ΔH_r) for the overall process is estimated by subtracting the heat of formation (at the process temperature) of the components in the feed from that of components in the product stream.

In this catalytic process, following exothermic and endothermic reactions are expected to occur simultaneously.

Exothermic reactions



Endothermic reactions



Results (Figs. 2.1.8 and 2.1.9) show that high methane conversion (> 90%) with almost 100% selectivity for both H₂ and CO (particularly when the conversion of H₂O and CO₂ is zero or positive) and H₂/CO product ratio of about 2.0 (which is suitable for methanol synthesis and Fischer-Tropsch processes) at very high space velocity (≈ 45,000 cm³.g⁻¹.h⁻¹) could be attained in this process. Because of the coupling of exothermic oxidation and the endothermic CO₂ and steam reforming reactions (reactions 1-5) over the same catalyst, this process can be made mildly endothermic, almost thermoneutral or mildly exothermic simply by manipulating the process conditions, particularly the reaction temperature and/or CH₄/O₂ ratio in the feed. Thus, this process can occur with requiring little or no external energy. The heat produced in the process or its exothermicity is decreased markedly

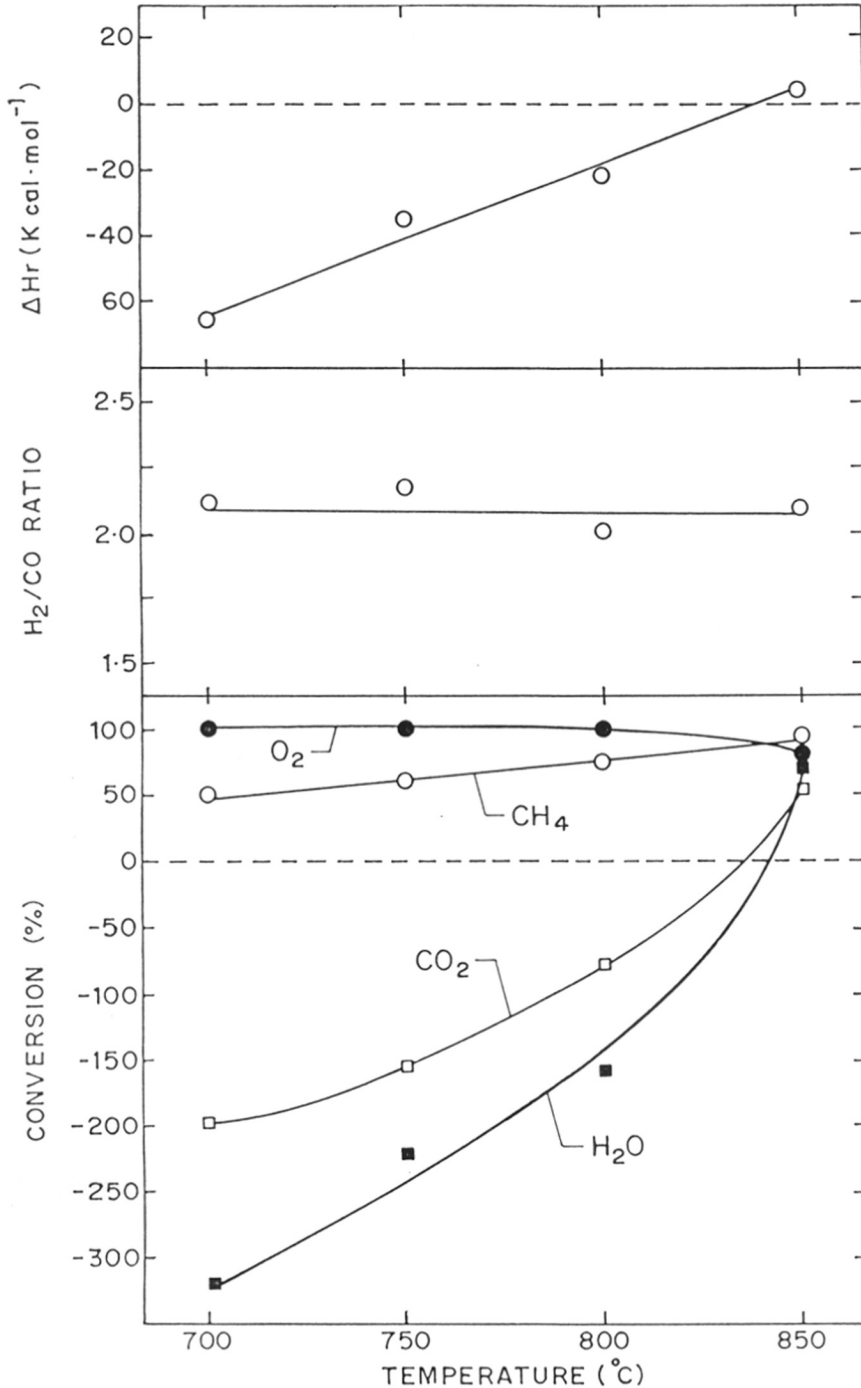


Fig. 2.1.8 : Influence of temperature on conversion, H_2/CO product ratio and net heat of reaction (ΔH_r) in the oxidative conversion of methane to syngas in presence of steam and CO_2 in the feed [$\text{CH}_4/\text{O}_2 = 2.1$, $\text{CH}_4/\text{H}_2\text{O} = \text{CH}_4/\text{CO}_2 = 12.0$ and $\text{GHSV} = 43,100 \text{ cm}^3\cdot\text{g}^{-1}\cdot\text{h}^{-1}$].

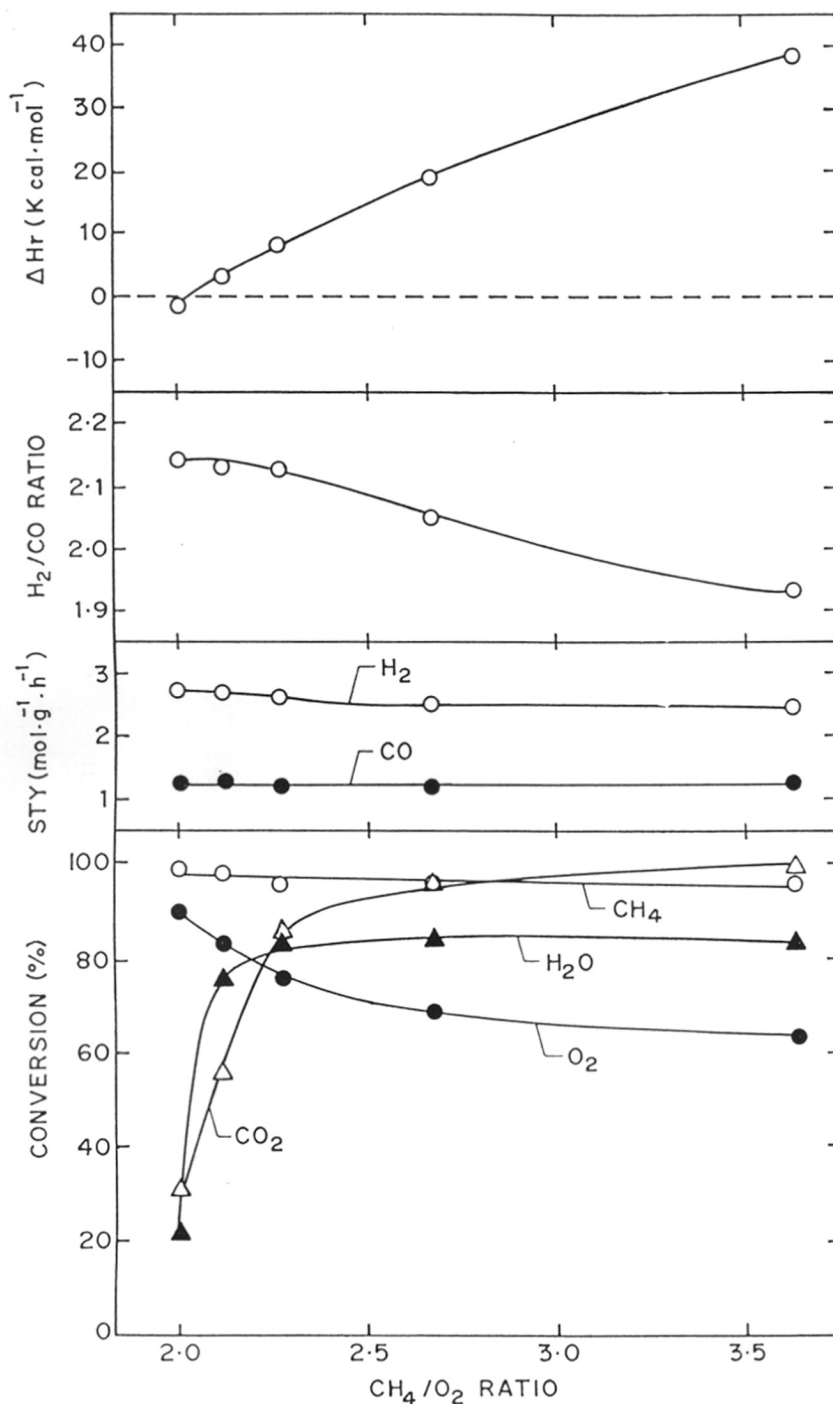


Fig. 2.1.9 : Influence of CH_4/O_2 ratio in the feed on conversion, space-time-yield, H_2/CO ratio and net heat of reaction (ΔH_r) in the simultaneous oxidative conversion, steam reforming and CO_2 reforming of methane to syngas at 850°C [$\text{CH}_4/(\text{O}_2 + 0.5\text{CO}_2 + 0.5\text{H}_2\text{O}) = 1.8$, $\text{CO}_2/\text{H}_2\text{O} = 1.0$ and $\text{GHSV} = 47,200 \text{ cm}^3 \cdot \text{g}^{-1} \cdot \text{h}^{-1}$].

with increasing the reaction temperature (Fig. 2.1.8) and/or CH_4/O_2 ratio in the feed (Fig. 2.1.9) due to the increase in the rate of endothermic steam and CO_2 reforming of methane (reactions 1 and 5). Since, the heat produced in the exothermic reactions (reactions 2-4) is used instantly in the endothermic reactions (reactions 1 and 5), the process is expected to occur in a most energy efficient manner, and also without forming hot spot on the catalyst, consequently avoiding reaction runaway conditions.

2.1.4 CONCLUSIONS

LaNiO_3 perovskite has a high potential as a catalyst for the selective partial oxidation of methane to syngas at extremely short contact time (≈ 0.8 ms). During the catalytic process, it is however transformed to $\text{Ni}^0/\text{La}_2\text{O}_3$, which is an active form of the catalyst during its operation in the catalytic process. However, the perovskite with partial substitution of its La by Ca or Sr or with partial or complete substitution of its Ni by Co shows inferior performance in the catalytic process. By carrying out the simultaneous oxidative conversion and steam and CO_2 reforming of methane over LaNiO_3 perovskite at $800\text{-}850^\circ\text{C}$ and high space velocity (contact time ≈ 9 ms), syngas (with H_2/CO ratio of about 2.0) can be obtained with high conversion ($> 90\%$) and almost 100% selectivity (based on methane) for both H_2 and CO , while the process is operated in a most energy efficient manner, requiring little or no external energy because of the coupling of exothermic oxidative conversion and endothermic steam and CO_2 reforming reactions over the same catalyst.

REFERENCES

1. R.E. Kirk and D.F. Othmer, eds., *Encyclopedia of Chemical Technology*, Vol. 12, 3rd Edn. (Wiley Interscience, New York, 1990) P. 398.
2. *Ullmann's Encyclopedia of Industrial Chemistry*, Vol. A 12, 5th revised Edn., (VCH Weinheim, 1989) P. 169.
3. A. Jess and K. Hedden, *Erdöl Erdgas Kohle*, 110 (1994) 365.
4. V.R. Choudhary, A.M. Rajput and B. Prabhakar, *Catal. Lett.*, 15 (1992) 363.
5. V.R. Choudhary, A.S. Mamman and S.D. Sansare, *Anew. Chem. Int.Ed.Engl.*, 31 (1992) 1189.
6. V.R. Choudhary, V.H. Rane and A.M. Rajput, *Catal. Lett.*, 22 (1993) 289.
7. V.R. Choudhary, A.M. Rajput and B. Prabhakar, *J. Catal.*, 139 (1993) 326.
8. L.D. Schmidt and D.A. Hickman, *Science*, 259 (1993) 343, *J. Catal.*, 138 (1992) 267.
9. D.A. Hickman, E.A. Haufear and L.D. Schmidt, *Catal.Lett.*, 17 (1993) 223.
10. P.M. Tornianan, X.. Chu, and L.D. Schmidt, *J.Catal.*, 146 (1994) 1.
11. J.A. Lapszewicz and X.Z. Jiang, *Prepr. Am. Chem. Soc., Div. Petr. Chem.*, 37 (1992) 252.
12. A.T. Ashcroft, A.K. Cheetham, J.S. Food, M.L.H. Green, C.P. Gray, A.G. Murrell, and P.D.F. Vernon, *Nature*, 344 (1990) 319.
13. R.H. Jones, A.T. Aschroft, D. Waller, A.K. Cheetham, and J.M. Thomas, *Catal.Lett.*, 8 (1991) 169.
14. P.D.F. Vernon, M.L.H. Green, A.K. Cheetham and A.T. Ashcroft, *Catal.Lett.*, 6 (1990) 181.
15. A.K. Bhattacharaya, J.A. Breach, S. Chand, D.K. Ghorai, A. Hartridge, J. Keary and K.K. Mallick, *Appl. Catal. A: General*, 80 (1992) L1.
16. Slagtern, A°, and Oslybe, V., *Appl.Catal. A: General*, 110 (1994) 99.
17. T. Hayakawa, A.G. Andersen, M. Shimizu, K. Suzuki and K. Takehira, *Catal. Lett.*, 22 (1993) 307.
18. P.D. Battle, J.B. Claridge, F.A. Coppystone, S.W. Carr and S.C. Tsang, *Appl.Catal. A: General*, 118 (1994) 217.
19. D. Dissanayake, M.P. Rosynek, K.C.C. Kharas, and J.H. Lunsford, *J.Catal.*, 132 (1992) 117.
20. V.R. Choudhary, A.M. Rajput and B. Prabhakar, *207th Annual ACS Meeting San Diego*, March 13 - 18, 1994 (in the symposium on Methane and Alkane Conversion Chemistry).
21. A.T. Ashcroft, A.K. Cheetham, J.S. Food, M.L.H. Green, C.P. Gray, A.G. Murrell and P.D.F. Vernon, *Nature*, 344 (1990) 319
22. V.R. Choudhary, A.M. Rajput and B. Prabhakar, *Catal. Lett.*, 32 (1995) 391.
23. V.R. Choudhary, A.M. Rajput and B. Prabhakar, *Angew. Chem. Int. Ed. Engl.*, 33 (1994) 2104.
24. D. Qin and J.A. Lapszewicz, *Catal. Today*, 21 (1994) 551

25. V.R. Choudhary and A.M. Rajput, *Ind. Eng. Chem. Res.*, .
26. L.G. Tejuca, J.L.G. Fierro and J.M.D. Tascon, *Adv. Catal.*, 36 (1989) 237.
27. T. Seiyama, *Catal. Rev. Sci. Eng.*, 34 (1992) 281.
28. J.L.G. Fierro and L.G. Tejuca, *J.Catal.*, 87 (1989) 126.
29. Z. Zhang and X.E. Verykios, *J. Chem. Soc. Chem. Commun.*, (1995) 71.
30. R. Blom, I.M. Dahl, A. Slagtern, B. Sortland, A. Spjelkavik and E. Tangstad, *Catal. Today*, 21 (1994) 535.
31. H.M. Swaan, V.C.H. Kroll, G.A. Martin and C. Mirodatos, *Catal. Today*, 21 (1994) 571.
32. A. Baiker, P.E. Marti, P. Keusch, E. Fritsch and A. Reller, *J. Catal.*, 146 (1994) 268.
33. J.L.G. Fierro, J.M.D. Tascon and L.G. Tejuca, *J.Catal.*, 89 (1984) 209.
34. J.L.G. Fierro, J.M.D. Tascon and L.G. Tejuca, *J.Catal.*, 93 (1985) 83.
35. A. Reller, G. Davoodabady, A. Portmann and H.R. Oswald, *Proc. Eur. Congr. Electron Microsc.*, 8th, Budapest (1984) 1165.
36. M. Crespin and W.K. Hall, *J. Catal.*, 69 (1981) 359.
37. M. Crespin, P. Levitz and L. Gatineau, *J. Chem. Soc. Faraday Trans II*, 79 (1983) 1181.

CHAPTER - 2.2

PARTIAL OXIDATION OF METHANE TO SYNGAS WITH OR WITHOUT SIMULTANEOUS CO₂ AND STEAM REFORMING REACTIONS OVER Ni/AlPO₄

2.2.1 INTRODUCTION

Energy efficient conversion of methane to syngas (a mixture of CO and H₂, which is a versatile feedstock for methanol, ammonia and different Fischer-Tropsch synthesis processes and also for the carbonylation and hydroformylation processes) is of great practical importance. In the past few years several studies have been reported on the use of nickel containing catalysts such as Ni/Al₂O₃ [1,2], NiO-MgO [3], NiO-CaO [4,5], and NiO-rare earth oxides [6,7], in the oxidative conversion of methane to syngas. Studies of NiO-CaO [8-10] in the coupling of exothermic oxidative conversion with the endothermic steam and/or CO₂ reforming of methane to syngas aimed at making the overall process more energy efficient and safe to operate.

Very recently, PdY [11,12] and NiY [13] zeolites have been used for the oxidative conversion of methane to CO and H₂ and for the CO₂ reforming of methane, respectively. The PdY, after reduction-reoxidation treatment, showed excellent activity and selectivity at 527°-727°C. The NiY also showed high catalytic activity in the reforming of methane with CO₂ at 577°C; the higher CO₂ conversion was, however, obtained over Ni supported on the non-acidic zeolite. Since, microporous crystalline aluminophosphates (e.g. ALPO-5) and silica (e.g. silicalite) molecular sieves have an electrically neutral framework with no ion exchange capacity, it is interesting to study the oxidative conversion of methane to syngas over Ni supported on these micoporous zeolite-like materials. The present investigation was, therefore, undertaken with the objective of studying the catalytic activity and selectivity in the partial oxidation of methane to CO and H₂ and also in the simultaneous oxidative conversion with the CO₂ and/or steam reforming of methane to syngas over NiO/ALPO-5 and NiO/silicalite-I catalysts.

2.2.2 EXPERIMENTAL

2.2.2.1 Catalyst Preparation

NiO/ALPO-5 and NiO/silicalite-I catalysts, both containing 16.4 wt.% NiO, were prepared by impregnating ALPO-5 (Al/P = 1.0) and silicalite-I (Si/Al > 10,000) with nickel nitrate from its aqueous solution by incipient wetness technique. This was followed by drying at 110°C for overnight, pressing binder-free, crushing to 22-30 mesh size particles and finally calcining at 900°C in static air for 4h. The preparation and the characterization of the ALPO-5 molecular sieve were given earlier [14]. The silicalite-I (a high silica ZSM) used in the catalyst preparation was that (silicalite Sr. No. S8 of ref. 14) prepared and characterised earlier [15]. The samples of ALPO-5 and silicalite-I, prepared earlier in our group by Dr. D.B. Akolekar [14, 15], have been used in the present study.

2.2.2.2 Catalytic Reaction

The schematic diagrams of experimental set-up and the quartz reactor used for catalytic partial oxidation of methane to syngas are shown in Figs. 2.1.1 and 2.1.2 (Chapter-2.1), respectively. For the catalytic oxidative conversion of methane in the presence of steam and/or CO₂, the reactor shown in Fig. 1.1.2 (Chapter- 1.1) was used.

The catalytic methane-to-syngas conversion reactions were carried out by passing continuously a gaseous feed containing pure methane (> 99.95%), oxygen (> 99.9%) with or without steam and CO₂ (99.99%) over the catalyst in a quartz microreactor at different process conditions. The reaction temperature was measured by a Chromel-Alumel thermocouple provided in the center of the catalyst bed. The gaseous products (after condensing the water from the product stream at 0°C) were analysed by on-line gas chromatography using a Spherocarb column. The C, H and O balances across the reactor were within about 2-5% error.

2.2.2.3 Catalyst Characterization

The NiO/ALPO-5 (before and after the simultaneous methane oxidative conversion and steam and/or CO₂ reforming reactions) and NiO/silicalite-I (before and after reduction by hydrogen at 800°C for 2 h) catalysts were subjected for their characterization by XRD (using Philips PW 1700 X-ray generator nickel filtered CuK_α radiation and a scintillation counter) and also by measuring

their N₂ sorption capacity at liquid nitrogen temperature (partial pressure of N₂ = 30 kPa) (using a Monosorb Surface Area Analyzer, Quanta-Chrome, USA).

2.2.3 RESULTS AND DISCUSSION

2.2.3.1 Catalyst Characterization

XRD spectra of NiO/ALPO-5, before and after reaction (simultaneous oxidative conversion and CO₂ and steam reforming of methane to syngas at 850°C, CH₄/O₂ = 2.1, CH₄/CO₂ = CH₄/H₂O = 10.0, GHSV = 47,000 cm³.g⁻¹.h⁻¹ and time-on-stream = 6 h), are presented in Fig. 2.2.1. Whereas, the spectra of NiO/silicalite-I, before and after reduction by H₂ at 800°C for 2 h, are shown in Fig. 2.2.2. The crystalline phases observed in these catalysts are listed in Table-2.2.1.

Table 2.2.1 : Crystalline phases and N₂ sorption capacity of ALPO-5 with and without catalyst loading.

Catalyst	Crystalline phases observed		N ₂ sorption (at 78 K)
	Major	Minor	
ALPO-5	AlPO ₄ -5	-	1.7
NiO/ALPO-5 (Unreduced, before reaction)	NiO AlPO ₄ -5	Tridymite	0.8
NiO/ALPO-5 (after reaction)	Ni ⁰ Tridymite	-	0.5
Silicalite-I	Silicalite-I	-	4.9
NiO/Silicalite-I (Unreduced)	NiO Silicalite-I	-	4.1
NiO/Silicalite-I (reduced at 800°C)	Ni ⁰ Silicalite-I	-	3.6

A comparison of the XRD spectra (Fig. 2.2.1) indicates that, by the deposition of NiO, the crystal structure of ALPO-5 is not affected except for a small phase transformation from ALPO-5 to tridymite. However, after the reaction, there is a drastic change in the crystal structure and

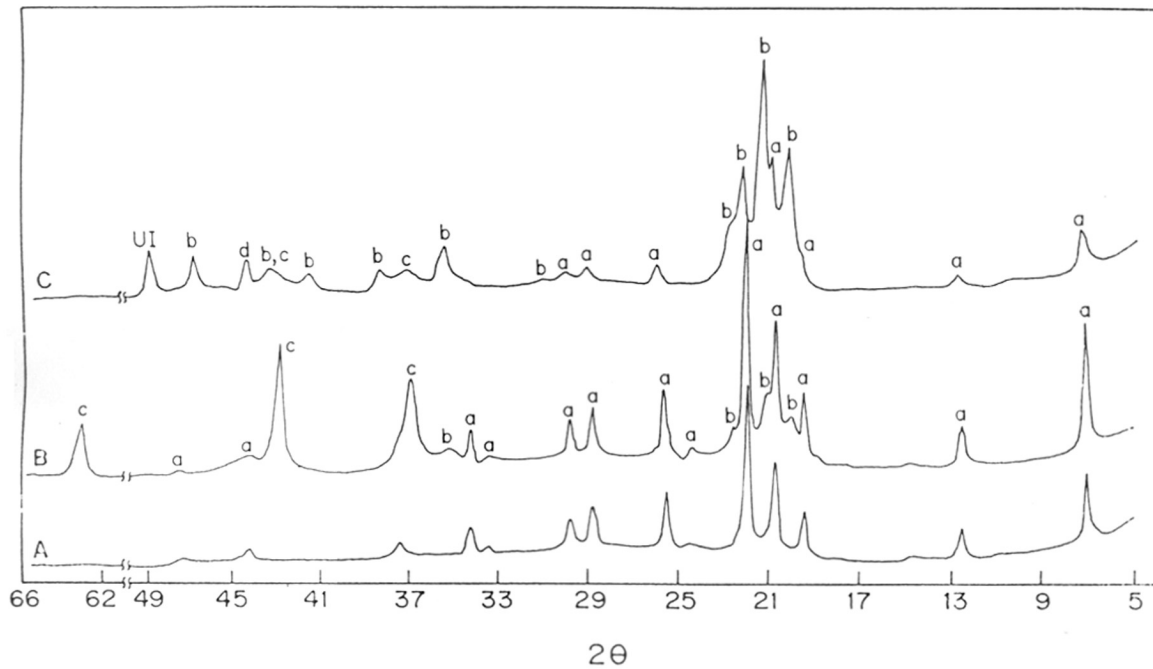


Fig. 2.2.1 : XRD spectra of a)ALPO-5 b)NiO/ALPO-5 (before reaction) and c)NiO/ALPO-5 (after reaction) [crystalline phases : a, $\text{ALPO}_4\text{-5}$; b, Tridymite; c, NiO; d, Ni^0 and UI, unidentified].

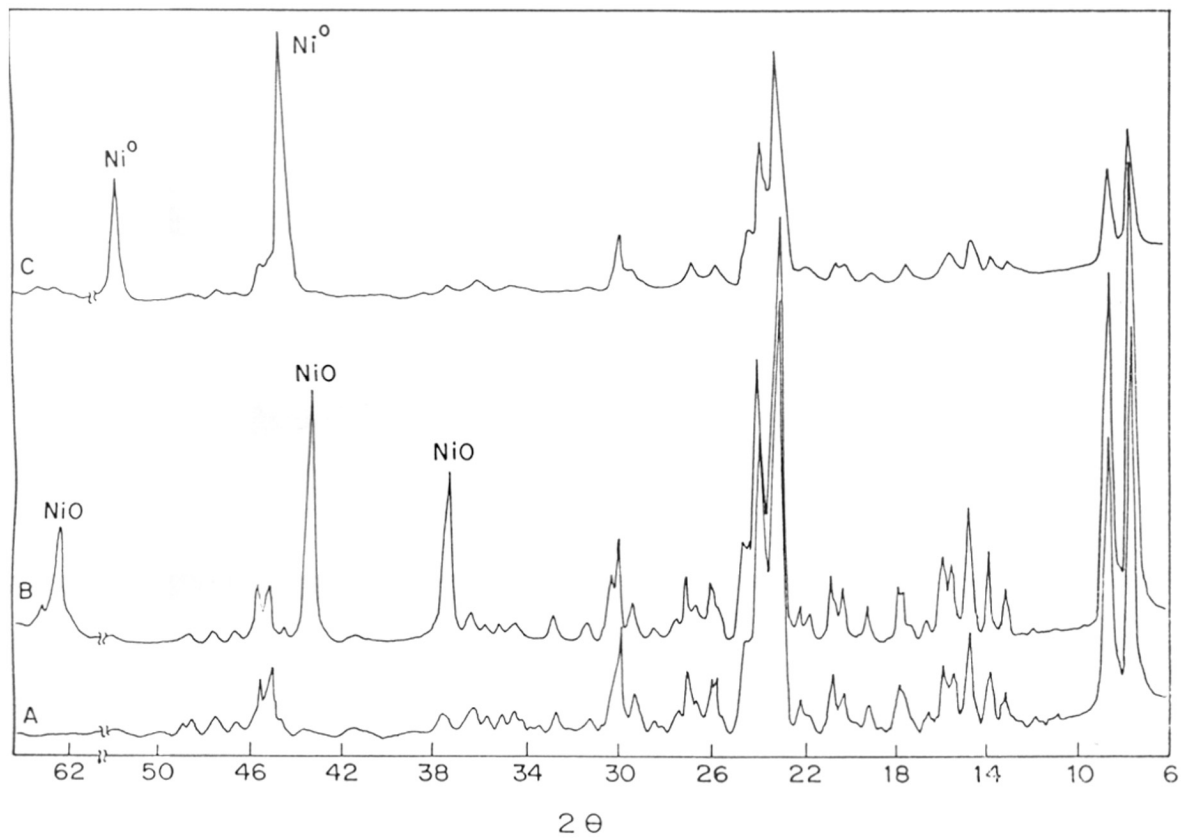


Fig. 2.2.2 : XRD spectra of A) Silicalite-I, B) NiO/Silicalite-I (unreduced) and C) NiO/Silicalite-I (reduced by H₂ at 800°C for 2 h)

crystalline phases of the catalyst; ALPO-5 and NiO phases are completely transformed to AlPO_4 (tridymite) and Ni^0 , respectively. The structural breakdown of ALPO-5 is expected because of its very poor hydrothermal stability [16]. In the catalytic process, NiO from the catalyst is reduced to Ni^0 in the initial reaction period, first by methane and then by the H_2 and CO produced in the methane reforming reactions. Thus, under the operating conditions, the catalyst is essentially metallic Ni dispersed on AlPO_4 (tridymite). The N_2 sorption capacity (at liquid nitrogen temperature and N_2 partial pressure of 30 kPa) of the ALPO-5 and NiO/ALPO-5 (Table-2.2.1) is in the following order: ALPO-5 > NiO/ALPO-5 (BR) > NiO/ALPO-5 (AR) [BR = before reaction, AR = after reaction]. The reduction in the N_2 sorption capacity is consistent with the transformation of the microporous ALPO-5 phase to the tridymite one.

In case of the NiO/silicalite-I catalyst, there is no significant change in the crystal structure and crystallinity of the support after deposition of NiO. However, after the reduction of NiO/silicalite-I by H_2 (at 800°C for 2 h), the crystallinity of the silicalite is reduced markedly and the NiO is transformed to Ni^0 (Fig 2.2.2). The N_2 sorption capacity is also reduced but to a smaller extent (Table 2.2.1).

2.2.3.2 Methane-to-Syngas Conversion over NiO/Silicalite-I

Results of the oxidative conversion of methane to syngas over NiO/silicalite-I are given in Table 2.2.2. The NiO/silicalite-I catalyst (without prereduction by H_2) showed very poor catalytic activity in the reaction even at 900°C . Hence the catalyst was reduced (by H_2 at 800°C for 2 h) before the reaction. However, the catalyst even when its all NiO is reduced completely to Ni^0 (Fig. 2.2.2c) showed poor performance in the reaction (Table 2.2.2). This is probably because of the following reason. Silicalite-I does not have ion-exchange capacity and moreover its hydroxyl groups are located mostly on the external crystal surface. Since the external surface is much more polar than the internal one, the nickel oxide or metallic nickel (after reduction) particles are expected to be concentrated at the polar external surface [17], thus causing an increase in the rate of sintering (crystal growth) of the active catalyst component (i.e. Ni^0) at the high reaction temperature and consequently resulting in a very poor catalytic activity.

Table 2.2.2 : Oxidative conversion of methane to CO and H₂ over NiO/Silicalite-I with or without prereduction [Feed : a mixture of CH₄ and O₂ with CH₄/O₂ ratio of 1.8; GHSV = 5.2 x 10⁵ cm³.g⁻¹.h⁻¹].

Catalyst	Temp. (°C)	CH ₄ conversion (%)	Selectivity (%)			H ₂ /CO ratio in product
			H ₂	CO	CO ₂	
Unreduced	900	2.8	90.6	98.0	2.0	1.8
	800	No reaction				
Reduced before reaction*	900	5.6	48.1	83.2	16.8	1.2
	800	2.1	-	-	-	-
	700	No reaction				

*Catalyst reduced by H₂ (20 mol% H₂ in N₂) for 2 h at 800°C.

2.2.3.3 Methane-to-Syngas Conversion over NiO/ALPO-5

Methane-to-syngas conversion over the NiO/ALPO-5 (without any prereduction) has been investigated by carrying out i) partial oxidation of methane at different temperatures (500° - 900°C), ii) CO₂ reforming of methane simultaneously with the oxidative conversion of methane with oxygen at 850°C and different CH₄/O₂ and CH₄/CO₂ ratios and iii) simultaneous steam reforming, CO₂ reforming and oxidative conversion of methane to syngas at different temperatures (750° - 900°C). The results of these reactions are presented in Figs. 2.2.3 - 2.2.6. Fresh catalyst was used for each of the above three reactions. No significant deactivation of the catalyst due to coke deposition in these reactions was observed (this was confirmed by repeating the first run on the catalyst used for these reactions). The net heat of reaction (ΔH_r) in the simultaneously occurring exothermic and endothermic methane conversion reactions was evaluated by subtracting the heat of formation (at reaction temperature) of components in feed from that in the product stream.

a) Oxidative conversion of methane to syngas

The results in Fig. 2.2.3 indicate that the catalyst shows good activity and selectivity, particularly at higher temperatures, in the partial oxidation of methane to CO and H₂. The selectivity for both CO and H₂ and also the H₂/CO product ratio are increased with increasing the temperature. However, the selectivity of the catalyst, particularly for H₂, is somewhat lower than that observed

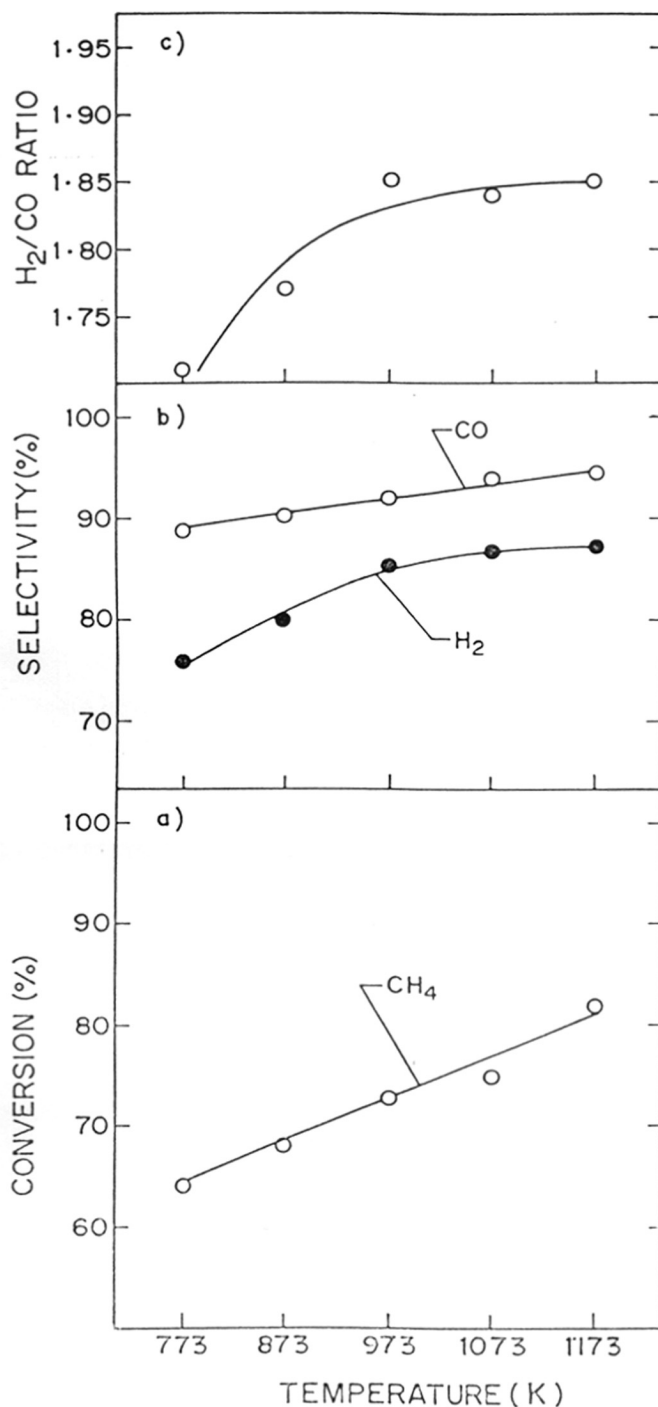


Fig. 2.2.3 : Influence of temperature on a) conversion, b) selectivity and c) H₂/CO product ratio in the oxidative conversion of methane to CO and H₂ over Ni/AlPO₄ [CH₄/O₂ ratio in feed = 1.8 and GHSV = 5.2 x 10⁵ cm³.g⁻¹.h⁻¹].

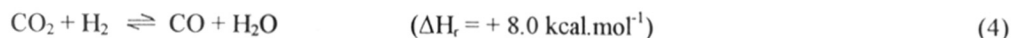
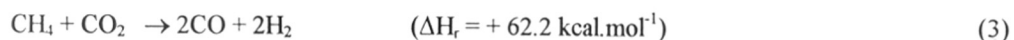
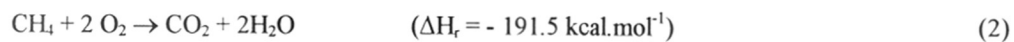
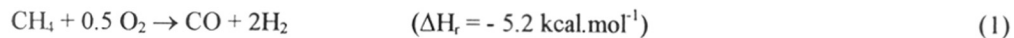
for the NiO-MgO [3], NiO-CaO [4] and NiO-Yb₂O₃ [7] catalysts. This suggests that the combustion of H₂ by O₂ and/or the reverse water gas shift reaction (CO₂ + H₂ → CO + H₂O) occur to a larger extent on the present catalyst.

b) Coupling of exothermic and endothermic methane-to-syngas conversion reactions

Simultaneous oxidative conversion and CO₂ reforming of methane

The results in Figs. 2.2.4 and 2.2.5 show a strong influence of CH₄/O₂ ratio (when the CH₄/(O₂ + 0.5CO₂) ratio in feed = 1.8) and of CH₄/CO₂ ratio (when the CH₄/O₂ ratio in feed = 2.1) on the conversion, selectivity for H₂, H₂/CO product ratio and also on the net heat of reaction (ΔH_r) in the simultaneous oxidative conversion and CO₂ reforming reactions of methane at 850°C. When the CH₄/O₂ ratio is increased while keeping the CH₄/(O₂ + 0.5CO₂) ratio constant, the conversion of CO₂ is increased appreciably and the H₂ selectivity, H₂/CO ratio and heat produced in the overall process are decreased markedly (Figs. 2.2.4a and 2.2.5a). The influence of the CH₄/CO₂ ratio in feed on the above is exactly the opposite (Figs. 2.2.4b and 2.2.5b). However, both the feed ratios have only small effects on the conversion of methane and O₂.

The following main exothermic and endothermic reactions are expected to occur simultaneously in this methane conversion process (at 850°C).



It may be noted that as long as there is a positive conversion of CO₂ (i.e. no net formation of CO₂ by reaction 2) in the process, the CO selectivity based on methane conversion is always 100%. However, the decrease and increase of the H₂ selectivity with increasing the CH₄/O₂ and CH₄/CO₂ ratios, respectively, indicate that the H₂ selectivity is changed mostly by the reverse water gas reaction (reaction 4). Since the net heat of reactions is strongly dependent on the CH₄/O₂ and CH₄/CO₂ ratios, the heat produced in the process can be controlled and the process can be made thermoneutral, mildly exothermic or mildly endothermic simply by manipulating the concentration of oxygen and CO₂ (in the feed) relative to that of methane. The H₂/CO ratio can be decreased by increasing the CO₂ concentration relative to that of O₂ in the feed.

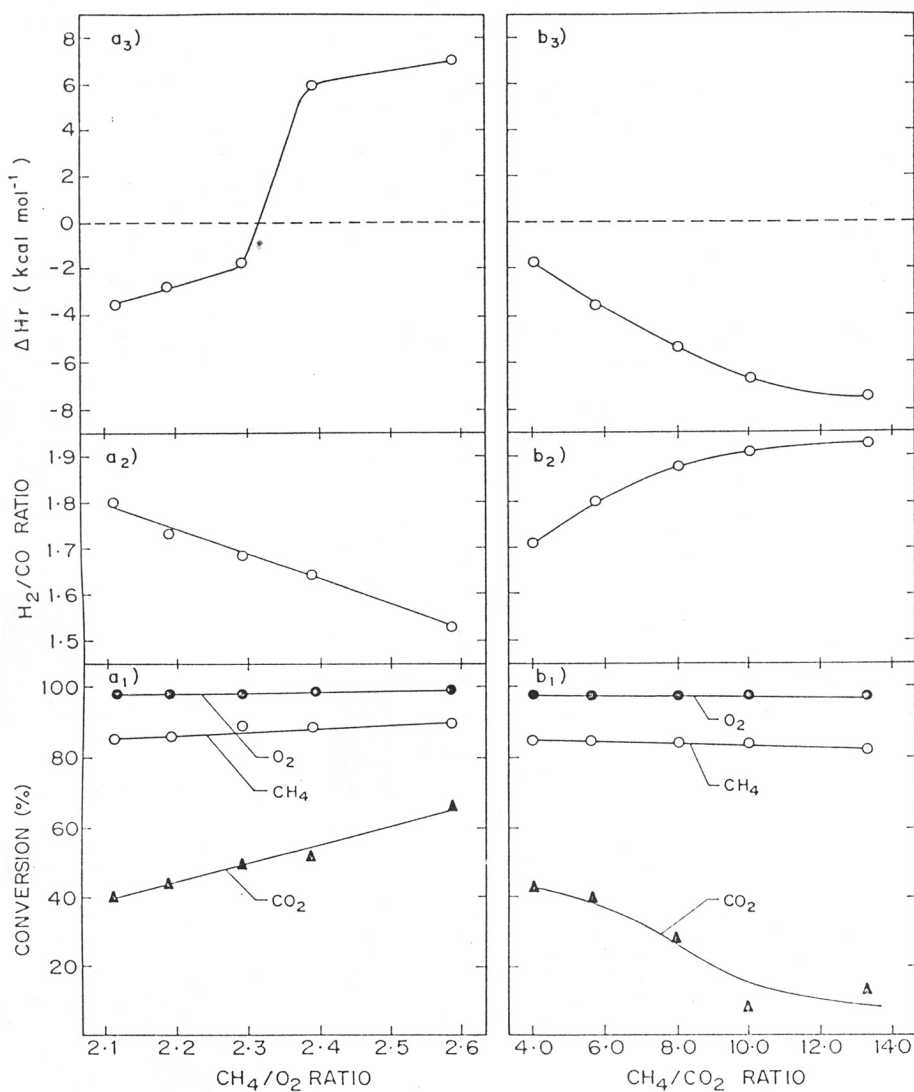


Fig. 2.2.4 : Influence of a) CH_4/O_2 ratio and b) CH_4/CO_2 ratio in feed on conversion, H_2/CO product and net heat of reaction (ΔH_r) in simultaneous oxidative conversion and CO_2 reforming over Ni/AlPO_4 at 850°C and GHSV of $47,000 \text{ cm}^3 \cdot \text{g}^{-1} \cdot \text{h}^{-1}$. [a) $\text{CH}_4/(\text{O}_2 + 0.5\text{CO}_2) = 1.8$ and b) $\text{CH}_4/\text{O}_2 = 2.1$].

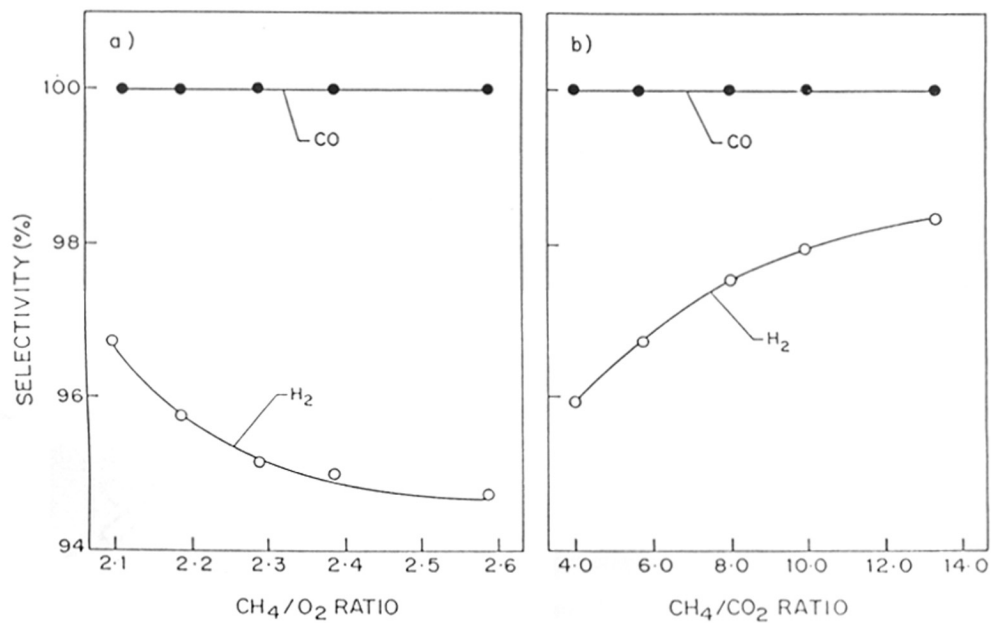
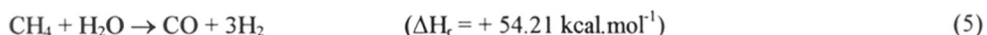


Fig. 2.2.5 : Influence of a) CH₄/O₂ ratio and b) CH₄/CO₂ ratio in feed on selectivity for H₂ in the simultaneous oxidative conversion and CO₂ reforming over NiO/AlPO₄.

Simultaneous oxidative conversion, CO₂ reforming and steam reforming of methane

The results in Fig. 2.2.6 show that the conversion, selectivity, H₂/CO product ratio and net heat of reaction in the simultaneous oxidative conversion and steam and CO₂ reforming reactions of methane over the NiO/ALPO-5 catalyst are strongly influenced by the reaction temperature. The negative conversion of CO₂ and water, observed at lower temperatures, is due to net formations of CO₂ and H₂O as side products due to complete combustion of methane (reaction 2). However, at the higher temperatures (above 800°C), the CO₂ reforming (reaction 3) and steam reforming (reaction 5)



also become predominant. Hence these endothermic reactions occur simultaneously with the oxidative conversion of methane (reactions 1 and 2). The selectivities for both H₂ and CO and the H₂/CO ratio are increased and the heat produced in the overall process is decreased with increasing the temperature. The decrease in the heat produced is because of the fact that the endothermic steam and CO₂ reforming reactions become more and more predominant with increasing the temperature above 800°C. Thus, the net heat of reactions can be controlled by the reaction temperature.

It may be noted that, whenever the steam and CO₂ reforming reactions occur simultaneously with the oxidative conversion and the conversion of CO₂ and H₂O is equal to or above zero, the selectivity (based on methane conversion) for H₂ and CO is always 100%.

The above results reveal that the Ni/AlPO₄ catalyst shows very good performance, comparable to that of NiO-CaO [8,10], in the methane-to-syngas conversion process involving simultaneous exothermic oxidative conversion and endothermic CO₂ and/or steam reforming reactions. Because of the coupling of the exothermic reactions with the endothermic reactions, the heat produced in the former reactions is used instantly for the later reactions. This makes the process operation very energy-efficient and safe. The formation of hotspots in the catalyst bed can be totally avoided due to the buffering action set in the reaction temperature. Also, it is possible to make the process almost thermoneutral, mildly exothermic or mildly endothermic by manipulating the process conditions (viz. reaction temperature and feed composition), thus requiring little or no external energy for the conversion of methane to syngas. The H₂/CO ratio in the syngas produced can be varied conveniently by manipulating the process conditions, particularly the relative concentrations of O₂, CO₂ and H₂O in the feed, similar to that observed earlier [8-10].

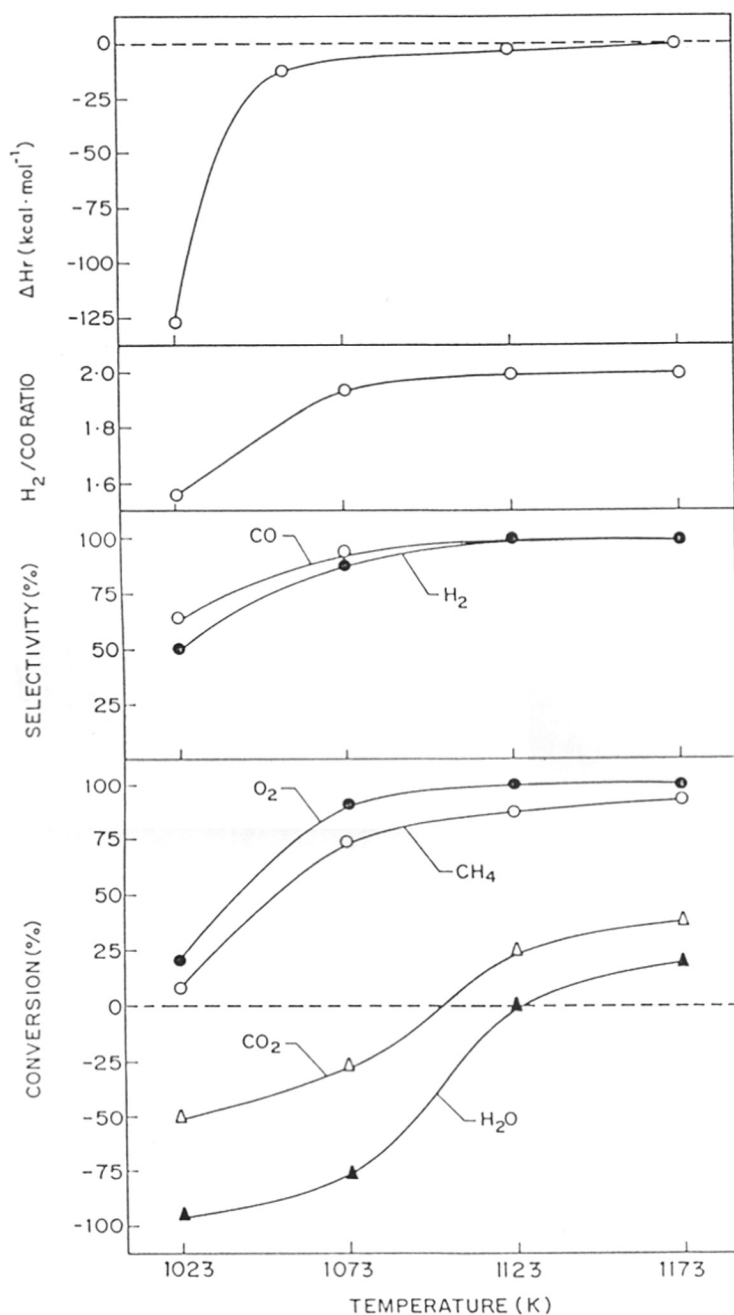


Fig. 2.2.6 : Influence of reaction temperature on conversion, selectivity, H₂/CO ratio and net heat of reaction (ΔH_r) in the simultaneous steam and CO₂ reforming and oxidative conversion of methane over NiO/AlPO₄ (GHSV = 47,000 cm³.g⁻¹.h⁻¹, CH₄/O₂ = 2.1 and CH₄/CO₂ = CH₄/H₂O = 10.0).

2.2.4 CONCLUSIONS

Ni/AlPO₄ catalyst shows good performance in the oxidative conversion of methane to syngas and also in the simultaneous methane-to-syngas conversion reactions, involving coupling of exothermic oxidative methane conversion and the endothermic CO₂ and/or steam reforming reactions of methane, over the same catalyst. However, NiO/silicalite-I shows extremely poor performance in the oxidative methane-to-syngas conversion.

The NiO/ALPO-5 catalyst under operating conditions is in the form of Ni⁰/AlPO₄ (tridymite). The former is transformed into the latter during a short initial reaction period at the high reaction temperature.

The methane-to-syngas conversion process involving simultaneous oxidative conversion and CO₂ and steam reforming reactions occur over the Ni/AlPO₄ catalyst in a very energy- efficient and safe manner, requiring little or no external energy. The process can be made almost thermoneutral or mildly exothermic or mildly endothermic. A desirable H₂/CO ratio can be obtained conveniently by manipulating the process conditions (viz. feed composition and reaction temperature).

REFERENCES

1. D. Dissanayake, M.P. Rosynek, K.C.C. Kharas and J.H. Lunsford, *J. Catal.*, 132 (1991) 117.
2. V.R. Choudhary, A.M. Rajput and B. Prabhakar, *J.Catal.*, 139 (1993) 326.
3. V.R. Choudhary, A.S. Mamman and S.D. Sansare, *Angew. Chem. Int. Ed. Engl.*, 31 (1992) 1189.
4. V.R. Choudhary, A.M. Rajput and B. Prabhakar, *Catal. Lett.*, 15 (1992) 363.
5. J.N. Theron, J.C.Q. Fletcher and C.T. O'Connor, *Catal. Today*, 21 (1994) 489.
6. V.R. Choudhary, V.H. Rane and A.M. Rajput, *Catal. Lett.*, 22 (1993) 289.
7. V.R. Choudhary, A.M. Rajput and V.H. Rane, *J. Phys. Chem.*, 96 (1992) 8686.
8. V.R. Choudhary, A.M. Rajput and B. Prabhakar, *Angew. Chem. Int. Ed. Engl.*, 33 (1994) 2104.
9. V.R. Choudhary, A.M. Rajput and B. Prabhakar, *207th Annual ACS Meeting San Diego*, March 13 - 18, 1994.
10. V.R. Choudhary, A.M. Rajput and B. Prabhakar, *Catal. Lett.*, 32 (1995) 391.
11. H. Matsumoto, *J. Phys. Chem. Lett.*, 98 (1994) 5180.
12. H. Matsumoto S. Tanabe, *J.Chem.Soc. Faraday Trans.*, 90 (1994) 3001.
13. G.J. Kim, D.-S. Cho, -H. Kwang and J.-H. Kim, *Catal. Lett.*, 28 (1994) 41.
14. V.R. Choudhary and D.B. Akolekar, *J.Catal.*, 103 (1987) 115.
15. V.R. Choudhary and D.B. Akolekar, *Mater. Chem. Phys.*, 20 (1988) 299.
16. V.R. Choudhary, D.B. Akolekar, A.P. Singh and S.D. Sansare, *J.Catal.*, 111 (1988) 254.
17. B. Kraushaar-Czarnetzki and J.H.C. Van Hooff, *Stud. Surf. Sci. Catal.*, 49B (1989) 1063.

CHAPTER - 2.3

OXIDATIVE CONVERSION OF METHANE TO SYNGAS WITH OR WITHOUT SIMULTANEOUS STEAM AND/OR CO₂ REFORMING OVER SUPPORTED NiO-MgO, NiO-CaO AND NiO-Yb₂O₃ CATALYSTS

2.3.1 INTRODUCTION

Under the present energy crisis, the catalytic oxidative conversion of methane to syngas (i.e. CO and H₂), which does not require external energy, is a process of great practical importance. Since last few years, extensive efforts have been made for converting methane by its partial oxidation with oxygen to syngas, using different catalysts [1-11].

Choudhary et.al. in their earlier studies reported that NiO-MgO [7], NiO-CaO [8] and NiO-Yb₂O₃ [9] catalysts shows very high activity/selectivity and also extremely high productivity in the oxidative conversion of methane to syngas. However, the pellets of these composite mixed metal oxide catalysts have poor mechanical strength (i.e. low crushing strength and poor attrition resistance). Also, because of the hygroscopic nature of the alkaline earth or rare earth metal oxide in the catalyst, the pellet strength is drastically reduced when exposed to atmospheric moisture. High mechanical strength is a basic requirement of any industrial catalyst. This could be achieved by supporting catalyst on a porous catalyst carrier having high mechanical strength and also very high thermal/hydrothermal stability. The present work was undertaken with this objective. In this paper, the influence of support on the catalytic activity/selectivity and productivity of NiO-MgO, NiO-CaO and NiO-Yb₂O₃ catalysts supported on a sintered low surface area porous commercial catalyst carrier (Appendix-1) in the catalytic oxidative conversion of methane to syngas has been investigated. Further, the oxidative conversion of methane in the presence of steam and/or CO₂ in the feed (involving simultaneous exothermic oxidative conversion and endothermic steam and CO₂ reforming reactions) over supported NiO-MgO catalyst has also been investigated.

2.3.2 EXPERIMENTAL

2.3.2.1 Catalyst Preparation

The supported catalysts- NiO-MgO/SA-5205 (Ni/Mg = 3.0), NiO-CaO/SA-5205 (Ni/Ca = 3.0), and NiO-Yb₂O₃/SA-5205 (Ni/Yb = 1.0) with a catalyst loading of 13 ± 0.2 wt.% were prepared by impregnating (using incipient impregnation technique) 22-30 mesh size particles of a commercial support SA-5205 (Appendix-1) with mixed nickel nitrate and magnesium nitrate or calcium nitrate or ytterbium nitrate solutions, drying and calcining in air at 900°C for 4 h.

2.3.2.2 Catalytic Reaction

The schematic diagram of experimental set-up and the quartz reactor used for the catalytic partial oxidation of methane to syngas are shown in Figs. 2.1.1 and 2.1.2, (Chapter-2.1), respectively. For the catalytic oxidative conversion of methane in the presence of steam and/or CO₂, the reactor shown in Fig. 1.1.2 (Chapter-1.1) was used.

The catalytic oxidative conversion of methane to syngas with or without simultaneous steam and CO₂ reforming of methane was carried out at 1 atm pressure by passing continuously a mixture of pure methane, O₂ with or without steam and CO₂ over the supported catalyst (0.02 or 0.3 gm) in a conventional quartz microreactor (i.d. 10 mm). The reaction temperature was measured with a Chromel-Alumel thermocouple located in the catalyst bed. The water from the product gas was condensed at 0°C. The feed and the products were analysed by an on-line GC using a spherocarb column. The C, H, and O balances were within 5%.

2.3.3 RESULTS AND DISCUSSIONS

Results showing influence of catalyst support on the performance of the supported NiO-MgO, NiO-CaO and NiO-Yb₂O₃ catalysts in the oxidative conversion of methane to syngas are shown in Table-2.3.1. Whereas, the results on the coupling of the exothermic oxidative conversion and the endothermic steam and CO₂ reforming reactions in the methane-to-syngas conversion over NiO-MgO/SA-5205 catalyst are presented in Fig. 2.3.1. The -ve conversion of H₂O and CO₂ (Fig. 2.3.1b), are just indicative of the formation of H₂O and CO₂ in the process, respectively. The net heat of reaction (ΔH_r) for the overall process is estimated by subtracting the heat of formation (at the

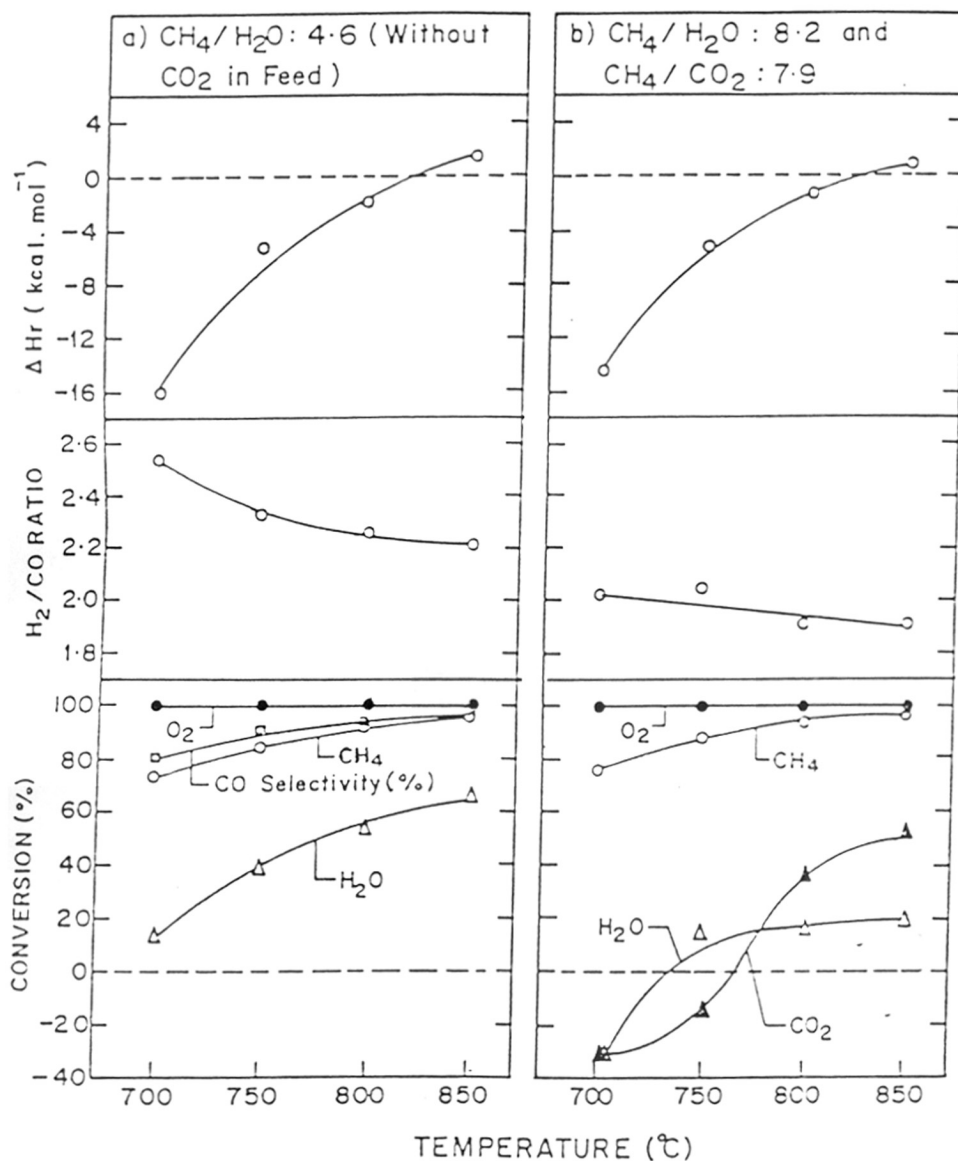


Fig. 2.3.1 : a) Simultaneous oxidative conversion and steam reforming of methane to syngas, and b) Simultaneous oxidative conversion and steam and CO₂ reforming of methane to syngas over NiO-MgO/SA-5205 [CH₄/O₂ = 2.1 and GHSV = 5.1 × 10⁵ cm³.(at STP).g⁻¹.h⁻¹][CO selectivity data are included in Fig. 2.3.1a]

process temperature) of the components in the feed from that of the components present in the product stream.

Table 2.3.1 : Influence of catalyst support on oxidative conversion of methane to syngas over supported NiO-MgO (Ni/Mg = 3.0), NiO-CaO (Ni/Ca = 3.0), and NiO-Yb₂O₃ (Ni/Yb =1.0) catalysts [Reaction conditions-Feed : a mixture of pure methane and O₂; CH₄/O₂ ratio : 1.8; GHSV : 5.2 x 10⁵ cm³ (at STP).g⁻¹.h⁻¹)]

Catalyst	Surface area (m ² .g ⁻¹)	Temp. (°C)	CH ₄ conversion (%)	Selectivity (%)		CO STY (mol.g ⁻¹ .h ⁻¹)
				CO	H ₂	
NiO-MgO	3.66	800	95.9	99.8	99.6	14.30
		700	90.9	96.6	94.0	13.10
		600	86.9	93.5	93.7	12.12
NiO-MgO/SA-5205	0.45	800	86.5	96.4	94.8	12.44
		700	80.3	92.2	90.9	11.05
		600	75.6	88.4	90.3	9.97
NiO-CaO	2.50	800	86.3	95.7	95.8	12.32
		700	81.4	94.1	93.1	11.43
		600	72.3	91.0	91.2	9.82
NiO-CaO/SA-5205	0.36	800	45.2	73.6	74.9	4.96
		700	No reaction			
NiO-Yb ₂ O ₃	6.30	800	91.3	96.3	96.5	13.12
		700	85.0	95.0	95.5	12.05
		600	79.0	93.2	91.4	10.98
NiO-Yb ₂ O ₃ /SA-5205	1.02	800	74.6	93.6	89.3	10.42
		700	64.3	90.5	84.4	8.68
		600	58.2	85.8	79.2	7.45

2.3.3.1 Oxidative Conversion of Methane to Syngas

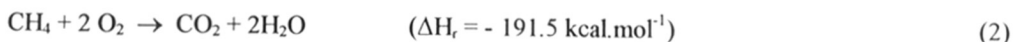
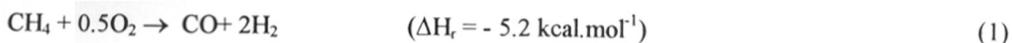
The results (Table-2.3.1) reveal that both the conversion and selectivity of the catalysts in the oxidative methane-to-syngas conversion are decreased because of the supporting the catalysts on the commercial catalyst carrier (SA-5205). This is mostly due to the formation of NiAl₂O₄ (spinel), which

is catalytically inactive and also very difficult to reduce, by a solid-solid reaction between NiO and Al₂O₃ (from support) to different extents depending upon the catalyst. The performance shown by the supported catalysts in the catalytic process is in the following order : NiO-MgO/SA-5205 > NiO-Yb₂O₃/SA-5205 >> NiO-CaO/SA-5205. The better performance of the supported NiO-MgO catalyst is attributed to a formation of MgAl₂O₄ (spinel) on the support surface, thus protecting to a certain extent the catalytically important component (NiO) from its reaction with surface Al₂O₃.

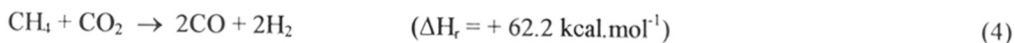
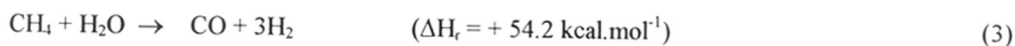
2.3.3.2 Coupling of Catalytic Exothermic and Endothermic Reactions

The results (Figs. 2.3.1a and 2.3.1b) reveal that by carrying out of the exothermic oxidative conversion and the endothermic steam with or without CO₂ reforming of methane simultaneously over NiO-MgO/SA 5205 catalyst, it is possible to make overall process mildly exothermic, near thermoneutral or mildly endothermic thus requiring little or no external energy. Further, methane can be converted to CO and H₂ (with H₂/CO ratio: 1.9 - 2.6) with very high conversion (> 90%) and selectivity (above 90% CO selectivity and 100% H₂ selectivity in the coupled process involving oxidative conversion and steam reforming of methane and 100% selectivity for H₂ and CO in the coupled process involving oxidative conversion and steam and CO₂ reforming of methane) and also with high productivity (about 12 mol.g⁻¹.h⁻¹). Following main exothermic and endothermic reactions occur simultaneously in the coupled processes.

Exothermic reactions



Endothermic reactions



The exothermicity of the coupled processes can, in general, be decreased with increasing the reaction temperature.

2.3.4 CONCLUSIONS

Because of the deposition of catalysts on the support, both the catalytic activity and selectivity in the oxidative methane-to-syngas conversion is decreased depending upon the catalyst, mostly due to the formation of NiAl_2O_4 (spinel), which is catalytically inactive and also very difficult to reduce. The performance shown by the supported catalysts in the catalytic process is in the following order : $\text{NiO-MgO/SA-5205} > \text{NiO-Yb}_2\text{O}_3/\text{SA-5205} \gg \text{NiO-CaO/SA-5205}$.

In the coupled processes over NiO-MgO/SA-5205 catalyst, methane can be converted to CO and H_2 (with H_2/CO ratio in the range of 1.9 - 2.6) with very high conversion (> 90%) and selectivity (above 90% CO selectivity and 100% H_2 selectivity in the coupled process involving oxidative conversion and steam reforming of methane and 100% selectivity for both H_2 and CO in the coupled process involving oxidative conversion and steam and CO_2 reforming of methane) with requirement of little or no external energy by making the process thermoneutral, mildly exothermic or mildly endothermic by manipulating the process conditions.

REFERENCES

1. A.T. Ashcroft, A.K. Cheetham, J.S. Foord, M.L.H. Green, C.P. Grey, A.J. Murrell and P.D.F. Vernon, *Nature*, 344 (1990) 319.
2. P.D.F. Vernon, M.L.H. Green, A.K. Cheetham, and A.T. Ashcroft, *Catal. Lett.*, 6 (1990) 181; *Nature*, 352 (1991) 225; *Catal.Today*, 13 (1992) 417.
3. D. Dissanayake, M.P. Rosynek, K.C.C. Kharas, and J.H. Lunsford, *J.Catal.*, 132 (1991) 117.
4. V.R. Choudhary, A.M. Rajput, and B. Prabhakar, *Catal. Lett.*, 16 (1992) 269; *J.Catal.*, 139 (1993) 326.
5. V.R. Choudhary, S.D. Sansare, and A.S. Mamman, *Appl. Catal.*, 90 (1992) L1.
6. V.R. Choudhary, A.M. Rajput, and V.H. Rane, *Catal. Lett.*, 16 (1992) 269.
7. V.R. Choudhary, A.S. Mamman, and S.D. Sansare, *Angew. Chem. Int. Ed. Eng.*, 31 (1992) 1189.
8. V.R. Choudhary, A.M. Rajput, and B. Prabhakar, *Catal. Lett.*, 15 (1992) 363.
9. V.R. Choudhary, A.M. Rajput, and V.H. Rane, *J. Phys. Chem.*, 96 (1992) 8686; *Catal. Lett.*, 22 (1993) 289.
10. H. Matsumoto, *J. Phys. Chem.*, 98 (1994) 5180.
11. P.M. Tornaiainen, X. Chu, and L.D. Schmidt, *J. Catal.*, 146 (1994) 1.

CHAPTER - 2.4

LARGE ENHANCEMENT IN METHANE-TO-SYNGAS CONVERSION ACTIVITY OF SUPPORTED Ni-CATALYSTS DUE TO PRECOATING OF CATALYST SUPPORTS WITH MgO, CaO OR RARE-EARTH OXIDE

2.4.1 INTRODUCTION

Nickel supported on alumina [1-6] and silica [7] is a commonly used catalyst in the conversion of methane to syngas (i.e. CO and H₂). Highly sintered low surface area (< 1 m².g⁻¹) porous catalyst carriers, containing silica and/or alumina, which have high thermal and hydrothermal stability and mechanical strength are most commonly used supports for the hydrocarbon oxidation catalysts and also for the catalysts used in the processes involving drastic reaction conditions (e.g. high temperatures, presence of steam in reaction mixture, sharp temperature changes, etc.). At high temperatures, a solid-solid reaction of Ni or NiO with Al₂O₃ and SiO₂ results in the formation of nickel aluminate (spinel) and nickel silicate phases, respectively, which are catalytically inactive for methane-to-syngas conversion reactions and also difficult to reduce, thus lowering catalytic activity and also causing catalyst deactivation during the high temperature process and/or in the catalyst regeneration cycles. The present investigation was undertaken with the objective of developing a highly stable nickel based supported catalyst which shows high catalytic activity, selectivity and productivity in the oxidative conversion of methane to syngas, steam and CO₂ reforming or both or in the simultaneous exothermic oxidative conversion with the endothermic steam and/or CO₂ reforming reactions.

2.4.2 EXPERIMENTAL

2.4.2.1 Catalyst Preparation

Supported nickel catalysts (Tables 2.4.1 and 2.4.2) were prepared by depositing nickel nitrate on 22-30 mesh size particles of commercial catalyst carriers (sintered low surface area porous catalyst carriers, obtained from Norton Co. USA) with or without precoating them by MgO, CaO or rare-earth oxide using incipient wetness impregnation technique, drying and

decomposing (or calcining) in air at 900°C for 4 h. The catalyst carriers were precoated with MgO, CaO or rare-earth oxide by impregnating the carriers with corresponding metal nitrate, drying and decomposing as above. The main components of the supports and their physiochemical properties are given in Appendix-1.

2.4.2.2 Catalytic Reaction

The schematic diagrams of experimental set-up and the quartz reactor used for catalytic partial oxidation of methane to syngas are shown in Figs. 2.1.1 and 2.1.2 (Chapter-2.1), respectively. For the catalytic steam and CO₂ reforming of methane to syngas reactions the reactor used is shown in Fig. 1.1.1 (Chapter- 1.1).

The methane-to-syngas conversion reactions over the supported nickel catalysts were carried out at atmospheric pressure in a conventional continuous flow quartz micro reactor [with i.d. of 4 mm (Fig. 2.1.1) and 9 mm (Fig. 1.1.1) for the oxidative methane conversion and steam/CO₂ reforming of methane, respectively], kept in a tubular furnace (i.d. 25mm). The reaction temperature was measured by Chromel-Alumel thermocouple located in the catalyst bed. Before the reaction, the catalyst was pretreated in-situ at 900°C in a flow of pure N₂ (50 cm³.min⁻¹) for 1 h. The water from the product stream was condensed at 0°C. The feed and the product gases were analyzed by an on-line gas chromatograph, using a spherocarb column.

2.4.3 RESULTS AND DISCUSSION

A comparison of the results (Tables 2.4.1 and 2.4.2) reveals that, in all the three methane-to-syngas conversion reactions, the catalytic activity (i.e. methane conversion), selectivity and space time yield (STY) or productivity of the supported nickel catalysts are drastically increased due to the precoating of the catalyst carrier with MgO, CaO or rare-earth oxide, before supporting (or depositing) NiO on them. The observed drastic improvement in the catalyst performance due to the precoating is attributed to the formation of a protective layer of the precoated metal oxide between the reactive component (e.g. Al₂O₃, SiO₂, etc) of the support and the deposited NiO, thus eliminating or drastically reducing the chemical interactions between them and consequently the formation of catalytically inactive spinel type binary metal oxide phases (e.g. NiAl₂O₄, Ni₂SiO₄, etc) by solid-solid reactions between NiO and Al₂O₃ or

SiO₂ from support. When NiO is directly deposited on the supports (without precoating), an extensive formation of these binary metal oxide phases has been observed. Also, even though these directly supported nickel catalysts were reduced before reaction by hydrogen at 500°C for 1 h, no improvement in the catalyst activity and selectivity was observed. Apart from providing a protective layer, the precoating of support (which results in an increase in the surface area) is also expected to result in an increase the dispersion of nickel oxide in the supported catalyst.

Table 2.4.1 : Results on oxidative conversion of methane^a to CO and H₂ over supported Ni catalysts prepared with or without precoating support by different metal oxides

Catalyst	CH ₄ convn. (%)	Selectivity (%)		CO STY (mol.g ⁻¹ .h ⁻¹)
		----- CO	H ₂	
NiO(12.0 wt %)/SA-5205	3.0	11.1	17.0	0.1
NiO(12.2 wt%)/MgO(5.6 wt%)/SA-5205	94.7	97.5	95.6	13.5
NiO(13.3 wt%)/CaO(9.7 wt%)/SA-5205	82.0	91.9	89.6	11.0
NiO(13.1 wt%)/Yb ₂ O ₃ (19.6wt%)/SA-5205	88.3	95.5	93.2	12.3
NiO(13.4wt%)/Sm ₂ O ₃ (15.3wt%)/SA-5205	87.2	93.8	91.2	12.0
NiO(14.8 wt %)/SC-5532	<0.1	-	-	-
NiO(12.9 wt%)/MgO(5.2 wt%)/SC-5532	89.0	95.8	97.2	12.5
NiO(18.0 wt %)/SC-5232	3.3	26.4	15.0	0.1
NiO(15.8 wt%)/MgO(7.5 wt%)/SC-5232	91.1	98.9	95.1	13.2
NiO(11.4 wt %)/SS-5231	5.9	39.1	10.0	0.3
NiO(10.3 wt%)/MgO(7.8 wt%)/SS-5231	91.8	95.8	95.1	12.9

^aReaction temperature, 800°C; feed, 65 mol% CH₄ and 35 mol% O₂; space velocity, 5.1 x 10⁵ cm³.(at STP).g⁻¹.h⁻¹

It may also be noted that the unsupported NiO-MgO (Ni/Mg = 3.0), NiO-CaO (Ni/Ca = 3.0) and NiO-Yb₂O₃ (Ni/Yb = 1.0) mixed metal oxide catalysts showed excellent performance in the oxidative conversion of methane to syngas [8-10]. However, when these catalysts are directly supported on SA-5205, their catalytic activity is found to be greatly reduced. This clearly shows

the importance of forming a protective layer (by the precoating of support) between support and NiO in the supported-Ni catalysts in order to avoid the chemical interactions between the support components and NiO.

The results (Table 2.4.1) show that the best catalyst performance in the oxidative methane-to-syngas conversion is observed when the catalyst carrier is precoated with MgO. This is mostly due to the formation of a protective layer of stable MgAl_2O_4 (spinel) and/or MgSiO_3 phases between the support surface and the active catalyst.

Table 2.4.2 : Results on steam and CO_2 reforming of methane to CO and H_2 over supported Ni catalyst prepared with or without precoating support by MgO

Catalyst	Steam reforming ^a			CO ₂ reforming ^b		
	CH ₄ convn	CO select.	H ₂ /CO ratio	CH ₄ convn	H ₂ select.	H ₂ /CO ratio
	(%)	(%)		(%)	(%)	
NiO(12.0 wt %)/SA-5205	<0.1	-	-	46.2	95.1	0.9
NiO(12.2wt%)/MgO(5.6wt%)/SA-5205	97.8	91.7	3.59	95.5	~100	1.0

^aReaction temperature, 800°C; feed, 39 mol% CH₄ and 61 mol% H₂O; space velocity, 22590 cm³.(at STP).g⁻¹.h⁻¹

^bReaction temperature, 800°C; feed, 50 mol% CH₄ and 50 mol% CO₂; space velocity, 8600 cm³.(at STP).g⁻¹.h⁻¹

2.4.4 CONCLUSIONS

Studies disclosing the beneficial effect of precoating of catalyst support (containing Al_2O_3 and SiO_2) with MgO , CaO or rare-earth oxide before depositing nickel oxide on the support, in the preparation of supported nickel catalysts, are reported in this chapter. Because of the precoating there is a very large increase in the methane-to-syngas conversion activity/selectivity of the supported nickel catalysts due to the elimination or drastic reduction in the formation of catalytically inactive NiAl_2O_4 (spinel) and/or Ni_2SiO_4 phases resulting from the chemical interactions between NiO and Al_2O_3 and/or SiO_2 from support at high temperatures. Among the alkaline and rare-earth metal oxides used for the support precoating, the best performance is shown by MgO , due to formation of stable protective layer of MgAl_2O_4 (spinel) and/or MgSiO_3 between the support surface and the active nickel catalyst.

REFERENCES

1. D. Dissanayake, M.P. Rosynek, K.C.C Kharas and J.H. Lunsford, *J. Catal.*, 132 (1991) 117.
2. V.R. Choudhary, A.M. Rajput and B. Prabhakar, *J. Catal.*, 139 (1993) 326.
3. S.M. Jackson, S.J. Thomson and G. Webb, *J. Catal.*, 70 (1981) 249.
4. W.J.M. Vermeiren, E. Blomsma, P.A. Jacobs, *Catal. Today*, 13 (1992) 427.
5. D.A. Goetsch and G.R. Say, *US patent* 4,877,550 (1989)
6. D.A. Goetsch, G.R. Say, J.M. Vargas and P.E. Ebexly, *US patent* 4,888,131 (1989)
7. L.J. Velenyi, C. Papparizos and P.A. Pesa, *European Patent EP 0 084 273 A2* (1983)
8. V.R. Choudhary, A.S. Mamman and S.D. Sansare, *Angew. Chem. Int. Ed. Engl.*, 31 (1992) 1189.
9. V.R. Choudhary, A.M. Rajput and B. Prabhakar, *Catal. Lett.*, 15 (1992) 363.
10. V.R. Choudhary, V.H. Rane and A.M. Rajput, *J. Phys. Chem.*, 96 (1992) 8686.

CHAPTER - 2.5

OXIDATIVE CONVERSION OF METHANE TO SYNGAS OVER NICKEL SUPPORTED ON COMMERCIAL LOW SURFACE AREA POROUS CATALYST CARRIERS PRECOATED WITH ALKALINE AND RARE EARTH OXIDES

2.5.1 INTRODUCTION

Catalytic oxidative conversion of methane to syngas with H_2/CO ratio of 2.0, a versatile feedstock for the methanol and Fischer-Tropsch synthesis processes, is a process of great commercial importance. Since last few years, extensive efforts have been made for converting methane by its partial oxidation with oxygen to syngas, using different nickel, cobalt and noble metal containing catalysts [1-15].

$NiO-MgO$ [6], $NiO-CaO$ [7] and $NiO-Yb_2O_3$ or other rare earth oxide [8] catalysts show high activity and selectivity at very low contact time (1-10 ms) and hence show very high productivity in the oxidative conversion of methane to syngas. However, because of their hygroscopic nature, the pellets of these composite mixed metal oxide catalysts have poor mechanical strength (i.e. low crushing strength and poor attrition resistance). The mechanical strength of a catalyst can be improved by supporting it on a porous catalyst carrier having high mechanical strength. But when the above three mixed metal oxide catalysts were deposited on a sintered low surface area porous silica-alumina catalyst carrier, the activity of the catalysts was reduced very significantly [15, Chapter-2.3]. This was due to the formation of $NiAl_2O_4$ (spinel), which is catalytically inactive and also very difficult to reduce, by a solid-solid reaction between NiO (from catalyst) and Al_2O_3 (from support).

In our recent preliminary studies [14, Chapter-2.4], supported nickel catalysts prepared using commercial sintered low surface area porous catalyst carriers (containing Al_2O_3 and/or SiO_2) precoated with MgO , CaO or rare-earth oxide show very much higher activity, selectivity and productivity in the oxidative conversion of methane to syngas than the catalysts prepared using the catalyst carriers without any precoating. The beneficial effect of the support precoating was attributed to the elimination or drastic reduction in the formation of catalytically inactive $NiAl_2O_4$.

(spinel) and/or Ni_2SiO_4 phases resulting from the chemical interactions between NiO and Al_2O_3 and/or SiO_2 from support at high catalyst calcination temperature. It is, therefore, interesting to investigate in details the effects of various parameters of the preparation of supported nickel catalyst (viz. use of different low surface area porous catalyst carriers, method of deposition, precoating agents, loading of precoating agent, loading of NiO and catalyst calcination temperature) on the temperature programmed reduction (TPR) and degree of reduction of nickel oxide from the catalyst, on the chemisorption of hydrogen (which is a measure of Ni surface area) on the catalyst after its reduction and also on the activity/selectivity of the supported Ni catalysts in the oxidative conversion of methane to syngas at very low contact time (≈ 1 ms). The present investigation was undertaken with these objectives.

2.5.2 . EXPERIMENTAL

2.5.2.1 Catalyst Preparation

Unsupported NiO-MgO with Ni/Mg ratio of 3.0 (Table 2.5.1) was prepared as per the procedure reported earlier [7]. NiO-MgO ($\text{Ni/Mg} = 3.0$) directly supported on different low surface area ($< 1 \text{ m}^2 \cdot \text{g}^{-1}$) porous catalyst carriers (SA-5205, SA-5218, SA-5552, SC-5532, SS-5231 and SZ-5564, obtained from M/S Norton Co., USA) were prepared by impregnating (using incipient wetness impregnation technique) 22-30 mesh size particles of the commercial supports with mixed nickel nitrate and magnesium nitrate solutions, drying and calcining in air at 900°C for 4 h. NiO supported on the different catalyst carriers precoated with different alkaline earth or rare-earth oxides were prepared by impregnating nickel nitrate from its aqueous solution on 22-30 mesh size particles of the precoated catalyst carriers, using incipient wetness impregnation technique, drying and calcining in air at different temperatures ($600^\circ - 1200^\circ\text{C}$) for 4 h. The catalyst carriers were precoated with alkaline earth or rare-earth oxide by impregnating the carriers with corresponding metal nitrate, drying and calcining in air at 900°C for 4 h. The main chemical constituents, surface area, pore volume and porosity of the different commercial catalyst carriers are given in Appendix-1. The catalyst carriers were crushed to 22-30 mesh size particles before using them for supporting the catalysts.

2.5.2.2 Catalyst Characterization

The catalysts were characterized for their surface area by the single point BET method, using a Monosorb Surface Area Analyser (Quantachrome Corp., USA). The catalysts were also characterized by their temperature programmed reduction (TPR) from 100° to 900°C with a linear heating rate of 20°C.min⁻¹ in a flow of H₂-Ar (3.7 mol% H₂) mixture (space velocity = 6000 cm³.g⁻¹.h⁻¹) in a quartz reactor (i.d. 4 mm) having a low dead volume. The hydrogen consumed in the TPR was measured quantitatively by TCD. Before the TPR, the catalyst was pretreated in a flow of He at 900°C for 1 h. The chemisorption of H₂ on the reduced catalysts was measured by saturating the catalyst with H₂ at 50°C in a flow of the H₂-Ar mixture for 4 h and then carrying out the temperature programmed desorption (TPD) of the adsorbed hydrogen from 50° to 700°C at a linear heating rate of 10°C.min⁻¹ in the flow of the H₂-Ar mixture (space velocity = 6000 cm³ g⁻¹.h⁻¹). The hydrogen desorbed (which corresponds to the amount adsorbed at 50°C) was measured quantitatively by the TCD. The H₂ desorption was complete upto 700°C. The experimental set-up used for the TPD/TPR studies is shown in Fig. 1.1.1 (Chapter-1.1).

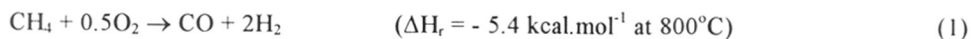
2.5.2.3 Catalytic Reaction

The schematic diagram of the experimental set-up and the quartz reactor used for the catalytic partial oxidation of methane to syngas are shown in Figs. 2.1.1 and 2.1.2 (Chapter-2.1), respectively.

The catalytic partial oxidation of methane to syngas was carried out by passing continuously a gaseous feed containing pure methane (> 99.95%) and oxygen (> 99.9%) over the catalyst (0.02 g) packed in a quartz reactor (i.d. 4 mm) kept in a tubular furnace (i.d. 25 mm). The temperature was measured/controlled by a Chromel-Alumel thermocouple provided in the center of the catalyst bed. The reaction temperature could be controlled within 5°C. The gas hourly space velocity (GHSV) of the feed was measured at 0°C and 1 atm pressure. The gaseous products (after condensing the water from the product stream at 0°C) were analysed by an on-line gas chromatograph using a spherocarb column.

2.5.3 RESULTS AND DISCUSSION

The partial oxidation of methane to syngas,



at very small contact time ($GHSV = 5.2 \times 10^5 \text{ cm}^3 \cdot \text{g}^{-1} \cdot \text{h}^{-1}$) has been carried out over following nickel containing catalysts with or without support at atmospheric pressure at two different temperatures (700° and 800°C).

- NiO-MgO (Ni/Mg = 1.2 and 3.0) without any support
- Mixed NiO-MgO (Ni/Mg = 3.0) supported on different commercial catalyst carriers, commonly used for supporting oxidation catalysts
- NiO supported on the catalyst carriers which are precoated with MgO
- NiO supported on a particular catalyst carrier (SA-5205) precoated with different alkaline earth and rare earth oxides
- NiO supported on SA-5205 precoated with MgO (NiO/MgO/SA-5205) with different loadings of MgO and NiO
- NiO/MgO/SA-5205 catalyst (Loading of NiO and MgO = 13.6 and 5.1 wt.%, respectively) calcined at different temperatures (600° - 1200°C).

The commercial catalyst carriers used for the supported nickel catalysts (Tables 2.5.1 and 2.5.2) are sintered low surface area, porous supports composed of refractory compounds, such as Al_2O_3 , SiO_2 , SiC , ZrO_2 and HfO_2 , etc. They have different chemical compositions and surface properties (viz. surface area, pore volume and porosity), as described earlier. The catalysts in their operating state (i.e. in their active form) are essentially Ni^0 dispersed on the alkaline earth and rare earth oxides supported on the different supports. The NiO from the catalysts is reduced in the initial short reaction period by its autocatalytic reaction with methane [6-8].

The catalysts have been characterized for their specific surface area. The reducibility (at different temperatures) and degree of reduction of the NiO supported on different catalyst carriers precoated with alkaline earth or rare earth oxides have been determined by carrying out TPR of the catalysts by H_2 (3.7 mol% H_2 in Ar) from 100° to 900°C at a linear heating rate of $20^\circ\text{C} \cdot \text{min}^{-1}$. The degree of NiO reduction is determined from the concentration of NiO in the catalyst and the amount of H_2 consumed in the TPR, assuming the reaction stoichiometry ($\text{NiO} + \text{H}_2 \rightarrow \text{Ni}^0 + \text{H}_2\text{O}$). The reduced catalysts are characterized by the chemisorption of H_2 at 50°C.

2.5.3.1 Influence of Support

The performance of the supported NiO-MgO (Ni/Mg = 3.0) catalysts in the oxidative conversion of methane to syngas is compared with that of the unsupported NiO-MgO (Ni/Mg = 3.0) in Table-2.5.1. The comparison clearly shows a strong influence of support on the performance of NiO-MgO catalyst. Both the activity and selectivity of the catalyst (NiO-MgO) are decreased after depositing it on the different catalyst carriers. The decrease in the catalytic performance is small when the catalyst is supported on SA-5205, SA-5218 and SZ-5564 supports but it is very large when the catalyst is deposited on the other supports. The catalyst supported on SA-5552 and SC-5532 shows a little or no activity even at 800°C.

Table 2.5.1 : Results of the oxidative conversion of methane to CO and H₂ over NiO-MgO (Ni/Mg = 3.0) mixed metal oxides deposited on the different supports (loading of NiO-MgO on support = 13 ± 1 wt.%) [Reaction conditions : CH₄/O₂ = 1.8 and GHSV = 5.2 × 10⁵ cm³.g⁻¹.h⁻¹]

Support	Catalyst surface area (m ² .g ⁻¹)	Reaction temp. (°C)	CH ₄ convn. (%)	Selectivity (%)		H ₂ /CO ratio	Productivity for CO (mol.g ⁻¹ .h ⁻¹)
				CO	H ₂		
Nil	3.66	800	95.9	99.8	99.6	2.00	14.3
		700	90.9	96.6	94.0	1.95	13.1
SA-5205	0.39	800	86.5	96.4	92.7	1.92	12.4
		700	80.3	92.2	90.9	1.97	11.1
SA-5218	0.34	800	82.8	95.9	92.1	1.92	11.9
		700	81.1	93.8	91.6	1.95	11.4
SA-5552	0.89	900	41.2	91.0	35.4	0.78	5.6
		800	1.8	-	-	-	-
SC-5532	0.36	900	1.9	-	-	-	-
		800	No reaction				
SZ-5564	0.57	800	86.2	95.7	92.5	1.93	12.3
		700	83.2	93.4	90.4	1.94	11.6
SS-5231	0.88	800	56.7	86.9	73.6	1.69	7.4

However, when the NiO is deposited on the different catalyst carriers precoated with MgO, the resulting supported nickel catalysts (Ni/Mg \approx 1.2) show the activity and selectivity in the catalytic process comparable to or even better (for SA-5205 and SZ-5564 supports) than that of the unsupported NiO-MgO (Ni/Mg \approx 1.2) catalyst (Table-2.5.2). These results reconfirm the earlier observed beneficial effect of precoating of catalyst support (containing Al₂O₃ and SiO₂) with MgO before depositing NiO on the support in the preparation of supported nickel catalyst [14, Chapter-2.4].

Table 2.5.2 : Results of the oxidative conversion of methane to CO and H₂ over NiO deposited on the different supports precoated with MgO (Loading of MgO and NiO on support = 6 ± 1 and 14 ± 2 wt.%, respectively) [Reaction conditions : CH₄/O₂ = 1.8 and GHSV = 5.2×10^5 cm³.g⁻¹.h⁻¹]

Support	Catalyst surface area (m ² .g ⁻¹)	Reaction temp. (°C)	CH ₄ convn. (%)	Selectivity (%)		H ₂ /CO ratio	Productivity for CO (mol.g ⁻¹ .h ⁻¹)
				CO	H ₂		
Without support ^a	5.9	800	93.5	92.9	96.9	2.07	13.0
		700	88.1	91.5	93.4	2.04	12.0
SA-5205	2.0	800	94.7	97.5	95.6	1.96	13.8
		700	89.7	94.3	95.0	2.01	12.6
SA-5218	1.6	800	92.9	99.8	97.1	1.86	13.9
		700	89.4	97.1	94.7	1.95	12.9
SA-5552	3.2	800	81.4	98.8	97.1	1.97	12.0
		700	78.8	97.5	96.8	1.99	11.5
SC-5532	1.7	800	91.5	96.8	96.1	2.00	13.2
		700	88.9	95.4	95.9	2.01	12.7
SS-5231	3.3	800	91.9	95.1	95.0	2.00	13.0
		700	88.2	92.8	94.0	2.04	12.2
SZ-5563	2.7	800	93.7	97.5	96.7	1.98	13.6
		700	89.5	94.2	94.8	2.01	12.5

^aUnsupported NiO-MgO catalyst having the Ni/Mg ratio (1.2) same as that for the supported catalysts.

The effect of support on the performance of the supported NiO-MgO catalyst (Table-2.5.1) arises mainly from the strong chemical interactions between the alumina and/or silica from the supports with the NiO from the mixed NiO-MgO deposited on the supports at the high calcination temperature (900°C). The chemical interactions are expected to result into formation of catalytically inactive binary metal oxide phases such as nickel silicate and/or aluminate, similar to that observed when NiO is directly supported on the silica and/or alumina containing catalyst carriers [14, Chapter-2.4]. The chemical interactions are expected to be stronger for the support containing larger concentration of Al₂O₃ and SiO₂ and/or having larger surface area. The results are quite consistent with this. For SZ-5564 support, which contains Al₂O₃ and SiO₂ at low concentrations, the decrease in the catalytic activity is small. For the silica-alumina supports (SA-5205, SA-5218 and SA-5552), the catalytic activity and selectivity of the supported Ni-catalyst is decreased with increasing the support surface area. The very low activity of the catalysts supported on high silica containing supports (viz. SS-5232 and SC-5532) may also be due to physical interactions of metallic nickel (formed during the initial period of the catalytic reaction), leading to its rapid crystal growth or sintering. This aspect of catalyst deactivation by support needs further investigation.

When the supports are precoated with MgO, at the high calcination temperature (900°C), there is a solid-solid reaction between the MgO and the Al₂O₃ and SiO₂ from the support surface, forming a stable protective layer of MgAl₂O₄ (spinel) and MgSiO₃, respectively, at the MgO-support interface [14, Chapter-2.4]. This protective layer is responsible for eliminating the chemical interactions between the active components of the supports (viz. Al₂O₃ and SiO₂) and the NiO, after its deposition on the MgO precoated supports.

The TPR curves for the NiO deposited on SA-5205, SA-5552, SS-5231 and SZ-5564 catalyst carriers precoated with MgO are presented in Fig. 2.5.1. Data on the degree of reduction of the NiO from the catalysts and H₂ chemisorption on the catalysts, after reduction at 900°C, are given in Table-2.5.3.

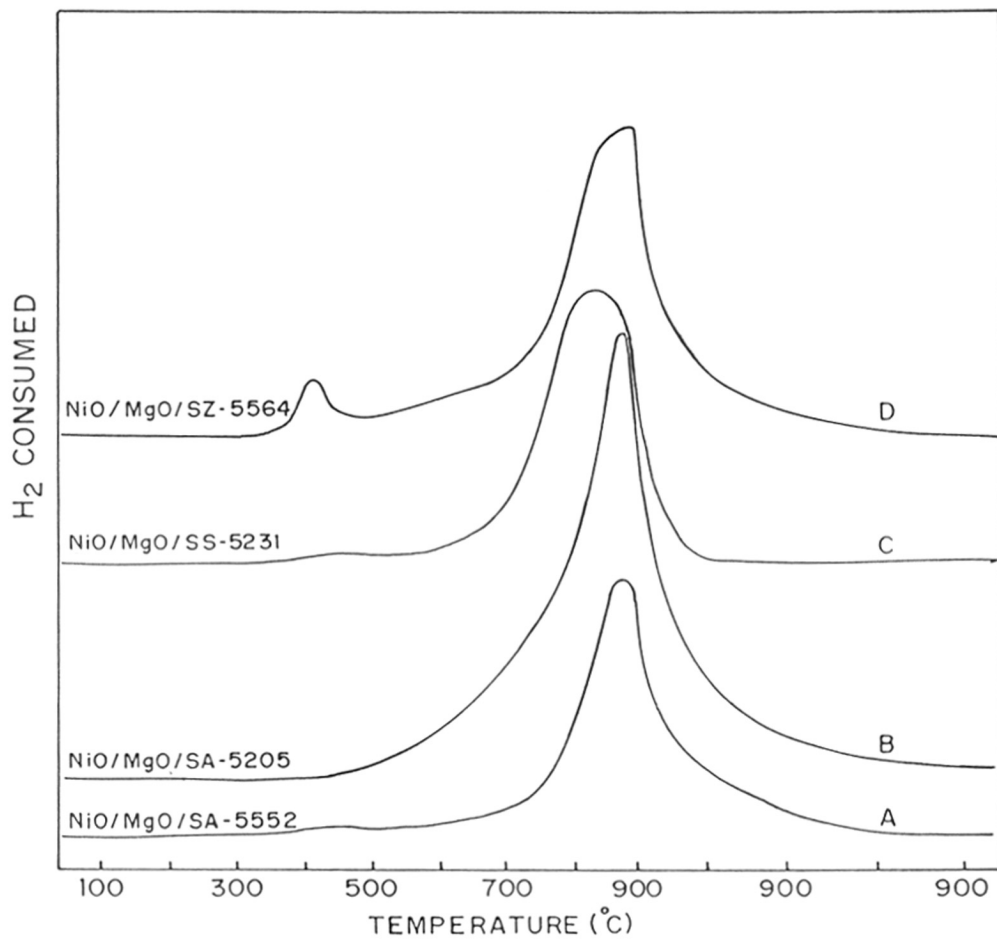


Fig. 2.5.1 : TPR of nickel oxide supported on different catalyst carriers precoated with MgO (Loading of MgO = 6.0 ± 1.0 wt.% and loading of NiO = 12.2 ± 1.5 wt.%)

Table 2.5.3 : Results showing the effect of support on the degree of reduction (by H₂ in TPR) of NiO deposited on different supports precoated with MgO and H₂ chemisorption on the reduced catalysts (loading of MgO and NiO : 6. ± 1 and 12.2 ± 1.5 wt.%, respectively)

Support	Redution (%)	H ₂ chemisorbed (μmol.g ⁻¹)
SA-5205	34.5	9.4
SA-5552	43.3	6.8
SS-5231	40.3	7.5
SZ-5564	36.7	8.9

The TPR of the NiO/MgO/SA-5205 catalyst is started above 400°C; it shows a single peak with a peak maximum above 800°C (Fig. 2.5.1B). The TPR is quite similar to that observed for a typical NiO-MgO complete solid solution [16, 17]. As expected for the solid solution, the degree of NiO reduction is small (34.5%). The high temperature TPR peak for the NiO/MgO/SA-5552, NiO/MgO/SS-5231 and NiO/MgO/SZ-5564 catalysts (Fig. 2.5.1A, C and D) and their low degree of reduction (Table-2.5.3) also indicate the formation of NiO-MgO solid solution in these catalysts. However, the observed small TPR peak between 400° and 500°C for these catalysts, indicating the presence of small amounts of free NiO, suggest that the formation of NiO-MgO solid solution is not complete. Thus, the comparison of the TPR and the degree of reduction of the different supported nickel catalysts shows a strong influence of support on the formation of NiO-MgO solid solution and consequently also on the degree of NiO reduction.

The H₂ chemisorption (which is a measure of the surface area of nickel) of the catalyst is also influenced significantly by the support; correlation exists between the H₂ chemisorption and the activity of the supported nickel catalysts (Tables 2.5.2 and 2.5.3). The catalytic activity is increased with increasing the H₂ chemisorption.

2.5.3.2 Influence of Support Precoating Agent

Results of the oxidative methane-to-syngas conversion over the NiO deposited on SA-5205 precoated with different alkaline earth or rare earth oxides are presented in Table-2.5.4. Also, results showing the influence of support precoating agent (alkaline earth or rare earth oxide) on the TPR and degree of NiO reduction of the catalysts and on the H₂ chemisorption, after their reduction, are given in Fig. 2.5.2 and Table-2.5.5.

Table 2.5.4 : Results showing effect of the precoating of catalyst support SA-5205 with different alkaline and rare earth metal oxides (MO_x) on the oxidative conversion of methane to CO and H₂ over NiO/MO_x/SA-5205 catalysts (loading of NiO on support = 13 ± 1 wt.%) [Reaction conditions : CH₄/O₂ = 1.8 and GHSV = 5.2 × 10⁵ cm³.g⁻¹.h⁻¹]

MO _x	Loading of MO _x (wt.%)	Catalyst surface area (m ² .g ⁻¹)	Reaction start temp. (°C)	Reaction temp. (°C)	CH ₄ convn (%)	Selectivity (%)		H ₂ /CO ratio	Productivity for CO (mol.g ⁻¹ .h ⁻¹)
						CO	H ₂		
Without precoating ^a	0.0	0.5	> 780	800 700	3.4 No reaction	12.1	-	-	0.06
MgO	5.0	2.0	635	800 700	94.7 89.7	97.5 94.3	95.6 95.0	1.96 2.01	13.8 12.6
CaO	6.5	1.3	675	800 700	82.0 73.4	91.9 87.2	89.6 85.8	1.95 1.97	11.2 9.6
SrO	16.6	0.8	> 800	900	4.7	85.7	-	-	0.6
BaO	8.6	0.7	> 800	900 800	6.1 1.6	54.0 33.8	- -	- -	0.5 0.1
Sm ₂ O ₃	15.3	0.9	514	800 700	87.2 80.6	93.8 90.2	91.2 88.1	1.94 1.95	12.2 10.9
Yb ₂ O ₃	19.7	2.1	538	800 700	88.3 81.6	95.5 93.6	93.2 91.9	1.95 1.96	12.6 11.4

^aNiO is deposited directly on the support.

The results (Table-2.5.4) show a very strong influence of the precoating agent on both the activity and selectivity in the catalytic process. In the absence of the precoating of the support, the

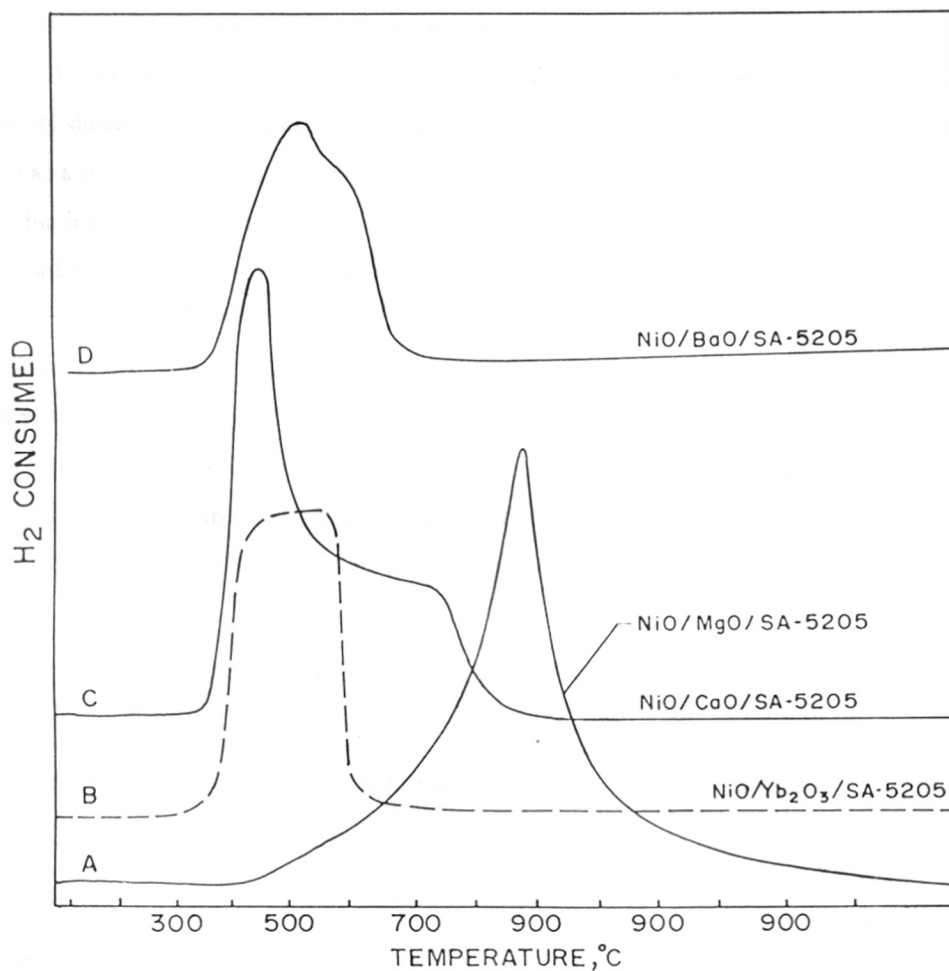


Fig. 2.5.2 : TPR of nickel oxide supported on catalyst carrier SA-5205 precoated with MgO, CaO, BaO or Yb₂O₃ (loading of NiO = 12.2 ± 1.5 wt.%, loading of MgO, CaO, BaO and Yb₂O₃ = 5.1, 6.5, 8.6 and 13.9 wt.%, respectively)

catalyst is not at all active and selective. When the support is precoated with SrO or BaO, the catalyst shows very poor performance. When the support is precoated with CaO, Sm₂O₃ or Yb₂O₃ the catalyst shows good performance. However, the best performance is observed for the catalyst prepared using MgO as a support precoating agent.

A comparison of the TPR (Fig. 2.5.2) and degree of NiO reduction (Table-2.5.5) for the catalysts shows a strong influence of the precoating agent on the state of NiO in the catalysts. For MgO as a precoating agent, the NiO reduction occurs at higher temperatures and also the degree of reduction is low because of the incorporation of Ni²⁺ deep in the MgO matrix forming NiO-MgO solid solution. However, in the case of other precoating agents, the NiO reduction starts at lower temperature (below 400°C) and also completes at much lower temperatures; the degree of reduction is also higher. The observed strong influence of the precoating agent on the TPR and degree of reduction of NiO from the supported nickel catalyst (Fig. 2.5.2 and Table 2.5.5) indicates that the nickel oxide in these catalysts exists in different forms; at least some part of the total NiO exists as a free-NiO. The presence of free-NiO was detected by XRD for the catalysts with CaO, SrO, BaO, Yb₂O₃ and Sm₂O₃ as precoating agents.

Table 2.5.5 : Results showing the effect of precoating agent (MO_x) on the degree of NiO reduction (by H₂ in TPR) of NiO/MO_x/SA-5205 catalysts and H₂ chemisorption on the reduced catalysts (NiO loading = 14 ± 2 wt.%)

Precoating agent (MO _x)	Reduction (%)	H ₂ chemisorbed (μmol.g ⁻¹)
MgO (5.1 wt.%)	34.5	9.4
CaO (6.5 wt.%)	53.9	5.2
BaO (8.6 wt.%)	57.4	1.7
Yb ₂ O ₃ (13.9 wt.%)	74.6	6.5

It is interesting to note from the results (Table 2.5.5) that the degree of NiO reduction for the catalysts with the precoating agent CaO, BaO and Yb₂O₃ is higher but the H₂ chemisorption on them (after the reduction) is lower than that for the catalyst with MgO as a precoating agent.

The observed lower H_2 chemisorption indicates sintering of nickel in the catalysts. The sintering is highest for the catalyst with BaO as a precoating agent. As expected, this catalyst also shows very poor activity and selectivity in the oxidative conversion of methane to syngas. The activity shown by the other catalysts is also consistent with their H_2 chemisorption (Tables 2.5.4 and 2.5.5); it is increased with increasing the H_2 chemisorption. However, interactions of nickel with the precoating agent and/or with the support itself may also be responsible for the observed large variation in the activity of the catalysts.

The observed higher H_2 chemisorption and hence higher stability of nickel against sintering for the catalyst with MgO as a precoating agent is attributed to the incorporation of Ni^{2+} in the MgO matrix forming a solid solution of NiO in MgO. In the reduction, the outermost Ni^0 atoms nucleate to form fine metal particles but some, which lie deeper, remain isolated in the MgO matrix either as Ni^0 or a charged Ni species in a low oxidation state. The reduced solid solution provides a strong ionic environment at the metal particle-support interface and even more so for the reduced species (Ni^0) which are at the surface but not fully exposed [16].

2.5.3.3 Influence of MgO Loading on Support

Results showing the influence of the loading of MgO (which acts as the best precoating agent among the alkaline earth and rare earth oxides) in the catalyst having almost the same NiO loading (13.4 ± 0.2 wt.%) on its performance in the partial oxidation of methane are presented in Fig. 2.5.3. TPR curves and H_2 chemisorption data for the catalyst with different MgO loadings (0 - 5.1 wt.%) are presented in Fig. 2.5.4 and Table 2.5.6, respectively.

In the absence of MgO, the catalyst has a very small activity with very poor selectivity for CO and H_2 . This is expected partly because of the strong chemical interaction of nickel with Al_2O_3 and SiO_2 from the support, resulting in formation of catalytically inactive binary metal oxide phases viz. $NiAl_2O_4$ and Ni_2SiO_4 [14, Chapter-2.4]. The degree of NiO reduction at the zero MgO loading is, however, higher than that observed in the presence of MgO. The TPR of the catalyst with zero MgO loading (Fig. 2.5.4A) is quite similar to that observed for pure NiO. These observations indicate presence of free-NiO as a major fraction of the total nickel in the catalyst. However, the H_2 chemisorption on the reduced catalyst is very low, indicating sintering of nickel to a large extent. Thus, the very low activity of the catalyst is attributed to both the strong nickel-support chemical interactions and sintering of the active catalyst component (Ni^0).

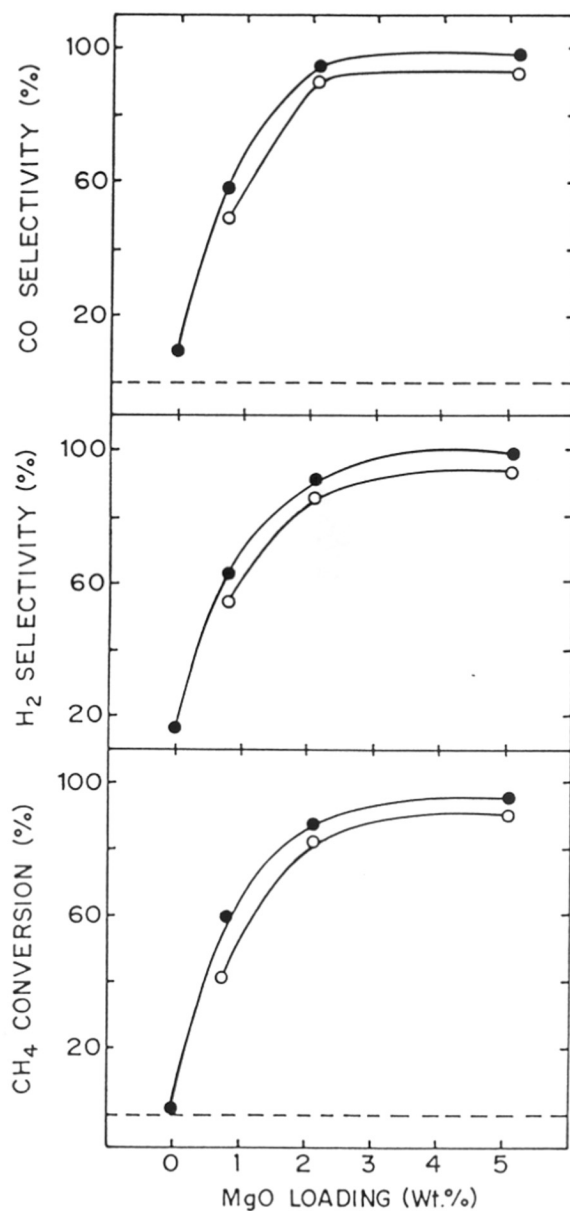


Fig. 2.5.3 : Variation of the conversion and selectivity in the oxidative methane-to-syngas conversion at 700°C (O) and 800°C (●) with the MgO loading for the NiO (12.2 ± 1.5 wt.)/MgO/SA-5205 catalyst [CH_4/O_2 ratio in feed = 1.8, GHSV = $5.2 \times 10^5 \text{ cm}^3 \cdot \text{g}^{-1} \cdot \text{h}^{-1}$]

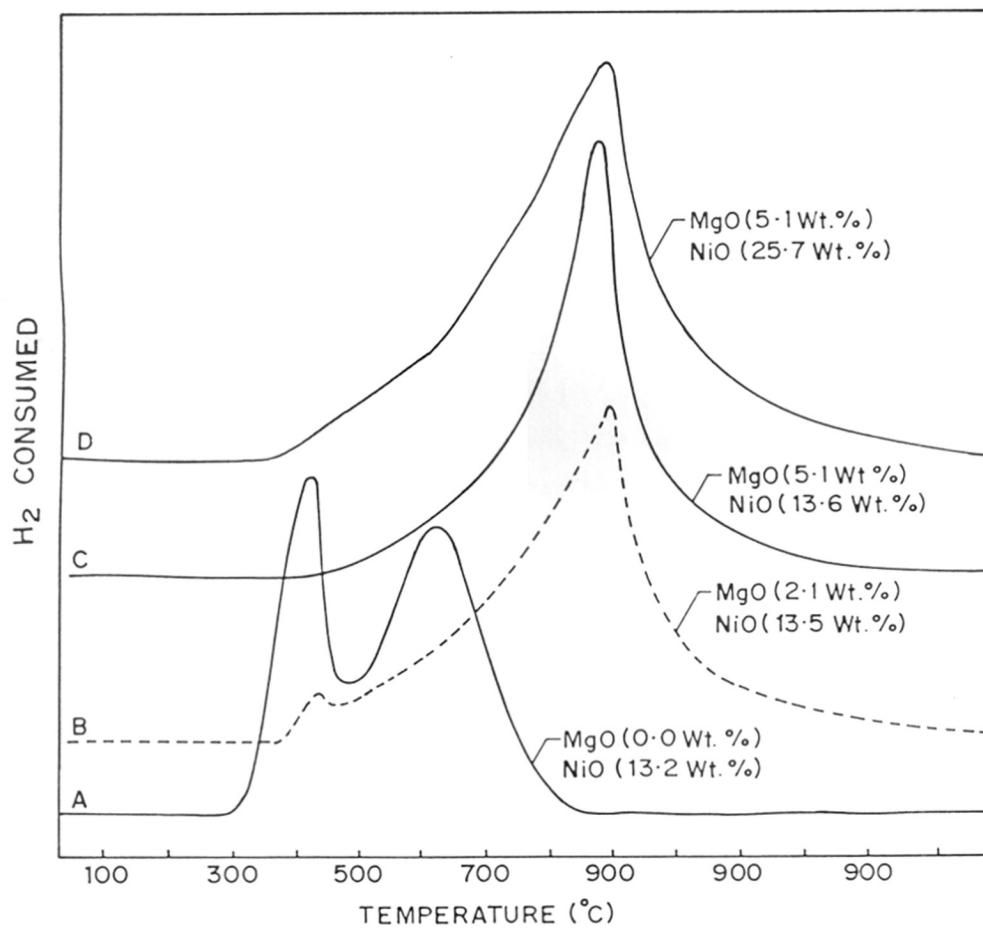


Fig. 2.5.4 : TPR of nickel oxide supported on catalyst carrier SA-5205 pre-coated with MgO with different loadings of MgO and NiO.

Table 2.5.6: Results showing the effect of NiO and MgO loadings on the degree of NiO reduction (by H₂ in TPR) of NiO/MgO/SA-5205 catalyst and H₂ chemisorption on the reduced catalyst.

Loading (wt.%)		Reduction (%)	H ₂ chemisorbed (μmol.g ⁻¹)
NiO	MgO		
13.2	0.0	64.5	1.1
13.5	2.1	35.0	6.2
13.6	5.1	34.5	9.4
25.7	5.1	42.9	5.7

Both the activity and selectivity of the catalyst are increased sharply with increasing the MgO loading. However, above the MgO loading of about 2 wt.%, the influence on the catalytic activity and selectivity is small. For the low MgO loading (2.1 wt.%), the TPR curve (Fig. 2.5.4B) shows a low temperature reduction peak (between 400° and 500°C), indicating the presence of free-NiO in the catalyst. But the presence of free-NiO is not observed for the catalyst with 5.1 wt.% MgO loading (Fig. 2.5.4C). A comparison of the TPR curves (Fig. 2.5.4A, B, C) clearly shows a sharp decrease in the free-NiO in the catalyst with increasing the MgO loading because of the increased dissolution of NiO in MgO. Consequently, the degree of NiO reduction is also decreased with increasing the MgO loading and the H₂ chemisorption on the reduced catalyst is increased (Table 2.5.6).

It may, however, be noted that, when the MgO loading is increased from 2.1 to 5.1 wt.%, the change in the NiO reduction is very small but that in the H₂ chemisorption and also in the activity and selectivity is appreciable. This shows that enough MgO on the support is essential for having a perfect NiO-MgO solid solution and also for stabilising nickel in the catalyst against sintering.

2.5.3.4 Influence of NiO Loading on MgO Precoated Support

Results showing the influence of NiO loading in the NiO/MgO/SA-5205 catalyst, having the same loading of MgO (5.1 wt.%), on its performance in the oxidative methane-to-syngas

conversion are presented in Fig. 2.5.5. TPR curves and the data on the degree of reduction and H₂ chemisorption for the catalyst with different NiO loadings (0 - 25.5 wt.%) are included in Fig. 2.5.4 and Table 2.5.6, respectively.

The influence of NiO loading as compared to that of MgO loading in the catalyst on its activity and selectivity is quite small. With the increase in the NiO loading from 1.6 to 25 wt.%, the CO selectivity is almost not changed but the methane conversion and H₂ selectivity are passed through a maximum (at the NiO loading of about 10 wt.%).

For the high NiO loading (25.7 wt.%), the TPR curve has a hump at low temperatures (350° - 550°C) and the reduction starts at lower temperatures (at about 350°C), indicating the presence of free-NiO to an appreciable extent. This is consistent with the high degree of NiO reduction as compared to that for the 13.6 wt.% NiO loading (Table 2.5.6). However, the H₂ chemisorption for the higher NiO loading is smaller. This indicates that, for the higher NiO loading, the sintering of nickel is more. The observed lower catalytic activity for the catalyst with 25.7 wt.% NiO loading is consistent with its lower H₂ chemisorption (Fig. 2.5.5 and Table 2.5.6).

2.5.3.5 Influence of Calcination Temperature

The influence of calcination temperature of the NiO (13.6 wt.%)/MgO(5.1 wt.%)/SA-5205 catalyst on its activity and selectivity in the catalytic process, TPR, degree of NiO reduction and H₂ chemisorption (after the reduction) is shown in Figs. 2.5.6-2.5.8. From the results, following general observations can be made.

The increase in the catalyst calcination temperature from 600° to 900°C has little or no effect on the catalytic activity and selectivity. But a further increase in the calcination temperature results in a decrease in the catalytic activity; the catalytic activity is totally killed by the calcination at 1200°C.

With the increase in the calcination temperature, the shape of TPR curve is changed, the temperature at which the reduction of the catalyst starts is gradually increased and also the TPR curve and also its peak maximum is gradually shifted towards the higher temperature side (Fig. 2.5.7). The degree of NiO reduction is also decreased appreciably (Fig. 2.5.8a). These observations suggest that the incorporation of Ni²⁺ in the MgO matrix forming NiO-MgO solid-solution is increased with increasing the temperature because of the higher diffusivity of the ionic Ni²⁺ and O²⁻ species in solid phase at higher temperature. However, at a very high calcination

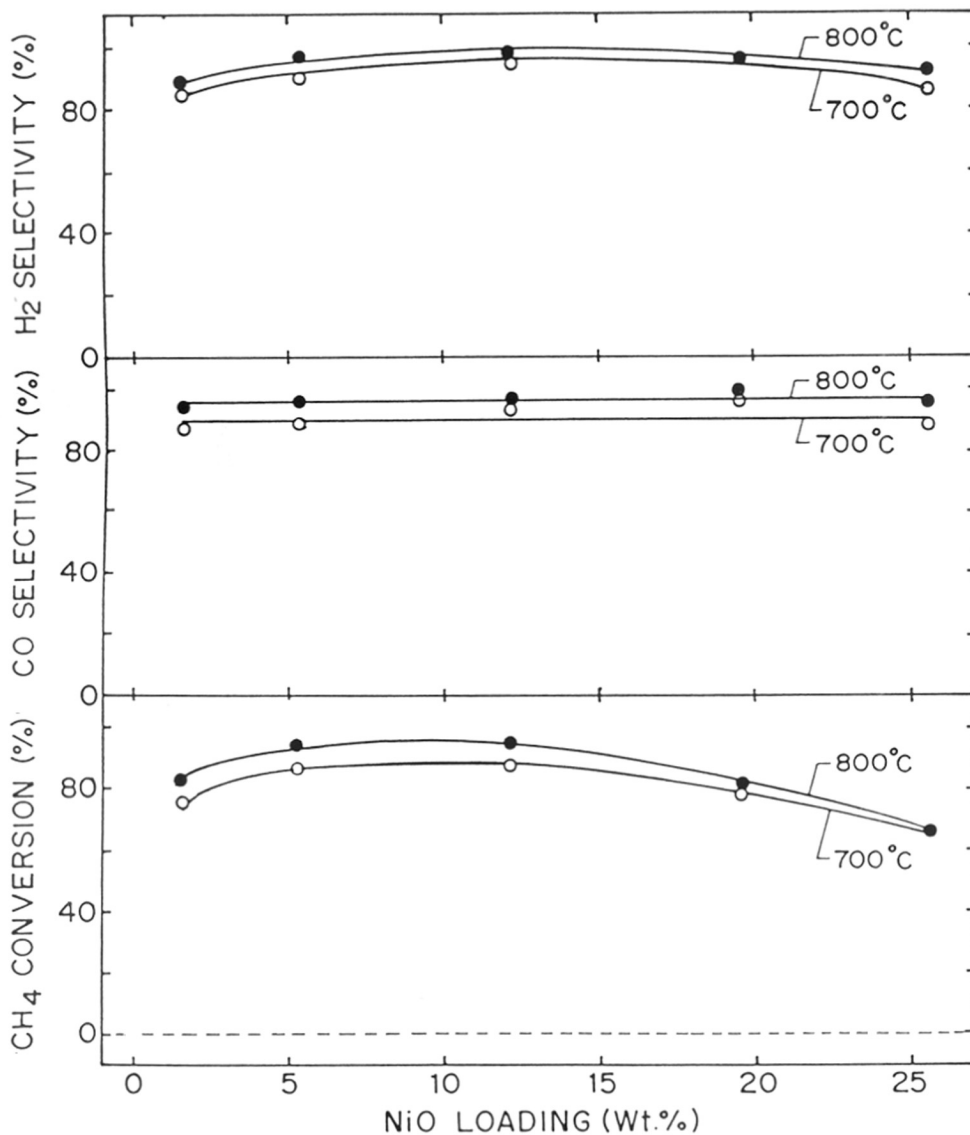


Fig. 2.5.5 : Variation of the conversion and selectivity in the oxidative methane-to-syngas conversion at 700°C (O) and 800°C (●) with the NiO loading for the NiO/MgO(5.1 wt.)/SA-5205 catalyst [CH_4/O_2 ratio in feed = 1.8, GHSV = $5.2 \times 10^5 \text{ cm}^3 \cdot \text{g}^{-1} \cdot \text{h}^{-1}$]

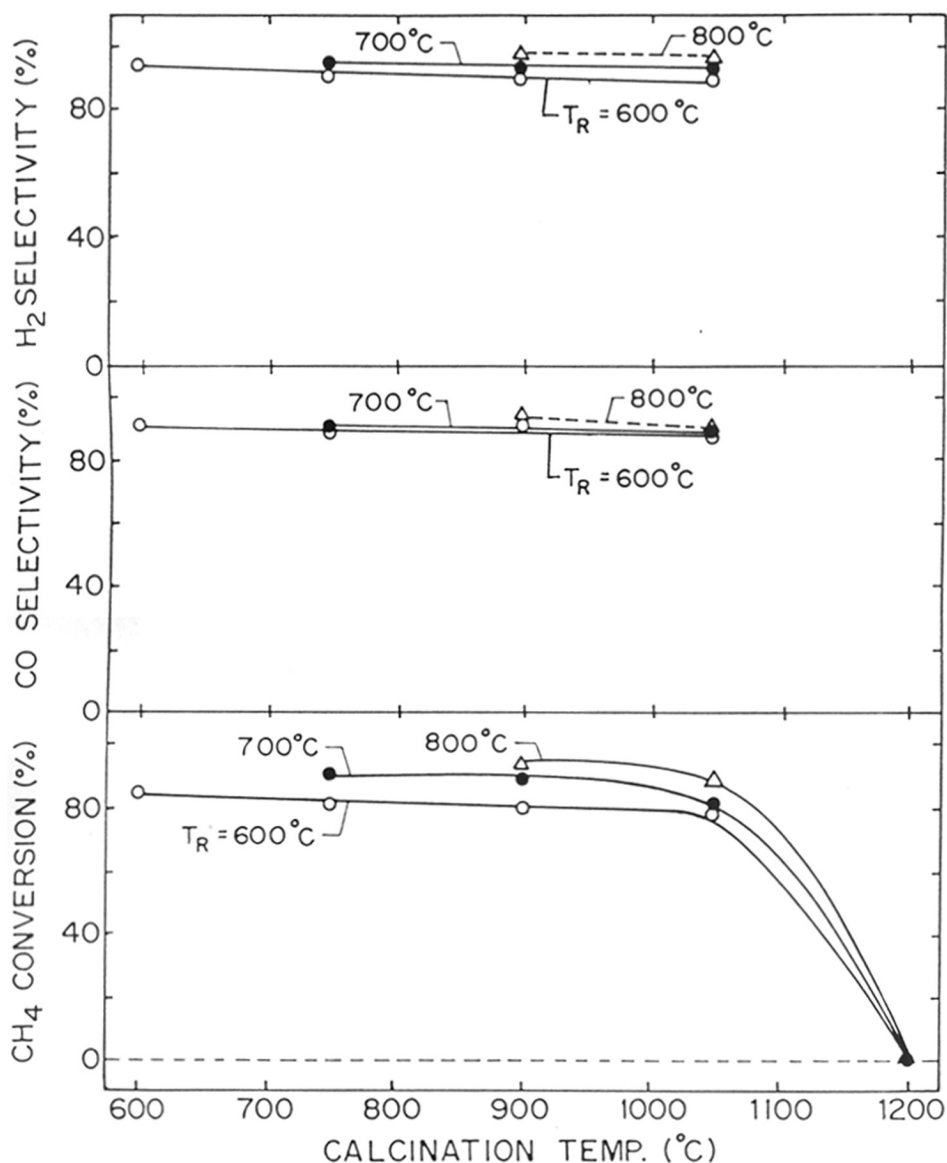


Fig. 2.5.6 : Dependence of the conversion and selectivity in the oxidative methane-to-syngas conversion over NiO (13.6 wt.)/MgO (5.1 wt.)/SA-5205 catalyst on its calcination temperature [Reaction temperature (T_R) : 600°C (O), 700°C (●) and 800°C (Δ); CH₄/O₂ ratio in feed = 1.8, GHSV = $5.2 \times 10^5 \text{ cm}^3 \cdot \text{g}^{-1} \cdot \text{h}^{-1}$]

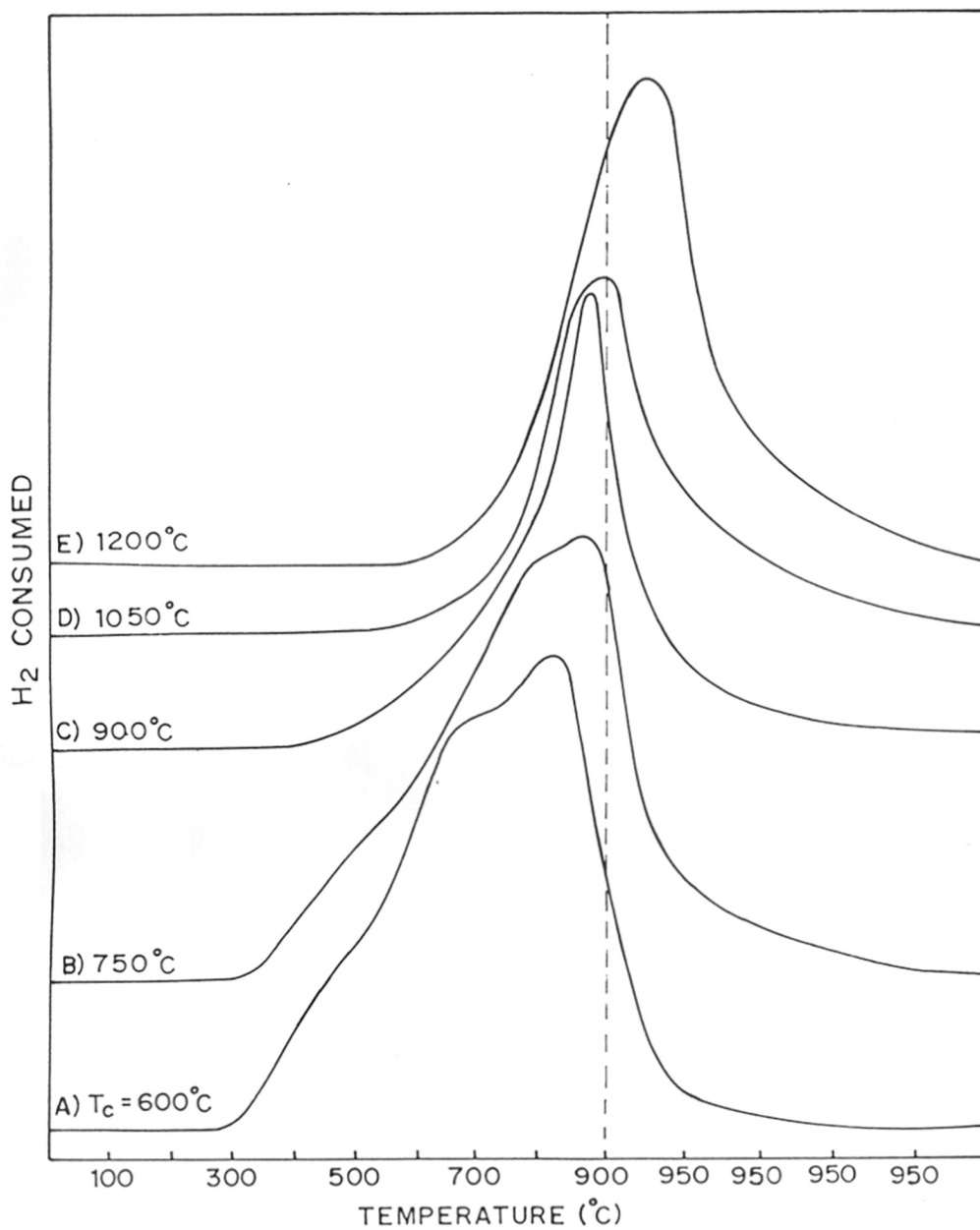


Fig. 2.5.7 : TPR of NiO/MgO/SA-5205 catalyst calcined in air at different temperatures (loading of MgO and NiO = 5.1 and 13.6 wt.%, respectively).

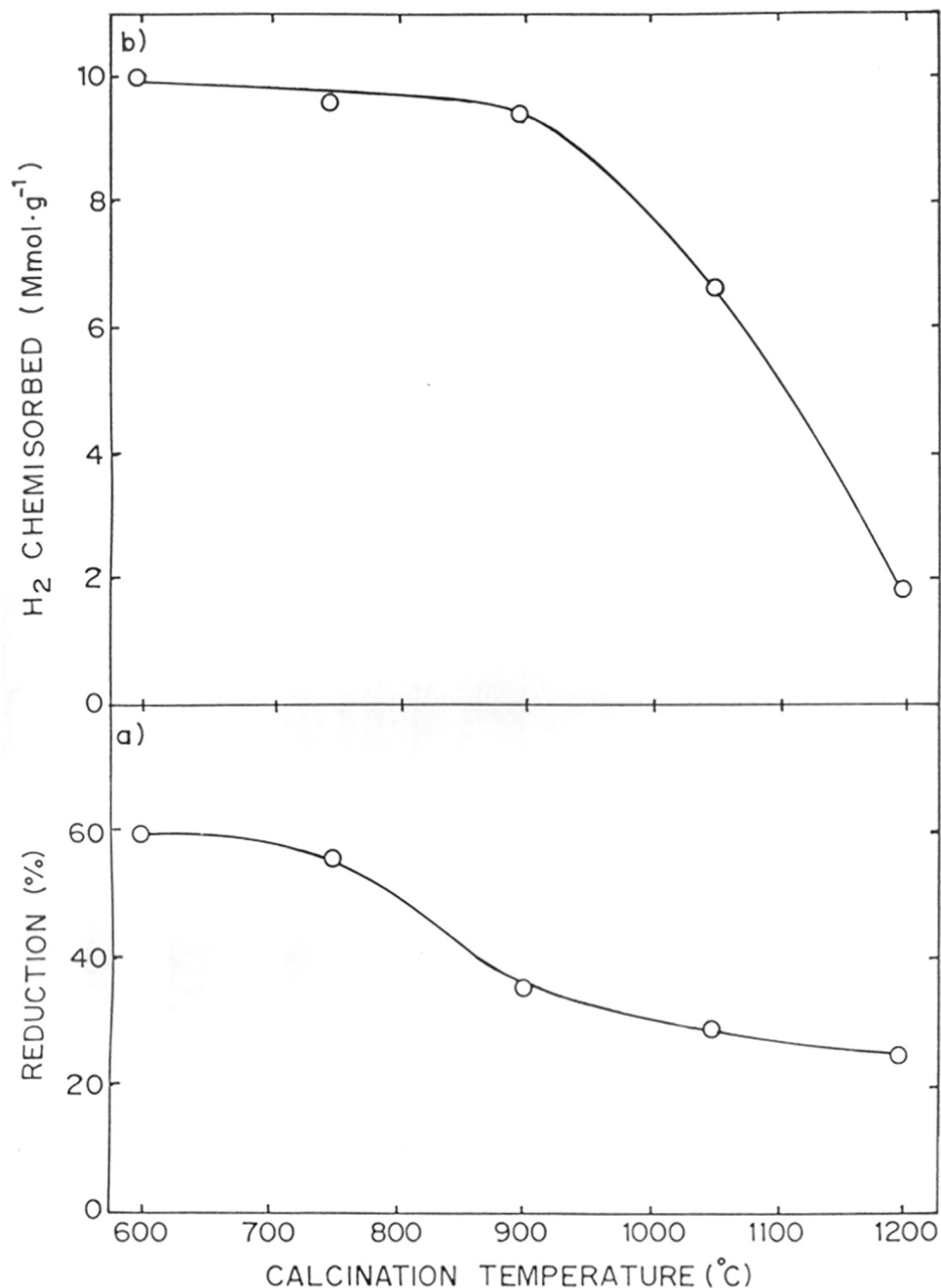


Fig. 2.5.8 : Effect of calcination temperature of NiO/MgO/SA-5205 catalyst on a) degree of NiO reduction and b) H₂ chemisorption on the reduced catalyst (loading of MgO and NiO = 5.1 and 13.6 wt.%, respectively).

temperature (1200°C), there is a high possibility of the formation of NiAl_2O_4 (spinel) because of the higher mobility of Ni^{2+} species. Indeed, the presence of NiAl_2O_4 as a major phase in the catalyst calcined at 1200°C, is confirmed by XRD. However, at the calcination temperature of 1050°C, the presence of this phase only in traces was observed.

The H_2 chemisorption is decreased with increasing the calcination temperature; the decrease is sharp above 900°C (Fig. 2.5.8b). The observed large decrease in the catalytic activity with increasing the calcination temperature above 900°C is quite consistent with the sharp decrease in the H_2 chemisorption. Thus, influence of the catalyst calcination temperature, particularly above 900°C is attributed to both the sintering of nickel and the strong nickel-support chemical interactions.

2.5.4 CONCLUSIONS

From the studies on the oxidative conversion of methane to syngas over the supported Ni-catalyst (prepared by different methods and using different commercial low surface area porous catalyst carriers or prepared with different compositions) and their TPR and H_2 chemisorption (after reduction), following important conclusions have been drawn.

1. The catalytic activity and selectivity of NiO-MgO are reduced markedly by depositing it on the catalytic carriers containing Al_2O_3 and SiO_2 at higher concentrations and having higher surface area. However, when the supported catalyst is prepared by depositing NiO on the catalyst carriers precoated with MgO, the influence of support is drastically reduced and the supported catalysts show performance in the catalytic process comparable to that of the unsupported NiO-MgO; the supported catalysts prepared using SA-5205 and SZ-5564 supports show even slightly superior performance. For these supported catalysts, the formation of NiO-MgO solid solution, degree of NiO reduction and H_2 chemisorption are strongly influenced by the support used.
2. The catalytic activity and selectivity, TPR, degree of NiO reduction and H_2 chemisorption (or nickel surface area) of the supported catalyst ($\text{NiO}/\text{MO}_x/\text{SA-5205}$, where MO_x is the support precoating agent (viz. MgO, CaO, SrO, BaO, Sm_2O_3 or Yb_2O_3) are strongly influenced by the precoating agent. The catalyst prepared using SrO or BaO as the support precoating agent shows little or no catalytic activity but that prepared using MgO as the support precoating

agent shows highest catalytic activity and selectivity. The catalyst characteristics are strongly influenced by the MgO loading, particularly at lower loadings (< 2 wt.%). However, the influence of NiO loading on the NiO/MgO/SA-5205 catalyst on its activity/selectivity and other characteristics is relatively much smaller.

3. In the supported Ni-catalysts prepared by depositing NiO on support precoated with MgO, the MgO plays two important roles - one, to avoid the chemical interactions of the catalytically active component (NiO) with the reactive components of support (viz. Al_2O_3 and SiO_2) by providing a stable protective layer of MgAl_2O_4 (spinel) and/or Mg-silicate on the support surface; and second, to stabilise nickel on the support surface against sintering by forming a NiO-MgO solid solution.
4. The NiO-MgO solid solution formation and consequently TPR and degree of NiO reduction of the NiO/MgO/SA-5205 catalyst are strongly influenced by its calcination at different temperatures (600° - 1200°C). The catalyst calcination upto 900°C has a little or no effect on the catalytic activity/selectivity and a small effect on the H_2 chemisorption but these are drastically reduced when the calcination temperature is increased further, particularly above 1050°C, because of sintering and/or formation of catalytically inactive NiAl_2O_4 .
5. The activity/selectivity of the different supported Ni-catalysts is consistent with their H_2 chemisorption, showing a good correlation between the two.

REFERENCES

1. A.T. Aschroft, A.K. Cheetham, J.S. Foord, M.L.H. Green, C.P. Grey, A.J. Murrell, and P.D.F. Vernon, *Nature* 344 (1990) 319.
2. P.D.F. Vernon, M.L.H. Green, A.K. Cheetham, and A.T. Aschroft, *Catal. Lett.* 6 (1990) 181; *Nature* 352 (1991) 225; *Catal. Lett.* 13 (1992) 417.
3. D. Dissanayake, M.P. Rosynek, K.C.C. Kharas, and J.H. Lunsford, *J. Catal.* 132 (1991) 117.
4. V.R. Choudhary, S.D. Sansare, and A.S. Mamman, *Appl. Catal.* 90 (1992) L1.
5. V.R. Choudhary, A.M. Rajput, and V.H. Rane, *Catal. Lett.* 16 (1992) 269.
6. V.R. Choudhary, A.S. Mamman, and S.D. Sansare, *Angew. Chem. Int. Ed. Engl.* 31 (1992) 1189.
7. V.R. Choudhary, A.M. Rajput, and B. Prabhakar, *Catal. Lett.* 15 (1992) 363..
8. V.R. Choudhary, A.M. Rajput, and V.H. Rane, *J. Phys. Chem.*, 96 (1992) 8686; *Catal. Lett.* 22 (1993) 289.
9. V.R. Choudhary, A.M. Rajput, and B. Prabhakar, *J. Catal.* 139 (1993) 329.
10. L.D. Schmidt, and D.A. Hickman, *Science*, 259, 343 (1993); *J. Catal.* 138 (1992) 267.
11. L.D. Schmidt, E.A. Haufear, and D.A. Hickman, *Catal. Lett.* 17 (1993) 223.
12. P.M. Tornianan, X. Chu, and L.D. Schmidt, *J. Catal.* 146 (1994) 1.
13. J.A. Lapszewicz, and X.Z. Jiang, *Prepr. Am. Chem. Soc., Div. Petr. Chem.* 37 (1992) 252.
14. V.R. Choudhary, B.S. Uphade, and A.S. Mamman, *Catal. Lett.* 32 (1995) 387.
15. B.S. Uphade, A.S. Mamman, and V.R. Choudhary, *Catalysis : Modern Trends*, N.M. Gupta and D.K. Chakraborty (Eds.), Narosa Publishing House, New Delhi, (1995) p. 380.
16. A. Bossi Highfield, and F.S. Stone, *Stud. Surf. Sci. Catal.* 16 (1983) 181.
17. A. Paramaliana, A. Arena, F. Frusteri, and N. Giordano, *J. Chem. Soc. Faraday Trans.* 86 (1990) 2663.

CHAPTER - 2.6

SIMULTANEOUS STEAM AND CO₂ REFORMING OF METHANE TO SYNGAS OVER NiO/MgO/SA-5205 IN PRESENCE AND ABSENCE OF OXYGEN

2.6.1 INTRODUCTION

Conversion of methane to CO and H₂ (i. e. syngas, which is a versatile feedstock for ammonia, methanol and Fischer-Tropsch synthesis processes and several other carbonylation and hydrogenation or reduction processes) in an energy efficient and safe manner by the coupling of the exothermic (partial oxidation with O₂) and endothermic (steam and/or CO₂ reforming) reactions of methane [1-3] is a process of great practical importance. A few studies have been reported earlier on oxy-steam reforming of methane over NiO-CaO, oxy-CO₂ reforming of methane over supported Rh, NiO-CaO and Ni/ALPO-5 catalysts [3, 4, 5], and also on oxy-steam and CO₂ reforming of methane over NiO-CaO, Ni/ALPO-5 and LaNiO₃ catalysts [1, 5, 6].

Recently, extensive studies [7-22] have been reported on the CO₂ reforming of methane over supported Pt group metals [7-11], NiO-alkaline earth oxides [12], Ni/La₂O₃ [13-15], Ni/Al₂O₃ [16-19], NiO-CaO [12, 14, 20], NiO-MgO [12, 21] and NiO/MgO-CaO [22] catalysts. In general, carbon deposition on catalyst in the CO₂ reforming is very fast [21]. Very recent studies on the steam and CO₂ reforming of methane over NiO-CaO [15] showed that the carbon deposition (which is very high in the CO₂ reforming) is drastically reduced when the steam and CO₂ reforming reactions are carried out simultaneously.

In an earlier studies reported by Choudhary et. al. [23], NiO-MgO catalyst showed high activity and selectivity in the partial oxidation of methane to syngas at extremely low contact time (\approx 1 ms). However, when this catalyst is supported directly on the alumina and/or silica containing catalyst carriers, its activity is reduced drastically [24, Chapter-2.3]. Supported nickel catalysts prepared using silica and/or alumina containing catalyst carriers precoated with MgO, CaO or rare earth oxides show much higher activity, selectivity and productivity in the methane-to-syngas conversion process than the catalysts prepared using the catalyst carriers without any

precoating [25, Chapter-2.4]. Among the precoating metal oxides, the best performance is shown by MgO. It is, therefore, interesting to study steam and/or CO₂ reforming of methane to syngas over NiO supported on MgO precoated commercial low surface area macroporous catalyst carrier (SA-5205, obtained from Norton Co., USA) in the presence and absence of oxygen at very low contact times. The present investigation was undertaken with the above objective.

2.6.2 EXPERIMENTAL

2.6.2.1 Catalyst Preparation

Supported nickel catalyst [NiO (13.6 wt.%)/MgO (5.1 wt.%)/SA-5205] used in this investigation was developed in our laboratory for the partial oxidation of methane to syngas at extremely small (≈ 1 ms) contact time. It has high thermal and hydrothermal stability and also has high mechanical strength. It was prepared by depositing nickel nitrate from its aqueous solution on 22-30 mesh size particles of commercial catalyst carrier - SA-5205 [sintered low surface area macroporous support, obtained from Norton Co., USA] precoated with MgO, using incipient wetness impregnation technique followed by drying and decomposing (or calcining) in air at 900°C for 4 h. The catalyst carrier was precoated with MgO by impregnating the carrier with Mg-nitrate, drying and decomposing as above. The support (Appendix-1) consists of mainly alumina (86.1 wt.%) and silica (11.8 wt.%) and its surface area, porosity, pore volume and average pore size are, $< 0.01 \text{ m}^2\cdot\text{g}^{-1}$, 54%, $0.35 \text{ cm}^3\cdot\text{g}^{-1}$ and $200 \text{ }\mu\text{m}$, respectively.

2.6.2.2 Catalyst Characterization

The catalyst was characterised for its surface area by the single point BET method, using a Monosorb Surface Area Analyser (Quantachrome Corp., USA). The catalyst after powdering was examined by XRD for the presence of different crystalline phases. The catalyst was also characterised by its temperature programmed reduction (TPR) from 100° to 900°C with a linear heating rate of $20^\circ\text{C}\cdot\text{min}^{-1}$ in a flow of H₂-Ar (3.7 mol% H₂) mixture (space velocity = $6,000 \text{ cm}^3\cdot\text{g}^{-1}\cdot\text{h}^{-1}$) in a quartz reactor (i.d. 4 mm) having a low dead volume. The hydrogen consumed in the TPR was measured quantitatively by a thermal conductivity detector (TCD). Before the

TPR, the catalyst was pretreated in a flow of He at 900°C for 1 h. The chemisorption of H₂ on the reduced catalyst was measured by saturating the catalyst with H₂ at 50°C in the flow of the H₂-Ar mixture for 2 h and then carrying out the temperature programmed desorption (TPD) of the chemisorbed hydrogen from 50° to 700°C at a linear heating rate of 10°C.min⁻¹ in the flow of the H₂-Ar mixture (space velocity = 6,000 cm³.g⁻¹.h⁻¹). The hydrogen desorbed (which corresponds to the amount chemisorbed at 50°C) was measured quantitatively by the TCD. The experimental set-up used for the TPD/TPR studies is shown in Fig. 1.1.1 (Chapter-1.1).

2.6.2.3 Catalytic Reaction

The schematic diagrams of experimental set-up and the quartz reactor used in the simultaneous steam and CO₂ reforming of methane to syngas in presence and absence of oxygen are shown in Fig. 2.1.1 (Chapter-2.1) and Fig. 1.1.1 (Chapter- 1.1), respectively.

The catalytic steam reforming, CO₂ reforming and simultaneous steam and CO₂ reforming of methane-to-syngas reactions in presence and absence of oxygen over the catalyst were carried out at atmospheric pressure in a continuous flow quartz reactor (i.d. 9 mm) packed with 0.3 g catalyst and provided with a Chromel-Alumel thermocouple located in the center of the catalyst bed. The feed was a mixture of pure methane (> 99.95%), CO₂ (99.995%) and/or steam with or without oxygen (> 99.9%). Water was added to the feed using a SAGE syringe pump and a specially designed evaporator. Before carrying out the reaction, the catalyst was heated insitu at 900°C in a flow (50 cm³.min⁻¹) of moisture free nitrogen for 1 h. The catalytic reactions were carried out at different temperatures, gas hourly space velocities (GHSV, measured at 0°C at 1 atm) and relative concentrations of methane, steam, CO₂ and O₂ in the feed. The product gases (after condensation of the water from them at 0°C) were analysed by an on-line gas chromatograph with TCD, using a Sphero carb column and He as a carrier gas. The C, H, and O balance across the reactor was within 2-6%. The experiments with larger error in the material balance were rejected. The H₂ and CO selectivities reported in this paper are based on the methane conversion alone.

2.6.3 RESULTS

2.6.3.1 Catalyst Characterization

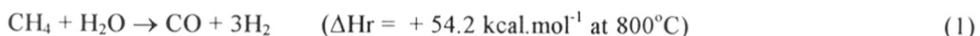
The surface area of the supported catalyst was $2.0 \text{ m}^2 \cdot \text{g}^{-1}$. The XRD analysis of the powdered catalyst showed no presence of a separate NiO phase, indicating a complete formation of a solid solution between NiO and MgO in the supported catalyst. However, a minor phase MgAl_2O_4 , resulting from a solid-solid reaction between MgO and Al_2O_3 (from the support) at the MgO-support interface, was observed. The formation of this phase (which consumes most of the alumina on the support surface) between the active catalyst mass (i.e. NiO-MgO solid solution) and the support is essential for avoiding chemical interactions between the nickel and alumina and consequently for avoiding the formation of catalytically inactive NiAl_2O_4 (spinel) phase, which is difficult to reduce [25, Chapter-2.4].

The TPR curve for the supported catalyst is shown in Fig. 2.6.1. In the TPR, the catalyst reduction starts at about 400°C and the peak maximum temperature is above 800°C . The TPR of the supported catalyst is quite similar to that observed for a typical NiO-MgO complete solid solution [26, 27]. From the knowledge of the concentration of NiO in the catalyst and the amount of H_2 consumed in the TPR, and assuming the reaction stoichiometry ($\text{NiO} + \text{H}_2 \rightarrow \text{Ni}^0 + \text{H}_2\text{O}$), the degree of reduction of NiO from the catalyst is estimated to be 34.5%.

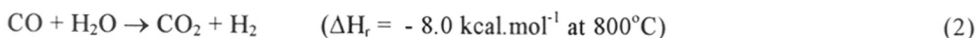
The TPD of H_2 (chemisorbed at 50°C) on the supported catalyst, after its reduction at 900°C for 1 h, is presented in Fig. 2.6.2. The amount of H_2 chemisorbed (at 50°C) on the reduced catalyst was $9.4 \mu\text{mol} \cdot \text{g}^{-1}$. The multiple peaks of the TPD show surface heterogeneity of hydrogen adsorption sites on the catalyst.

2.6.3.2 Steam and/or CO_2 Reforming of Methane

Results showing the influence of temperature and space velocity on the conversion of methane and water, CO selectivity and H_2/CO product ratio in the steam reforming of methane (reaction-1) over the supported catalyst are presented in Fig. 2.6.3.



The observed higher H_2/CO ratio (> 3.0) indicates that water gas shift reaction,



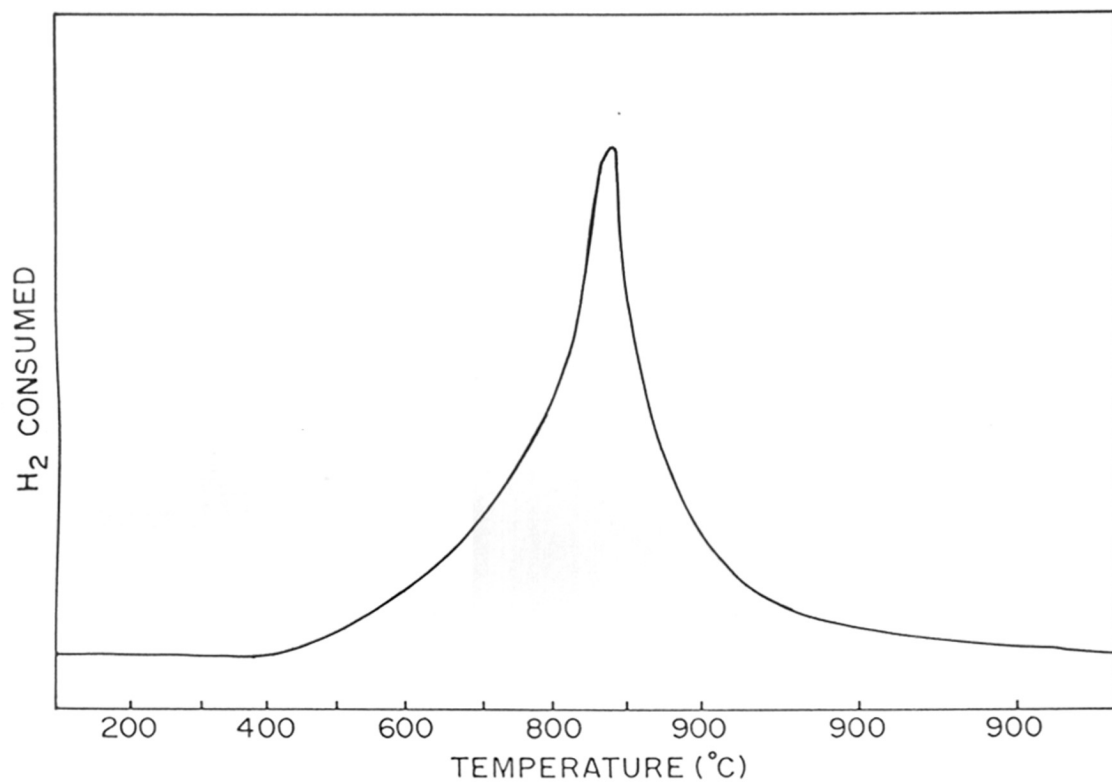


Fig. 2.6.1 :. TPR of NiO/MgO/SA-5205 catalyst.

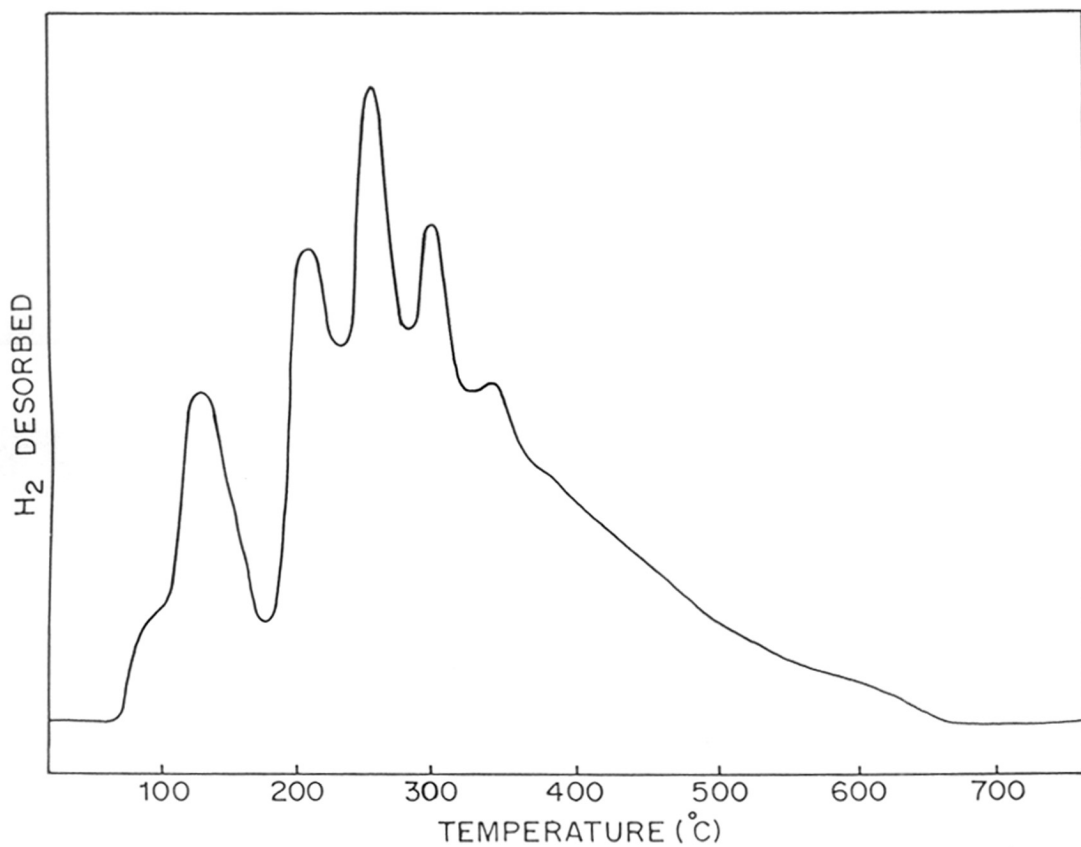


Fig. 2.6.2 : TPD of NiO/MgO/SA-5205 catalyst reduced earlier at 900°C.

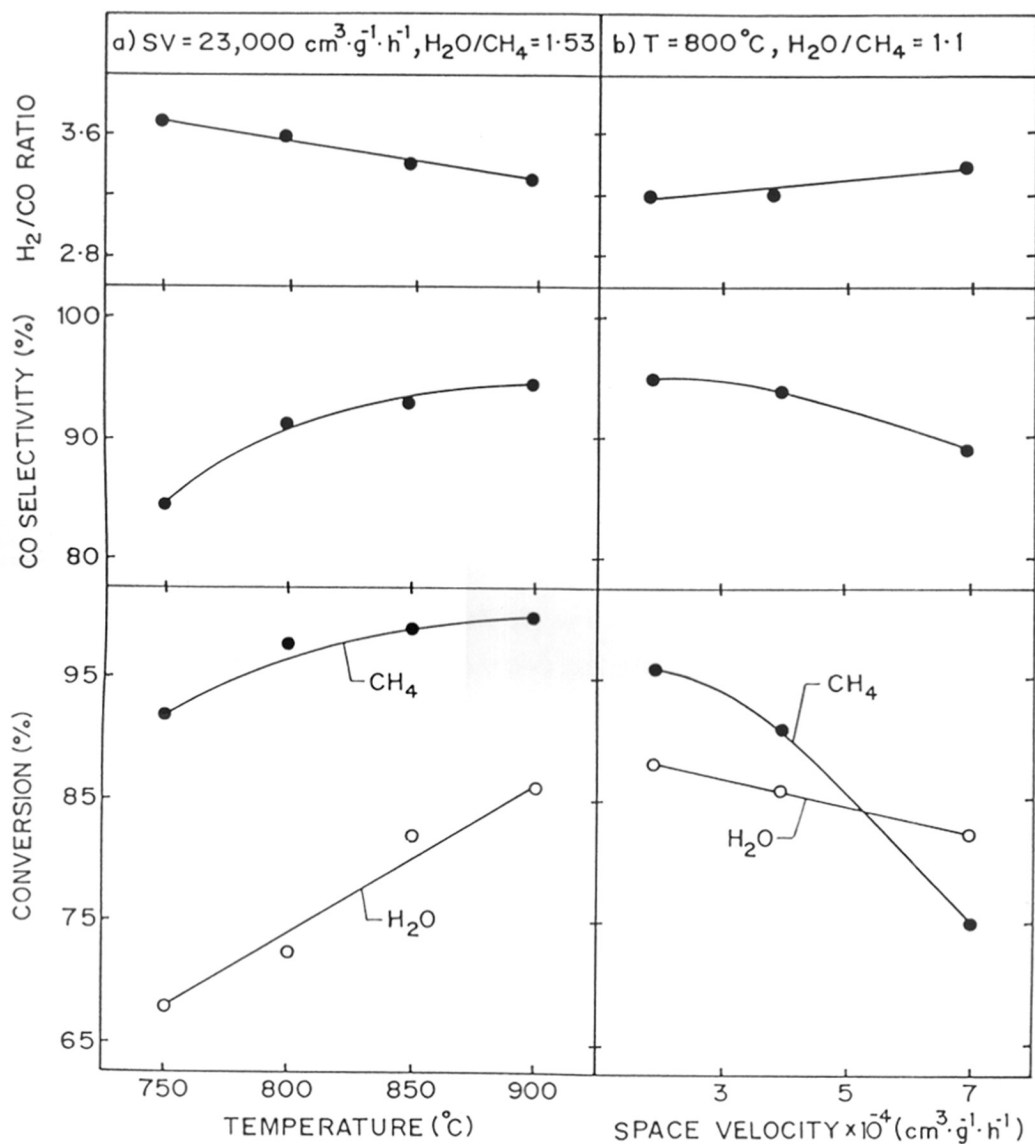


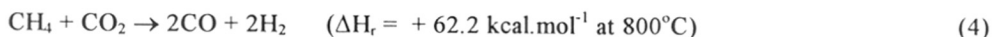
Fig. 2.6.3 : Influence of a) reaction temperature and b) space velocity on the conversion, CO selectivity and H₂/CO product ratio in the steam reforming of methane to syngas.

occurs to an appreciable extent simultaneously with the steam reforming. The increase in the CO selectivity and the decrease in H₂/CO ratio with increasing the temperature are consistent with the fact that water gas shift reaction is not favored thermodynamically at higher temperatures. However, the observed small decrease in the H₂/CO ratio with increasing the space velocity indicates that the temperature inside the catalyst particles may be somewhat lower than that measured by the thermocouple at the higher space velocities because of the high endothermic nature of the steam reforming. This is consistent with the fact that the conversion of water relative to that of methane is increased with increasing the space velocity due to the occurrence of water gas shift reaction to a larger extent.

Results in Fig. 2.6.4 show the influence of reaction temperature and space velocity on the conversion, H₂ selectivity and H₂/CO product ratio in the CO₂ reforming of methane. The conversion of both CH₄ and CO₂ is increased almost linearly with increasing the temperature and decreased exponentially with increasing the space velocity. The H₂ selectivity and H₂/CO ratio are increased with increasing the temperature but decreased with increasing the space velocity. The fact, that the conversion of CO₂ is higher than that of methane and also the H₂/CO ratio is less than 1.0, indicates occurrence of reverse water-gas shift reaction



simultaneously with the CO₂ reforming reaction,



depending upon the process conditions. It is interesting to note that, although the thermodynamic feasibility of reaction-4 is increased with increasing the temperature, unexpectedly the H₂ selectivity is increased with increasing the temperature. The H₂ selectivity is lower when the CO₂ conversion is lower (i.e when the CO₂ at higher concentration is available for the reverse shift reaction), and hence it is controlled essentially by the reaction kinetics rather than the reaction thermodynamics.

Results showing the influence of space velocity (at 800°C and 850°C) on the conversion and H₂/CO product ratio in the simultaneous steam and CO₂ reforming of methane are presented in Fig. 2.6.5. In this process, both the CO₂ and H₂O are converted simultaneously by their reaction with methane (reactions 1 and 4). Hence, as long as the conversion of both CO₂ and H₂O is ≥ 0, the formation of H₂ and CO is controlled only by reactions 1 and 4. Under this

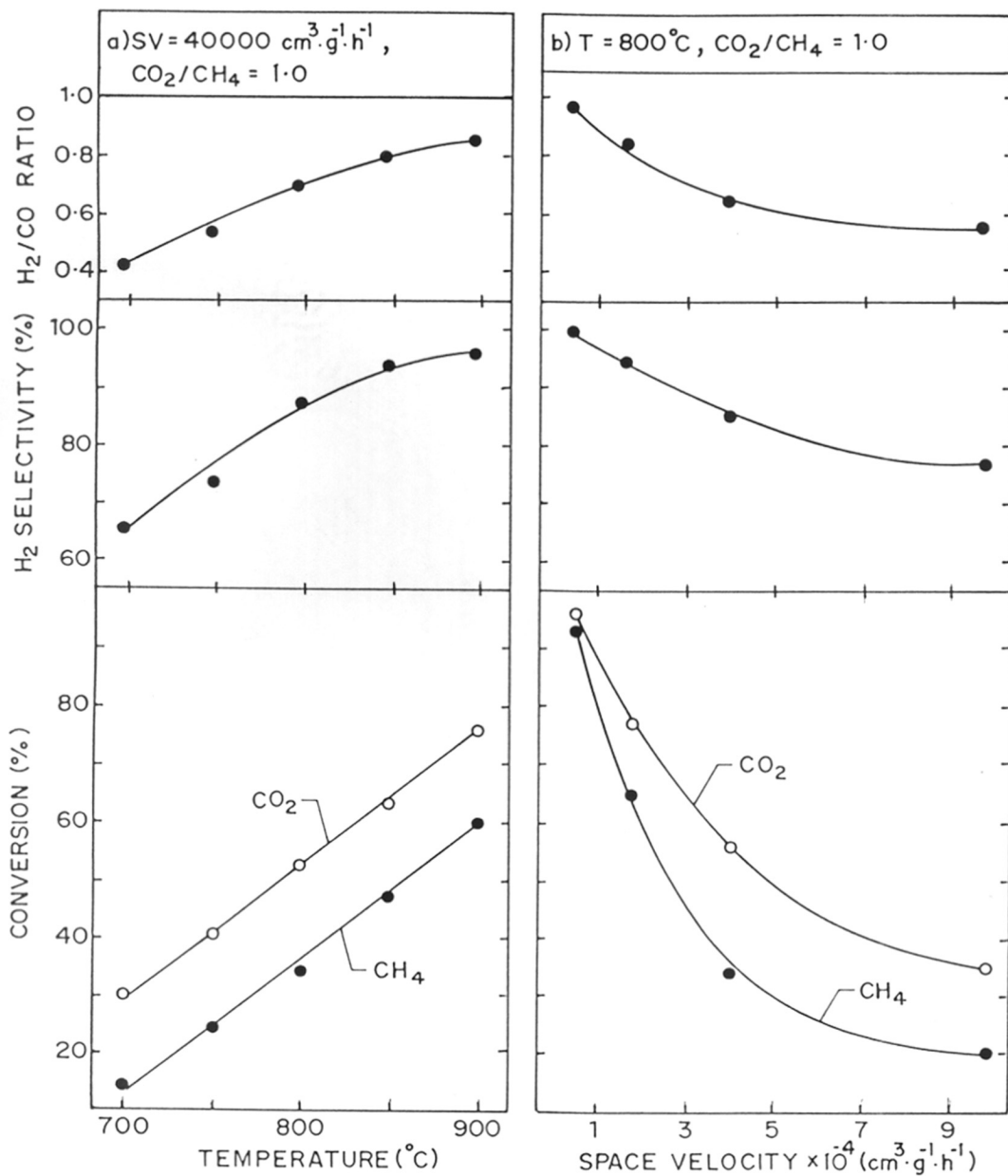


Fig. 2.6.4 : Influence of a) reaction temperature and b) space velocity on the conversion, H_2 selectivity and H_2/CO product ratio in the CO_2 reforming of methane to syngas.

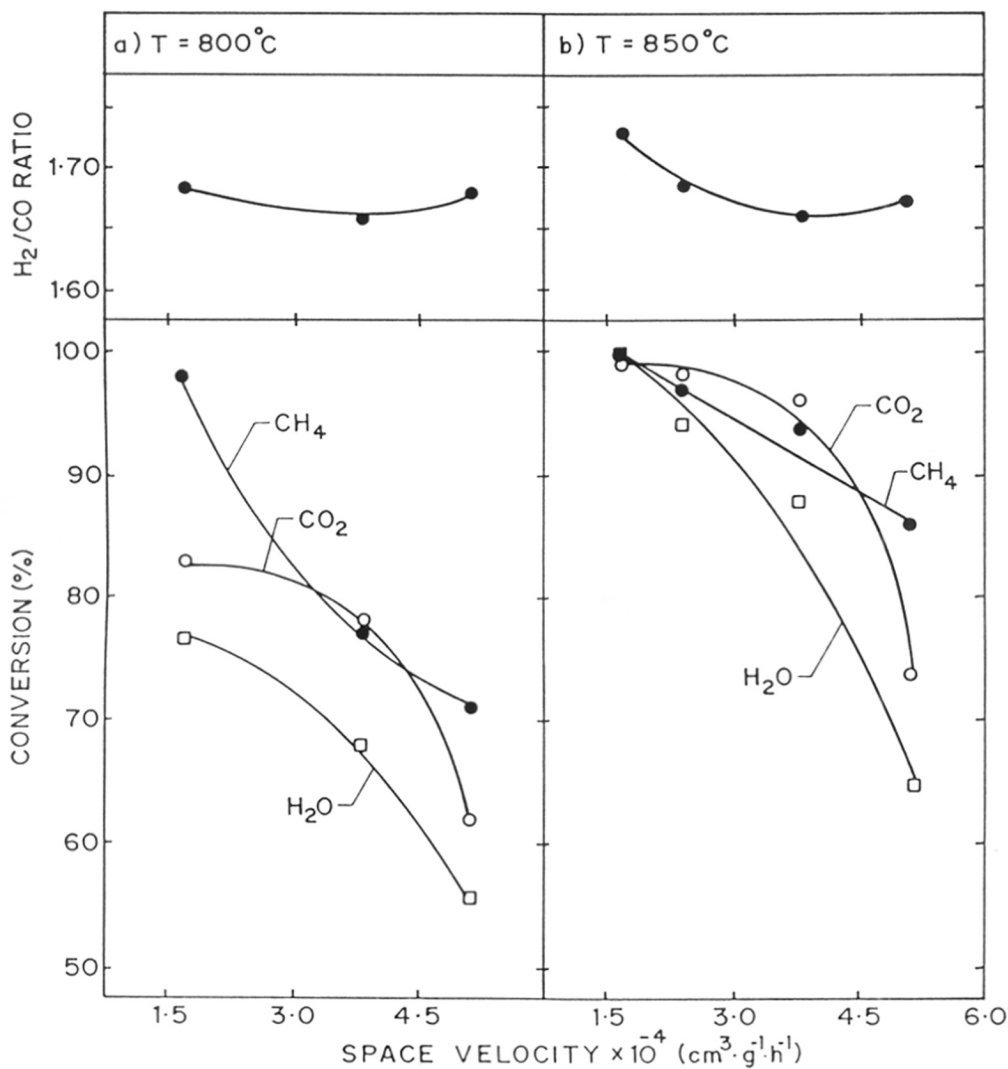


Fig. 2.6.5 : Influence of space velocity on the conversion and H_2/CO product ratio in the simultaneous steam and CO_2 reforming of methane at 800° and $850^\circ C$ ($H_2O/CH_4 = CO_2/CH_4 = 0.56$).

situation, the selectivity for both H₂ and CO is always 100% and also it is not dependent upon the process conditions (e.g. temperature, pressure and space velocity). The H₂/CO ratio, however, depends strongly on the relative concentration of CO₂ and H₂O in the feed, as shown in Fig. 2.6.6. The increase in the CO₂/H₂O ratio from 0 to 1.86 has not affected the methane conversion significantly but caused a large decrease in the H₂/CO ratio (from 3.2 to 1.3). The conversion of methane even at the high space velocity (25100 cm³.g⁻¹.h⁻¹) is very high (\approx 97% at 850°C) (Fig. 2.6.6).

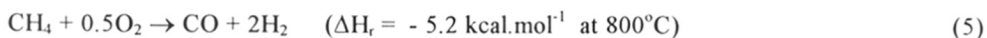
2.6.3.3 Oxy-Steam Reforming of Methane

Results showing the influence of CH₄/O₂ and CH₄/H₂O ratios in the feed [when CH₄/(O₂ + 0.5H₂O) = 1.82] at two different temperatures (800° and 850°C) on the conversion, selectivity, H₂/CO product ratio and net heat of reaction (ΔH_r) in the oxy-steam reforming of methane at high space velocity (47200 cm³.g⁻¹.h⁻¹) are presented in Fig. 2.6.7. The net heat of reaction (ΔH_r) for the overall process is estimated by subtracting the heat of formation (at the process temperature) of the components in the feed from that of the components in the product stream.

When the CH₄/O₂ ratio is increased and corresponding CH₄/H₂O ratio is decreased while keeping the CH₄/(O₂ + 0.5H₂O) ratio constant, the process is influenced as follows:

- The conversion of O₂ (which is nearly 100%) and methane is almost not changed but that of water is increased markedly.
- The selectivity (based on methane) of H₂ (which is 100%) is not changed but that of CO is decreased significantly and hence the H₂/CO ratio is increased.
- The net heat of reaction (ΔH_r) is increased, indicating a decrease in the reaction exothermicity and/or an increase in the reaction endothermicity.

The above observations indicate that the oxidative methane-to-syngas conversion reaction,



occurs simultaneously with the methane steam reforming and water-gas shift reactions (reactions 1 and 2, respectively). The decrease in the CO selectivity shows that the rate of water-gas shift reaction is increased with increasing the relative concentration of water in the feed.

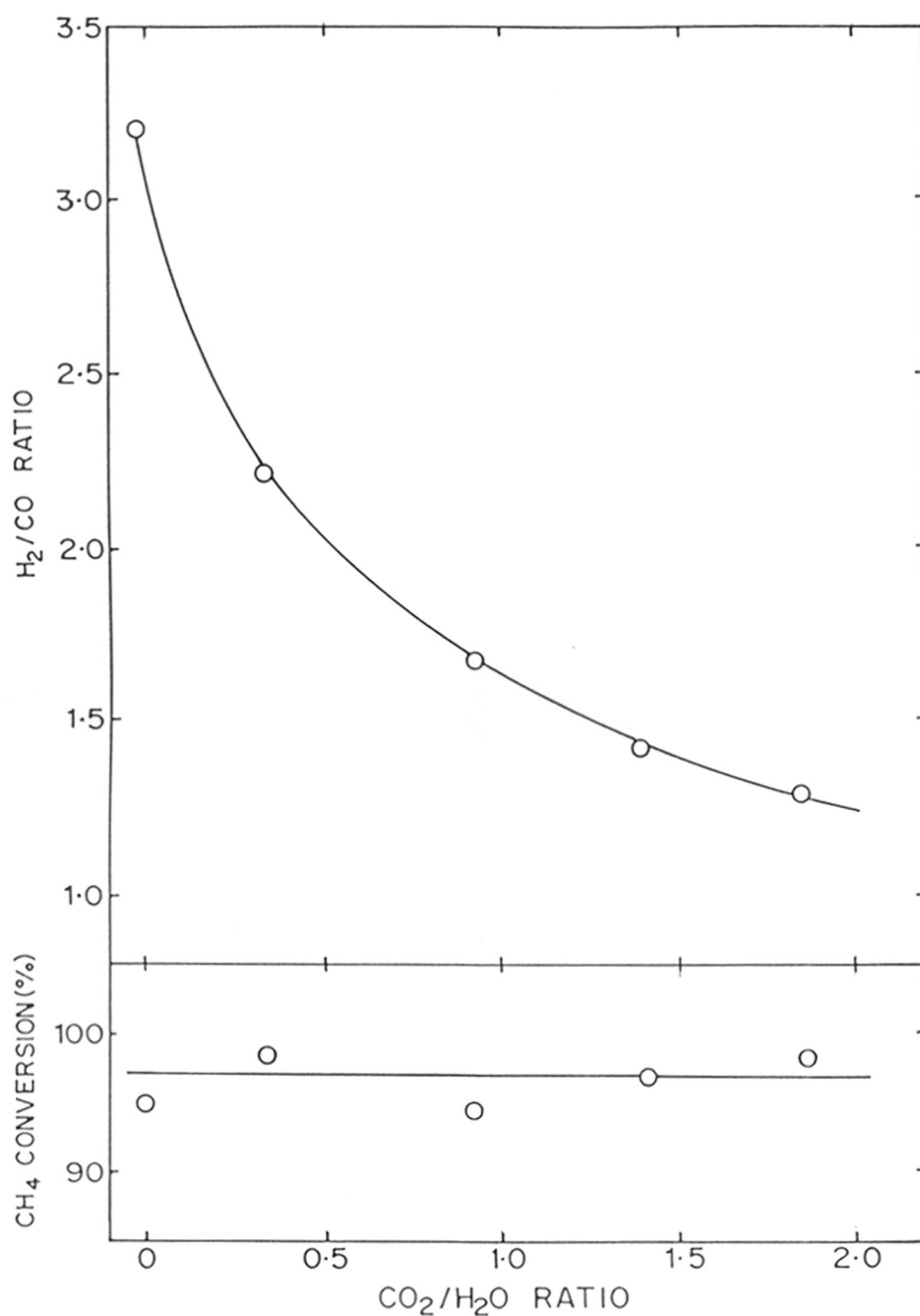


Fig. 2.6.6 : Influence of CO₂/H₂O ratio in feed on the methane conversion and H₂/CO product ratio in the simultaneous steam and CO₂ reforming of methane at 850°C [CH₄/(CO₂ + H₂O) ratio in feed = 0.86, space velocity = 2.51 × 10⁴ cm³.g⁻³.h⁻¹].

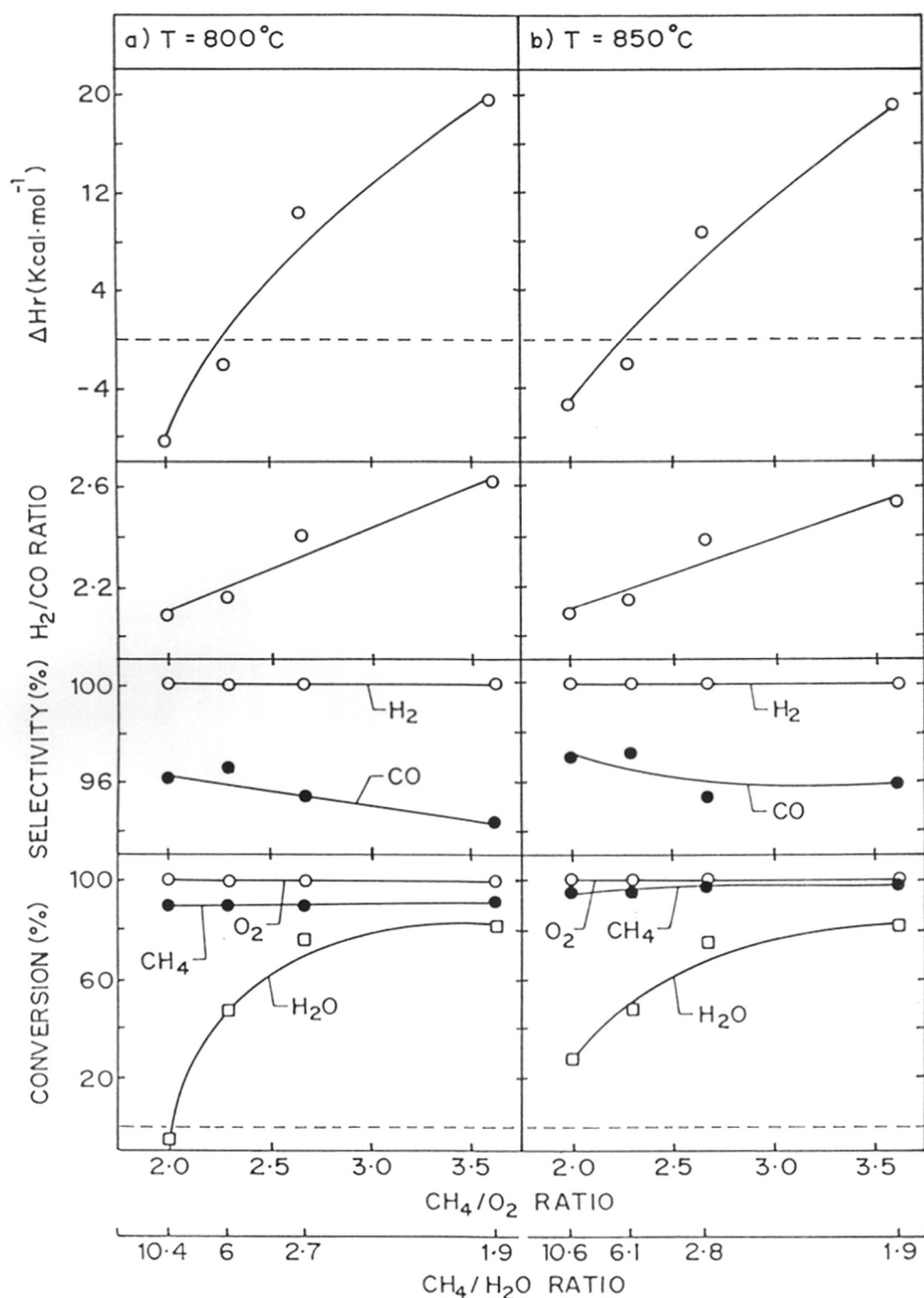


Fig. 2.6.7 : Influence of CH_4/O_2 ratio in feed on the conversion, selectivity, H_2/CO product ratio and net heat of reaction (ΔH_r) in the simultaneous exothermic oxidative conversion and endothermic steam reforming of methane to syngas at 800° and 850°C . [$\text{CH}_4/(\text{O}_2 + 0.5\text{H}_2\text{O})$ mole ratio in feed = 1.8 and space velocity = $4.72 \times 10^4 \text{ cm}^3\cdot\text{g}^{-1}\cdot\text{h}^{-1}$].

2.6.3.4 Oxy-CO₂ Reforming of Methane

Results showing the influence of reaction temperature and CH₄/O₂ and CH₄/CO₂ ratios in the feed [when CH₄/(O₂ + 0.5CO₂) = 1.85] on process performance in the oxy-CO₂ reforming of methane over the catalyst at high space velocity (45800 cm³.g⁻¹.h⁻¹) are presented in Fig. 2.6.8. In this case also, the conversion of O₂ is nearly 100%. The CO selectivity (based on methane) is 100%, as the conversion of CO₂ is positive. With the increase in the temperature, the conversion of CO₂ and CH₄ and the H₂ selectivity are increased and the heat produced in the process is decreased markedly; the H₂/CO ratio is, however, not changed (Fig. 2.6.8a). When the CH₄/O₂ ratio is increased or CH₄/CO₂ ratio is decreased while keeping the CH₄/(O₂ + 0.5CO₂) ratio constant, the conversion of methane is decreased to a small extent but that of CO₂ is increased appreciably and the H₂ selectivity, H₂/CO ratio and net heat produced in the process are decreased markedly (Fig. 2.6.8b).

The H₂ selectivity is lower than 100% because of the reverse shift reaction (reaction-3) occurring simultaneously with the oxidative conversion and CO₂ reforming of methane to syngas.

2.6.3.5 Oxy-Steam and CO₂ Reforming of Methane

Results of the oxy-steam and CO₂ reforming of methane over the catalyst at 800° and 850°C [CH₄/(O₂ + 0.5H₂O + 0.5CO₂) = 1.8, CO₂/H₂O = 1.1, GHSV = 47200 cm³.g⁻¹.h⁻¹], showing the influence of CH₄/O₂ or CH₄/(0.5H₂O + 0.5CO₂) ratio in the feed on the process performance are presented in Fig. 2.6.9. The negative conversion of H₂O and CO₂ observed at the lower CH₄/O₂ ratio [or at the higher CH₄/(0.5H₂O + 0.5CO₂) ratio] is indicative of the net formation of CO₂ and H₂O in the process, respectively. However, when the conversion of both H₂O and CO₂ is ≥ 0, the selectivity (based on methane) for both CO and H₂ is 100%. The influence of CH₄/O₂ or CH₄/(0.5H₂O + 0.5CO₂) ratio [when the CH₄/(O₂ + 0.5H₂O + 0.5CO₂) ratio is kept constant] on the conversion of CO₂ and H₂O, H₂/CO product ratio and also on the net heat of reaction (ΔH_r) is strong but there is a little or no effect of the feed ratios on the conversion of O₂ and CH₄ (Fig. 2.6.9). When the CH₄/O₂ ratio is increased or the CH₄/(0.5H₂O + 0.5CO₂) ratio (when CO₂/H₂O = 1.1) is decreased, the heat produced in the overall process is decreased markedly and the H₂/CO ratio is decreased. The variation of H₂/CO ratio is, however, expected to be dependent upon the CO₂/H₂O ratio in the feed.

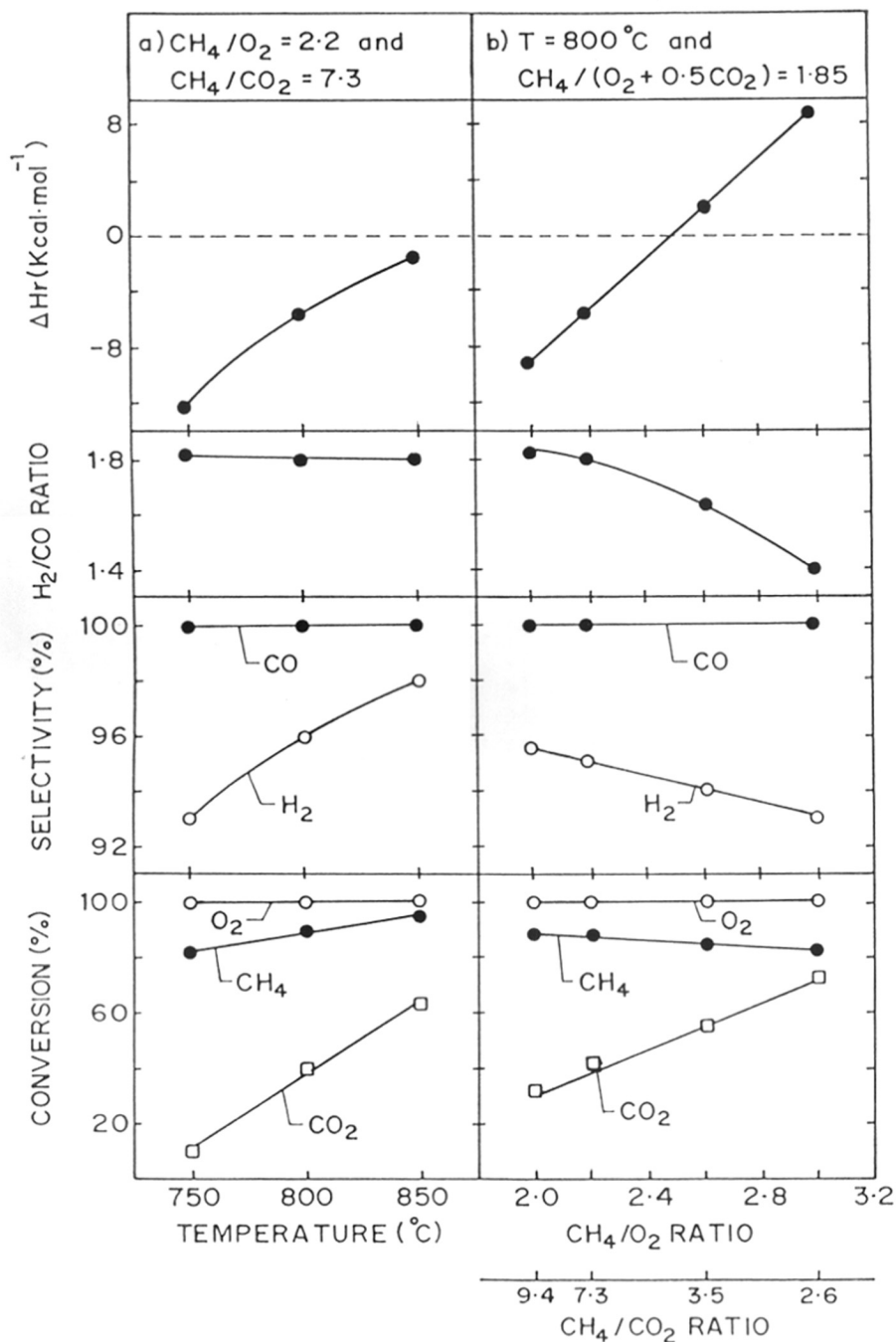


Fig. 2.6.8 : Influence of reaction temperature and CH₄/O₂ ratio in feed on the conversion, selectivity, H₂/CO product ratio and net heat of reaction (ΔH_r) in the simultaneous exothermic oxidative conversion and endothermic CO₂ reforming of methane to syngas. (space velocity = 4.58 × 10⁴ cm³·g⁻¹·h⁻¹).

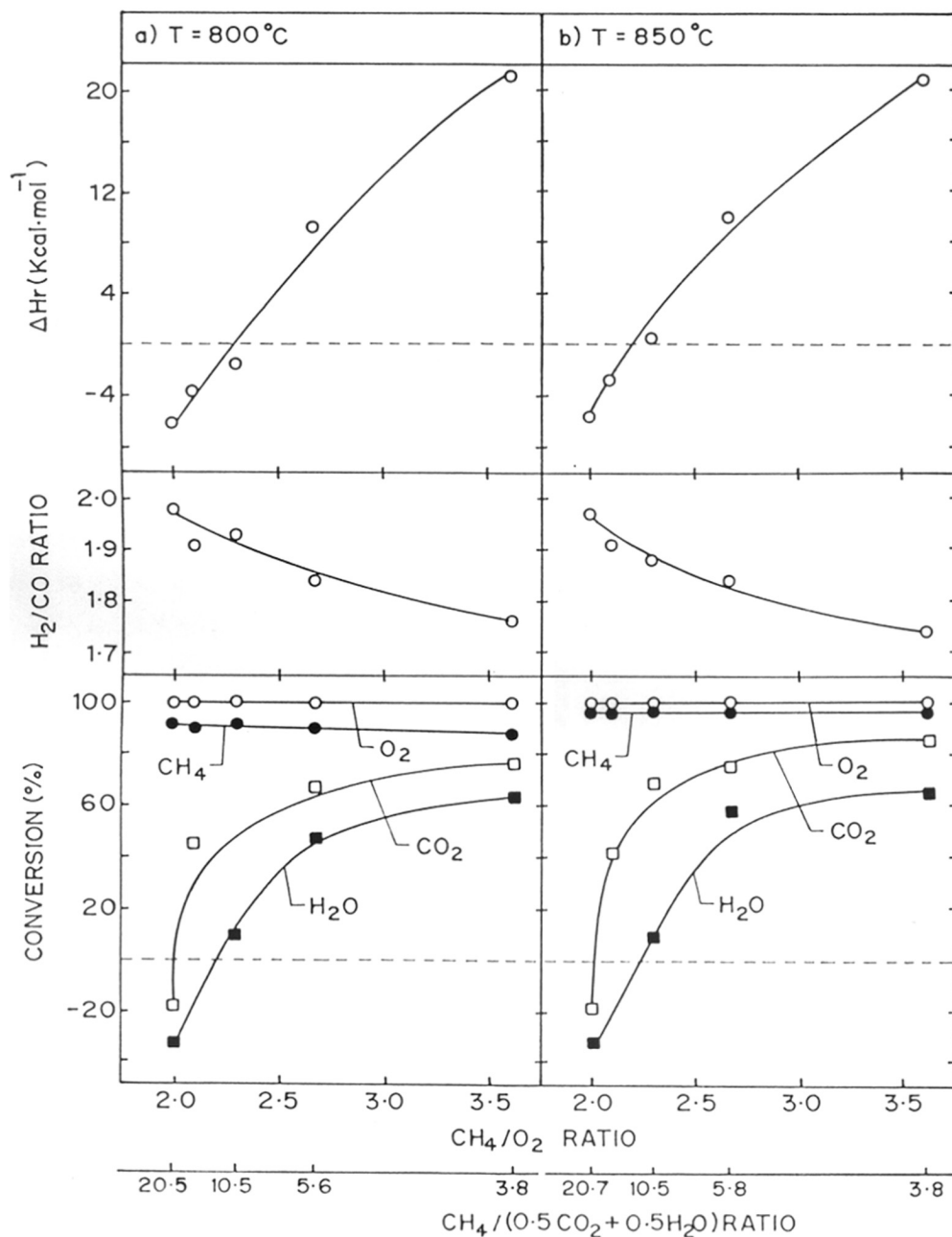


Fig. 2.6.9 : Influence of CH_4/O_2 ratio in feed on the conversion, H_2/CO product ratio and net heat of reaction (ΔH_r) in the simultaneous exothermic oxidative conversion and endothermic steam and CO_2 reforming of methane to syngas at 800° and 850°C. [$\text{CH}_4/(\text{O}_2 + 0.5\text{H}_2\text{O} + 0.5\text{CO}_2)$ mole ratio in feed = 1.8, $\text{CO}_2/\text{H}_2\text{O}$ mole ratio = 1.1 and space velocity = $4.72 \times 10^4 \text{ cm}^3\cdot\text{g}^{-1}\cdot\text{h}^{-1}$].

Results in Fig. 2.6.10 show that, when the $\text{CO}_2/\text{H}_2\text{O}$ ratio is increased while keeping the CH_4/O_2 and $\text{CH}_4/(\text{O}_2 + 0.5\text{H}_2\text{O} + 0.5\text{CO}_2)$ feed ratios constant, there is no significant change in the methane conversion but the H_2/CO ratio is decreased markedly and heat produced in the process is also decreased significantly. This is expected because of the occurrence of the CO_2 reforming reaction (which is more endothermic and yields syngas with lower H_2/CO ratio than the steam reforming) to a larger extent than that of the steam reforming reaction with increasing the $\text{CO}_2/\text{H}_2\text{O}$ ratio.

2.6.4 DISCUSSION

The supported-Ni catalyst ($\text{NiO}/\text{MgO}/\text{SA-5205}$) shows high activity at high space velocity (i.e. at low contact time) in the different methane-to-syngas conversion reactions (Figs. 3-10). Because of the precoating of the support with MgO, before depositing NiO on it, a protective layer of a thermally stable MgAl_2O_4 (spinel); resulting from solid-solid reaction between MgO and Al_2O_3 (from support), at the MgO-support interface is formed. This has avoided the formation of catalytically inactive NiAl_2O_4 (spinel) phase, and hence avoided the consumption of nickel, the active component of the catalyst. This and the formation of solid solution of NiO and MgO [which is supported by the TPR (Fig. 2.6.1) and low degree of NiO reduction (34.5%)] are responsible for the high catalytic activity of the present supported Ni catalyst. The catalyst in its operating state is expected to be in a form of Ni^0 dispersed on MgO supported on SA-5205. The NiO from the catalyst is reduced in the initial short reaction period by its autocatalytic reaction with methane [23].

The reduced catalyst shows surface heterogeneity for its H_2 adsorption sites (i.e. nickel sites), as indicated by the multiple H_2 TPD peaks (Fig. 2.6.2). The heterogeneous sites are expected to be Ni^0 in different chemical environments. The reducibility of Ni^{2+} is controlled by the incorporation of Ni^{2+} in the MgO matrix forming a solid solution of NiO in MgO. The degree of reduction of the Ni^{2+} ions even at the high temperature (900°C) is low (34.5%). In the reduction, the outermost Ni^0 atoms nucleate to form fine metal particles but some, which lie deeper, remain isolated in the MgO matrix either as Ni^0 or a charged Ni species in a low oxidation state. The observed multiplicity in the H_2 TPD curve is consistent with the fact that the reduced solid solution provides a strongly ionic environment at the metal particle-support

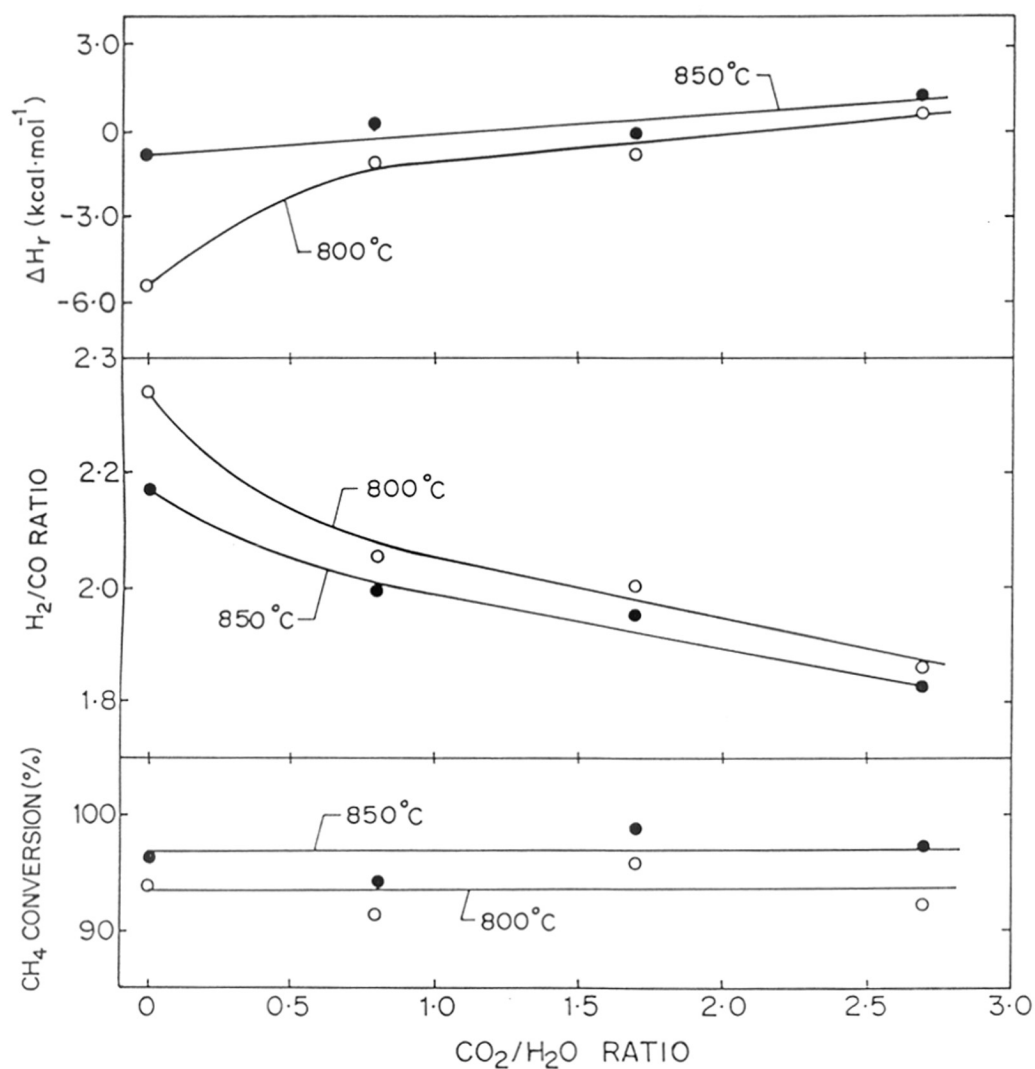


Fig. 2.6.10 : Influence of CO₂/H₂O ratio in feed on the methane conversion, H₂/CO product ratio and net heat of reaction (ΔH_r) in the simultaneous oxidative conversion and steam and CO₂ reforming of methane to syngas at 800°C (O) and 850°C (●). [CH₄/O₂ ratio in feed = 2.11, CH₄/(O₂ + 0.5H₂O + 0.5CO₂) mole ratio in feed = 1.8, space velocity = 4.8 x 10⁴ cm³·g⁻¹·h⁻¹].

interface and even more so for the reduced species (Ni^0) which are at the surface but not fully exposed [26].

2.6.4.1 Steam and/or CO_2 Reforming of Methane

The results on the steam and/or CO_2 reforming of methane (Figs. 2.6.3-2.6.6) show trends quite similar to those observed earlier over NiO-CaO [20]. However, the filamental carbon deposition on the NiO-CaO [20] and NiO-MgO [28] in the CO_2 reforming of methane under similar conditions was found to be so fast that there was a sharp increase in the pressure drop across the catalyst bed in a very short reaction period (≤ 0.5 h). But for the present catalyst, no increase in the pressure drop across the catalyst bed even for much longer reaction period (20 h) is observed. This indicates that the carbon deposition on the present catalyst by the Boudouard reaction,

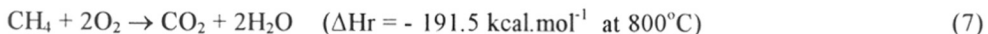


is much less than that on the unsupported NiO-MgO or NiO-CaO catalysts.

The carbon deposition by the Boudouard reaction on the catalyst is expected to be reduced by carrying out the CO_2 reforming simultaneously with the steam reforming [20]. In the simultaneous steam and CO_2 reforming over the present catalyst, methane can be converted almost completely to syngas of desirable H_2/CO ratio (2.0 ± 0.5) with 100% selectivity for both CO and H_2 at high space velocity ($\geq 25000 \text{ cm}^3 \cdot \text{g}^{-1} \cdot \text{h}^{-1}$). The H_2/CO ratio in this process can be controlled by manipulating the relative concentrations of steam and CO_2 in the feed.

2.6.4.2 Oxy-Steam and/or CO_2 Reforming of Methane

In the oxy-steam and/or CO_2 reforming processes, the exothermic methane conversion reactions, involving the partial oxidation of methane to H_2 and CO (reaction-5) and to a smaller extent the complete combustion of methane,



occur simultaneously with the endothermic steam reforming (reaction-1) and/or CO_2 reforming (reaction-4) over the same catalyst. Because of the simultaneous occurrence of the exothermic and endothermic methane conversion reactions, the process operates in a most energy efficient manner and also in a safe manner. The net heat produced or absorbed in the process can be controlled by manipulating the process conditions (viz. reaction temperature and feed

composition) and the process can be made mildly exothermic, thermoneutral or mildly endothermic. In general, the net heat produced in the process is decreased with increasing the temperature (Fig. 2.6.8a) mainly because of the increase in the rate of the endothermic steam and/or CO₂ reforming reactions. It is also decreased with decreasing the concentration of O₂ relative to that of steam and/or CO₂ in the feed (Figs. 2.6.7, 2.6.8b and 2.6.9) due to the decrease in the rate of the exothermic oxidative methane conversion reactions relative to those of the endothermic steam and/or CO₂ reforming reactions. In these processes, the methane conversion is high and the H₂/CO product ratio can be controlled, within the limits decided by stoichiometry of the reactions involved, by manipulating the relative concentrations of O₂, steam and/or CO₂ in the feed.

In the oxy-steam reforming process, when the H₂O conversion is ≥ 0 , the H₂ selectivity (based on methane) is 100%. The CO selectivity in this process is also high (above 94%). However, it is decreased with increasing the concentration of steam relative to that of O₂ in the feed, due to the increase in the rate of the water-gas shift reaction, resulting in an increase in the H₂/CO ratio above 2.0 (Fig. 2.6.7).

In the oxy-CO₂ reforming of methane, the CO selectivity is 100% when the CO₂ conversion is ≥ 0 . However, the H₂ selectivity (which is above 92%) is decreased with increasing the concentration of CO₂ relative to that of O₂ in the feed, because of the increased rates of the reverse water-gas shift reaction, and consequently the H₂/CO product ratio is also decreased below 2.0 (Fig. 2.6.8b).

However, in the oxy-steam and CO₂ reforming process, methane can be converted to syngas almost completely with 100% selectivity for both H₂ and CO. Moreover, the H₂/CO ratio close to 2.0 (which is desirable for the methanol and Fischer-Tropsch synthesis processes) can be obtained by manipulating the relative concentrations of CO₂ and H₂O in the feed; it is decreased with increasing the CO₂/H₂O ratio in the feed (Fig. 2.6.10). In this process, the H₂/CO ratio is not affected by the forward or reverse water-gas shift reaction; it is controlled by the three individual methane-to-syngas conversion reactions-partial oxidation (reaction-5), steam reforming (reaction-1) and CO₂ reforming (reaction-4), occurring to different extents depending upon the process conditions.

The present supported nickel catalyst showed high activity and selectivity in the above methane-to-syngas reactions at low contact times without deactivation, atleast during its operation for the data collection for the above reactions. The performance in the oxy-steam and/or CO₂ reforming of methane of the present catalyst is much superior to that reported earlier for the NiO-MgO/SA-5205 (prepared by depositing mixed NiO-MgO directly on SA-5205) [24, Chapter-2.3], LaNiO₃ [6, Chapter-2.1] and NiO/ALPO-5 [5, Chapter-2.2]. Unsupported NiO-CaO catalyst showed a comparable performance for the activity/selectivity in these processes [1-3]. But, in the CO₂ reforming, this catalyst showed a high tendency for the formation of filamental carbon, causing a drastic increase in the pressure drop across the catalyst bed in a short (0.5 h) reaction period [12, 20]. Unsupported NiO-MgO catalyst also showed a high tendency for the filamental carbon formation in the methane-to-syngas conversion reactions; particularly when the CO₂ reforming is involved [28]. The present catalyst showed no tendency for fast carbon deposition on it; no filamental carbon growth on the catalyst (when examined by SEM), at least during its operation in the reactions, is observed. Further studies are, however, essential for investigating in details the carbon deposition on the present catalyst and its deactivation by other means in the different methane-to-syngas conversion reaction.

2.6.5 CONCLUSIONS

Following important conclusions from the steam and/or CO₂ reforming and oxy-steam and/or CO₂ reforming reactions of methane for its conversion to syngas over the supported Ni catalyst, prepared by depositing NiO on the MgO pre-coated SA-5205 support, have been drawn.

1. The NiO and MgO in the catalyst exist in the form of their solid solution supported on SA-5205. The reduction of NiO from the catalyst is only partial (34.5%) and the Ni sites on the reduced catalyst are heterogeneous.
2. The catalyst shows high activity and selectivity in the above methane-to-syngas conversion reactions at low contact times. The carbon deposition on the catalyst is much less than that observed for the unsupported NiO-MgO and NiO-CaO catalysts.
3. In the simultaneous steam and CO₂ reforming process, methane can be converted to syngas with H₂/CO ratio close to 2.0 with 100% selectivity for both H₂ and CO.
4. In the oxy-steam and CO₂ reforming processes, the exothermic oxidative methane-to-syngas conversion occurs simultaneous with the endothermic steam and CO₂ reforming reactions of methane and hence there is a direct coupling of the exothermic and endothermic reactions over the same catalyst. Because of this, the process occurs in a most energy efficient and safe manner. It can be made mildly exothermic, thermoneutral and mildly endothermic by manipulating the reaction temperature and/or concentration of O₂ in the feed, and hence it requires little or no external energy. Moreover, the syngas with desirable H₂/CO ratio (close to 2.0) can be obtained by manipulating the relative concentrations of steam and CO₂ in the feed.

REFERENCES

1. V.R. Choudhary, A.M. Rajput, and B. Prabhakar, *Angew. Chem. Int. Ed. Engl.* 33 (1994) 2104.
2. V.R. Choudhary, A.M. Rajput, and B. Prabhakar, *Catal. Lett.* 32 (1995) 391.
3. Choudhary, V.R., Rajput, A.M., and Prabhakar, B., *Methane and Alkane Conversion Chemistry* (Proc. Am. Chem. Soc. Symp. 207th Annual Meeting San Diego, March 13018, 1994) Eds. M.M. Bhasin and D.W. Slocum, Penum Publ. Corp., New York, (1995) 305.
4. A.T. Ashcroft, A.K. Cheetham, M.L.H. Green, and P.D.F. Vernon, *Nature* 352 (1991) 225.
5. V.R. Choudhary, B.S. Uphade, and A.S. Mamman, *Zeolites* (in press)
6. V.R. Choudhary, B.S. Uphade, and A.A. Belhekar, *J. Catal.*, 163 (1996) 312.
7. F. Solymosi, Gy. Kutsan, and A. Erdohelyi, *Catal. Lett.*, 11 (1991) 149.
8. J.S.H.Q. Perera, J.W. Couves, G. Sankar, and J.M. Thomas, *Catal. Lett.*, 11 (1991) 219.
9. A. Erdohelyi, J. Cserenyi, and F. Solymosi, *J. Catal.*, 141 (1993) 287.
10. J. Nakamura, K. Aikawa, K. Sato, and T. Uchijima, *Catal. Lett.*, 25 (1994) 265.
11. M.F. Mark, and W.F. Maier, *Angew. Chem. Int. Ed. Engl.* 33 (1994) 1657.
12. E. Ruckenstein, and Y.H. Hu, *Appl. Catal. A: Gen.*, 133 (1995) 149.
13. Z. Zhang, and X.E. Verykios, *J. Chem. Soc. Chem. Commun.*, (1995) 71.
14. Z. Zhang, X.E. Verykios, S.M. MacDonald, and S. Affrossman, *J. Phys. Chem.*, 100 (1996) 744.
15. Z. Zhang, and X.E. Verykios, *Appl. Catal. A: Gen.*, 138 (1996) 109.
16. Z. Cheng, Q. Wu, J. Li, and Q. Zhu, *Catal. Today*, 30 (1996) 147.
17. T. Horiuchi, K. Sakuma, F. Takehisa, Y. Kubo, T. Osaki, and T. Mori, *Appl. Catal. A: Gen.*, 144 (1996) 111.
18. E. Ruckenstein, and Y.H. Hu, *J. Catal.*, 162 (1996) 230.
19. Y. Chen, and J. Ren, *Catal. Lett.*, 29 (1994) 39.
20. V.R. Choudhary, and A.M. Rajput, *Ind. Eng. Chem. Res.*, 35 (1996) 3934.
21. J.R. Rostrup-Nielsen, and J.H. Bak-Hansen, *J. Catal.*, 144 (1993) 38.
22. O. Yamazaki, T. Nozaki, K. Omata, and K. Fusimao, *Chem Lett.*, (1992) 1953.
23. V.R. Choudhary, A.S. Mamman, and S.D. Sansare, *Angew. Chem. Int. Ed. Engl.*, 31 (1992) 1189.

24. B.S. Uphade, A.S. Mamman, and V.R. Choudhary, *Catalysis : Modern Trends*, N.M. Gupta and D.K. Chakraborty (Eds.), Narosa Publishing House, New Delhi, (1995) 380.
25. V.R. Choudhary, B.S. Uphade, and A.S. Mamman, *Catal. Lett.* 32 (1995) 387.
26. Highfield., A. Bossi, and F.S. Stone, *Stud. Surf. Sci. Catal.*, 16 (1983) 181.
27. A. Parmaliana, A. Arena, F. Frusteri, and N. Giordano, *J. Chem. Soc. Faraday Trans.*, 86, (1990) 2663.
28. V.R. Choudhary, and A.S. Mamman, (Unpublished results).

PART-III

COMPLETE COMBUSTION OF METHANE FOR ITS EMISSION CONTROL

CHAPTER-3.1 : LOW TEMPERATURE COMPLETE COMBUSTION OF METHANE OVER Mn-, Co-, AND Fe-STABILIZED ZrO₂

CHAPTER-3.2 : LOW TEMPERATURE TOTAL OXIDATION OF METHANE OVER Ag-DOPED LaMO₃ PEROVSKITE OXIDES

CHAPTER - 3.1

LOW TEMPERATURE COMPLETE COMBUSTION OF METHANE OVER Mn-, Co- AND Fe-STABILIZED ZrO₂

3.1.1 INTRODUCTION

The concentration of methane in the atmosphere is increasing continuously [1]. Since methane has much larger greenhouse effect (causing global warming) than carbon dioxide, the control of methane emission from the natural gas engines and power plants and also from the petroleum and petrochemical industries by its complete combustion to carbon dioxide is a must. Methane is most inert among the hydrocarbons and hence its oxidative destruction by complete combustion at low temperature (below 600°C, for economic reasons) is rather difficult. Noble metal catalysts show high activity in the combustion of light hydrocarbons [2-4] or methane [5-10] at low temperature. However, the use of noble metal catalysts for the methane emission control is limited because of the scarcity and high cost of noble metals. Worldwide efforts are, therefore, being made to replace noble metal catalysts by mixed metal oxide catalysts based on perovskite oxides [11-18] of ABO₃ type (where A = La or other rare earth, with or without partial substitution by alkaline earth, and B = transition metal viz. Mn, Fe, Co, Ni, etc).

Stabilization of ZrO₂ in its cubic phase by doping with Mn [19-22], Fe [23, 24], and Co [25] has been reported earlier. It is interesting to study the activity of transition metal (viz. Mn, Co, Fe, Cr, Ni, Cu, etc.) doped ZrO₂ (cubic) catalysts in the combustion of methane. The present work was undertaken for this purpose.

3.1.2 EXPERIMENTAL

3.1.2.1 Catalyst Preparation

The transition metal (viz. Cr, Mn, Fe, Co, Ni or Cu)-stabilized ZrO₂ (cubic) catalysts were prepared by mixing aqueous solutions of zirconyl nitrate and the appropriate transition metal nitrates (transition metal/Zr mole ratio = 0.25), coprecipitating metal hydroxides from the solution with aqueous tetramethylammonium hydroxide (25%) under vigorous stirring at 30°C and a pH of 8, washing with deionized water, drying the resulting precipitate at 110°C for 2 h, and finally calcining it

in air at 500°C for 8 h and then at 600°C for 1 h. The pure ZrO₂ catalyst was also prepared by above procedure but without the addition of any transition metal compound. The Mn-impregnated ZrO₂ (Mn/Zr = 0.05 and 0.25) was prepared with ZrO₂ and Mn-nitrate by the incipient wetness method and calcining as above. For the purpose of comparison, the perovskite oxide catalysts were prepared by coprecipitating the metal carbonate, decomposing it at 500°C for 4 h, powdering and pelleting, and finally calcining in air at 900°C for 6 h.

3.1.2.2 Catalyst Characterization

The stabilization of transition metal doped ZrO₂ catalysts in their cubic form was confirmed by XRD. Powder X-ray diffraction patterns of Cr-, Mn-, Fe-, Co-, and Ni- stabilized ZrO₂ are given in Fig. 3.1.1. In all cases no free transitional metal oxide was observed. The perovskite oxide structure of the catalysts was also confirmed by XRD. The surface area of the catalysts was measured by the single-point BET method by measuring the adsorption of nitrogen at liquid nitrogen temperature from a N₂-He mixture containing 30 mol% N₂, using a Monosorb Surface Area Analyzer (Quantachrome Corp. USA).

3.1.2.3 Catalytic Reaction

The schematic diagram of the quartz reactor and the experimental set-up used in the complete combustion of methane are shown in Figs. 1.1.2 and 1.1.2, respectively. The experimental set-up used for the pulse reaction of pure methane in the absence of free-O₂ is shown in Fig. 3.1.2.

The methane combustion activity of all the catalysts at different temperatures was measured at atmospheric pressure, fixed bed, quartz-microreactor (i.d. 10 mm) containing 0.1 g catalyst (22-30 mesh size) mixed uniformly with 0.4 g inert α -Al₂O₃ particles (22-30 mesh size). Methane in air (1 mol%) was fed at a space velocity (measured at 0°C and 1 atm pressure) of 51,000 cm³.g⁻¹.h⁻¹. The reaction temperature was measured by a Chromel-Alumel thermocouple located in the centre of the catalyst bed. The products (after condensing the water from the product stream at 0°C) were analyzed by an on-line GC using the molecular sieve and Sphero carb columns. The pulse reaction of methane over the catalyst in the absence of free-O₂ was carried out with He carrier gas in a quartz pulse microreactor connected to GC described earlier [26]. No formation of carbon monoxide (or no partial oxidation of methane) was observed in any of the methane conversion reactions.

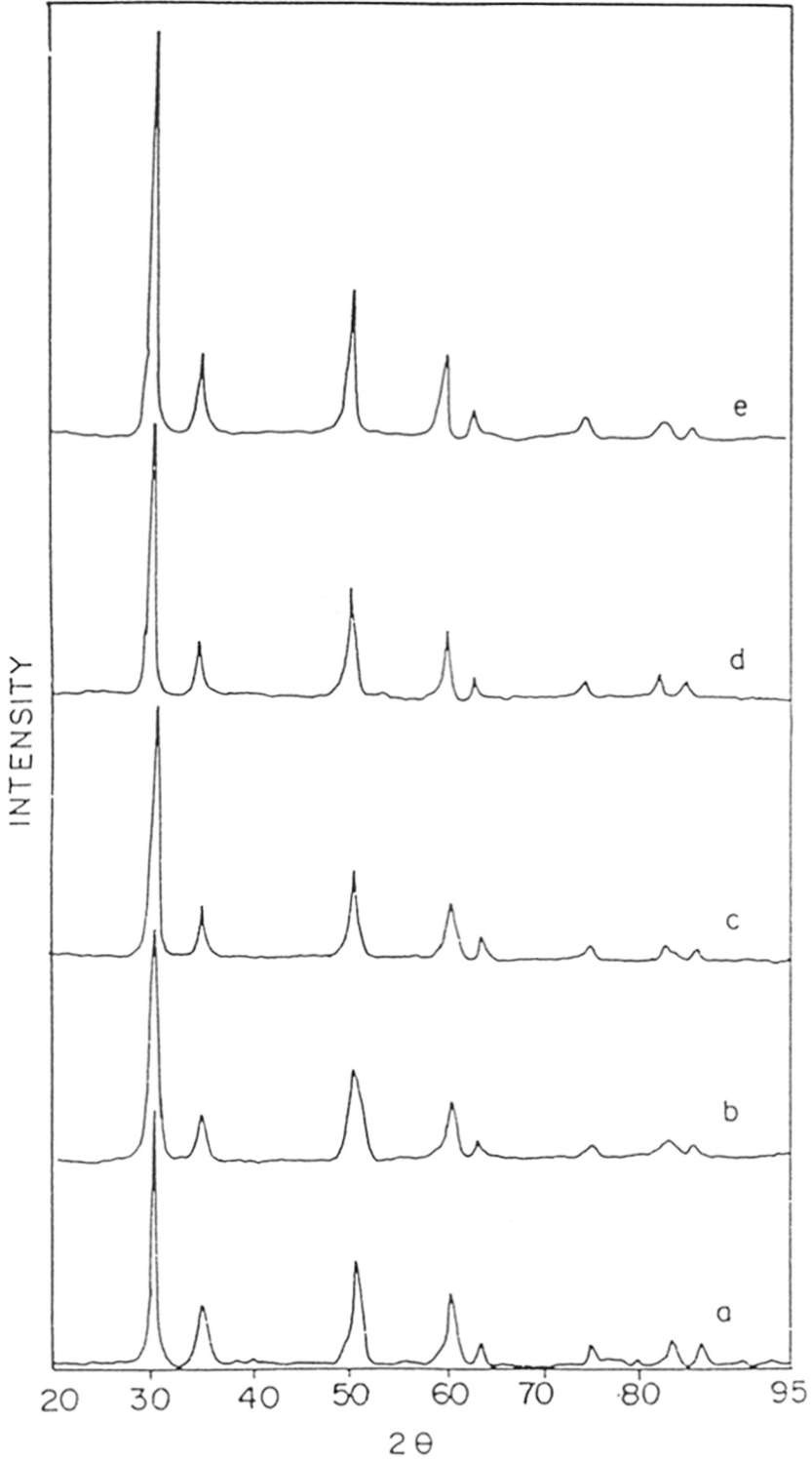


Fig. 3.1.1 : XRD patterns of ZrO₂ stabilised with transition metal Cr (a), Mn (b), Fe (c), Co (d) and Ni (e)

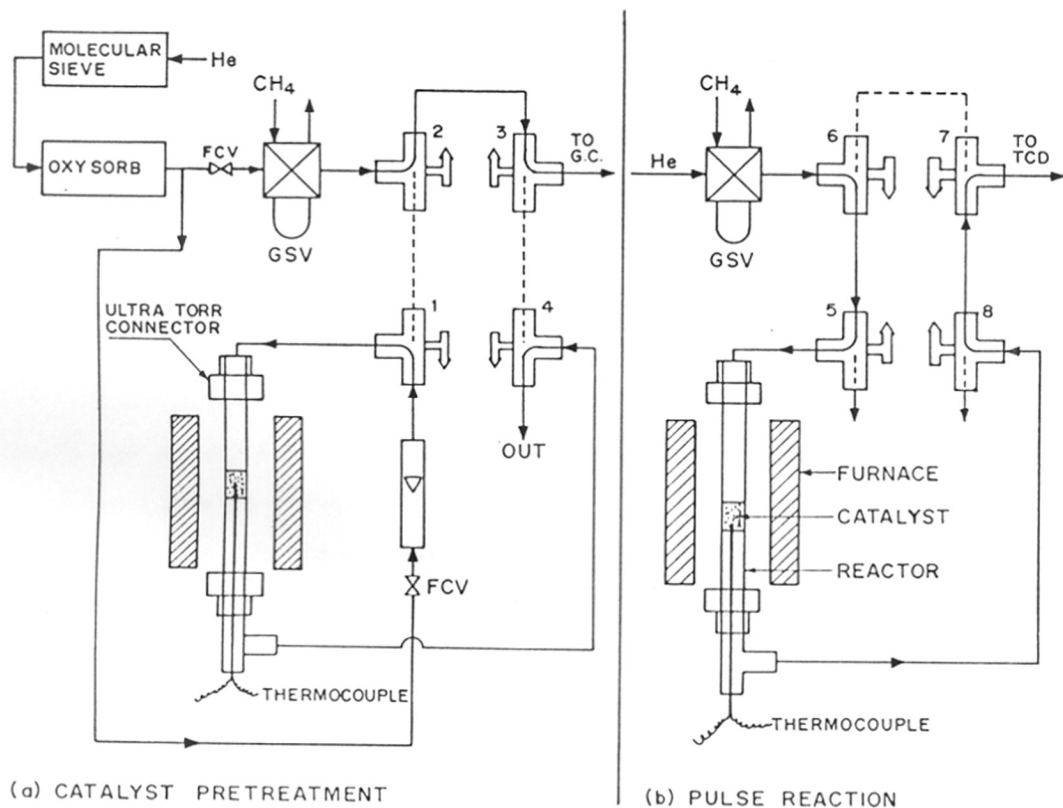


Fig. 3.1.2: Experimental set-up for a) *in-situ* pretreatment (or reoxidation) of catalyst and b) methane oxidation on the catalyst in the pulse-reactor in absence of free-O₂ [FCV = Flow control valve, GSV = Gas sampling valve, 1-8 = Three way ball valve]

3.1.3 RESULTS AND DISCUSSION

Results in Fig. 3.1.3 show that the methane combustion activity of ZrO_2 (monoclinic) is increased drastically due to its stabilization in its cubic form by the incorporation of the transitional metals, particularly Mn, Co, Fe and Cr, at the concentration of 20 mol% in the bulk structure of zirconia. The Mn-stabilized ZrO_2 shows the highest catalytic activity and its activity is much larger than that of the Mn-impregnated ZrO_2 with Mn/Zr ratio of 0.25 [which is a mixture of MnO_2 and ZrO_2 (monoclinic)]. Mn-impregnated ZrO_2 with a much lower Mn/Zr ratio (0.05) and bulk MnO_2 (i.e. Mn/Zr = ∞) also showed much lower methane combustion activity (methane conversion : 26.3 and 9.6%, respectively) at 500°C. The Mn-stabilised ZrO_2 shows no sign of catalyst deactivation when operated continuously for 50 h at 500°C in the methane combustion process.

In the pulse reaction of pure methane over the Mn-stabilized ZrO_2 at 500°C in the absence of free- O_2 , high conversion of methane to carbon dioxide is observed for the first pulse (Fig. 3.1.4). The conversion is, however, decreased with increasing the pulse number and, subsequently, it is reduced to a very low value after the 45th pulse. However, the initial high conversion is regained after the reoxidation of the deactivated catalyst by air (at 500°C for 30 min). This clearly shows the involvement of lattice oxygen from the catalyst in the methane combustion and also confirms that a redox mechanism is operative in the catalytic methane combustion process. The observed somewhat higher conversion after the reoxidation for the initial few pulses may be due to the chemisorbed oxygen on the catalyst and/or due to the partial reduction of the virgin catalyst during storage before testing.

The Mn-stabilized ZrO_2 , Mn-impregnated ZrO_2 (Mn/Zr = 0.20) and pure ZrO_2 catalysts are compared in Fig. 3.1.5 for the reactivity of their lattice oxygen in the methane combustion by carrying out the methane pulse reaction (in the absence of free- O_2) at different temperatures. The observed very high conversion of methane over the Mn-stabilized ZrO_2 as compared to that over the other two catalysts reveals that the reactivity of lattice oxygen of zirconia catalyst is drastically increased due to the Mn doping which stabilizes the cubic phase as well. Our studies on the temperature programmed reaction of pure methane (in the absence of free- O_2) over the catalysts also indicated that the reactivity of lattice oxygen of all the transitional metal-stabilized ZrO_2 catalysts is much higher than that of pure ZrO_2 and is in the order of the observed methane combustion activity (in the presence

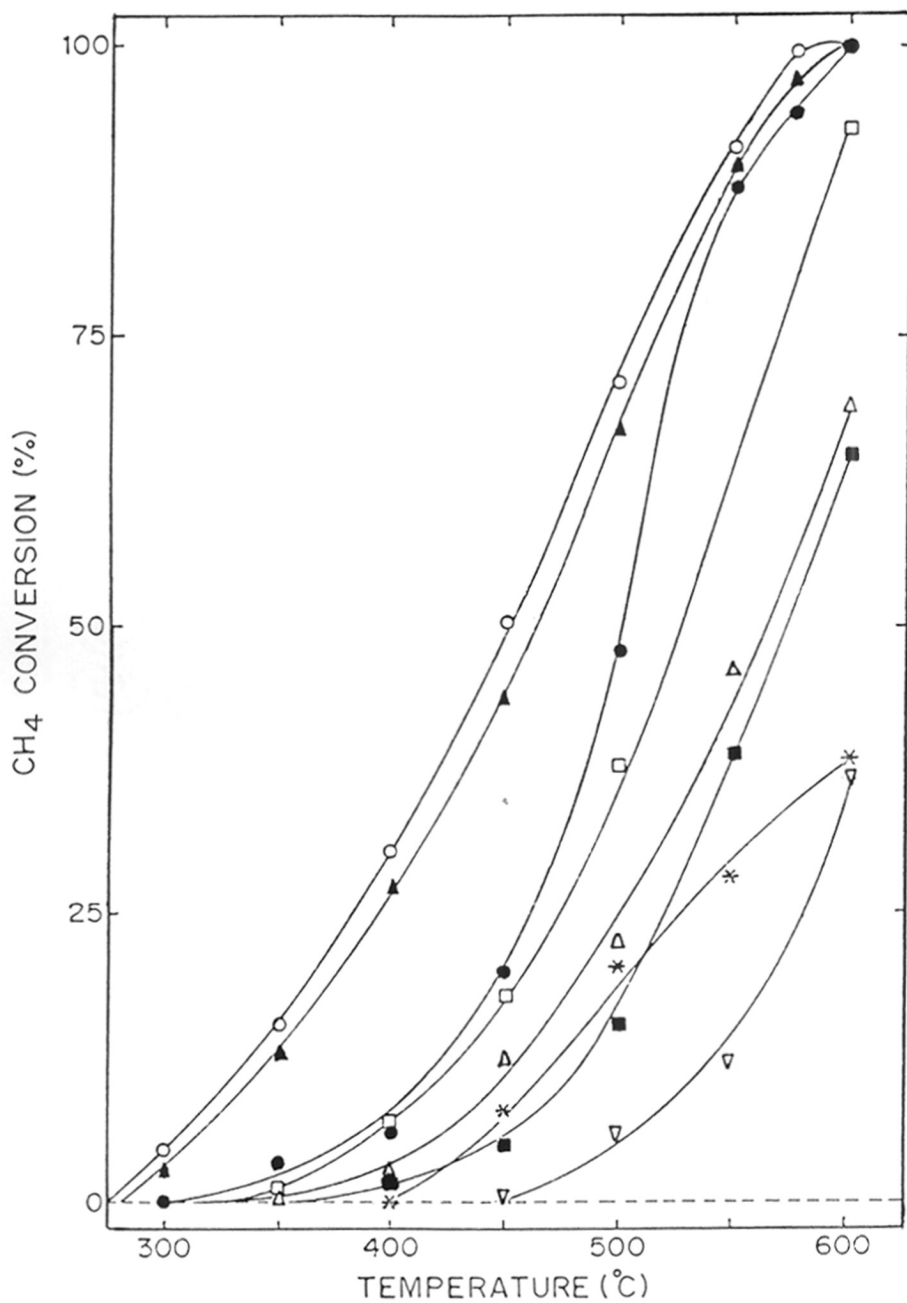


Fig. 3.1.3: Temperature dependence of the conversion of methane in its complete combustion over Mn-stabilized ZrO₂ (O), Co-stabilized ZrO₂ (▲), Fe-stabilized ZrO₂ (●), Cr-stabilized ZrO₂ (□), Cu-stabilized ZrO₂ (△), Ni-stabilized ZrO₂ (■), Mn-impregnated ZrO₂ (*) and pure ZrO₂ (▽) [Feed = 1 mol% CH₄ in air, space velocity = 51,000 cm³.g⁻¹.h⁻¹].

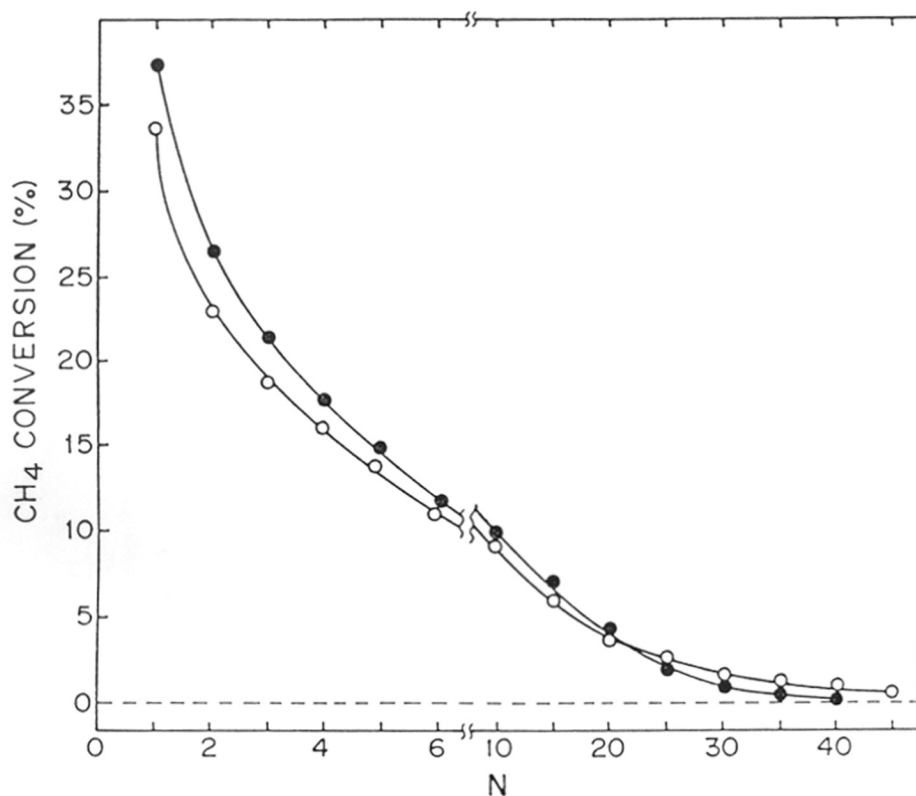


Fig. 3.1.4 : Variation of methane conversion with pulse number (N) in the pulse reaction of methane (in the absence of free-O₂) at 500°C over fresh Mn-stabilized ZrO₂ (O) and deactivated Mn-stabilized ZrO₂ after its reoxidation by air at 500°C (●) [pulse : 0.2 cm³ of pure methane, carrier gas : He (30 cm³.min⁻¹), amount of catalyst : 0.1 g]

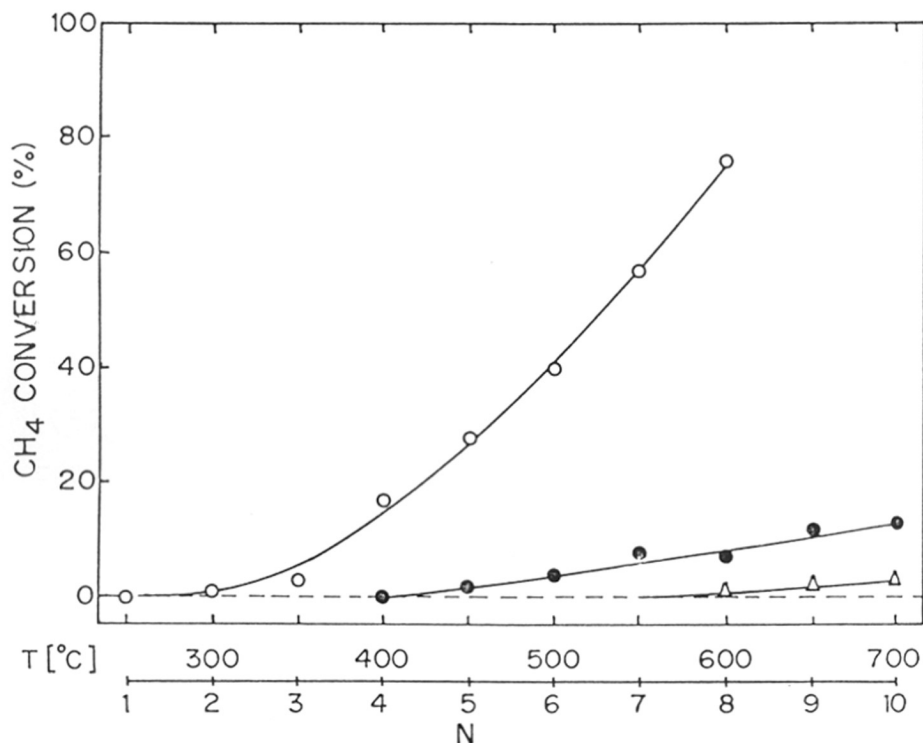


Fig. 3.1.5 : Temperature dependence of methane conversion in the pulse reaction of methane (in the absence of free-O₂) over Mn-stabilized ZrO₂ (O), Mn-impregnated ZrO₂ (●) and pure ZrO₂ (Δ) [amount of catalyst : 0.1 g, pulse : 0.2 cm³ of pure methane, carrier gas : He (30 cm³.min⁻¹)]

of free-O₂) of these catalysts. These observations reveal that the high catalytic activity in the methane combustion is attributed to the high reactivity of lattice oxygen of the catalyst.

Table 3.1.1 : Comparison of Mn-, Co- and Fe-stabilized ZrO₂ (cubic) catalysts with perovskite oxide and noble metal catalysts for complete combustion of methane (GHSV= 51,000 cm³.g⁻¹.h⁻¹)

Catalyst	Surface area (m ² .g ⁻¹)	Temperature required for	
		50% conversion	90% conversion
LaNiO ₃	4.5	793	>> 800
La _{0.7} Sr _{0.3} NiO ₃	3.5	620	740
LaCoO ₃	2.4	633	750
La _{0.7} Sr _{0.3} CoO ₃	2.2	637	753
LaMnO ₃	3.2	693	793
La _{0.7} Sr _{0.3} MnO ₃	5.9	670	760
LaFeO ₃	6.8	617	713
La _{0.7} Sr _{0.3} FeO ₃	5.3	610	712
La _{0.7} Sr _{0.3} Co _{0.5} Fe _{0.5} O ₃	3.5	660	775
Pt/Al ₂ O ₃ (1 wt% Pt) (ref. 7)	-	545	650
Pd/Al ₂ O ₃ (1 wt% Pd) (ref. 7)	-	400	445
Fe-stabilized ZrO ₂	102	503	557
Co-stabilized ZrO ₂	98	464	550
Mn-stabilized ZrO ₂	105	450	545

The Mn-, Co- and Fe-stabilized ZrO₂ catalysts are compared with the perovskite oxide catalysts (known for high methane combustion activity) and noble metal catalysts for their methane combustion activity at the same space velocity in Table 3.1.1. The comparison clearly shows that the stabilized zirconia catalysts have much higher activity than the perovskite oxide catalysts and their activity is comparable with that of the noble metal catalysts. The stabilized ZrO₂ catalysts, particularly Mn-, and Co-stabilized ZrO₂ catalysts have high potential for their use as low temperature

combustion catalyst in the methane emission control. The high methane combustion activity of these catalysts at low temperature is attributed to the high reactivity of their lattice oxygen and also to the high mobility of oxygen in the stabilized zirconia, facilitating the redox process in the catalytic methane combustion. The Mn-doped ZrO_2 in its cubic form is stable upto $700^\circ C$ [19-22].

The enhancement in the reactivity of lattice oxygen due to the stabilization of zirconia by Mn or other transitional metals may be due to creation of crystal defects, resulting in the formation of low coordinated lattice oxygen and transition metal sites on the surface and also increasing the mobility of oxygen both on the surface and in the bulk of the catalyst. Further work is necessary for understanding this.

3.1.4 CONCLUSIONS

The Mn-, Co-, and Fe-stabilized ZrO_2 (cubic) catalysts display much higher methane combustion activity at low temperature than the perovskite oxide catalysts; the activity is somewhat comparable to that of the noble metal catalysts. Furthermore, incorporation of the transition metal in the ZrO_2 bulk structure not only stabilizes the metal oxide cubic (fluorite) modification but also drastically increases the reactivity of the lattice oxygen, which can be used for low-temperature complete combustion of methane.

REFERENCES

1. R.E. Dickinson and R.J. Cicerone, *Nature*, 319 (1986) 109.
2. R.B. Anderson, K.C. Stein, J.J. Freenan and L.J.E. Hofer, *Ind. Eng. Chem.*, 53 (1961) 809.
3. C. Cullis, D. Keene and D.L. Trimm, *J.Catal.*, 19 (1970) 378.
4. K.R. Thampi, J. Kiwi and M. Graztel, *Catal. Lett.*, (1990) 4549.
5. T.R. Baldwin and R. Burch, *Appl. Catal.*, 66 (1990) 337.
6. T.R. Baldwin and R. Burch, *Appl. Catal.*, 66 (1990) 359.
7. N. Mouaddib, C. Feumi-Jantou, E. Garbbowski and M. Primet, *Appl. Catal. A: General*, 87 (1992) 129.
8. Y. Mizushima and M. Hori, *Appl. Catal. A: General*, 88 (1992) 137.
9. Y. Li and J.N. Armor, *Appl. Catal. B: Environment*, 3 (1994) 275.
10. T. Ishihara, H. Sumi and Y. Takita, *Chem. Lett.*, (1994) 1499.
11. L.G. Tejuca, J.L.G. Fierro and J.M.D. Tascon, *Adv. Catal.*, 36 (1989) 237.
12. T. Seiyama, *Catal. Rev. -Sci. Eng.*, 34 (1992) 281.
13. H. Arai, T. Yamada, K. Eguchi and T. Seiyama, *Appl. Catal.*, 26 (1986) 265.
14. H.M. Zhang, Y. Teraoka and N. Yamazoe, *Catal. Today*, 6 (1989) 155.
15. J.G. McCarty and H. Wise, *Catal. Today*, 8 (1990) 231.
16. B. de Collongue, E. Garbowski and M. Primet, *J. Chem. Soc., Faraday Trans.*, 87 (1991) 2493.
17. P.E. Marti and A. Baiker, *Catal. Lett.*, 26 (1994) 71.
18. P.E. Marti, M. Maciejewski and A. Baiker, *Appl. Catal. B: Environment*, 4 (1994) 225.
19. H.J. Stöcker and R. Collongues, *Compt. Rend.*, 245 (1957) 695.
20. H.J. Stöcker, *Ann. Chim.*, 5 (1960) 1495.
21. A. Keshavaraj and A.V. Ramaswamy, *J. Mater. Res.*, 9 (1994) 837.
22. V.P. Dravid, V. Ravikumar, M.R. Notis, C.E. Lyman, G. Dhaleane and A. Revcolevschi, *J. Am. Ceram. Soc.*, 77 (1994) 2758.
23. S. Davison, R. Kershaw, K. Dwight and A. Wold, *J. Solid State Chem.*, 73 (1988) 45
24. I.B. Inwang, F. Chyad and I.J. McColm, *J. Mater. Chem.*, 5 (1995) 1209.
25. P. Wu, R. Kershaw, K. Dwight and A. Wold, *Mater. Res. Bull.*, 23 (1988) 475.
26. V.R. Choudhary and V.H. Rane, *J. Catal.*, 135 (1992) 310.

CHAPTER - 3.2

LOW TEMPERATURE TOTAL OXIDATION OF METHANE OVER Ag- DOPED LaMO_3 PEROVSKITE OXIDES

3.2.1 INTRODUCTION

Methane has 20 - 30 times larger green-house effect relative to carbon dioxide. Hence, the control of methane emission from natural gas engines/power plants and petroleum and petrochemical industries is essential. However, since methane is most inert among the hydrocarbons, its oxidative destruction by complete combustion to CO_2 is difficult. Because of scarcity and high cost of noble metals, worldwide efforts are being made to replace noble-metal catalysts (which show high methane combustion activity at low temperature) by non-noble metal catalysts, particularly ABO_3 type perovskite oxides (where A = rare earth, B = transition metal such as Cr, Mn, Fe, Co, Ni, etc) with or without partial substitution of A by other elements (e.g. Sr) [1-8]. Earlier studies [3, 5] showed that LaMO_3 (M = Co, Mn, Ni, Fe) and Sr-doped LaCoO_3 and LaMO_3 perovskite oxides have high methane combustion activity. ABO_3 type perovskites with partial substitution at both the sites (i.e. A and B) also have been reported for complete combustion of methane. Earlier studies [9, 10] showed that LaCoO_3 with partial substitution of La by Sr and of Co by Fe or Ni has high methane combustion activity. The present investigation was undertaken to study influence of the doping of these ABO_3 type perovskites by Ag on their activity in the complete combustion of methane.

3.2.2 EXPERIMENTAL

3.2.2.1 Catalyst Preparation

Ag-doped LaMO_3 (M = Mn, Co or Ni) Perovskites

The LaMO_3 and $\text{La}_{0.7}\text{Sr}(\text{or Ag})_{0.3}\text{MO}_3$ (M = Mn, Co, Ni) perovskite oxides were prepared by coprecipitating mixed metal carbonates of La and transition metal (viz.: Mn, Co, Ni) with or without Sr or Ag from their mixed-nitrate solution with sodium carbonate, ageing the precipitate for 12 h, filtering and washing it thoroughly with deionized water, drying (at 100°C overnight), decomposing at 500°C under static air for 5 h, powdering, washing with boiling deionized water to remove traces of sodium, again filtering and drying (at 100°C overnight) pelletizing and calcining at 750°C (for Ag

containing perovskites) or 900°C (for other perovskites) for 6h under static air and crushing the calcined pellets to 22-30 mesh size particles.

Ag-doped $\text{La}_{1-x}\text{Sr}_x\text{Fe}_{1-y}\text{Co}_y\text{O}_3$ perovskites

The LaFeO_3 , $\text{LaFe}_{0.5}\text{Co}_{0.5}\text{O}_3$, $\text{La}_{0.7}\text{Sr}(\text{or Ag})_{0.3}\text{FeO}_3$ and $\text{La}_{0.7}\text{Sr}(\text{or Ag})_{0.3}\text{Fe}_{0.5}\text{Co}_{0.5}\text{O}_3$ perovskite oxides were prepared by coprecipitating mixed metal carbonates of La and transition metal(s) (viz.: Fe and Co) with or without Sr or Ag from their mixed nitrate solution with sodium carbonate, ageing the precipitate for 12 h, filtering and washing it thoroughly by deionized water, drying (at 100°C overnight), decomposing at 500°C under static air for 5 h, powdering, washing with boiling deionized water to remove traces of sodium, again filtering and drying (at 100°C overnight) pelletizing and calcining at 750°C (for Ag containing perovskites) or 900°C (for other perovskites) for 6 h under static air and crushing the calcined pellets to 22-30 mesh size particles.

Ag-impregnated LaMO_3 ($M = \text{Mn}, \text{Fe}, \text{Co}$ or Ni) perovskites

Ag-impregnated LaMO_3 ($M = \text{Mn}, \text{Fe}, \text{Co}$ or Ni) and $\text{LaCo}_{0.5}\text{Fe}_{0.5}\text{O}_3$ type perovskite oxides were prepared by impregnating 22-30 mesh size particles of these perovskites (prepared as described earlier) with aqueous Ag-nitrate, drying (at 100°C overnight) and calcining in static air at 750°C for 6 h.

3.2.2.2 Catalyst Characterization

The perovskite oxide structure of all the catalysts was confirmed by XRD. The XRD spectra for the perovskite oxides are given in Figs. 3.2.1-3.2.5. The XRD spectra for all the Ag-doped perovskites show presence of free metallic Ag, a minor crystalline phase along with the perovskite oxide phase.

The surface area of the catalysts was measured by the single-point BET method by measuring the adsorption of nitrogen at liquid nitrogen temperature from a N_2 -He mixture containing 30 mol% N_2 , using a Monosorb Surface Area Analyzer (Quantachrome Corp. USA).

3.2.2.3 Catalytic Reaction

The schematic diagram of the quartz reactor and the experimental set-up used in the total combustion of methane are shown in Figs. 1.1.2 and 1.1.3, respectively. The experimental set-up used for the pulse reaction of pure methane in the absence of free O_2 is given in Fig. 3.1.2.

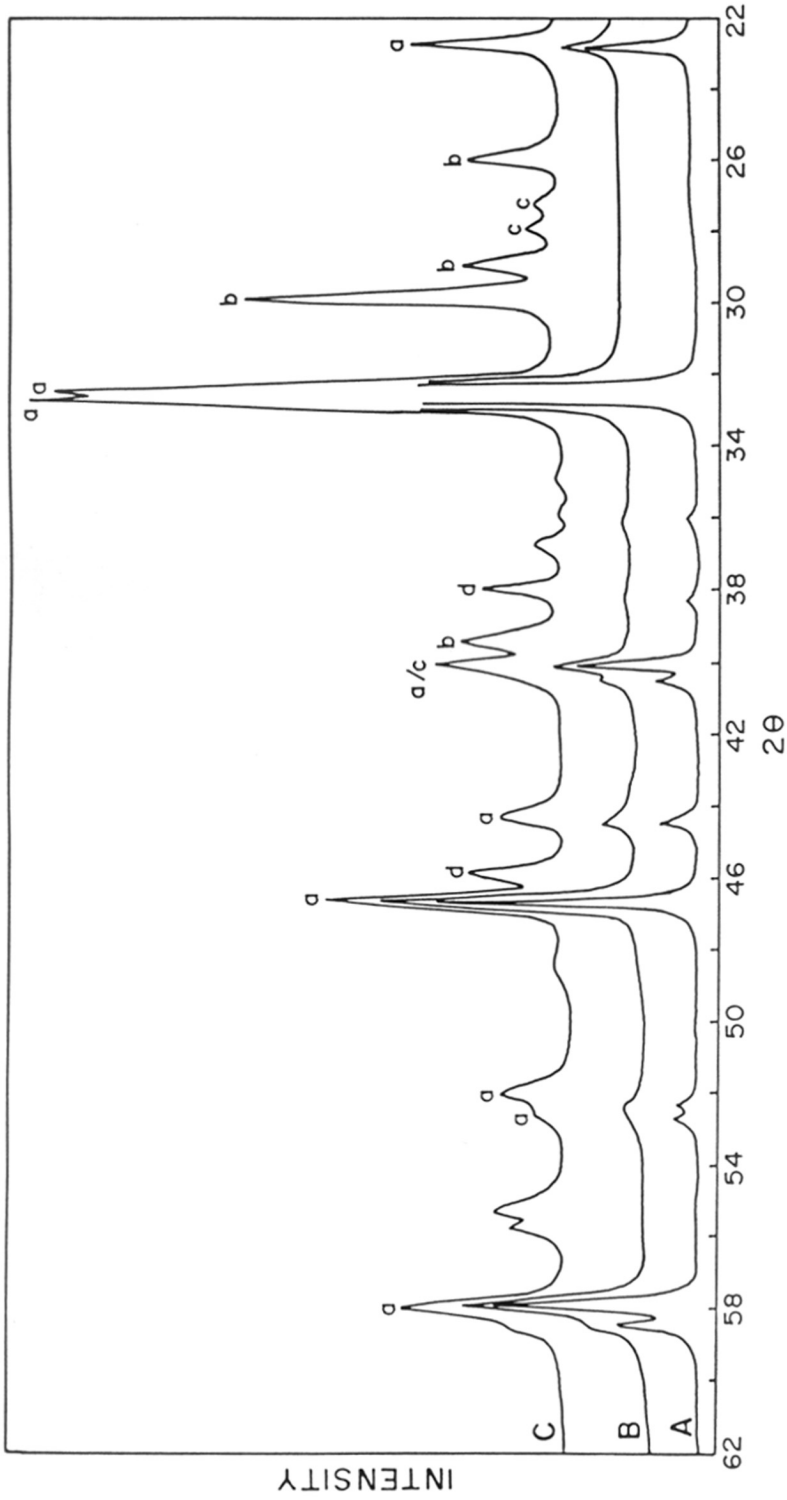


Fig. 3.2.1 : XRD spectras of LaMnO_3 (A), $\text{La}_{0.7}\text{Sr}_{0.3}\text{MnO}_3$ (B) and $\text{La}_{0.7}\text{Ag}_{0.3}\text{MnO}_3$ (C) perovskite oxides [crystalline phases : (a) perovskite, (b) La_2O_3 , (c) $\text{La}(\text{OH})_3$ and (d) Ag^0]

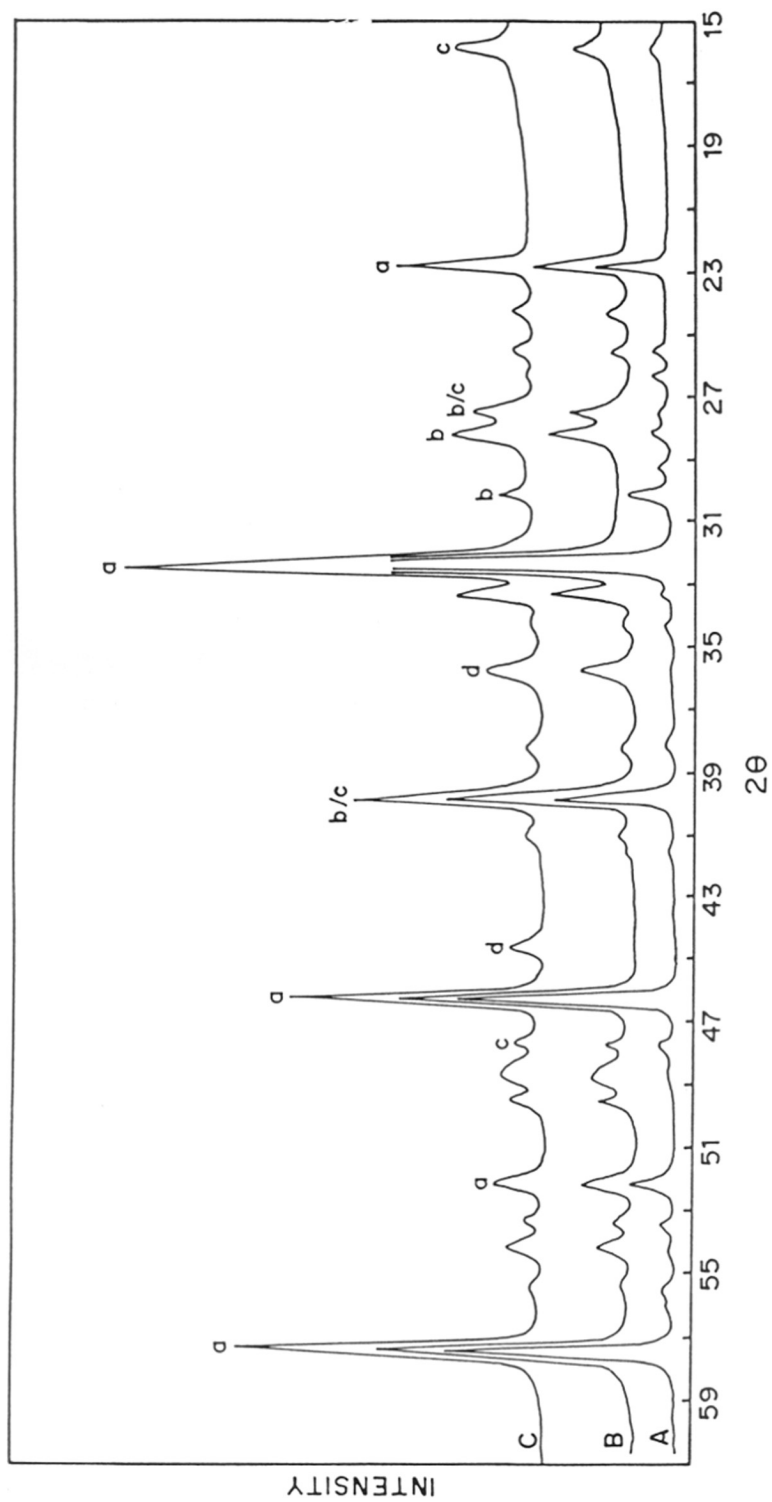


Fig. 3.2.2 : XRD spectras of LaFeO_3 (A), $\text{La}_{0.7}\text{Sr}_{0.3}\text{FeO}_3$ (B) and $\text{La}_{0.7}\text{Ag}_{0.3}\text{FeO}_3$ (C) perovskite oxides [crystalline phases : (a) perovskite, (b) La_2O_3 , (c) $\text{La}(\text{OH})_3$ and (d) Ag^0]

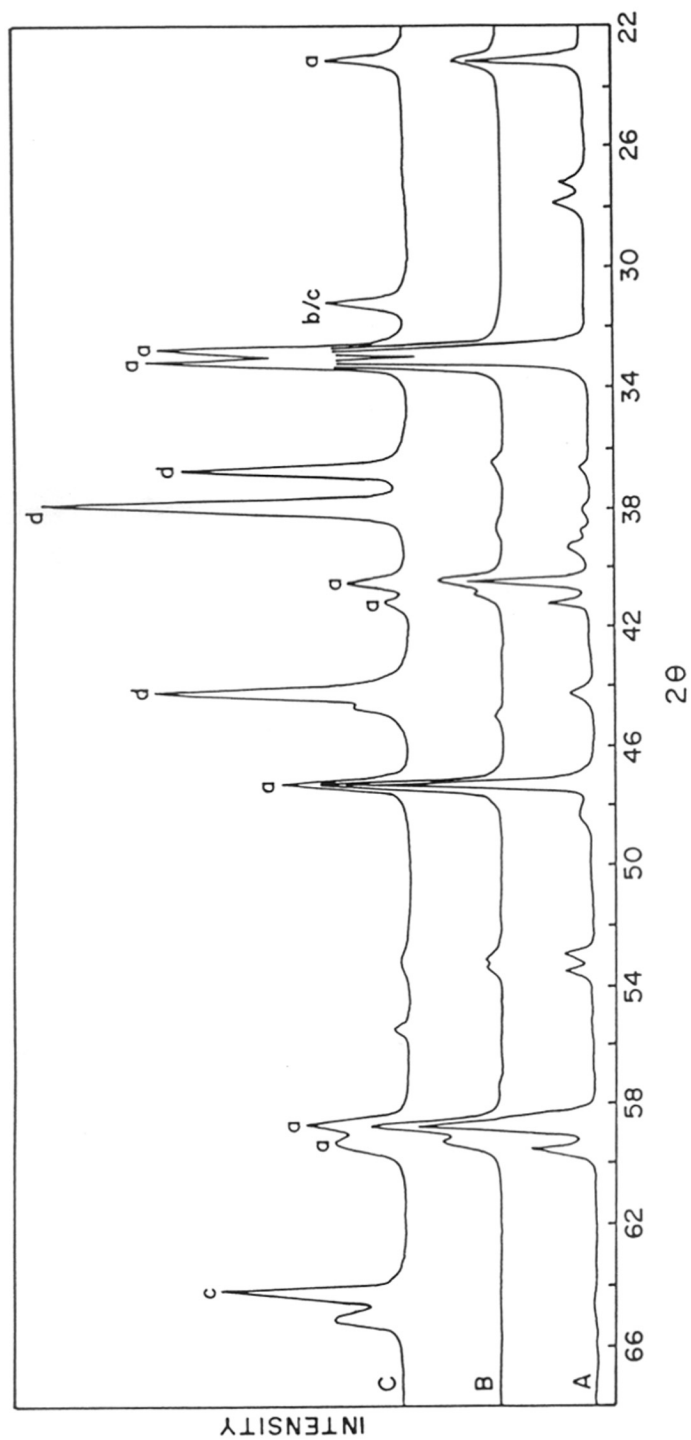


Fig. 3.2.3 : XRD spectras of LaCoO_3 (A), $\text{La}_{0.7}\text{Sr}_{0.3}\text{CoO}_3$ (B) and $\text{La}_{0.7}\text{Ag}_{0.3}\text{CoO}_3$ (C) perovskite oxides [crystalline phases : (a) perovskite, (b) La_2O_3 , (c) Co_3O_4 and (d) Ag^0]

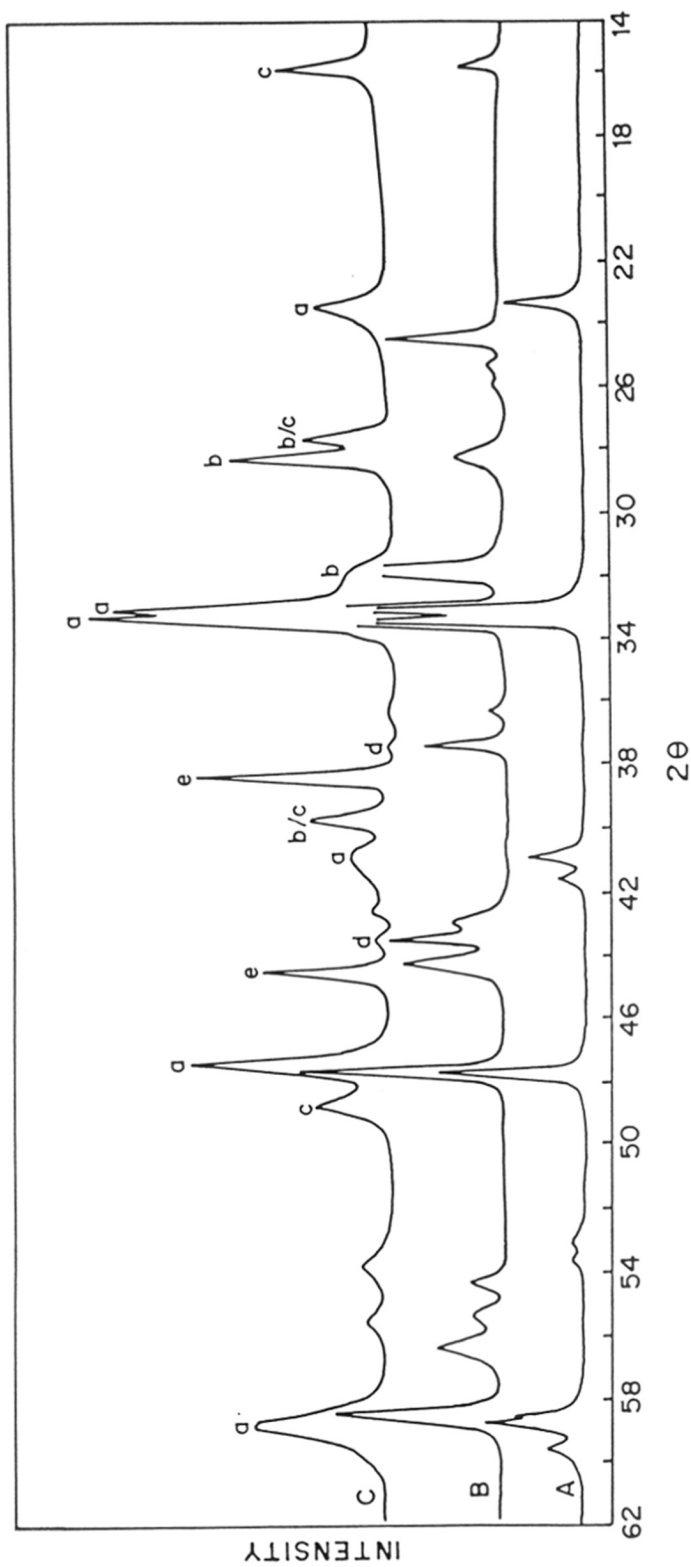


Fig. 3.2.4 : XRD spectras of LaNiO_3 (A), $\text{La}_{0.7}\text{Sr}_{0.3}\text{NiO}_3$ (B) and $\text{La}_{0.7}\text{Ag}_{0.3}\text{NiO}_3$ (C) perovskite oxides
[crystalline phases : (a) perovskite, (b) La_2O_3 , (c) $\text{La}(\text{OH})_3$, (d) NiO and (e) Ag^0]

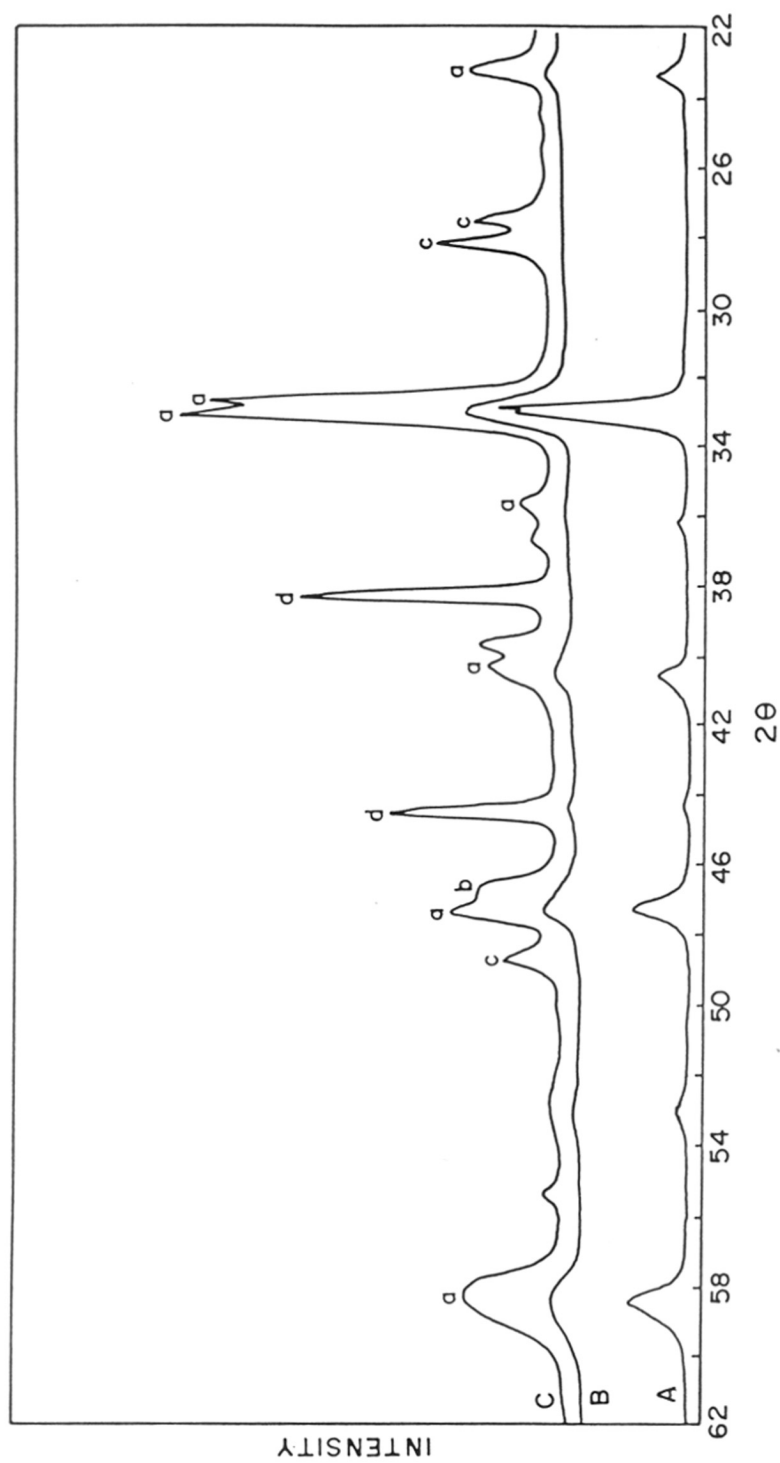


Fig. 3.2.5: XRD spectra of $\text{LaC}_{0.5}\text{Fe}_{0.5}\text{O}_3$ (A), $\text{La}_{0.7}\text{Sr}_{0.3}\text{Co}_{0.5}\text{Fe}_{0.5}\text{O}_3$ (B) and $\text{La}_{0.7}\text{Ag}_{0.3}\text{Co}_{0.5}\text{Fe}_{0.5}\text{O}_3$ (C) perovskite oxides [crystalline phases : (a) perovskite, (b) La_2O_3 , (c) $\text{La}(\text{OH})_3$ and (d) Ag^0]

The methane combustion activity of all the perovskite oxide catalysts was determined at atmospheric pressure in a continuous fixed-bed quartz microreactor (i.d. = 10 mm) packed with 0.1 g catalyst (particle size = 22-30 mesh), mixed uniformly with 0.9 g inert α -Al₂O₃ particles, at different temperatures using 4 mol% methane in air as a feed at a space velocity (measured at 0°C and 1 atm pressure) of 51,000 cm³.g⁻¹.h⁻¹. The reaction temperature was measured by a Chromel-Alumel thermocouple placed in the centre of the catalyst bed. The products (after condensing the water from the product stream at 0°C) were analyzed by an on-line GC using molecular sieve and Sphero carb column. The temperature programmed reactions of methane (in the absence of free O₂) over the catalysts were carried out in a quartz reactor. The products were sampled at different temperatures using a multiloop gas-sampling valve and analysed by GC. The pulse reaction of pure methane (in the absence of free O₂) over the catalyst was carried out at 550°C in a quartz-pulse microreactor connected to a GC, described earlier[11], using He as a carrier gas. In both the presence and absence of free O₂, the combustion of methane over the catalysts was complete with no formation of CO.

3.2.3 COMPLETE COMBUSTION OF METHANE OVER Ag-DOPED LaMO₃ (M = CO, Mn, Ni)

Results in Table 3.2.1 reveal that the reaction temperature required for 50 and 90% methane conversion is reduced markedly when La is partially substituted by Ag, instead of Sr, in the LaMnO₃, LaCoO₃ and LaNiO₃ perovskites. Among the perovskite oxide catalysts, Ag-doped LaCoO₃ shows the highest methane combustion activity. It shows no sign of deactivation in the catalytic process when tested for 50 h at 600°C.

In the absence of free O₂, a high conversion of methane is observed in the pulse-reaction of pure methane over the Ag-doped LaCoO₃ catalyst at 550°C (Table 3.2.2). The conversion is decreased upon increasing the number of pulses and is reduced to a very low value after the 30th pulse. However, the initial high conversion is regained after reoxidation of the catalyst by O₂. This reveals the involvement of lattice oxygen in a redox mechanism in the methane combustion over the catalyst. The observed higher conversion, after reoxidation, for the initial 15 pulses may be due to chemisorbed oxygen on the catalyst.

Table 3.2.1 : Results of complete combustion of methane over different perovskite oxide catalysts (concentration of CH₄ in air = 4 mol% and GHSV = 51,000 cm³.g⁻¹.h⁻¹)

Catalyst	Surface area (m ² .g ⁻¹)	Reaction temperature (°C) for	
		50% conversion	90% conversion
LaMnO ₃	3.2	693	793
La _{0.7} Sr _{0.3} MnO ₃	5.9	670	760
La _{0.7} Ag _{0.3} MnO ₃	9.8	592	683
LaCoO ₃	1.2	634	743
La _{0.7} Sr _{0.3} CoO ₃	2.2	637	753
La _{0.7} Ag _{0.3} CoO ₃	4.1	560	653
LaNiO ₃	1.5	793	>> 800
La _{0.7} Sr _{0.3} NiO ₃	3.5	620	740
La _{0.7} Ag _{0.3} NiO ₃	6.7	580	673

Table 3.2.2 : Pulse reaction of pure methane over La_{0.7}Ag_{0.3}CoO₃ at 550°C (in the absence of free O₂ [amount of catalyst, 0.1 g; pulse, pure methane (0.2 cm³); carrier gas, He (30 cm³.min⁻¹)])

Pulse number	Methane conversion (%)	
	Fresh catalyst	Reoxidised catalyst ^a
1	24.0	37.8
2	23.1	26.0
5	19.8	20.0
10	13.8	14.3
15	9.9	10.5
20	6.5	6.5
25	4.8	4.7
30	1.1	1.2

^aAfter the 30th pulse the catalyst was pretreated in O₂ at 550°C for 1 h.

Results of the temperature programmed reaction of methane over the LaCoO_3 and Sr- and Ag-doped LaCoO_3 catalysts in the absence of free O_2 (Fig. 3.2.6) clearly show that the lattice oxygen of Ag-doped LaCoO_3 is much more reactive at lower temperatures than that of LaCoO_3 and Sr-doped LaCoO_3 catalysts. Because of the higher reactivity of lattice oxygen, the Ag-doped LaCoO_3 is catalytically more active in the methane combustion at lower temperatures.

In summary, the doping of LaMO_3 ($M = \text{Mn, Co, Ni}$) perovskites by Ag results in a large increase in their methane combustion activity at lower temperatures (below 700°C) and high space velocity ($51,000 \text{ cm}^3 \cdot \text{g}^{-1} \cdot \text{h}^{-1}$) due to the increase in the reactivity of their lattice oxygen. The Ag-doped LaCoO_3 is a highly promising catalyst for the complete combustion of methane for its emission control.

3.2.4 COMPLETE COMBUSTION OF METHANE OVER Ag-DOPED $\text{LaFe}_{1-x}\text{Co}_x\text{O}_3$

The methane combustion activity of all the perovskite oxide catalysts at different temperatures is shown in Fig. 3.2.7. The data on the reaction temperature required for 50% and 95% methane conversion over the different perovskite oxide catalysts are compared in Table 3.2.3. The reaction temperature required for 50% or 95% conversion is reduced markedly when La is partially substituted by Ag, instead of Sr, in the LaFeO_3 and $\text{LaFe}_{0.5}\text{Co}_{0.5}\text{O}_3$ perovskites. It is clear from the results that the Ag-doped (viz. LaFeO_3 and $\text{LaFe}_{0.5}\text{Co}_{0.5}\text{O}_3$) perovskite oxide catalysts show the highest methane combustion activity. It shows no sign of catalyst deactivation when operated continuously for 50 h at 600°C in the methane combustion process.

The $\text{LaFe}_{0.5}\text{Co}_{0.5}\text{O}_3$ and $\text{La}_{0.7}\text{Sr}$ (or $\text{Ag}_{0.3}\text{Fe}_{0.5}\text{Co}_{0.5}\text{O}_3$) perovskite oxide catalysts are compared in Fig. 3.2.8 for the reactivity of their lattice oxygen in the methane combustion by carrying out the methane pulse reaction (in the absence of free- O_2) at different temperatures. The observed higher conversion over the Ag-doped $\text{LaFe}_{0.5}\text{Co}_{0.5}\text{O}_3$ as compared to that over the other two catalysts reveals that the lattice oxygen of the Ag-doped perovskite oxide catalyst is much more reactive at lower temperatures than that of other two catalysts. Because of the higher reactivity of lattice oxygen, the Ag-doped $\text{LaFe}_{0.5}\text{Co}_{0.5}\text{O}_3$ is catalytically more active in the methane combustion at lower temperatures.

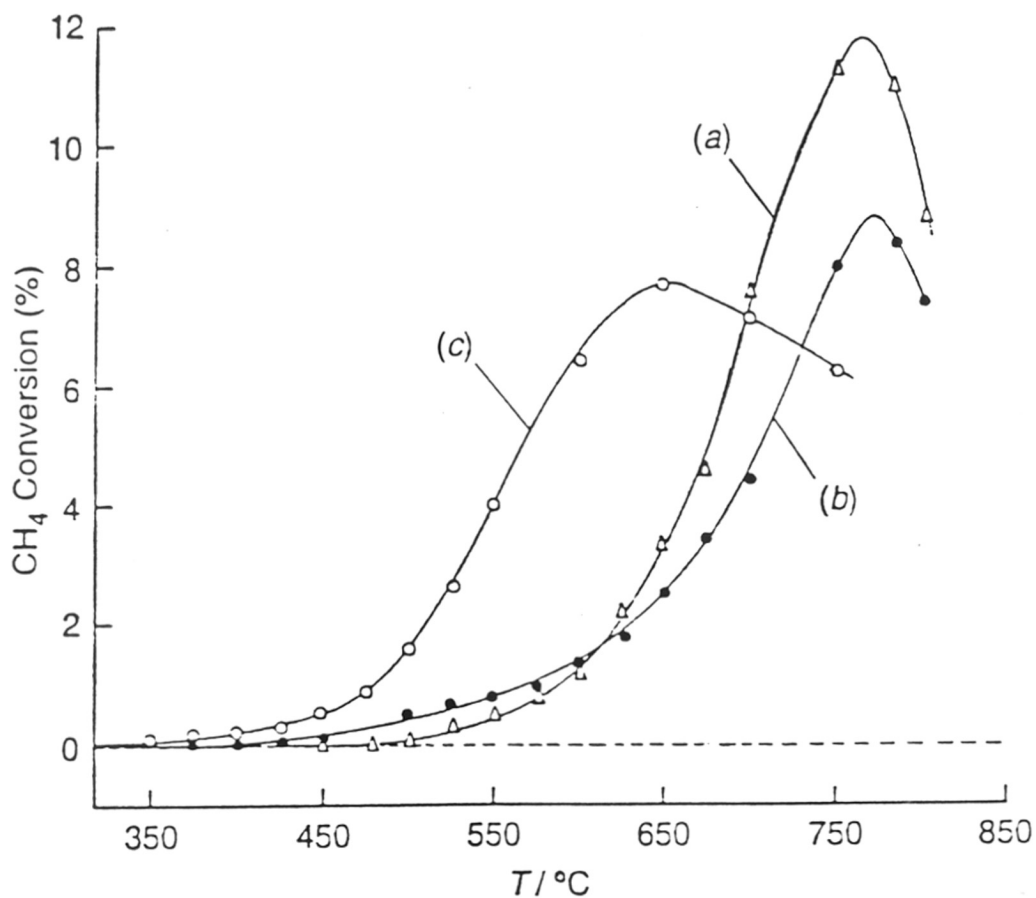


Fig. 3.2.6: Temperature programmed reaction of methane over LaCoO_3 (a), $\text{La}_{0.7}\text{Sr}_{0.3}\text{CoO}_3$ (b) and $\text{La}_{0.7}\text{Ag}_{0.3}\text{CoO}_3$ (c) in the absence of free O_2 [amount of catalyst, 0.5 g; feed, 5 mol% CH_4 in He ($100 \text{ cm}^3 \cdot \text{g}^{-1}$); linear heating rate, $20^\circ\text{C} \cdot \text{min}^{-1}$]

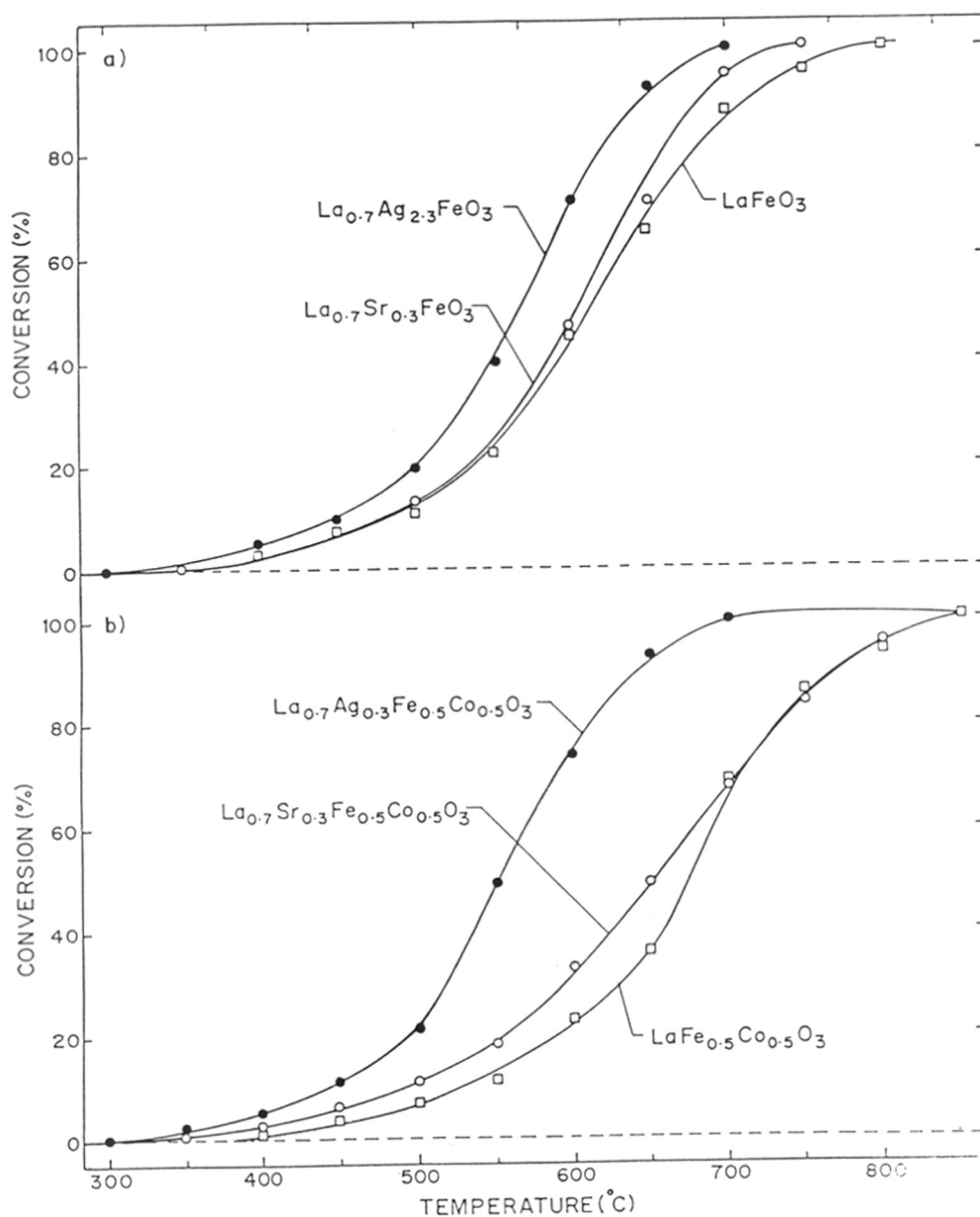


Fig. 3.2.7: Temperature dependence of the complete combustion of methane over the perovskite oxide catalysts [Feed = 4% CH_4 in air, GHSV = $51,000 \text{ cm}^3 \cdot \text{g}^{-1} \cdot \text{h}^{-1}$]

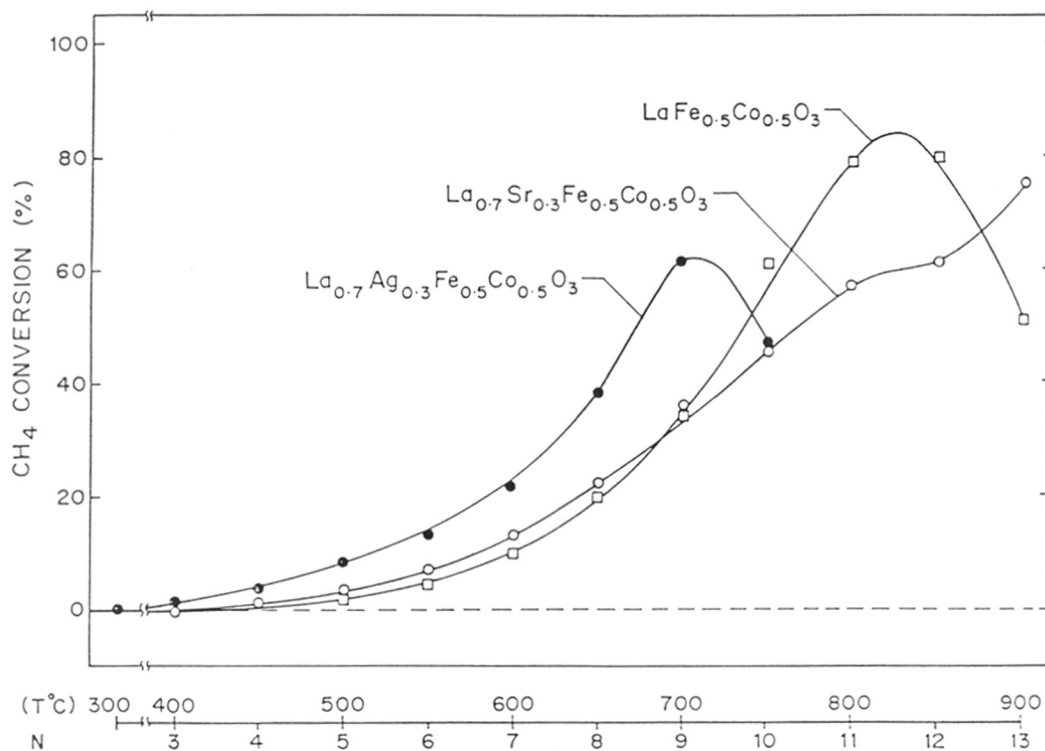


Fig. 3.2.8: Temperature dependence of the conversion in the pulse reaction of methane over the perovskite oxide catalysts in the absence of free-O₂ [amount of catalyst = 0.1 g, pulse = 0.2 cm³ of pure methane, carrier gas = He (30 cm³.min⁻¹)] (N = pulse number)

In summary, the doping of LaFeO_3 and $\text{LaFe}_{0.5}\text{Co}_{0.5}\text{O}_3$ perovskites by Ag results in a large increase in their methane combustion activity at lower temperatures due to the increase in the reactivity of their lattice oxygen. The Ag-doped $\text{LaFe}_{0.5}\text{Co}_{0.5}\text{O}_3$ is a highly promising catalyst for the complete combustion of methane for its emission control.

Table 3.2.3.: Results of complete combustion of methane over different perovskite oxide catalysts (Concentration of CH_4 in air = 4 mol% and GHSV = $51,000 \text{ cm}^3 \cdot \text{g}^{-1} \cdot \text{h}^{-1}$)

Catalyst	Surface area ($\text{m}^2 \cdot \text{g}^{-1}$)	Reaction temperature ($^\circ\text{C}$)	
		50% conversion	95% conversion
LaFeO_3	6.8	613	743
$\text{La}_{0.7}\text{Sr}_{0.3}\text{FeO}_3$	5.4	603	705
$\text{La}_{0.7}\text{Ag}_{0.3}\text{FeO}_3$	12.9	568	667
$\text{LaFe}_{0.5}\text{Co}_{0.5}\text{O}_3$	3.8	675	800
$\text{La}_{0.7}\text{Sr}_{0.3}\text{Fe}_{0.5}\text{Co}_{0.5}\text{O}_3$	3.5	653	800
$\text{La}_{0.7}\text{Ag}_{0.3}\text{Fe}_{0.5}\text{Co}_{0.5}\text{O}_3$	8.6	550	665

3.2.5 COMPLETE COMBUSTION OF METHANE OVER Ag-IMPREGNATED PEROVSKITE OXIDES

Since the Ag-doped perovskites contain free metallic Ag (as detected by their XRD), it is interesting to know the effect of direct deposition of Ag by impregnation on the perovskites on their methane combustion activity.

The methane combustion activity (at different temperature) of the perovskites is compared with that of the Ag-doped and Ag-impregnated perovskites in Table 3.2.4. From these results following important observations have been made.

- The methane combustion activity of Ag-impregnated LaMnO_3 , LaCoO_3 and $\text{LaCo}_{0.5}\text{Fe}_{0.5}\text{O}_3$ perovskites is lower than their Ag-doped counterparts and it is comparable to that of the perovskites without Ag.

Table 3.2.4 : Results of complete combustion of methane over different perovskite oxide catalysts (concentration of CH₄ in air = 4 mol% and GHSV = 51,000 cm³·h⁻¹·g⁻¹).

Catalyst	Ag/La ratio	Calcination temp. (°C)	Methane conversion (%) at different temperatures (°C)														
			350	400	450	500	550	600	650	700	750	800	850				
LaMnO ₃	0.0	900	0.0	0.0	1.8	7.1	9.6	23.6	38.7	65.4	87.4	100					
Ag-doped LaMnO ₃	0.3	750	0.0	3.0	7.9	14.8	27.7	52.5	79.9	94.5	100						
Ag-impregnated LaMnO ₃	0.3	750	0.0	2.4	5.7	9.0	14.6	28.5	43.7	63.0	77.0						
LaFeO ₃	0.0	900	0.0	3.4	7.6	10.9	22.3	44.8	64.7	88.2	95.8	100					
Ag-doped LaFeO ₃	0.3	750	1.9	4.7	7.8	19.2	39.9	70.9	93.3	99.0	100						
Ag-impregnated LaFeO ₃	0.3	750	0.0	2.3	4.9	9.6	16.0	42.4	57.2	78.8	91.7	100					
LaCoO ₃	0.0	900	0.0	1.9	2.9	6.0	15.7	34.4	57.2	77.2	91.7	96.3	100				
Ag-doped LaCoO ₃	0.3	750	0.0	4.0	12.2	19.4	41.1	65.6	86.2	98.2	100						
Ag-impregnated LaCoO ₃	0.3	750	0.0	1.3	2.1	5.8	12.7	31.9	40.5	61.4	87.6						
LaNiO ₃	0.0	900	0.0	0.0	0.0	0.0	0.0	3.5	8.4	16.7	32.8	54.6	68.3				
Ag-doped LaNiO ₃	0.3	750	0.0	2.4	7.3	15.6	35.6	51.2	83.2	96.8	100						
Ag-impregnated LaNiO ₃	0.3	750	0.0	2.5	9.0	17.6	32.7	49.8	80.6	95.0	100						
LaCo _{0.5} Fe _{0.5} O ₃	0.0	900	0.0	0.0	1.8	18.6	26.9	43.9	63.0	91.1	98.4	100					
Ag-doped LaCo _{0.5} Fe _{0.5} O ₃	0.3	750	6.7	8.8	11.7	29.6	58.0	86.7	100								
Ag-impregnated LaCo _{0.5} Fe _{0.5} O ₃	0.3	750	0.0	0.0	1.6	5.5	14.2	33.3	56.7	81.0	95.6	100					

- The methane combustion activity of Ag-impregnated LaNiO_3 is comparable to that of the Ag-doped LaNiO_3 . The activity of both the catalyst is much higher than that of LaNiO_3 without Ag. The results clearly show that the doping of LaMO_3 type perovskite oxides with Ag enhances the methane combustion activity of the perovskite. This may be due to an incorporation of part of Ag in the perovskite lattice by a partial substitution of La by Ag. However, further studies are necessary for confirming the partial substitution by Ag.

REFERENCES

1. L.G. Tejuca, J.L.G. Fierro and J.M.D. Tascon, *Adv.Catal.*, 36 (1989) 237.
2. T. Seiyama, *Catal.Rev.Sci.Eng.*, 34 (1992) 281.
3. H. Arai, T. Yamada, K. Eguchi and T. Seiyama, *Appl.Catal.*, 26 (1986) 265.
4. H.M. Zhang, Y. Teraoka and N. Yamazoe, *Catal.Today*, 6 (1989) 155.
5. J.G. McCarty and H. Wise, *Catal.Today*, 8 (1990) 231.
6. A. de Collongue, E. Garbbowski and M. Primet, *J.Chem.Soc. Faraday Trans.*, 87 (1991) 2493.
7. G.E. Marti and A. Baiker, *Catal.Lett.*, 26 (1994) 71.
8. G.E. Marti, M. Maciejewski and A. Baiker, *Appl.Catal. B: Environ.*, 4 (1994) 225.
9. J. Kirchnerova, D. Klavana, J. Vaillancourt and J. Chaouki, *Catal. Lett.*, 21 (1993) 77.
10. D. Klavana, J. Vaillancourt, J. Kirchnerova and J. Chaouki, *Appl. Catal. A: General*, 109 (1994) 181.
11. V.R. Choudhary and V.H. Rane, *J.Catal.*, 135 (1992) 310.

Appendix 1: Chemical composition and physiochemical properties of different supports
(Obtained from Norton Co., USA)

Support	Shape	Composition	Surface area ($\text{m}^2\cdot\text{g}^{-1}$)	Pore volume ($\text{cm}^3\cdot\text{g}^{-1}$)	Porosity (%)
SA-5205	spherical	Al_2O_3 (86.1 %), SiO_2 (11.8 %), K_2O (0.6 %), CaO (0.4 %), MgO (0.4 %), Na_2O (0.4 %), Fe_2O_3 (0.2 %) $\text{ZrO}_2 + \text{HfO}_2$ (< 0.05 %)	< 0.05	0.35	54
SA-5218	spherical	Al_2O_3 (86.1 %), SiO_2 (12.0 %), CaO (0.6 %), MgO (0.4 %), K_2O (0.6 %), TiO_2 (0.2 %), Na_2O (0.2 %), Fe_2O_3 (0.1 %), ZrO_2 (< 0.05 %)	< 0.05	0.20	40
SA-5552	rings	Al_2O_3 (93.1 %), SiO_2 (5.6 %), Fe_2O_3 (0.3 %), MgO (0.3 %), TiO_2 (0.1 %), CaO (0.1 %), Na_2O (0.1 %), K_2O (0.1 %), $\text{ZrO}_2 + \text{HfO}_2$ (< 0.05 %)	0.33	0.39	59
SC-5532	rings	SiC (65.8 %), SiO_2 (28.5 %), Al_2O_3 (4.7 %), Fe_2O_3 (0.3 %), CaO (0.2 %), MgO (0.1 %), Na_2O (0.1 %), K_2O (0.1 %), $\text{ZrO}_2 + \text{HfO}_2$ (< 0.05 %), TiO_2 (< 0.01 %), leachable iron = 17 ppm	0.15	0.23	45
SS-5231	spherical	SiO_2 (95.0 %), Al_2O_3 (4.1 %), Fe_2O_3 (0.3 %), TiO_2 (0.2 %), CaO (0.1 %), MgO (0.1 %), Na_2O (0.1 %), K_2O (0.1 %), $\text{ZrO}_2 + \text{HfO}_2$ (< 0.05 %)	0.22	0.25	35
SZ-5564	rings	$\text{ZrO}_2 + \text{HfO}_2$ (94.1 %), CaO (3.5 %), SiO_2 (1.6 %), Al_2O_3 (0.4 %), MgO , Na_2O and K_2O (< 0.02 %)	0.10	0.15	45

Appendix-2 : List of chemicals

The following chemicals have been used.

Ammonium hydroxide	: Special Grade (S.D. Fine Chemicals)
Barium nitrate	: AR Grade (S.D. Fine Chemicals)
Calcium acetate	: GR Grade (Loba-Chemie)
Calcium hydroxide	: Special (Qualigens, SQ)
Calcium nitrate	: GR Grade (Loba Chemie).
Calcium oxide	: GR Grade (Loba Chemie).
Cobalt nitrate	: GR Grade (Loba Chemie)
Copper nitrate	: GR Grade (Loba Chemie)
Chromium nitrate	: GR Grade (Loba Chemie)
Ferric nitrate	: Special (Qualigens, SQ)
Lanthanum acetate	: AR Grade (99.9%, Sas Chemicals)
Lanthanum nitrate	: GR Grade (Loba Chemie).
Lanthanum oxide	: Aldrich (99.9%)
Lithium acetate	: Extra pure (Sisco Research Laboratories).
Lithium nitrate	: GR Grade (Loba-Chemie)
Manganous acetate	: Sepcial (Qualigens, SQ)
Magnesium acetate	: AR grade (Thomas Baker Chemicals).
Magnesium nitrate	: AR Grade (S.D. Fine Chemicals)
Magnesium oxide	: GR (Loba-Chemie)
Nickel nitrate	: GR Grade (99.9%, Loba-Chemie)
Samarium nitrate	: Aldrich (99.9 %)
Silver nitrate	: Chemically pure (National Refinery Pvt. Ltd., Mumbai)
Sodium carbonate	: AR Grade (S.D. Fine Chemicals)
Sodium hydroxide	: AR Grade (S.D. Fine Chemicals)
Strontium nitrate	: GR Grade (99.9%, Loba Chemie)
TMAOH	: Aldrich (25% solution in water)
Urea	: Extrapure (S.D. Fine Chemicals)
Ytterbium nitrate	: Aldrich (99.9 %)
Zirconyl nitrate	: Practical Grade (Loba-Chemie)

Appendix-3 : List of gases

The following gases have been used

Ammonia	:	High purity (99.995%) obtained from L'Air Liquide France.
Carbon dioxide	:	High purity (99.995%) obtained from L'Air Liquide France.
Ethane	:	High purity (99.995%) obtained from L'Air Liquide France.
Ethylene	:	High purity (99.99%) obtained from AIRCO Industrial Gases, USA.
Hydrogen	:	IOLAR-II grade obtained from Indian Oxygen Ltd., Bombay.
Helium	:	IOLAR-II grade obtained from Indian Oxygen Ltd., Bombay.
Methane	:	High purity (99.995 %) obtained from L'Air Liquide France.
Nitrogen	:	IOLAR-II grade obtained from Indian Oxygen Ltd., Bombay.
Oxygen	:	IOLAR-II grade (99.99 %) obtained from Indian Oxygen Ltd Bombay.

PUBLICATIONS *based on the thesis work*

Research papers

1. Metal oxide-support interaction in supported Li-promoted MgO catalysts for oxidative coupling of methane
V.R. Choudhary, S.A.R. Mulla and **B.S. Uphade**
Mater. Chem. Phys. (communicated)
2. Oxidative coupling of methane over Sr-promoted La₂O₃ catalyst supported on low surface area porous catalyst carrier
V.R. Choudhary, **B.S. Uphade** and S.A.R. Mulla
Ind. and Eng. Chem. Res. (communicated)
3. Oxidative conversion of methane to syngas over LaNiO₃ perovskite with or without simultaneous steam and CO₂ reforming reactions : Influence of partial substitution of La and Ni
V. R. Choudhary, **B. S. Uphade** and A. Belhekar
J. Catal., 163, 312 (1996).
4. Partial oxidation of methane to syngas with or without simultaneous CO₂ and steam reforming reactions over Ni/AlPO₄
V.R. Choudhary, **B.S. Uphade** and A.S. Mamman
Zeolites (in press)
5. Large enhancement in methane-to-syngas conversion activity of supported Ni catalysts due to precoating of catalyst support with MgO, CaO or rare earth oxide
V.R. Choudhary, **B.S. Uphade** and A.S. Mamman
Catal. Lett., 32, 387 (1995)
6. Oxidative conversion of methane to syngas over nickel supported on the low surface area porous porous catalyst carriers precoated with alkaline and rare earth oxides
V.R. Choudhary, **B.S. Uphade** and A.S. Mamman
J. Catal. (Communicated)
7. Simultaneous steam and CO₂ reforming of methane to syngas over NiO/MgO/SA-5205 in presence and absence of oxygen
V.R. Choudhary, **B.S. Uphade** and A.S. Mamman
J. Catal. (Communicated)
8. Low temperature complete combustion of methane over Mn-, Co- or Fe-stabilised ZrO₂
V. R. Choudhary, **B. S. Uphade**, S. G. Patsakar and A.Keshavaraja
Angew. Chem. Int. Ed. Engl., 35, 2393 (1996).

9. Complete combustion of methane over Mn-doped ZrO_2 (cubic)
V.R.Choudhary, **B.S.Uphade** and A.Keshavraja
Appl. Catal. B: Environment (To be communicated)
10. Low temperature total oxidation of methane over Ag-doped $LaMO_3$ perovskite oxides
V.R. Choudhary, **B.S. Uphade**, S.G. Pataskar and G.A. Thite
J. Chem. Soc. Chem. Commun., 1021 (1996)

PAPERS PRESENTED IN THE NATIONAL SEMINARS/SYMPOSIUMS

1. Influence of Metal Oxide-Support Interactions in Supported La-Promoted CaO Catalysts for Oxidative Coupling of Methane
B.S. Uphade, S.A.R. Mulla and V.R. Choudhary
paper accepted for the poster presentation in *13th National Symposium on Catalysis*, IIP, Dehradun, April 2-4, 1997.
2. Oxidative conversion of methane to syngas with or without simultaneous steam and/or CO_2 reforming over supported NiO-MgO, NiO-CaO and NiO-Yb $_2$ O $_3$ catalysts
B.S. Uphade, A.S. Mamman and V.R. Choudhary
Presented in *12th National Symposium on Catalysis*, Bombay, Dec. 19-22, 1994.
3. Complete combustion of methane over $La_{1-x}Sr_x$ (or Ag) $_x$ Co (or Mn) O_3 perovskites: Influence of partial substitution of La by Sr or Ag.
V.R. Choudhary, S.G. Pataskar, **B.S. Uphade**, G.A. Thite and L.R. Kamath
Presented in *Indo-British Seminar on Catalysis in Energy and the Environment*, IICT, Hyderabad, January 30 - 31, 1995.

LIST OF US & INDIAN PATENT APPLICATIONS FILED

1. Process for the preparation of an improved supported catalyst containing nickel and cobalt, with or without noble metals, useful for the oxidative conversion of methane, natural gas and biogas to syngas.
V.R.Choudhary, **B.S.Uphade**, A.S.Mamman, A.M.Rajput
In India : Filing No. 624/DEL/94 (dtd. 20.5.94)
In USA : Patent Application Filed by CSIR. Filing No. 08/359035 (1994)
2. Process for oxidative conversion of methane or natural gas to syngas in an energy efficient manner, using an improved supported catalyst containing nickel and cobalt.
V.R.Choudhary, **B.S.Uphade**, A.S.Mamman, A.M.Rajput
In India : Filing No. 632/DEL/94 (dtd. 20.5.94)
In USA : Patent Application Filed by CSIR. Filing No. 08/37260 (1994)

PUBLICATIONS *other than thesis work*

Research papers

1. Coupling of endothermic thermal cracking with exothermic oxidative dehydrogenation of ethane to ethylene using a diluted SrO/La₂O₃/SA-5205 catalyst
V.R.Choudhary, **B.S.Uphade** and S.A.R.Mulla
Angew. Chem. Int. Ed. Engl., **34**, 665 (1995)
2. Oxidative coupling of methane over supported MgO, La₂O₃ and La-promoted MgO catalysts : Influence catalyst support interaction
V.R. Choudhary, S.A.R. Mulla and **B.S. Uphade**
Ind. and Eng. Chem. Res. (in press)
3. Oxidative conversion of methane to syngas over NiO/MgO/SA5205 with or without containing cobalt and noble metals
V.R. Choudhary, A.S. Mamman and **B.S. Uphade**
Appl. Catal. A: Gen. (To be communicated)
4. Simultaneous steam and CO₂ reforming of methane over CoO-NiO/MgO/SA5205 catalysts
V.R. Choudhary, A.S. Mamman and **B.S. Uphade**
J. Chem. Tech. Biotech. (To be communicated)
5. Coupling of exothermic and endothermic methane-to-syngas conversion reactions over CoO-NiO/MgO/SA5205 catalysts
V.R. Choudhary, A.S. Mamman and **B.S. Uphade**
Ind. and Eng. Chem. Res. (To be communicated)
6. Oxidative Dehydrogenation of Ethane to Ethylene over Sr-Promoted La₂O₃ Catalyst Supported on Low Surface Area Porous Catalyst Carrier.
S.A.R. Mulla, **B.S. Uphade** and V.R. Choudhary
paper accepted for the poster presentation in *13th National Symposium on Catalysis*, IIP, Dehradun, April 2-4, 1997.

LIST OF US & INDIAN PATENT APPLICATIONS FILED

1. Process for the preparation of an improved supported catalyst useful for the oxidative coupling of methane to higher hydrocarbons, for oxidative conversion of natural gas to ethylene and other lower olefins and oxidative dehydrogenation of ethane to ethylene.
V.R.Choudhary, **B.S.Uphade**, S.A.R.Mulla
In India : Filing No. 370/DEL/94 (dtd. 31.3.94)
Patent applications filed by CSIR in USA on 5.6.95. Filing number is awaited.
2. Energy efficient process for the oxidative conversion of ethane or C₂ - C₄ paraffins to ethylene and higher olefins, using the improved supported catalyst".
V.R.Choudhary, **B.S.Uphade**, S.A.R.Mulla
In India : Filing No. 371/DEL/94 (dtd. 31.3.94)
Patent applications filed by CSIR in USA on 5.6.95. Filing number is awaited.
3. Energy efficient process for the oxidative conversion of methane or natural gas to ethylene, ethane and higher hydrocarbons using the improved supported catalyst".
V.R.Choudhary, **B.S.Uphade**, S.A.R.Mulla
In India : Filing No. 372/DEL/94 (dtd. 31.3.94)
Patent applications filed by CSIR in USA on 5.6.95. Filing number is awaited.